

# **Evolution of Lubricant Degradation and Lubricant Behaviour in a Piston Assembly of a Reciprocating Gasoline Engine**

Rai Bahadur Raman Singh Notay

MEng(Hons)

Submitted in accordance with the requirements for the degree of  
Doctor of Philosophy

The University of Leeds  
School of Mechanical Engineering

April 2013

The candidate confirms that the work submitted is his/her own and that appropriate credit has been given where reference has been made to the work of others.

This copy has been supplied on the understanding that it is copyright material and that no quotation from the thesis may be published without proper acknowledgement.

The right of Rai Bahadur Raman Singh Notay to be identified as Author of this work has been asserted by him in accordance with the Copyright, Designs and Patents Act 1988.

© 2013 The University of Leeds and Rai Bahadur Raman Singh Notay

*“aharan math vaedh hatheear”*

Consider your mind as your anvil and knowledge as your hammer

Sri Japji Sahib, recited by Sri Guru Nanak Dev Ji (1<sup>st</sup> Sikh Guru)

*For my family*

## **Abstract**

The most difficult and challenging area for the tribology of reciprocating internal combustion engines to improve efficiency and life is the lubricant health within the piston ring pack. It is here where extreme temperatures, pressures and noxious gases interact with the small volume of lubricant designed to protect the components. There is a lack of knowledge of the correlation between the lubricant condition and its performance. This research is an original contribution to this field and addressed the influence of lubricant degradation on lubricant film thicknesses and residence times in the piston ring pack.

A laser induced fluorescence (LIF) system was first implemented on an operating motored gasoline engine to examine the piston ring to cylinder wall lubricant film thickness. A bespoke optical setup was designed and developed with excellent spatial resolution incorporating an argon ion laser, operating at 488 nm, combined with photomultiplier tubes to measure reference laser and incoming fluorescent light via a sapphire window in the cylinder liner. Lubricants were doped with Pyrromethene 567A fluorescent dye and the fluorescence signals were calibrated through a strict method, which allowed the fluorescence of degraded samples, and hence the lubricant film thickness, to be quantified. A range of degraded engine lubricant samples were acquired from Mercedes Benz, Leeds, UK and Southwest Research Institute, Texas, USA. The LIF system was then adapted and transferred to a high speed, fired Ricardo Hydra single cylinder gasoline engine. The capability of the LIF system was finally extended to examine lubricant flow in the piston ring pack through a novel tracer technique, which enabled direct measurement of piston ring pack lubricant residence time.

A LIF system was developed that could clearly distinguish between lubricants of different viscosities and degradation state. It was found that degraded lubricants, with increased viscosity compared to fresh lubricant, produce thicker lubricant films in the piston ring to cylinder wall interface, which would directly impact on engine efficiency. Additionally, it was found that engine speed, load and lubricant viscosity influence the piston ring pack lubricant residence time and the replenishment of the lubricant within the piston ring pack.

## Acknowledgments

First and foremost, I would like to thank my Waheguru (Wonderful Lord). He provides me with the breath of life so that I can perform at what I do best.

I would like to express my sincere thanks to my supervisor Prof. Martin Priest for his consistent help throughout my studies at University. His vast knowledge was an invaluable resource and always welcomed. I would also like to thank Prof. Richard C Coy and Prof. Malcolm F Fox whose guidance and encouragement throughout this research pushed me to reach my full potential. No acknowledgement would be complete without a mention to Dr Peter M Lee, who was initially my primary supervisor, and opened my mind to challenging theories and the impossibilities that expanded my knowledge and skill.

There are many colleagues in the Mechanical Engineering Department who I must thank for helping me and making my time here enjoyable. Without the technicians; Paul Banks, Mark Batchelor, Ron Cellier, Graham Jakeman and Brian Leach, this experimental program would not have been possible. Jonathan Stephenson for the use of his workshop, I am grateful for that and all the advice he has provided. They have all been more than work colleagues. Dr Richard Chittenden provided knowledge and help too. Adrian Eagles was very welcoming when it came to last minute profile scans of piston rings and cylinder liners. The many PhD students, too many to list, that have provided help and advice along the way, I thank you.

Thanks go to Jonny Atkinson, technician at Mercedes Benz (Leeds, UK), for supplying the degraded gasoline lubricants and also to Dr Chris Warrens, Senior Technologist at BP (Reading, UK), for the viscosity analysis of the lubricant samples.

I would like to thank my family; Dad, Mum, Surjeet, Harpreet, Jaspal, Manvinder, Amreet and little Harsimar, whose confidence in me has been priceless to me. Words cannot express the feelings I have for you. I would not be here if it was not for my family who consistently offered unconditional love and support.

Finally, I would like to acknowledge the most important person in my life, my fiancée Navinder. She has been a constant source of strength, and her love, dedication and patience (and sometimes a kick in the backside when I needed one) has encouraged me to see this project through to the end. I love you Navinder, more than mere words can possibly say.

# Contents

<b>Abstract</b> .....	<b>v</b>
<b>Acknowledgments</b> .....	<b>vi</b>
<b>Contents</b> .....	<b>vii</b>
<b>List of Tables</b> .....	<b>xii</b>
<b>List of Figures</b> .....	<b>xiii</b>
<b>Notation</b> .....	<b>xx</b>
<b>Abbreviations</b> .....	<b>xxii</b>
<b>Chapter 1      Opening</b> .....	<b>1</b>
1.1 Introduction .....	1
1.2 The role of the piston ring pack.....	4
1.3 Piston ring design .....	7
1.4 An introduction to engine lubrication.....	10
1.5 Scope of this project .....	13
1.6 Structure of the thesis .....	14
<b>Chapter 2      Literature Review</b> .....	<b>17</b>
2.1 Engine lubricant degradation.....	17
2.1.1 Thermal degradation and evaporation .....	18
2.1.2 Mechanical molecular degradation.....	19
2.1.3 Dilution.....	19
2.1.4 Oxidation and nitration.....	20
2.1.5 Additive depletion .....	21
2.1.6 Methods of bulk engine lubricant degradation detection.....	22
2.1.7 In-situ lubricant sampling methods for piston ring pack degradation .....	24
2.2 Theoretical piston ring research .....	28
2.3 Experimental piston ring research.....	33
2.3.1 Lubricant transport and consumptions mechanisms.....	33

---

2.4	Lubricant film thickness measurement methods .....	39
2.4.1	Electrical methods .....	39
2.4.2	Laser Induced Fluorescence (LIF) method.....	43
2.4.3	Ultrasound method .....	47
2.4.4	Summary of the measured film thicknesses in the literature .....	51
2.5	Summary .....	52
<b>Chapter 3</b>	<b>Development of a Laser Induced Fluorescence Technique on a Motored Engine.....</b>	<b>54</b>
3.1	VW horizontal piston motored engine .....	54
3.1.1	Specifications and previous OFT work on engine.....	54
3.1.2	Modifications to lubricant and coolant supply .....	57
3.1.3	Modifications to crankcase breather system.....	58
3.1.4	Modifications to cylinder pressure .....	60
3.2	Laser induced fluorescence (LIF).....	63
3.2.1	Fluorescence principles .....	63
3.2.2	Stokes shift .....	65
3.3	LIF system.....	65
3.3.1	Laser system and optical arrangement.....	66
3.3.2	New collimator probe and window design .....	70
3.4	LIF Calibration .....	74
3.4.1	Lubricant film thickness calibration methods.....	75
3.4.2	Temperature effects .....	81
3.4.3	Dye concentration.....	82
3.4.4	Sample opacity .....	84
3.4.5	Surface reflectivity .....	85
3.5	Summary .....	86
<b>Chapter 4</b>	<b>Implementation and Results of Testing on the Motored Engine.....</b>	<b>88</b>
4.1	Implementation.....	88
4.1.1	Setting the focal point of lenses.....	88
4.1.2	Black coating of window seat.....	91
4.1.3	Piston rings .....	91
4.1.4	Cylinder liner thermocouples .....	91

---

4.1.5	Installation of the optical encoder and engine TDC position .....	92
4.1.6	Cylinder head pressure transducer.....	94
4.2	Engine Lubricant samples .....	96
4.2.1	Lubricant chemical analysis .....	97
4.2.2	Lubricant viscosity analysis.....	99
4.3	Testing and test matrix .....	102
4.4	Results and Discussion.....	104
4.4.1	End of test (EOT) components .....	115
4.5	Conclusions .....	117
<b>Chapter 5</b>	<b>Development and Testing of a LIF System on a Ricardo Hydra</b>	
	<b>Fired Test Engine.....</b>	<b>119</b>
5.1	Ricardo Hydra gasoline single cylinder engine.....	119
5.2	Implementation of the LIF system on the Hydra.....	120
5.2.1	Design and manufacture of Hydra barrel.....	120
5.2.2	Cylinder liner thermocouples and mid-stroke sampling tube.....	125
5.2.3	Piston rings and running-in.....	127
5.2.4	Engine lubricant samples.....	129
5.3	Testing and test matrix .....	130
5.4	Results and Discussion.....	132
5.4.1	EOT components .....	143
5.5	Conclusions .....	146
<b>Chapter 6</b>	<b>Piston Ring Pack Lubricant Residence Times and the Influence</b>	
	<b>of Top Ring Zone Sampling on Piston Ring Lubricant Film Thickness .....</b>	<b>148</b>
6.1	Previous Studies of Piston Ring Pack Residence Time.....	149
6.2	Using the LIF Technique to Measure Piston Ring Pack Residence Time.....	150
6.2.1	Implementation on the Hydra Engine.....	152
6.2.2	Temperature Controlled Lubricant Sumps .....	153
6.2.3	Engine Lubricant Samples.....	153
6.3	Using the LIF Technique to Investigate the Influence of TRZ Sampling on Piston Ring Pack Lubrication.....	155
6.4	Testing and Test Matrix .....	156
6.5	Method Used to Measure Piston Ring Pack Residence Time .....	157
6.6	Results and Discussion.....	161

---

6.6.1	Piston Ring Pack Residence Time .....	161
6.6.2	Top Ring Zone Sampling .....	167
6.7	Conclusions .....	171
<b>Chapter 7</b>	<b>Data Acquisition System .....</b>	<b>173</b>
7.1	LIF Data Acquisition System .....	173
7.2	DAQ Channels .....	174
7.3	Engine control unit .....	178
7.4	Introduction to LabVIEW .....	178
7.5	LabVIEW DAQ Programs .....	179
7.5.1	LIF Calibration Program .....	180
7.5.2	Piston Ring Pack Oil Film Thickness Measurement Program .....	183
7.5.3	Post Processing Program .....	186
7.5.4	Additional LabVIEW Programs .....	187
7.6	Data Averaging and Error Analysis .....	188
7.7	Summary .....	192
<b>Chapter 8</b>	<b>Conclusions and Recommendations for Future Research .....</b>	<b>193</b>
8.1	Introduction .....	193
8.2	Major Conclusions .....	194
8.3	Detailed Conclusions.....	195
8.3.1	Motored Engine Experimental Work.....	195
8.3.2	Ricardo Hydra Gasoline Engine Experimental Work.....	196
8.3.3	Piston Ring Pack Lubricant Residence Time and Top Ring Zone Sampling Investigation.....	197
8.4	Novel Aspects of the Research.....	198
8.5	Recommendations for Further Work.....	198
8.6	Recommendations for Future Research.....	200
	<b>References.....</b>	<b>202</b>
	<b>Appendix.....</b>	<b>218</b>
<b>A.</b>	<b>Optical Parts Inventory and Optical Specifications.....</b>	<b>218</b>
A.1	Optical Parts Inventory.....	218

---

A.2	Photosensor Module Specification (H5783-20) .....	219
A.3	Photosensor Module Power Supply (C7169) .....	221
A.4	Thorlabs Excitation/ Emission Filters and Dichroic Mirror Specification .....	222
<b>B.</b>	<b>Engineering Technical Drawings.....</b>	<b>223</b>
B.1	Sapphire Window Technical Drawing .....	223
B.2	Motored Engine Cylinder Liner Machining Guide to Fit Window .....	224
B.3	Motored Engine LIF Collimator Probe Sleeve.....	225
B.4	Ricardo Hydra Cylinder Liner Machining Guide.....	227
B.5	Ricardo Hydra Engine LIF Collimator Probe Sleeve.....	231
B.6	Ricardo Hydra Barrel Machining Guide .....	232
<b>C.</b>	<b>Engine Lubricant LIF Calibration Tests .....</b>	<b>237</b>
C.1	Fresh Sample A – Castrol Edge SAE 0W30 plus 35mg/l dye.....	237
C.2	Degraded Sample B – MB Medium Size Car, Castrol Edge SAE 0W30 plus 100mg/l dye .....	238
C.3	Degraded Sample C – MB Sports Car, Castrol Edge SAE 0W30 plus 100mg/l dye.....	239
<b>D.</b>	<b>Pyrrromethene 567A Dye Specification.....</b>	<b>240</b>
<b>E.</b>	<b>Monarch 280 Carbon Black Powder Specification .....</b>	<b>242</b>
<b>F.</b>	<b>Test Oil Specifications.....</b>	<b>243</b>
F.1	Castrol Edge SAE 0W30.....	243
F.2	Shell Extra High Viscosity Index (XHVI) 8.2 .....	244
F.3	Shell Helix HX7 AG SAE 5W30.....	245
<b>G.</b>	<b>Ricardo Hydra Engine Specifications .....</b>	<b>246</b>
<b>H.</b>	<b>List of Presentations.....</b>	<b>247</b>

## List of Tables

Table 2-1: A summary of the lubricant film thickness as measured at the piston ring through various experimental techniques and conditions by previous researchers .....	51
Table 3-1: Variation of peak cylinder pressures with and without forced induction at 11.6:1 cr .....	62
Table 3-2: Variation of peak cylinder pressures with and without forced induction at 9.4:1 cr .....	62
Table 3-3: Variation of peak cylinder pressures with and without forced induction at 7.4:1 cr .....	62
Table 4-1: A list of the lubricants acquired for the investigation of piston ring to cylinder wall film thickness measurements .....	97
Table 4-2: Percentage area increase in the oxidation region of the gasoline lubricant samples when compared to the fresh sample .....	99
Table 5-1: Running-in test procedure .....	127
Table 5-2: Hydra engine test matrix for test lubricant Sample A .....	131
Table 6-1: Piston ring pack residence times (in minutes) over a wide range of engine operating conditions (error $\pm$ 1.0 min) as measured by Lee (Lee 2006).....	150
Table 6-2: Test oil kinematic viscosity specification.....	154
Table 6-3: Test matrix to investigate piston ring pack residence time (X denotes test point, area shaded in orange is test range as investigated by Lee 2006).....	157
Table 6-4: Test matrix to investigate the effect of TRZ sampling on piston ring pack lubrication (X denotes test point).....	157
Table 6-5: TRZ sample pipe flow rate (l/min) as measured by Lee (Lee 2006).....	169
Table A-1: Optical parts inventory .....	218
Table G-1: Ricardo Hydra Engine specifications .....	246

## List of Figures

Figure 1-1:	Current and future emission legislation from around the world (LNG 2010) .	3
Figure 1-2:	Cross section of a typical gasoline 4 stroke internal combustion engine.....	5
Figure 1-3:	A typical piston ring pack arrangement for a gasoline engine.....	8
Figure 1-4:	Summary of modern automotive piston ring designs (Neale 1994) .....	9
Figure 1-5:	A modified Stribeck diagram detailing lubricant property influence. Adapted from Priest (2000) (Priest and Taylor 2000).....	10
Figure 1-6:	Fuel energy losses with large contribution from piston rings. After Tung and McMillan (2004).....	12
Figure 2-1:	Effect of shear rate on viscosity of lubricant (Mortier and Orszulik 1992) ...	19
Figure 2-2:	Two phase reactor model of an engine. Reproduced from Lee (Lee 2006)...	24
Figure 2-3:	Method to attach sample pipe to connecting rod (Lee 2006).....	26
Figure 2-4:	TRZ lubricant sample collection method as used by Lee (Lee 2006) .....	26
Figure 2-5:	Current TRZ sampling linkage designed by Notay (Notay 2008).....	27
Figure 2-6:	Watson's probe for in-situ infrared absorbance measurements (Watson and Wong 2010) .....	28
Figure 2-7:	Minimum film thickness as predicted by Priest when adopting different cavitation models (Priest 1996) .....	30
Figure 2-8:	Oil accumulating ahead of ring (Gamble, Priest et al. 2003).....	32
Figure 2-9:	Inertia and gas forces fight to keep the ring stable (Tian 2002) .....	34
Figure 2-10:	Dynamics of ring twisting cause the lubricant to squeeze out of piston groove. Reproduced from (Thirouard and Tian 2003).....	35
Figure 2-11:	Oil Flow observed when ring gaps are all 180° out of phase with each other (Nakashima, Ishihara et al. 1995) .....	36
Figure 2-12:	Oil Flow observed when ring gaps are all in phase (Nakashima, Ishihara et al. 1995) .....	36
Figure 2-13:	Flow of oil in an engine, reproduced from (Burnett, Bull et al. 1995) .....	37
Figure 2-14:	Cross sectional view of the capacitance transducers mounted in the top and scraper ring by Takiguchi (Takiguchi, Sasaki et al. 2000) .....	41
Figure 2-15:	Lubricant film thickness measurements of the top ring across all four engine strokes (Takiguchi, Sasaki et al. 2000) .....	42

Figure 2-16:	LIF method through the liner as used by Yilmaz (Yilmaz, Tian et al. 2004)	44
Figure 2-17:	2D LIF system as used by Thirouard (Thirouard, Tian et al. 1998)	46
Figure 2-18:	Oil misting due to blow-by gases in the ring gaps (Thirouard and Tian 2003)	46
Figure 2-19:	Comparison of oil film velocity by PIV with average piston speed $V_{pt}$ at various engine speeds (Baba, Suzuki et al. 2007)	47
Figure 2-20:	Ultrasonic transducer mounted to outside of liner (Dwyer-Joyce, Green et al. 2006)	50
Figure 2-21:	Typical OFT measurement of the piston ring – liner interface using ultrasound at a motored engine speed of 840 rpm (Avan, Mills et al. 2010)	50
Figure 3-1:	A schematic of the modified motored engine used for the development of the LIF system	55
Figure 3-2:	A cross section of the experimental cylinder. Adapted from (Radcliffe 1993)	56
Figure 3-3 :	Original crankcase breather system (Radcliffe 1993)	59
Figure 3-4:	Schematic of how compression ratio of cylinder was adapted	61
Figure 3-5:	Diagram illustrating fluorescence process (Hauglan 2005)	63
Figure 3-6:	Illustration of Stokes Shift theory	65
Figure 3-7:	A schematic of the original optics arrangement as used by Rahimiardali (Rahimiardali 2008)	66
Figure 3-8:	LIF Optical System	67
Figure 3-9:	Original complete assembled collimator probe and dismantled probe	68
Figure 3-10 :	Illustration of crush bush sealing and conical window seating in the liner	69
Figure 3-11:	Talysurf profile of the misaligned conical window in the liner	70
Figure 3-12:	New dynamic collimator probe and step window design	71
Figure 3-13:	A schematic of the new optical probe setup on the motored engine	72
Figure 3-14:	Illustrating the importance of fibre optic aperture on optical convolution	74
Figure 3-15:	Four grooves turned into the piston skirt for dynamic calibration	75
Figure 3-16:	Surface profile scan of the four grooves on the piston skirt	76
Figure 3-17:	Oil feed to calibration grooves on skirt to prevent local lubricant cavitation	76
Figure 3-18:	An attempt at fluorescence calibration using an increasing oil film thickness trapped between two microscope cells	77
Figure 3-19:	Typical calibration graph obtained from the wedged cells	78
Figure 3-20:	Calibration setup designed and manufactured	79
Figure 3-21:	Part of a piston and piston ring used as the reflective surface for calibration	79
Figure 3-22:	Increased level of dye concentration is required for degraded lubricants	83

---

Figure 3-23:	Contamination with carbon black (CB) influences the sample opacity.....	84
Figure 3-24:	The importance of opacity becomes apparent when the samples are calibrated.....	85
Figure 3-25:	Influence of surface reflectivity when PMT sensitivity is increased.....	85
Figure 4-1:	Illustration of the position of the focal point of the lenses.....	89
Figure 4-2:	The reflectivity of the window seating surface was reduced to minimise the effects of stray light.....	90
Figure 4-3:	Thermocouples used to monitor cylinder liner temperatures.....	92
Figure 4-4:	Liner temperature trace at 1000 rpm and 10 bar cylinder peak pressure.....	93
Figure 4-5:	Four-way pressure splitter used to help calibrate Kistler 601 pressure transducer.....	95
Figure 4-6:	Calibration graphs for pressure transducer sensors 601 and 4045.....	95
Figure 4-7:	Motored engine cylinder pressure measurement showing correction applied for pressure drift.....	96
Figure 4-8:	FTIR spectra of Sample A showing most common absorbance peaks.....	98
Figure 4-9:	FTIR spectra of oxidation and nitration absorption for all samples.....	98
Figure 4-10:	Dynamic viscosity of all samples at 40°C and 100°C.....	99
Figure 4-11:	HTHS viscosity at increasing temperature for Samples A, B, C and D.....	101
Figure 4-12:	Motored engine test matrix for test lubricant Sample A.....	103
Figure 4-13:	Perspex piece used to mount the piston and allow the rings to be in tension ready for a profilometric scan. As used by Priest (Priest 1996).....	104
Figure 4-14:	Three measurement locations taken on the piston rings.....	105
Figure 4-15:	Before engine testing new piston ring profiles.....	105
Figure 4-16:	EOT used piston ring profiles.....	106
Figure 4-17:	Typical LIF profile with the piston rings superimposed (compression stroke), Sample A at 120°C, 800rpm and 22 bar peak cylinder pressure.....	107
Figure 4-18:	LIF profile on intake stroke shows a mirror like image to the compression stroke profile. Sample A at 120°C, 800rpm and 22 bar peak cylinder pressure.....	107
Figure 4-19:	The effect of lubricant temperature on MOFT across the complete piston ring pack for the MB gasoline lubricant samples at 800 rpm and 22 bar pressure.....	109
Figure 4-20:	The effect of lubricant temperature on MOFT across the complete piston ring pack for the SwRI diesel lubricant sample at 800 rpm and 22 bar pressure.....	109

---

Figure 4-21: Compression ring MOFT vs HTHS viscosity, 80 °C, 800 rpm and 22 bar pressure .....	110
Figure 4-22: Compression ring MOFT vs HTHS viscosity, 100 °C, 800 rpm and 22 bar pressure .....	110
Figure 4-23: Compression ring MOFT vs HTHS viscosity, 120 °C, 800 rpm and 22 bar pressure .....	110
Figure 4-24: The effect of cylinder peak pressure on the piston ring pack MOFT for the MB gasoline lubricant samples at 800 rpm and 120°C .....	112
Figure 4-25: The effect of cylinder peak pressure on the piston ring pack MOFT for the SwRI diesel lubricant sample at 800 rpm and 120°C .....	112
Figure 4-26: The effect of engine speed on the piston ring pack MOFT for the MB gasoline lubricant samples at 16 bar cylinder pressure and 100°C .....	113
Figure 4-27: The effect of engine speed on the piston ring pack MOFT for the SwRI diesel lubricant sample at 16 bar cylinder pressure and 100°C .....	113
Figure 4-28: The influence of temperature and engine speed on Sample A lubricant shear rate at 16 bar peak cylinder pressure .....	114
Figure 4-29: The influence of temperature and engine speed on Sample C lubricant shear rate at 16 bar peak cylinder pressure .....	115
Figure 4-30: Thrust side of cylinder liner at EOT .....	116
Figure 4-31: Anti-thrust side of cylinder liner at EOT .....	116
Figure 4-32: Cross section of engine without cylinder head showing the piston crown deposits .....	117
Figure 5-1: Illustration of modified Hydra barrel .....	121
Figure 5-2: A picture of the coolant intake re-positioned on the engine flywheel side ..	122
Figure 5-3: Modified cylinder liner with extra material at 3 locations .....	123
Figure 5-4: The top view of the barrel complete with liner and probe sleeve .....	124
Figure 5-5: A cross sectional view of the interface between the liner and the probe sleeve .....	124
Figure 5-6: Mid-stroke liner temperatures for various engine speeds and loads .....	126
Figure 5-7: Mid-stroke sampling tube and thermocouple wires on the thrust side as the probe .....	126
Figure 5-8: Piston ring profiles before engine run-in .....	127
Figure 5-9: Piston ring profiles after engine run-in .....	128
Figure 5-10: A 3D scan of the Hydra liner shows the window is flush with the running surface .....	129
Figure 5-11: A 2D profile scan of the window in the liner in the direction of the piston motion .....	130

---

Figure 5-12:	A 2D profile scan of the window in the liner in the circumferential direction .....	130
Figure 5-13:	Typical 4 stroke LIF profile for Sample A at 1000 rpm, 50 % load, 60 °C. ....	132
Figure 5-14:	Piston ring MOFT at 1000rpm, no load (motoring), 30 °C.....	134
Figure 5-15:	Piston ring MOFT at 1000rpm, 50% load (firing), 60 °C.....	134
Figure 5-16:	The effect of engine speed at maximum load on piston ring MOFT .....	136
Figure 5-17:	MOFT against HTHS – compression ring, 4000 rpm, 100 % load, 95 °C... ..	137
Figure 5-18:	MOFT against HTHS – scraper ring, 4000 rpm, 100 % load, 95 °C .....	137
Figure 5-19:	MOFT against HTHS – oil control ring, 4000 rpm, 100 % load, 95 °C .....	137
Figure 5-20:	The effect of engine load on piston ring MOFT at engine speeds of 1000 and 3000 rpm.....	139
Figure 5-21:	The influence of engine load and engine speed on Sample A lubricant shear rate during the compression stroke .....	140
Figure 5-22:	The influence of engine load and engine speed on Sample C lubricant shear rate during the compression stroke .....	140
Figure 5-23:	The influence of engine load and engine speed on Sample A lubricant shear rate during the power stroke .....	141
Figure 5-24:	The influence of engine load and engine speed on Sample C lubricant shear rate during the power stroke .....	141
Figure 5-25:	FTIR spectra of lubricant Sample C; before engine testing, mid-stroke and sump samples.....	142
Figure 5-26:	Spark plug noise at the start of ignition as observed on the oscilloscope ....	143
Figure 5-27:	Thrust side of EOT cylinder liner .....	144
Figure 5-28:	Thrust side of EOT piston.....	144
Figure 5-29:	Anti-thrust side of EOT cylinder liner .....	145
Figure 5-30:	Anti-thrust side of EOT piston.....	145
Figure 5-31:	The use of a prism to observe the area around the window in the liner.....	146
Figure 6-1:	A flow diagram of the complete engine lubricant supply .....	150
Figure 6-2:	An illustration of the oil flow for the switchable valve .....	151
Figure 6-3:	Lubricant supply switch valve on Hydra engine with LIF collimator probe .....	152
Figure 6-4:	Ricardo Hydra engine equipped with 3 sump lubricant supply .....	154
Figure 6-5:	TRZ sampling linkage complete with sample pipe, connecting rod and piston assembly .....	155
Figure 6-6:	Oscilloscope image of fluorescence and ignition during the switch of lubricant supply at 3000 rpm and 50 % load .....	158

---

Figure 6-7:	Oscilloscope image of fluorescence and ignition at the start of Sump 2 lubricant entering the piston ring pack at 3000 rpm and 50 % load .....	158
Figure 6-8:	Oscilloscope image of fluorescence and ignition with increasing concentration of Sump 2 lubricant at 3000 rpm and 50 % load.....	159
Figure 6-9:	Oscilloscope image of fluorescence and ignition with further increase in concentration of Sump 2 lubricant at 3000 rpm and 50 % load.....	159
Figure 6-10:	Oscilloscope image of fluorescence and ignition once all Sump 1 lubricant has been displaced from the piston ring pack at 3000 rpm and 50 % load..	160
Figure 6-11:	Piston ring pack residence time for lubricant supply switch from Sump 1 to Sump 2.....	161
Figure 6-12:	The number of engine cycles required for the lubricant to reach the piston ring pack for both test lubricants when the supply is switched from Sump 1 to Sump 2.....	163
Figure 6-13:	Piston ring pack residence time for lubricant switch from Sump 2 to Sump 1 .....	164
Figure 6-14:	The number of engine cycles required for the lubricant to exit the piston ring pack for both test lubricants when the supply is switched from Sump 2 to Sump 1 .....	164
Figure 6-15:	The influence of engine load on piston ring pack residence time.....	165
Figure 6-16:	Compression ring MOFT of test lubricants at 1500 rpm with increasing load .....	166
Figure 6-17:	Scraper ring MOFT of test lubricants at 1500 rpm with increasing load.....	166
Figure 6-18:	Oil control ring MOFT of test lubricants at 1500 rpm with increasing load	166
Figure 6-19:	Effect of engine speed on TRZ sampling – compression ring, 50 % load...	168
Figure 6-20:	Effect of engine speed on TRZ sampling – scraper ring, 50 % load .....	168
Figure 6-21:	Effect of engine speed on TRZ sampling – oil control ring, 50 % load .....	168
Figure 6-22:	Effect of engine load on TRZ sampling – compression ring, 1500 rpm.....	170
Figure 6-23:	Effect of engine load on TRZ sampling – scraper ring, 1500 rpm .....	170
Figure 6-24:	Effect of engine load on TRZ sampling – oil control ring, 1500 rpm .....	170
Figure 7-1:	Schematic diagram of transducer connection to NI hardware. Adapted from (NI 2013) .....	173
Figure 7-2:	Four times the resolution is possible with quadrature shaft encoders.....	176
Figure 7-3:	Data flow chart of the DAQ system.....	177
Figure 7-4:	LVDTs have a limited operable range .....	180
Figure 7-5:	Dataflow diagram of the LIF calibration program.....	181
Figure 7-6:	Front panel of LIF calibration program .....	182

---

Figure 7-7:	Dataflow diagram of the piston ring pack OFT measurement program .....	183
Figure 7-8:	Front panel of the piston ring pack OFT measurement program.....	185
Figure 7-9:	Example of averaging process used for all LIF OFT profiles.....	188
Figure 7-10:	Standard deviation analysis for different averaging ranges during the compression stroke of the Hydra engine operating at a motoring speed of 2000 rpm.....	190
Figure 7-11:	Standard deviation analysis for different averaging ranges during the power stroke of the Hydra engine operating at a motoring speed of 2000 rpm.....	190
Figure 7-12:	Standard deviation analysis for different averaging ranges during the compression stroke of the Hydra engine operating at a firing speed of 2000 rpm.....	191
Figure 7-13:	Standard deviation analysis for different averaging ranges during the power stroke of the Hydra engine operating at a firing speed of 2000 rpm.....	191
Figure 8-1:	Curved linkage design idea for in-situ LIF probe .....	200
Figure A-1:	MF475-35 – Blue Excitation Filter .....	222
Figure A-2:	MF535-22 - Green Emission Filter .....	222
Figure A-3:	DMLP605 – Dichroic Mirror .....	222
Figure D-1:	Pyrrromethene 567A dye absorption spectrum .....	241

## Notation

$A$	Absorptivity (-)
$B$	Bulk modulus (N/m <sup>2</sup> )
$C$	capacitance (F)
$E$	energy (J)
$F_q^0$	unquenched fluorescence intensity (W)
$F_q$	actual fluorescence intensity (W)
$F(T, \lambda)$	constant relating to wavelength and temperature (-)
$I_o$	intensity of incident light (W)
$I$	intensity of fluorescence (W)
$K(\lambda)$	constant relating to wavelength (-)
$[Q]$	concentration of quenching lubricant molecules (mol/l)
$R$	gas constant (J/mol.K)
$R_c$	reflection coefficient (-)
$S$	transducer surface area (m <sup>2</sup> )
$S_0$	internal ground energy state (-)
$S_1$	internal semi-stable energy state (-)
$S_2$	internal unstable energy state (-)
$b$	path length (m)
$c$	molar concentration (mol/l)

---

$c_s$	speed of sound (m/s)
$h$	Planck's constant (J.s)
$h_{ex}$	incident (excited) light energy (J)
$h_{em}$	fluorescence (emitted) light energy (J)
$h_{OFT}$	oil film thickness (m)
$k$	stiffness (N/m)
$k_c$	molecular collision rate ( $Jm^2/Ns.mol$ )
$s$	wavespeed (m/s)
	density ( $kg/m^3$ )
	frequency (Hz)
$ex$	frequency of excited light (Hz)
$em$	frequency of emitted light (Hz)
	angular frequency (rad/s)
$z$	acoustic impedance ( $Ns/m^3$ )
	wavelength (m)
$ex$	wavelength of excited light (m)
$em$	wavelength of emitted light (m)
	molar extinction coefficient (litres/mol.cm)
$s$	material dielectric constant ( $Fm^{-1}$ )
$o$	vacuum dielectric constant (-)
	dynamic viscosity ( $Ns/m^2$ )
$\dagger_0$	fluorophore lifetime (s)
$\emptyset$	diameter (m)

## Abbreviations

ADC	Analogue to Digital Conversion
AFR	Air Fuel Ratio
API	American Petroleum Institute
ASTM	American Society for Testing and Materials
ATDC	After Top Dead Centre
BDC	Bottom Dead Centre
Bhp	Brake horse power
BTDC	Before Top Dead Centre
BP	British Petroleum
CA	Crank Angle
cc	cubic capacity
CB	Carbon Black
CCD	Charge Coupled Device
cr	compression ratio
CR	Compression Ring
DAQ	Data Acquisition
deg	degrees
DECC	Department of Energy and Climate Change
DFT	Department for Transport
EOT	End of test

---

FTIR	Fourier Transform Infrared Spectroscopy
GM	General Motors
HTHS	High temperature high shear
ILSAC	International Lubricant Standardisation and Approval Committee
JSAE	Japanese Society of Automotive Engineers
LabVIEW	Laboratory Virtual Instrumentation Engineering Workbench
LIF	Laser Induced Fluorescence
LVDT	Liner Variable Differential Transformer
mA	milli Ampere
MB	Mercedes Benz
mg	milli gram
min	minute
µm	micrometre
MOFT	Minimum Oil Film Thickness
mW	milli Watt
NI	National Instruments
nm	nanometre
Nm	Newton metre
OCR	Oil Control Ring
OEM	Original Equipment Manufacture
OFT	Oil Film Thickness
pc	personal computer
PCV	Positive Crankcase Ventilation

---

pH	Potential of Hydrogen
PMT	Photomultiplier Tube
PTFE	Polytetraflouroethylene
PVC	Polyvinyl chloride
rpm	revolutions per minute
SAE	Society of Automotive Engineers
sec	seconds
SR	Scraper Ring
SwRI	Southwest Research Institute
TAN	Total Acid Number
TBN	Total Base Number
TDC	Top Dead Centre
TRZ	Top Ring Zone
TTL	Transistor – transistor logic
UK	United Kingdom
USA	United States of America
VI	Viscosity Index
VW	Volkswagen
XHVI	Extra High Viscosity Index

# Chapter 1 Opening

The proposition of this research thesis is that the lubricant film thickness experienced between a piston ring and the cylinder wall is the most sensitive parameter when considering the tribological response of the internal combustion engine as the lubricant degrades with service time. The lubricant within this region degrades more rapidly than anywhere else within the engine and the piston ring film thickness ultimately governs the outcome of lubricant flow, friction and wear in the piston assembly to the cylinder wall. There is a lack of knowledge when considering the correlation between engine performance and lubricant degradation through normal operating use. Even in the commercial automotive market, there are a wide range of lubricant service intervals and lubricant viscosity grades. This can clearly be seen by different service schedules presented by manufacturers for the same engine size and engine technology. In passenger vehicles, the lubricant service is determined by on-board duty cycle algorithms with many reflecting different service requirements and no measurement of lubricant properties. A more scientific correlation would greatly assist in optimising this process, increasing vehicle lifecycle efficiency, improving durability and reducing lubricant usage and waste.

In this opening chapter, the role, technology and operating conditions of piston rings are investigated, along with the tribological performance in terms of the lubrication characteristics.

## 1.1 Introduction

In the current environment, the reciprocating internal combustion engine is considered the primary means of propulsion, whether that be for ground or sea transport. It is widely recognised that without it our quality of life would suffer. According to recent Department for Transport statistics (DFT 2011), in the UK alone there were 35.7 million vehicles registered for road use in 2010. Of these 41.3% were fuelled by gasoline, 58.4% by diesel and 0.3% by liquid petroleum gas or were electric powered vehicles.

The internal combustion engine has improved as technology has advanced, allowing faster and more reliable engines. However, the internal combustion engine, whether it be diesel or

petrol powered, has many weaknesses. Overall engine efficiency is poor, being at most 25%, with much of this attributed to low thermal and mechanical efficiencies. Much of the available energy from fuel is lost as heat and friction. Coupled with this, internal combustion engines emit harmful exhaust emissions, such as oxides of nitrogen, hydrocarbons, particulate matter and the greenhouse gas carbon dioxide. As a means to overcome the drawbacks, improved vehicle technology has led to more efficient vehicles with better economy thanks to innovations such as the auto start stop function, brake energy regeneration, aerodynamics, weight reduction, tyre pressure monitoring systems and use of tyres with less rolling resistance. Better marketing and awareness has also improved driving habits by introducing information on increasing fuel economy from vehicles, through simple measures such as checking tyre pressures regularly and having a well maintained vehicle. Alternative prime movers to improve economy and reduce environment impact are now beginning to invade the motor market, but current examples of hybrid engine and electric fuel cell powered vehicles are expensive. It is therefore safe to assume that the internal combustion engine will still be used for many years to come.

With so many internal combustion engines in service emitting harmful pollutants and affecting the global climate, any slight improvement in efficiency in terms of reduced fuel consumption is much welcomed. Government legislation gets tighter yearly, demanding reductions in emissions, and as a result the combustion event of the engine is considered the first place to make improvements for increased efficiency. Generally the piston assembly of an internal combustion engine is widely recognised as having a significant effect on performance and economy, and any improvement in efficiency is a leap forward for society as a whole.

The battle to achieve lower vehicle emissions each year is seen across the continents of the world. Each major territory has their own emission regulations, but the focus towards emission reduction is the same. Figure 1-1 details the emission regulations internationally and also shows future trends. Such trends have triggered new technology such as hybrid, fuel cell and full electric vehicles to be presented in the market as a means of achieving emission targets, but currently at a premium cost. Engine downsizing on vehicle models, whereby a turbocharger unit is fitted to a smaller engine than its predecessor, is becoming more common. They emit less carbon dioxide (CO<sub>2</sub>), have a lower fuel consumption and the overall vehicle weight is lower since the engine is smaller whilst providing the same amount of power. It is therefore safe to assume that the reciprocating piston engine is not yet superseded. The European emission requirements were first established in 1992 with the Euro 1 standard, which detailed that gasoline engines required catalytic converters on

exhaust systems and single point fuel injection to replace carburettors. Since that first standard, a further four have been introduced with stricter emission regulations, with a sixth standard now scheduled for 2014. An overall emissions reduction of a massive 74% in gasoline vehicle emissions has been achieved since the introduction of Euro 1. Legislation introduced in 2012 levies fines on automotive manufacturers based upon the amount of CO<sub>2</sub> their vehicles emit above a target of 120 CO<sub>2</sub> g/km (Mortier, Fox et al. 2009). As a side note, the sulphur content in liquid fuels was also reduced heavily in 1999 in gasoline to 0.1% of mass and in diesel fuel to 1% of mass, as it was recognised that harmful emissions of sulphur dioxide contribute to atmospheric acidification, increasing acid rain, and also affect human respiratory health (Department for Environment 1999). Vehicle fuel economy is an additional factor that constantly needs improving as the price of a barrel of crude oil increases. As will be made apparent later in this chapter, the automotive industry would struggle without the engine, fuel, lubricant and additive manufacturers to achieve improved fuel economy and exhaust emission targets. As a result, lubricant standards, such as the recently introduced ILSAC GF-5, issued by The International Lubricant Standardization and Approval Committee in the USA, covers a number of critical factors including fuel economy, emissions control and engine cleanliness that a lubricant needs to meet (Canter 2010). Although GF-5 is an American standard, the European market, with standards set by ACEA (European Automobile Manufacturers Association), recognise and employ the new standard in current lubricant formulations (Lubrizol 2010).

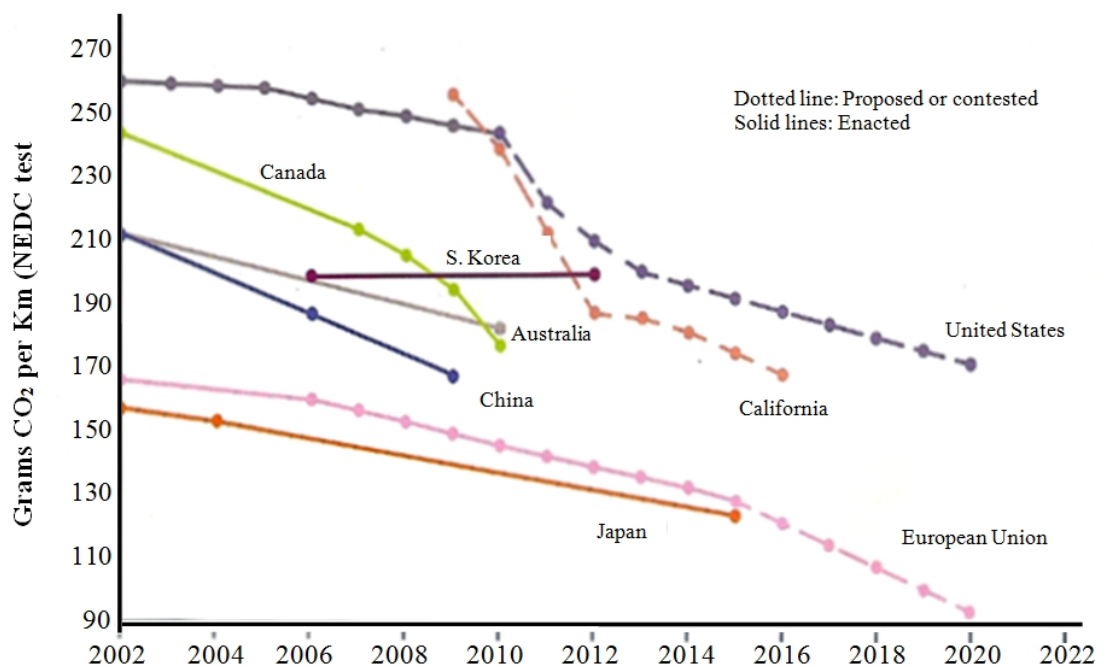


Figure 1-1: Current and future emission legislation from around the world (LNG 2010)

## 1.2 The role of the piston ring pack

In short, the internal combustion engine takes in fuel and air as a mixture and burns this in its combustion chamber. As a result of burning, the hot combustion gases expand rapidly over a piston stroke length and this energy is transformed into kinetic energy through the piston, connecting rod and crankshaft, providing rotational motion to drive the vehicle wheels.

To help illustrate the role of the piston ring pack, consider the schematic in Figure 1-2 which details a typical layout of a four stroke gasoline engine. On the first stroke, with the inlet valve open and exhaust valve closed, the piston moves from top dead centre (TDC), this being the highest piston height in the chamber, drawing in air and fuel mixture from the inlet manifold. The mixture is drawn in since there is a pressure gradient between the chamber and the inlet manifold. When the piston reaches bottom dead centre (BDC), this being the lowest piston height in the chamber, the inlet valve closes and the piston begins to start its second stroke where it compresses the charge mixture heading for TDC. Just before the piston reaches TDC the mixture is ignited by a spark delivered from the spark plug and the mixture burns. The flame front propagates as the mixture is burnt and a rapid increase in cylinder pressure and temperature results that forces the piston back towards BDC. This is where the fuel energy is converted into useful kinetic energy for propulsion through the crankshaft and ultimately the wheels. As the piston begins to complete its final stroke, heading back towards TDC, the exhaust valve opens to release the combustion gases. The inlet valve reopens just before the piston reaches TDC, in preparation to begin the first stroke of the next cycle.

In terms of the efficiency of the power stroke, it can be seen that any leakage of hot gases past the piston is detrimental to the available power output. It is therefore necessary to maintain a seal between the piston and the cylinder bore throughout the piston stroke. The piston ring maintains this seal by providing an interface in the gap between the piston and the bore. It can also be seen that any leakage, whether that be hot gases, in the form of 'blow-by' gases which simply blow past the piston ring, and unburnt fuel from the combustion into the crankcase would eventually escape into the atmosphere through the crankcase breather, a vent, and contribute to environment pollutants. In modern engines, this emission contributor has been reduced through use of a positive crankcase ventilation (PCV) system. A PCV system utilises a one way valve between the crankcase breather and the inlet manifold of the engine. The blow-by gases and unburnt fuel that escape past the piston rings into the crankcase are drawn into the combustion chamber during the intake stroke, when the inlet manifold is experiencing a lower pressure, and burnt in the combustion event.

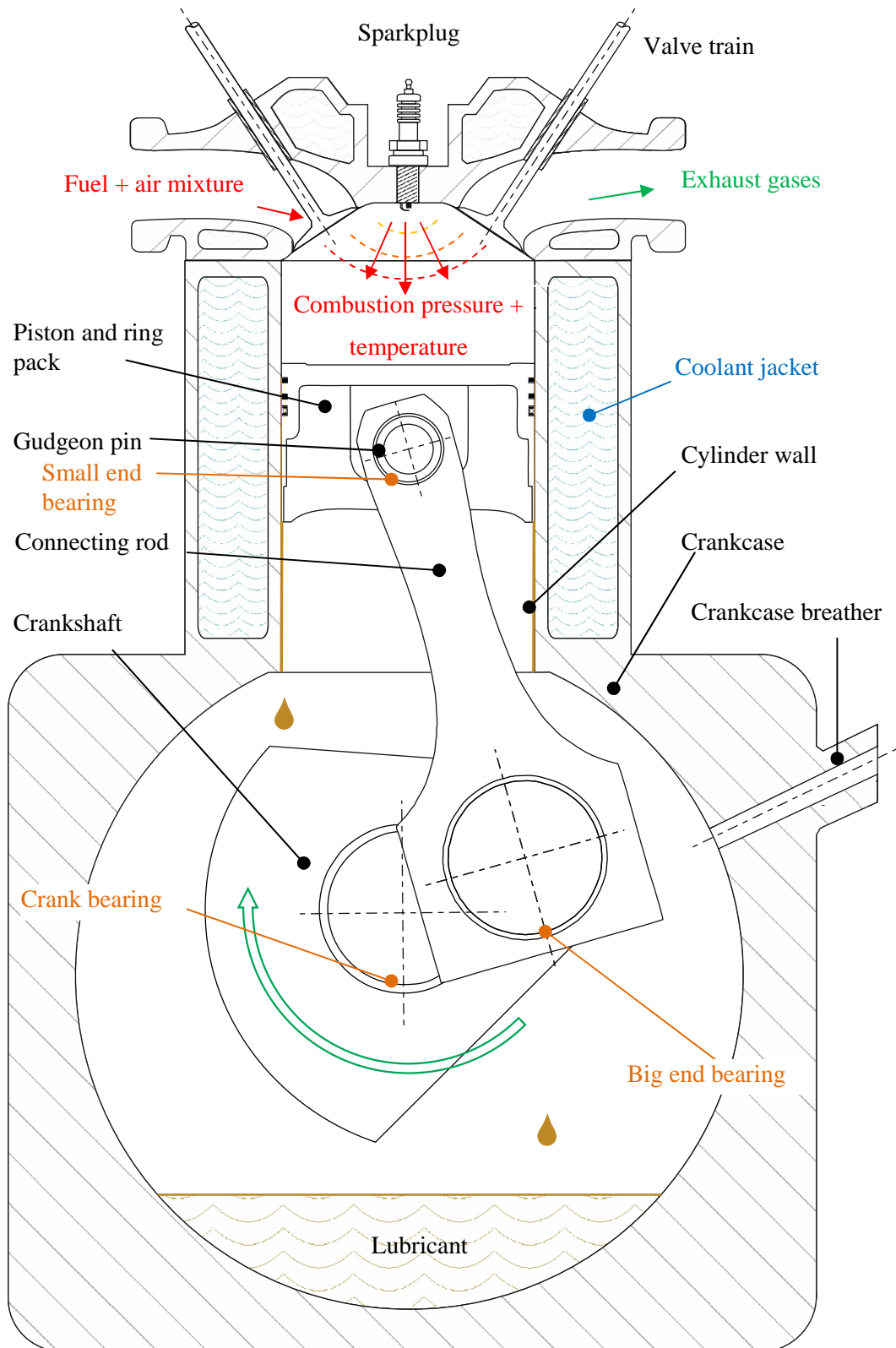


Figure 1-2: Cross section of a typical gasoline 4 stroke internal combustion engine

Two additional contributors to pollutant emissions, especially hydrocarbon emissions, include the lubricant left on the cylinder wall which is exposed to the combustion chamber and also where the lubricant flows from the crankcase into the combustion chamber, a phenomenon known as 'reverse blow-by.' The latter occurs when gas pressure builds up between the piston rings, known as inter-ring gas pressure, which is greater than the pressure above the top piston ring and pushes lubricant upwards towards the combustion chamber. Consequently, any lubricant mist in the crankcase would be 'caught' in the reverse blow-by and exit the exhaust pipe into the atmosphere.

A secondary function of the piston ring is to provide a means of heat conduction. The combustion event can increase chamber temperatures up to 600°C and any heat generated needs to be dissipated to prevent overheating of the cylinder bore, which could cause premature lubricant degradation and evaporation, possibly leading to engine seizure. The piston ring transfers heat from the piston to the cylinder wall and the water jacket, on the opposite side of the cylinder wall.

A final role of the piston ring is to control the amount of oil that can possibly flow into the combustion chamber in an attempt to minimize hydrocarbon exhaust emissions.

One must also consider the design of the piston and the ring, and their completeness in combustion sealing. On modern engines the top of the piston, above the top ring, is slightly tapered so the crown diameter, which is the topmost part of the piston, is smaller than the piston skirt, the bottommost part of the piston. The difference in diameter, known as the piston crevice, is to allow the top of the piston to expand as a result of the very high temperatures experienced in the chamber due to combustion. As a flame front progresses at the beginning of the power stroke, any charge mixture which has been trapped in the crevice will remain un-burnt since the flame cannot progress into the small volume. As a result, on the exhaust stroke the un-burnt charge will be exhausted and further contribute to hydrocarbon emissions.

Wentworth, (Wentworth 1971), first discovered that the design of the piston has a great influence on hydrocarbon emissions with a revised design of a narrower piston crevice volume. Further improvements in piston design are particularly rare but changes in piston ring design have been popular in attempts to meet stringent emission legislation.

### 1.3 Piston ring design

John Ramsbottom, (Ramsbottom 1854), first proposed a ring as a means of providing a compression seal for locomotive steam engines and the same concept of using a piston ring is still used in modern engines today. The proposed design was an open ended ring, which was ten percent greater in diameter than the cylinder bore, and located in a groove in the piston circumference. Once compressed and installed, the elasticity of the ring provided an effective seal against gas compression, limiting any leakage of steam past the piston and therefore improving efficiency. A single ring does not provide a complete compression seal, due to the ring being open ended, and as a result it is more common to see a collection of two or three compression rings generally known as a 'ring pack.'

Since the introduction of the piston ring in 1854 by Ramsbottom, there have only been a few changes to the initial idea. A year after its introduction, Ramsbottom (Ramsbottom 1855) himself declared that during initial tests it was found that the proposed ring caused uneven circumferential wear from uneven loading due to the elasticity of the ring itself. It was found that the ring must not follow a free circular shape but have a slightly larger radius at the ring gap as manufactured to ensure even pressure loading on the cylinder bore when fitted and hence even wear. One further improvement to the ring design was that of Miller, (Miller 1862), who investigated the use of high steam pressure from the compression to act on the inside face of the ring and push the ring out to the bore, and provide additional sealing force without the use of springs. Miller's idea of using the compression pressure is still fundamental to many ring designs in use today for modern automotive engines.

No further major designs changes have been made to date to the basic ring concept evolved by Ramsbottom (Ramsbottom 1855) and Miller (Miller 1862). Smaller modifications such as multi-piece ring designs and rings with edge profiles designed to reduce lubricant consumption through better lubricant scraping capabilities and better compression sealing and having shorter running-in periods are now common, reducing engine friction and lubricant consumption.

A typical piston ring pack of a gasoline engine is shown in Figure 1-3. Generally in gasoline engines there are three rings; a compression ring, scraper and an oil control ring. The top compression ring is the primary seal from combustion pressure. It usually has a barrel shaped profile since being closest to the combustion it experiences high temperatures and pressure loading. Often the barrel ring would have an internal bevel or step (see Figure 1-4 7a), which is useful in encouraging positive twisting, that being the inner edge of the ring making contact with the piston groove to limit the lubricant flow upwards into the combustion

chamber (Federal-Mogul 2008). The scraper ring is also a secondary compression ring, but its primary function is to limit the amount of lubricant flowing upwards towards the top compression ring and into the combustion chamber. It generally has a step removed from the lower running edge, known as a Napier type ring, to improve the scraping action. The third

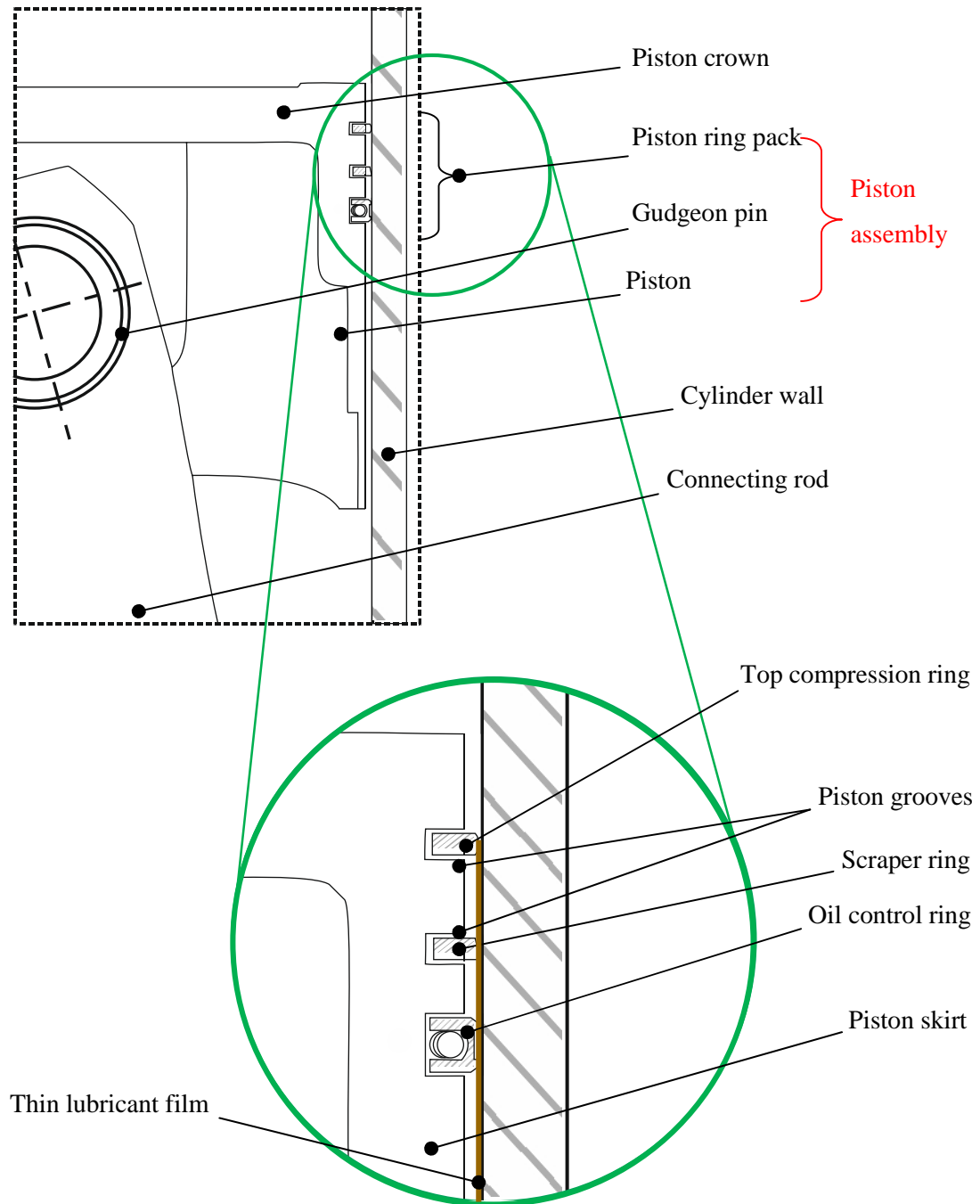


Figure 1-3: A typical piston ring pack arrangement for a gasoline engine

ring is the oil control ring and as the name suggests, it limits the amount of lubricant on the cylinder bore in an attempt to minimise lubricant consumption. It is generally a multi-piece ring with a steel coil between either one or two-piece rails. The coil allows the complete ring to conform to bore distortions, (Federal-Mogul 2008), but also allows any lubricant to flow through it towards the piston groove where holes drilled radially through the piston transport excess lubricant back towards the crankcase.

Figure 1-4, taken from (Neale 1994), details typical piston rings as found in many modern engines.

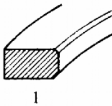
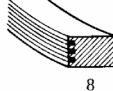
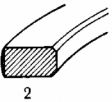
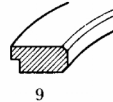
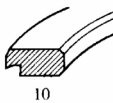
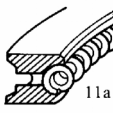
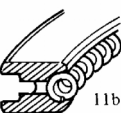
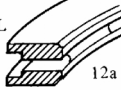
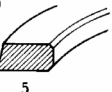
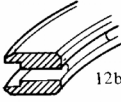
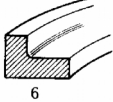
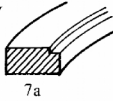
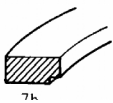
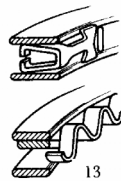
COMPRESSION RINGS		OIL CONTROL RINGS		
Ring type	Description	Ring type	Description	
STRAIGHT-FACED RECTANGULAR	The most simple ring can be chromium-plated on peripheral face to give longer life	GROOVED INLAID	Materials such as chrome, bronze and ferrox are inlaid in multi-groove configurations, providing good scuff resistance	
 1		 8		
BARREL-FACED CHROMIUM-PLATED	Widely used as top compression ring in diesel and petrol engines. Gives quick bed-in, good scuff resistance and long life. Has neutral oil control characteristic	EXTERNALLY-STEPPED COMPRESSION AND SCRAPER	Combines gas sealing and oil control functions, the step giving the ring a torsional twist when fitted	
 2		 9		
RECTANGULAR INLAID	Various low-wear-rate scuff-resistant materials, such as electroplated chrome, sprayed chrome, molybdenum, etc. are set into ring periphery. Outer lands give edge protection to deposited material	NAPIER	Variation of externally stepped ring; hooked relief gives sharp scraping edge with good oil control	
SEMI-INLAID		 10		
 3a		COIL SPRING LOADED SLOTTED OIL CONTROL	Very popular ring particularly in high-speed diesels. Main wall pressure is derived from butting helical coil expander. Chromium-plated for wall pressures above 700 kN/m <sup>2</sup>	
 3b		 11a		
KEYSTONE	A common top ring in diesel engines prevents sticking due to carbon formation fitted in groove with similar taper	BEVELLED EDGE TYPE	 11b	
HALF KEYSTONE		 4a		
 4b		SLOTTED OIL CONTROL	A common form of bulk oil scraper with two scraping lands separated by drainage slots or holes	
TAPER FACED	Normally between $\frac{1}{2}^\circ$ to $1\frac{1}{2}^\circ$ , gives quick bed-in and combines gas sealing and oil control features. A witness land at periphery is often added	 12a		
 5		BEVELLED EDGE TYPE	 12b	
DYKES PRESSURE BACKED	Mainly used in high-speed racing applications to prevent blow-by due to 'flutter' under high inertia loading. Fitted in a groove of similar shape	STEEL RAIL MULTIPIECE		(a) Combined spacer expander
 6		(b) Separate spacer expander	These rings allow very high scraping pressures to be applied with good conformability, and have chromium-plated rails	
INTERNALLY STEPPED POSITIVE TWIST TYPE	Step or bevel relief on inner edge causes ring to dish when fitted, giving bottom edge contact and good oil control	 7a		
NEGATIVE TWIST TYPE		 7b		
		 13		

Figure 1-4: Summary of modern automotive piston ring designs (Neale 1994)

Piston ring materials for modern engines tend to be either spring steel or grey cast iron. The running faces tend to have various coatings to improve wear, scuffing and corrosion resistance such as chromium plating, PVD (Physical Vapour Deposition) and nitriding. Other surface treatments such as phosphating, improve the running-in of the ring and black oxidizing provides corrosion resistance (Federal-Mogul 2008). Diamond-Like-Carbon (DLC) coatings for engine mechanical components are now becoming increasingly common. The coating has been found to provide low frictional characteristics for piston rings (Araujo and Banfield 2012; Hanke, Fahr et al. 2012), and have now been tested in commercial vehicles with improvements of approximately 5% in highway fuel economy (Read, Vazquez et al. 2012).

#### 1.4 An introduction to engine lubrication

This project was concerned with engine lubrication, in particular the thin lubricant films between the piston and the cylinder wall. It is therefore appropriate to highlight the different regimes of lubrication experienced by the piston assembly.

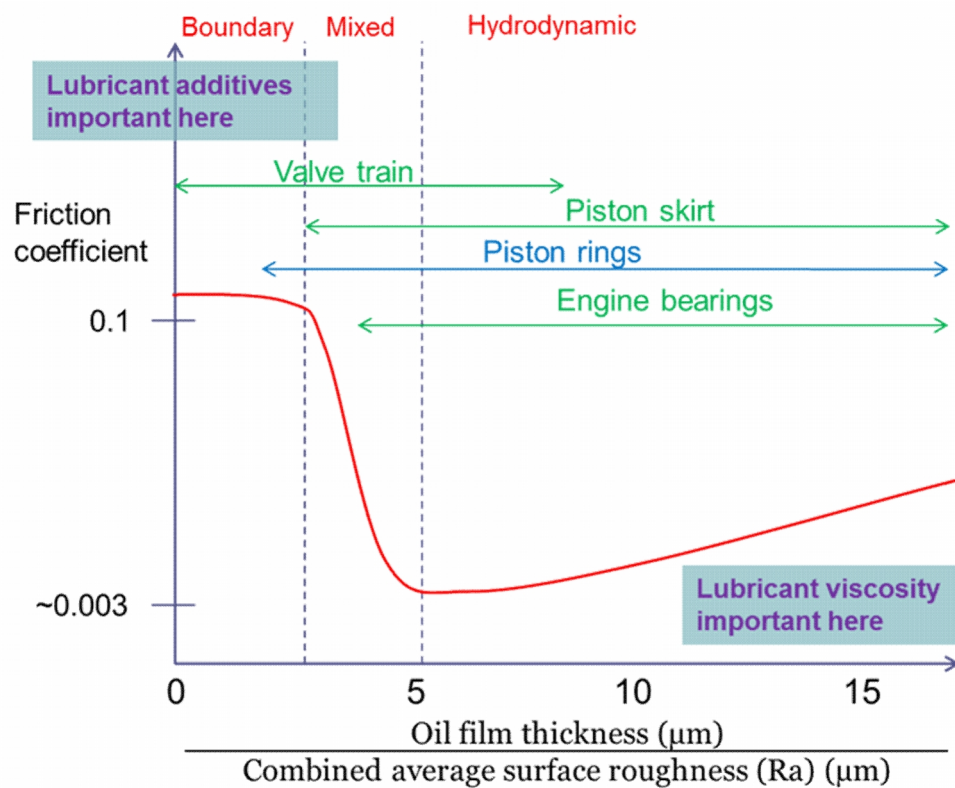


Figure 1-5: A modified Stribeck diagram detailing lubricant property influence.

Adapted from Priest and Taylor (2000) (Priest and Taylor 2000)

It is possible to investigate different lubrication regimes that can take place between a contact and how the overall performance is influenced by friction by means of a Stribeck diagram. A Stribeck diagram for automotive engines is shown in Figure 1-5 from Priest (2000). The diagram has been adapted to demonstrate where the lubricant additives and viscosity become important for different regimes.

There are four lubrication regimes; boundary, mixed, elastohydrodynamic and hydrodynamic. Boundary lubrication is where the surface asperities come into contact at an interface. There is usually a lubricant film ( $< 0.01\mu\text{m}$ ) between the interfaces but because it is smaller than the asperity height on the surfaces, contact takes place. As a result the asperities interact and slide over each other causing high boundary friction. Hydrodynamic lubrication is where the lubricant film is sufficiently thick ( $>1\mu\text{m}$ ) to prevent any surface contact. Any friction generated from the contact is purely caused by the viscous shearing of the lubricant film. Mixed lubrication regime is where boundary and hydrodynamic regimes both occur in the interface. In the mixed regime, the friction generated when the two surfaces slide is a result of combined asperity contact and the viscous shearing of the lubricant film, between  $0.05\mu\text{m}$  and  $1\mu\text{m}$ . Finally, elastohydrodynamic lubrication is caused by sufficiently high loads deforming the surface and the surface asperities, increasing the loading capacity of the surface. A small lubricant film, between  $0.1\mu\text{m}$  and  $1\mu\text{m}$ , exists to separate the interface which undergoes a rapid increase in viscosity with the ability to support the load, so no contact occurs. Interfaces experiencing elastohydrodynamic lubrication have very low friction coefficients due to thinner films and elastic deformation of the surfaces and the asperities. More information on the basics of tribology can be found in (Williams 2005).

In a modern engine the piston assembly, especially the piston rings, can experience all modes of lubrication during operation as a simple consequence of the reciprocating motion. The piston rings would normally operate in hydrodynamic lubrication at piston mid stroke since the piston speed is at its maximum. The lubricant film is thickest here and can vary between  $10\mu\text{m}$  and  $20\mu\text{m}$  depending on absolute speed and load (Brown and Hamilton 1977). Frictional power loss is also observed at piston mid-stroke, since the piston speed is at its maximum. Upon approaching the extreme ends of the stroke, TDC and BDC, the piston speed reduces and momentarily halts at its highest and lowest positions respectively. Here large amounts of boundary and mixed frictional force, much greater than when the piston is at midstroke, have been observed (Kovach, Tsakiris et al. 1982; Mufti 2004; Mufti and Priest 2005; Mufti, Priest et al. 2006) due to the piston becoming stationary and reversing direction but also because the lubricant films are thin. However, the friction observed at the dead centres is only momentarily during the reversal process. The thinnest lubricant films, in the

order of  $0.1\mu\text{m}$ , have been predicted to occur just after top dead centre where hydrodynamic lubricant is unlikely and elastohydrodynamic lubrication is more likely (Dowson, Ruddy et al. 1983). Hence, it is not strange to see that piston rings can experience all lubrication regimes as shown in Figure 1-5 and by other researchers (Lloyd 1969; Dowson, Ruddy et al. 1983; Hoshi 1984; Tian 2002).

Holmberg et al. (Holmberg, Andersson et al. 2011) examined the energy consumption within passenger vehicles and from a collection of analyses from various authors, determined that the average engine friction losses are as follows; 45% consumed in the piston assembly, 30% in engine bearings, 15% valve train friction and the final 10% consumed by pumping losses. A more specific case by Tung and McMillan (Tung and McMillan 2004) estimated that 7.4% of the potential fuel energy losses is lost as engine friction, 25% of which originates from the piston rings, as shown in Figure 1-6 below. Clearly the lubricant has a major impact on engine performance and efficiency.

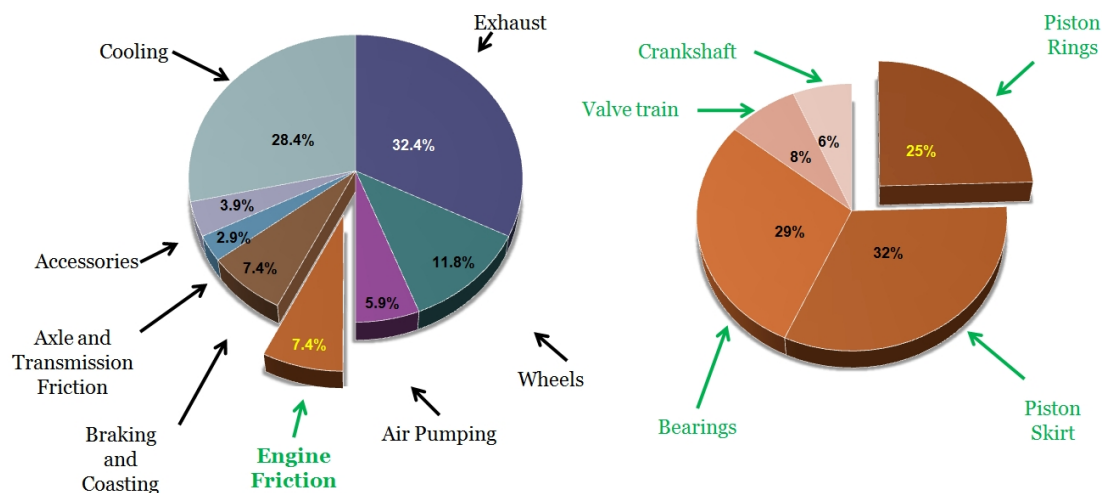


**Figure 1-6: Fuel energy losses with large contribution from piston rings. After Tung and McMillan (2004)**

The engine lubricant has been enhanced over the years to meet the operating conditions and performance characteristics of modern engines. As engines have become more powerful and better manufacturing techniques have been employed, it is down to the lubricant to still perform at its best when faced with ever tougher situations.

Previously, the lubricant itself was comprised of mineral oil refined from crude oil, which provides the majority of hydrocarbons it contains. However, as engine technology has

evolved, lubricant base stocks have also changed to include semi-synthetic and fully synthetic formulations which have greater thermal stability. These base fluids, despite providing some reduced friction and wear of parts, are poor at the extreme conditions experienced in modern engines. They decrease in viscosity as the temperature increases. As a result the base stock contains 15-20% additives (Mortier, Fox et al. 2009) for performance improvement and to increase lubricant service drain intervals. Apart from friction and wear reduction, a lubricant must also act as a cooling agent by removing heat from the metallic parts (Mortier, Fox et al. 2009). As can be seen from Figure 1-5, lubricant surface active additives are important when contact occurs between interfaces and the lubricant viscosity, when a sufficiently thick film exists between the interfaces.

The lubricant temperature and the proximity of the interfaces are the key factors in how the lubricant copes with both viscosity change and performance. The increase in lubricant temperature dictates the oxidation stability and the lubricant viscosity. Viscosity index improver additives are used to recover the loss of viscosity with temperature (Mortier, Fox et al. 2009). Any reduction in viscosity and the friction and wear of components becomes more apparent. Friction modifier additives such as MoDTC (molybdenum dithiocarbamate) have a strong molecular hexagonal type structure where a single molybdenum molecule is enclosed by six sulphur atoms. The bonds between the sulphur and the molybdenum are strong covalent bonds whereas between the sulphur, the bonds are dictated by the Van der Waal forces. Hence a low energy is required to slide the bonds between the sulphur atoms. ZDDP (Zinc-dialkyl-dithiophosphate) is multifunctional with uses as an anti-oxidant, anti-wear and extreme pressure additive with thick films forming on surfaces in the order of 50-150nm thick (Mortier, Fox et al. 2009).

Deposits, from combustion activity, are held in suspension by the use of lubricant dispersant additives, and detergent additives keep lubricated components clean. Other additives such as antifoam, antiwear, antioxidant, demulsifiers and corrosion inhibitors are usually present in a fully formulated lubricant. More information on these additives can be found in Chapter Two and various literature specific to automotive lubricants, for example (Bell 1993; Mortier, Fox et al. 2009).

## **1.5 Scope of this project**

This project aims were to investigate the changes in the tribological performance of the piston ring pack with the influence of lubricant degradation through measurements of lubricant film thickness.

The objectives of this study are as follows:

- Develop a method of oil film thickness measurement for the piston ring – cylinder bore interface through the cylinder wall of a horizontally opposed motored engine
- Investigate the influence of lubricant degradation on lubricant film thickness within the piston ring – cylinder bore vicinity using lubricant samples of known degradation in the motored engine
- Adapt the same lubricant film thickness measurement system, as used on the horizontally opposed motored engine, to a Ricardo Hydra fired gasoline engine to investigate oil film profiles at higher engine speeds and loads
- Further this method to investigate residence time with the use of a switchable twin lubricant sump on the Ricardo Hydra engine
- Investigate the implications of sampling lubricant from the top ring groove of a piston, during engine operation, on the piston ring pack lubricant film thicknesses

## **1.6 Structure of the thesis**

### Chapter 1 - Opening

The difficulties the automotive industry is facing with increasing pressures from government legislation, environment and economic concerns, and customer demands and expectations is discussed in this introductory chapter. A brief summary on how the emission regulations have got increasingly tighter over the past twenty years is explained. An introduction to gasoline internal combustion engines and piston ring design has been discussed with the importance of piston ring lubrication being highlighted. This chapter also describes the nature of this research thesis.

### Chapter 2 – Literature Review

Chapter 2 is a literature review on previous work on Engine Tribology with a prime focus on piston ring lubrication. A review of theoretical and experimental research is covered. An investigation into the three main types of piston ring lubricant film thickness techniques; capacitance, laser induced fluorescence and ultrasound, was made with a direct comparison between all three techniques.

---

### Chapter 3 – Development of a Laser Induced Fluorescence Technique on a Motored Engine

In this chapter, the development of a motored engine test and previous work on this engine is discussed. The motored engine was modified to improve the crankcase breather, oil and coolant supply. This allowed the laser induced fluorescence (LIF) system to be developed into an operational technique. A new cylinder liner was machined to have a greater wall thickness, which provided a greater support for the LIF probe. The design considerations to implement the same LIF system on the fired engine are made in Chapter 5. A brief introduction into fluorescence theory is made along with the design considerations for the new optical system is also discussed. Laser fluorescence calibration methods have also been discussed.

### Chapter 4 – Implementation and Results of Testing on the Motored Engine

Lubricant samples were acquired from customer vehicles at Mercedes Benz Leasing, Leeds, UK during oil service intervals and these were used as the test degraded samples. A fresh lubricant of the same kind was also acquired and used as a reference to monitor the influence of lubricant degradation on piston ring lubricant film thickness during motored conditions on the simulated engine. The test strategy included the influence of engine speed, compression peak pressure and engine temperature on the minimum lubricant film thickness experienced by the piston ring pack. Results are also presented and discussed.

### Chapter 5– Development and Testing of a LIF system on a Ricardo Hydra Fired Test Engine

The design and manufacture of the LIF system on the fired engine is described. A spare unfinished Hydra barrel was machined to accept the LIF probe and completed to work on the engine. An additional cylinder liner was machined to have a larger wall thickness similar to the design used for the motored engine. The same test lubricants as used in Chapter 4 were used on the fired engine with a test strategy which involved varying engine speed and torque. Results are presented and discussed.

### Chapter 6 – Piston Ring Pack Lubricant Residence Times and the Influence of Top Ring Zone Sampling on Piston Ring Lubricant Film Thickness

The flow of lubricant within the engine, based on engine speed and torque, is investigated by examining the residence time of the lubricant within the piston ring pack. A switchable twin sump system supplying lubricant to the crankcase bearings and piston assembly was used to examine the residence time. One sump contained fresh lubricant and the other sump contained the same lubricant but had been mixed with fluorescent dye. Both sumps were

---

maintained at the same temperature and by using the LIF system as a tracer technique, it was possible to examine the lubricant residence times. An investigation into the effects of sampling lubricant from the top ring zone of the piston on the piston ring lubrication was also made.

#### Chapter 7 – Data Acquisition System

All the instrumentation and the data acquisition system employed to simultaneously measure piston ring pack lubricant film thickness along with crank angle position, cylinder liner temperatures and pressures to perform this research is explained in great detail.

#### Chapter 8 – Conclusions and Recommendations for Future Research

Finally, the conclusions arising from this research work are presented in Chapter eight along with suggestions for further development techniques and future ideas to combine in-situ infrared spectroscopy measurement of the piston ring lubricant condition and film thickness.

All the Appendices are given at the end of this thesis.

## **Chapter 2 Literature Review**

There has been much development in piston assembly lubrication for internal combustion engines in terms of reduced power loss, through minimising frictional characteristics, and improvements in engine lubricants and drain intervals, which have improved engine fuel economy and reduced exhaust emissions.

Tribological engine research has been both theoretical and experimentally based. Theoretical based modelling does not usually require much expense, but much computing and predictions can be made. However, boundary conditions applied to any models are important. Experimental research, depending on how intrusive and complex a system, can be expensive but more rewarding if the system is adaptable to consider additional test variables that may have initially been considered as constants.

This chapter outlines the process of lubricant degradation and detection along with theoretical and experimental piston ring research, with a main focus on lubricant transport and consumption where the influence of lubricant film thickness, within the piston ring – cylinder wall interface, is drawn.

### **2.1 Engine lubricant degradation**

For an engine to remain in a clean and problem-free condition it is necessary to change the oil regularly since it degrades and reduces in performance. With the price of oil continually increasing (BP 2012), lubricant engineers are trying to increase the oil drain intervals of vehicles and this is one of the reasons why it is necessary to understand how the engine lubricant degrades.

Lubricant degradation can be considered a phase where the remaining useful life of the lubricant starts to reduce. Lubricant degradation is caused by a combination of high operating temperatures and pressures, contamination with unburnt fuel and water from the combustion process, and combustion gases, such as oxides of nitrogen, that promote lubricant acidity (Korcek and Jensen 1976; Korcek and Johnson 1993; Winborn and Shayler 2001). Through degradation, additive depletion, that being a reduction in additive performance, results (Kumar, Mishra et al. 2005) and the lubricant presents reduced

performance characteristics. Eventually the lubricant degrades to a point where any further use of the lubricant would be detrimental to engine performance. The lubricant viscosity has been found to increase as a consequence of degradation (Spearot 1974; Yasutomi, Maeda et al. 1981b; Fox 1997), and this is detrimental to frictional power loss and engine efficiency (Taylor 1997).

The lubricant can degrade through many means such as:

- Thermal degradation and evaporation
- Mechanical molecular degradation
- Dilution
- Oxidation and nitration
- Additive depletion

### **2.1.1 Thermal degradation and evaporation**

High temperatures, in excess of 120°C, are observed in the engine itself with temperatures of ~200°C being experienced in the piston assembly. A consequence of high temperature is reduced lubricant viscosity. The atoms between the long hydrocarbon chains are excited and vibrate, due to the increase in thermal energy, causing the molecular bonds to break. Consequently the lubricant viscosity decreases. If the lubricant is allowed to cool, the viscosity is recoverable. However, too high a temperature can cause permanent viscosity damage. In an internal combustion engine, high temperatures cause the lubricant viscosity to reduce and therefore, it is necessary to use viscosity index improver additives to slow down the rate of decrease of viscosity with increasing temperature. Viscosity index improvers are generally polymers and mainly consist of polymethylmethacrylates (PMAs) and olefin copolymers (OCPs) (Mortier, Fox et al. 2009). Another consequence of high temperature is lubricant evaporation, which is considered to be a major contributor to the total lubricant consumed in an engine (Yilmaz, Tian et al. 2004) and the greater the lubricant film temperature, the greater the rate of evaporation (Bailey and Ariga 1990). The volatility of a lubricant, defined as an indication of the propensity of lubricant loss by vaporisation (Mortier, Fox et al. 2009), plays an important part in the rate of evaporation; the more volatile a lubricant the greater the tendency and rate of evaporation (Mortier and Orszulik 1992; Yilmaz, Tian et al. 2004).

### 2.1.2 Mechanical molecular degradation

In the piston assembly, high speed reciprocating parts shear the polymer additives in the lubricant. At high shear rates the polymers, which have a long chain molecular structure, stretch and distort, causing the lubricant viscosity to reduce. If the shearing is not excessive the molecular structure can ‘spring’ back to its original shape. This is known as temporary shearing and is a reversible effect. The molecular structure can only take so much shearing and excessive shearing causes this structure to break and collapse, resulting in reduced viscosity. This is permanent shear damage, which is irreversible and only occurs at very high shear rates, greater than  $10^5 \text{ sec}^{-1}$  (Mortier and Orszulik 1992). A reduced viscosity will ultimately reduce the oil film thickness that is present between an interface. Figure 2-1 shows the effect of increasing shear rate on viscosity of a lubricant, as drawn by Mortier (Mortier and Orszulik 1992).

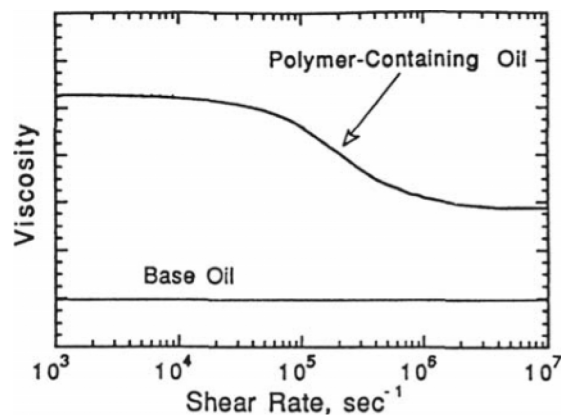


Figure 2-1: Effect of shear rate on viscosity of lubricant (Mortier and Orszulik 1992)

### 2.1.3 Dilution

Fuel is used in the combustion process and one by-product of combustion is water. In a sealed combustion system, fuel can absorb into the lubricant in the sump and the water can form an emulsion with the lubricant both causing lubricant contamination. Water can also be absorbed into the lubricant on cold start conditions from condensation build up on the crankcase walls. Other fluids present in the engine such as the antifreeze, glycol, do not contaminate the lubricant unless there is a physical leak in the cylinder head gasket.

The use of renewable energy is seen as the solution to the world energy crisis. Newer fuels now have a small content of biofuel, derived from ethanol for gasoline fuels and biomass for

diesel fuels, which are sustainable without exhausting natural resources. Currently in the UK, ethanol content accounts for 4% in gasoline fuel, and an increase by 0.5% annually until 2014 has already been confirmed (DECC 2011). Ethanol however, does attract water and therefore any unburnt fuel which rests in the lubricant sump will ultimately increase water dilution levels (Boons, Van Den Bulk et al. 2008).

Winborn modelled fuel transport, and found that blow-by pressure causes unburnt fuel to be transported past the piston into the crankcase. Eventually this dilutes the bulk oil in the sump (Winborn and Shayler 2001). Short trip, cold start engine operation can cause fuel and water concentrations to exceed 5% (Tung and McMillan 2004), which is enough to cause engine corrosion problems. This is usually referred to as ‘Aunt Minnie’ driving conditions, where mileage accumulation is low from short start stop journeys and cold starts are regular enough not to allow the lubricant to fully warm up. In these conditions the majority of the fuel is absorbed into the oil films from the blow-by and is carried into the crankcase. Clearly with ethanol based fuels, this problem escalates as the ethanol is highly hydroscopic. As the lubricant temperature increases, the rate of fuel absorption decreases and some of the unburnt fuel then flows through the crankcase vent via the blow-by pressure. This process, absorption and desorption, eventually reaches some equilibrium state once the lubricant fully warms up (Winborn and Shayler 2001).

#### **2.1.4 Oxidation and nitration**

The principle of the oxidation process is described below, (Korcek and Jensen 1976; Mortier and Orszulik 1992).

The lubricant undergoes oxidation as soon as it is exposed to the atmosphere. So in an engine, where oxygen is presented to the lubricant in a more pressurised state and at higher temperatures, one can imagine the rate of lubricant degradation to be higher. This is usually considered an autoxidation process if the oxidation stage is self-propagating. Generally this occurs in the low temperature region, <120°C, which sub-divides further into four distinct stages:

- Initiation – slow construction of free radicals
- Propagation – these free radicals react rapidly with oxygen to form alkyl radicals and slowly forming hydroperoxides

- Chain branching - hydroperoxides are cleaved only at higher temperatures ( $>100^{\circ}\text{C}$ ) or with catalysts leading to an 'autocatalytic' phase. The time taken from the start of oxidation to the autocatalytic process is known widely as the 'induction period.'
- Termination – hydrogen becomes completely used and any further chain branching is terminated. The degradation process ceases.

At higher temperatures ( $>120^{\circ}\text{C}$ ) oxidation is a two phase process. The first stage is similar to that of the low temperature oxidation process but the reaction rate is greater. Here the cleavage of hydroperoxides is the most vital part, leading to hydroxyl radicals. The acidity of the lubricant increases and the introduction of carbonyl products, such as ketones, begins. In the second stage, the viscosity of the bulk base lubricant increases due to the production of polymerisation and polycondensation reactions. Eventually these reactions create products, known as 'sludge,' which are insoluble in the bulk lubricant. This sludge generally settles in the sump, but in the piston assembly where there are thin oil films, these products deposit on the piston with a varnish like appearance. Apart from physical appearance and feel, the lubricant increases in molecular weight due to the creation of these degradation products (Mortier and Orszulik 1992).

Nitrogen forms the majority of air and hence is involved in the combustion process. However, the majority of nitrogen is not reacted with any by-products of the combustion, but due to high temperatures, it reacts with the lubricant when in contact with the blow-by gases, causing the lubricant to degrade, reducing its useful life (Korcek and Johnson 1993). This process is known as nitration.

### **2.1.5 Additive depletion**

The additive concentration in a lubricant formulation tends to decrease with use (Kumar, Mishra et al. 2005). It has been shown (Lee, Stark et al. 2004; Lee, Priest et al. 2006) that fully formulated lubricant actually undergoes a 'degradation free' service period, which is the time taken for the additives, generally those with antioxidant characteristics, to be consumed, thereby delaying any initial degradation. They are depleted through general use within specifications, destroyed through extreme use outside specifications, or consumed via the exhaust process of the engine cycle.

As mentioned previously the viscosity changes with degradation. A lubricant has viscosity improver additives added to suppress the rate of viscosity decrease with temperature increase (Mortier and Orszulik 1992), and if these begin to deplete the viscosity will reduce. It is the

high temperatures and shearing effects which cause the bonds to break, reducing the additive effectiveness (Mortier and Orszulik 1992; Taylor 2002).

When an anti-wear or corrosion inhibitor additive is active in the lubricant system, it forms a film on the surface, usually by chemisorption. This film can be removed by excessive abrasive wear from loose wear particles in the engine. Providing there is still additive reserve remaining in the lubricant, another film will be formed over the wear (Mortier and Orszulik 1992).

Some additives such as dispersants, which surround contaminant products, will only be effective once and are not reusable. That means that these additives can only cope with so much contamination (Mortier and Orszulik 1992).

Apart from additive depletion, the physical appearance of degraded oil is darker than the equivalent fresh sample. Hammond (Hammond 2003) from the University of York in the UK, investigated the autoxidation of ketones, which are part of the chemical Carbonyl group present when a lubricant degrades, as a means to investigate what happens to a lubricant as it degrades. He used UV radiation and oxygen alone to investigate lubricant colour change with degradation. He found through controlled oxidative tests of Nanon-5-one, which is a hydrocarbon found in automotive lubricant formulations and in its purest form is colourless, turned a pale yellow colour, caused by the formation of oxidation products. Although it cannot account for the complete colour change, it does provide some indication that oxidation of the lubricant is the source of a colour change.

### **2.1.6 Methods of bulk engine lubricant degradation detection**

One of the major signs of preliminary degradation is that the lubricant acidity increases (Hsu, Ku et al. 1986). The most common method of detection is that of the ASTM D-664 standard which measures the total acid number (TAN) (ASTM D-664-09). The number determines the acidity of the lubricant sampled. It is believed that the acidity of the lubricant increases due to the exposure to nitric acids, which are present in blow-by gases (Korcek and Johnson 1993; Stark, Wilkinson et al. 2004). TAN is the opposite to Total Base Number (TBN) (ASTM D-2896) which is a standard measure of the alkalinity of the base (ASTM D2896-07a) and as expected, decreases with increased TAN. Both must be referenced to the values of a fresh sample of the lubricant to determine the degradation level.

One of the first chemical signs of degradation is the formation of nitrate and carbonyl compounds when oxidation begins. Carbonyl compounds consist of carboxylic acids, and ketones (Mortier and Orszulik 1992; Powell and Compton 1993; Toms 1998).

Another simple method of acid detection, apart from using extensive TAN and TBN methods, is to use the pH scale (Kumar, Mishra et al. 2005; Endo, Watanabe et al. 2009). Although this provides a quick insight into lubricant degradation in terms of lubricant acidity, it does not however indicate by how much the lubricant has degraded or what species have caused the degradation. A lubricant may initially degrade, but this does not rule out its service life. It is only when the lubricant begins to change its composition and present poorer performance behaviour that concern for engine protection should be raised. This, however, may take a long time.

Another factor to consider is that any strange substance, for example coolant contamination occurring from leakage at the cylinder head gasket, would be difficult to detect by traditional TAN and pH methods, where the former has been considered in the past a vital measure of oil quality (Hsu, Ku et al. 1986). Here coolant, being of alkaline nature, would suppress any acid formed in a degraded lubricant sample, leaving the user convinced the lubricant is still fairly fresh. Over the years, the majority of researchers interested in lubricant degradation (Coates and Setti 1986; Powell and Compton 1993; Natrass, Thompson et al. 1994; Dong, Van De Voort et al. 2000; Dahmani and Gupta 2002) have used infrared spectroscopy as a method of detection.

Infrared spectroscopy can be used to measure the state of lubricant degradation and is now widely accepted as an industry standard (ASTM E 2412-04). Fourier Transform infrared spectroscopy (FTIR) is usually the popular method used, since it offers fast and reliable data capture. The infrared region between the visible and microwave regions (0.7 and 500 $\mu$ m in the electromagnetic spectrum), is employed and passed through a sample for investigation. The compounds absorb infrared radiation and absorption peaks are mapped on an absorption spectrum against infrared frequency. The benefit of using FTIR over traditional techniques is that it not only provides the state of degradation, but the level of compound activity. A fresh sample of the lubricant is required to measure the extent of degradation. Providing the user has a library of information on the absorption frequencies for lubricants and their compounds, quick identification of compounds contained in the lubricant sample is possible. Also any strange fluid, such as a coolant leak in the above example, would be easily detected, resulting in an additional means of engine protection. Monitoring in this way makes sure the engine is running in an optimum condition and maintaining lower fuel

consumption through oil quality control (Powell and Compton 1993). It has also been possible to determine TBN from FTIR spectroscopy (Dong, Van De Voort et al. 2001).

Apart from additive depletion and contamination from other fluids, the characteristic properties, such as the lubricant viscosity, change with mechanical degradation, as mentioned earlier, and degradation caused by the by-products of combustion. In diesel engines, soot contamination causes an additional increase in lubricant viscosity (Yasutomi, Maeda et al. 1981b).

### 2.1.7 In-situ lubricant sampling methods for piston ring pack degradation

It is necessary to examine the lubricant within the piston ring pack, since it is here that the lubricant experiences extreme operating conditions. This section introduces the concept of piston ring pack lubricant residence time and the need to examine the chemical changes to the lubricant in the ring pack.

#### 2.1.7.1 Piston ring pack lubricant residence time

The engine can be considered as a two phase reactor model with two, well mixed, homogenous oil volumes; the piston ring pack (small volume) and the sump (large volume) (Yasutomi, Maeda et al. 1981a), Figure 2-2. The lubricant residing in the piston ring pack area experiences greater temperatures, pressures and interaction with noxious combustion gases than the lubricant that resides in the sump (Lee 2006).

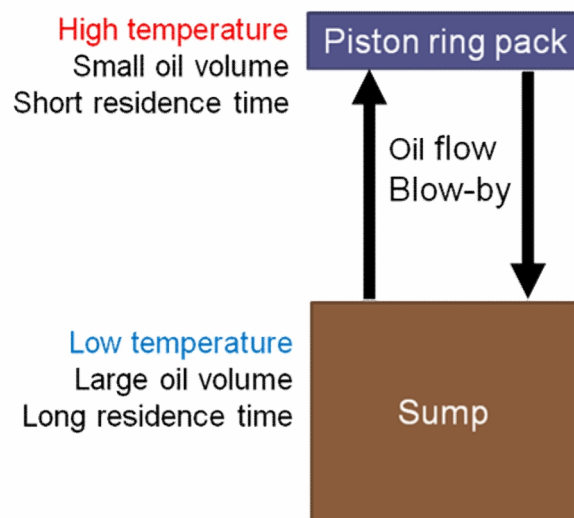


Figure 2-2: Two phase reactor model of an engine. Reproduced from Lee (Lee 2006)

The lubricant in the sump resides for a longer period than that in the piston ring pack. The lubricant in the sump is at relatively low temperatures and low rates of degradation whereas the lubricant in the ring pack is subjected to higher temperatures (Yasutomi, Maeda et al. 1981a). There is a flow of lubricant from the sump to the piston ring pack and back to the sump, and this is a cyclic activity (Burnett, Bull et al. 1995). In terms of the influence of lubricant degradation, the lubricant residence time can therefore be defined as the time to exchange the small volume of degraded lubricant in the piston ring pack with an equivalent amount of lubricant volume in the sump.

The piston ring pack lubricant residence time was first reported to be measured by Saville et al. (Saville, Gainey et al. 1988). They measured the ring pack residence time by using a tracer marker in the lubricant sump and extracting lubricant samples from the top compressing ring. By comparing the concentration of the tracer in the sump and the extracted piston ring samples it was possible to calculate an estimation of the ring pack residence time as three minutes in a Caterpillar 1Y73 diesel engine at an engine speed of 1200 rpm. Stark et al. (Stark, Gamble et al. 2005) followed the same approach as Saville et al. on a Ricardo Hydra single cylinder gasoline engine and measured the ring pack residence time to be 60 seconds at 1500 rpm and 50 % load.

It is therefore of greater interest to examine the lubricant in the piston ring pack as opposed to the lubricant in the sump to determine state of degradation and ultimately the ring pack performance.

### **2.1.7.2 Top ring zone (TRZ) lubricant sampling**

The lubricant towards the top piston ring has been found to be more degraded, in terms of carbonyl oxidation (Lee 2006; Lee, Priest et al. 2006) and fuel dilution (Smith, Priest et al. 2006), than the bulk lubricant in the engine sump. Lubricant has been sampled from the top ring zone (TRZ) of the engine by many researchers in the past (Thompson 1990; Burnett, Bull et al. 1995; Fox 1997; Moritani and Nozawa 2003; Lee, Priest et al. 2006). These researchers have made use of grasshopper type linkages that attach to the big end bearing of the connecting rod with the sole purpose of carrying a lubricant sample pipe from the piston assembly to the outside of the engine. A small hole drilled into either the top ring groove (Thompson 1990; Burnett, Bull et al. 1995; Lee, Priest et al. 2006) or the second land (Moritani and Nozawa 2003), feeds blow-by samples containing a mist of lubricant down the pipe into a collection vial for post analysis. The difference in pressure from the combustion pressure in the chamber to the atmospheric pressure outside the engine forces this gas stream

down the pipe (Lee 2006). At University of Leeds, many linkages have been used in the past to help facilitate sampling but with many failures. An extensive research into the different types of grasshopper linkages used at University of Leeds, on the Ricardo Hydra gasoline engine, with improvements in sample flow rates can be followed in (Lee 2006). Lee, (Lee 2006), used a PTFE pipe that fed through a stainless steel tube attached to the front face of the connecting rod to improve the reliability of the pipe, see Figure 2-3. From the crankshaft, the pipe fed around a single axial constraint creating a coil spring before feeding out of the side of the crankcase through a window and into a vial to collect the sample, Figure 2-4.

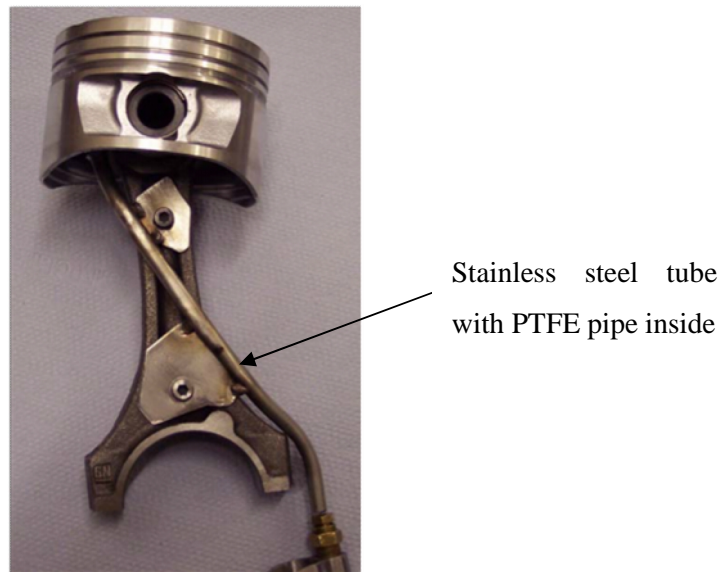


**Figure 2-3: Method to attach sample pipe to connecting rod (Lee 2006)**

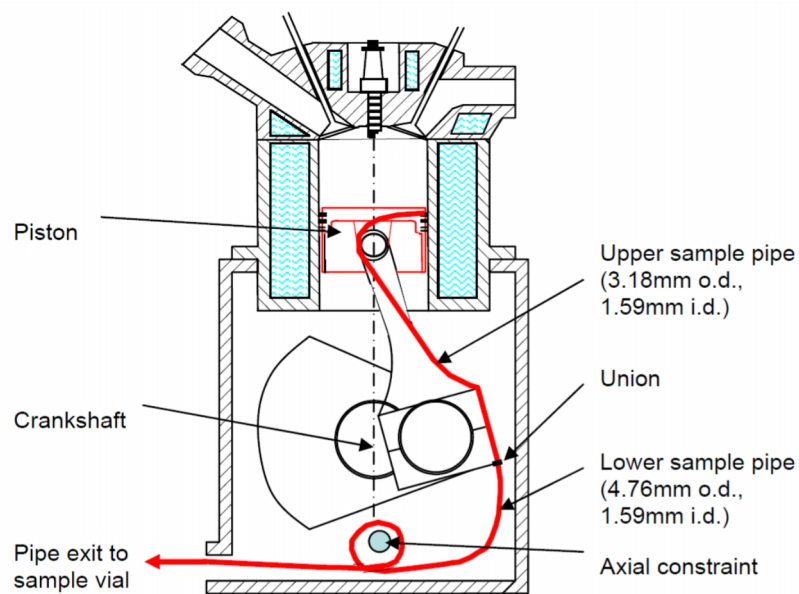


**Figure 2-4: TRZ lubricant sample collection method as used by Lee (Lee 2006)**

The system as used by Lee was reliable up to 2500 rpm and was tested for 250 hours. Lee managed sample rates of approximately 25 ml over 40 hours of testing. There was always a desire for sampling at higher speeds since this would also improve the sample flow rates down the pipe. In 2008, Notay (Notay 2008), an undergraduate student at University of Leeds, designed and manufactured a grasshopper linkage for the Hydra engine, Figure 2-5, which was tested at speeds in excess of 5000 rpm without failure. The linkage was fixed to the bottom end of the connecting rod and anchored to the side wall of the crankcase. A PTFE sample pipe is routed through the steel tube of the existing connecting rod, Figure 2-3, the linkage and then out of a hole in the crankcase window for sample collection.

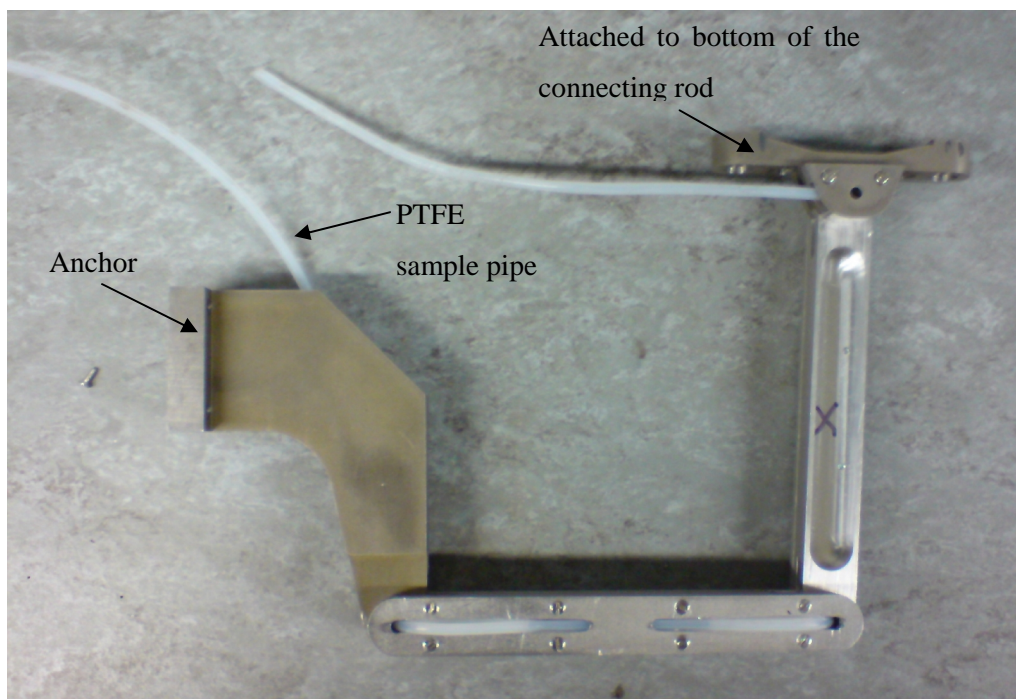


**Figure 2-5: Current TRZ sampling linkage designed by Notay (Notay 2008)**

Extracting actual lubricant samples from the piston ring pack is one method of analysing the quality of the lubricant in terms of chemical analysis via infrared spectroscopy and viscosity check. However, it is not yet sure whether removing samples from the TRZ affects the piston ring lubrication.

### **2.1.7.3 In-situ infrared absorption**

An alternative to removing samples for chemical analysis is to measure the infrared absorption directly in the piston ring pack during engine operation. In the past, researchers

have used various novel in-situ infrared absorption analyses to measure the influence of lubricant degradation (Natrass, Thompson et al. 1994; Thompson and Natrass 1996; Watson and Wong 2010). Natrass and Thompson of Shell Research Ltd, UK (Natrass, Thompson et al. 1994; Thompson and Natrass 1996) both investigated just the carbonyl oxidation absorption of the infrared spectrum to improve the signal to noise ratio whereas Watson and Wong of Massachusetts Institute of Technology (MIT), USA (Watson and Wong 2010) managed to measure the complete spectrum but only for approximately two minutes since the infrared fibre optic became detached from the probe window as engine vibration increased on start-up. However, the MIT method, Figure 2-6, had the benefit over the Shell Research approach in that a complicated triggering system was not required and the measurement was not sensitive to the thermal effects of the piston assembly since it was nitrogen gas cooled. One of the more interesting finds in the Shell Research approach was that it was found that the carbonyl absorption levels changed between strokes and were predominantly lower in the intake and compression strokes with absorbances similar to that of fresh lubricant (Thompson and Natrass 1996).

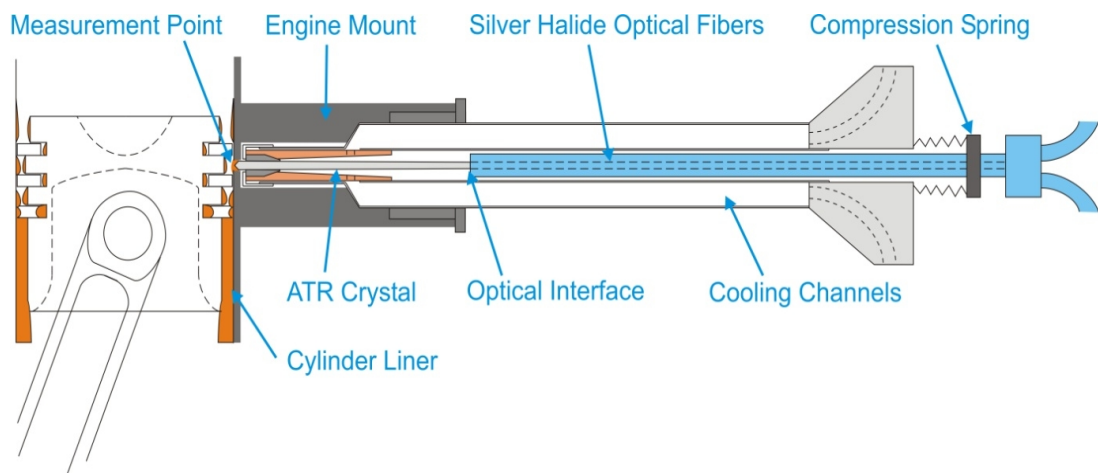


**Figure 2-6: Watson's probe for in-situ infrared absorbance measurements (Watson and Wong 2010)**

## 2.2 Theoretical piston ring research

In 1959, Furuhashi (Furuhashi 1959) modelled the lubricant film thickness between the piston ring and the cylinder liner. He adapted the Reynolds equation to take into account the

squeeze term, which is considered in the dynamic theory, and showed its importance since it was assumed earlier by Eilon and Saunders and later by Lloyd (Eilon and Saunders 1957; Lloyd 1968), that the film thickness is zero at zero speed, i.e. at the dead centres. Subsequently, Furuhamma went on to investigate the gaseous flow past the piston ring pack (Furuhamma 1961a). This was done by measuring the gas flow rate through a narrow gap in the ring of a piston. Increase in chamber temperature was also investigated simultaneously and the discharge coefficient, that being the ratio between actual flow rate and the ideal flow rate with the same conditions, was found to be 0.86. This value, obtained experimentally, was used to predict the pressure distribution and gas leakage of piston rings in a volume model, (Furuhamma 1961b). The results obtained theoretically matched closely experimental work.

The access to a cost effective computer system in large institutions became easier from the 1960's onwards, which greatly facilitated modelling research. Lloyd, (Lloyd 1968) was one of the first to take advantage of the computer models with the addition of complex variables and also included changes in ring velocity, which had never been investigated before.

The use of the computer proved beneficial, with an exceptional two part paper series produced by Ting and Mayer in 1974 (Ting and Mayer 1974a; Ting and Mayer 1974b). They produced a model that was able to predict cylinder bore wear over the complete four engine strokes. The Reynolds equation was used to examine the pressure distribution between the piston ring and the cylinder liner in a manner similar to the method developed by Furuhamma and Tada (Furuhamma 1961a; Furuhamma 1961b). Coupling this with lubricant film thickness analysis, based on the film thickness being greater than a lower limit before boundary contact takes place; it was shown how the Archard wear law, whereby the total wear debris between an interface is inversely proportional to the surface hardness of the softer material (Williams 2005), could be adapted to determine the wear along both the thrust and anti-thrust sides of the cylinder wall. The analytical method in Part I of the series (Ting and Mayer 1974a) was compared to wear patterns from a collection of engines with different mileages in Part II (Ting and Mayer 1974b). The agreement between the theory and practice was found to be good (Ting and Mayer 1974b).

Modelling of lubricant film thicknesses was also investigated by Sreenath and Venkatesh in 1973 (Sreenath and Venkatesh 1973), and a year later by Hamilton and Moore (Hamilton and Moore 1974a; Hamilton and Moore 1974b). Hamilton and Moore were unsuccessful in obtaining an agreement between measured film thicknesses and film thicknesses predicted from hydrodynamic equations. Predicted film thicknesses, were a factor of eight larger than

those films measured experimentally. It was concluded that an error in the boundary conditions explained the difference and that it was important to include lubricant starvation in models (Hamilton and Moore 1974b). Sreenath and Venkatesh, also making use of the hydrodynamic theory, found that there was a zero film thickness predicted at the dead centres but during practice this was not the case (Sreenath and Venkatesh 1973). Dowson, Ruddy et al. (Dowson, Ruddy et al. 1983), were the first to investigate the possibility of elastohydrodynamic lubrication in piston ring operation. They also mentioned that the film thickness is not zero at the dead centres but is a minimum shortly after the piston has passed top dead centre and can be as small as  $0.1 \mu\text{m}$  (Dowson, Ruddy et al. 1983).

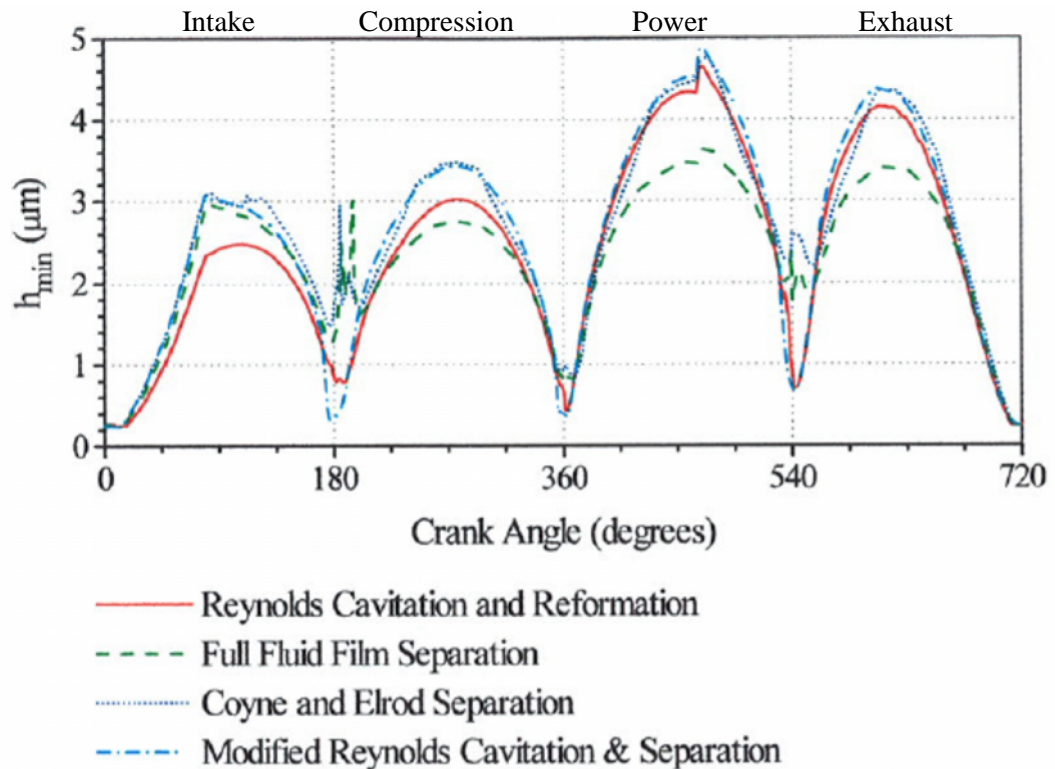


**Figure 2-7: Minimum film thickness as predicted by Priest when adopting different cavitation models. Adapted from Priest (Priest 1996)**

It has been noted by Priest (Priest 1996; Priest, Dowson et al. 2000) that mathematical models used to predict lubricant cavitation, that being a volume of space in the fluid with the inability to sustain large negative pressures (Priest, Dowson et al. 2000), in piston ring lubrication and dynamics are sensitive to the boundary conditions applied. When predicting the minimum oil film thickness for a single diesel compression ring, Priest found a small

variation in the film thickness when different cavitation models were applied as shown in Figure 2-7. The film thickness was predicted at the mid-stroke position, where the lubricant entrainment velocity is large. From Figure 2-7, it can be seen that each model has a similar cyclic shape corresponding to the variation in the film thickness. From 0-360° crank angle, the film thickness, as predicted by all models, is smallest throughout the entire cycle, since this represents the power and exhaust strokes where high chamber pressures push the piston rings out towards the cylinder wall. The small spike at around 470° is believed to be caused by ring lift (Priest 1996; Priest, Dowson et al. 2000).

From a mechanical efficiency perspective, piston ring and cylinder wall friction has also been modelled by many researchers including Dowson, Economou et al (Dowson, Economou et al. 1979), and Wakuri, Hamatake et al (Wakuri, Hamatake et al. 1992), again based on hydrodynamic theory. They obtained frictional forces from calculations of oil film thickness. Dowson, Economou et al stated that the curvature of a piston ring face along with its height, influences the lubricant film thickness and ultimately friction (Dowson, Economou et al. 1979). An investigation by Wakuri et al. (Wakuri, Hamatake et al. 1992) into (a) fully flooded lubrication, where the interface is filled completely with lubricant since there is an unlimited supply of lubricant at the inlet to the ring and operating under hydrodynamic lubrication and (b) starved lubrication, where the interface has an inadequate lubricant supply which experiences boundary lubrication causing unwanted high friction and component wear. They found that the frictional force in starved lubrication was at least twice that when fully flooded due to thinner films. Taylor (Taylor 1997) took frictional analysis of engines a step further by investigating cold start and fully warmed conditions and the impact on frictional power loss. The main focus of the paper was engine friction as a whole, including bearing and valve train losses, and the importance of lubricant rheology. It was found that engine friction is particularly sensitive to lubricant characteristics such as viscosity. He also noted that engine friction under cold start conditions was up to five times greater than with fully warmed normal operating conditions.

The running-in of the piston ring and the cylinder wall leads to a reduction in component roughness. This in turn increases the specific film thickness ratio and a move from boundary to hydrodynamic lubrication. Even after a short run period the piston ring profile changes from new (Ting and Mayer 1974a; Ting and Mayer 1974b; Sreenath and Raman 1976; Sreenath and Raman 1976). The ring profile has a great influence on the oil film present between the ring and cylinder wall interface (Ting and Mayer 1974b). So, as the ring wears a shift in lubrication regime from boundary/mixed to hydrodynamic is very likely, causing changes in lubricant film profiles.

Another area analysed in piston ring tribology, not particularly specific just to lubrication, is the absorption and desorption of fuel into and out of the lubricant films on the cylinder wall. This, as mentioned earlier, contributes to unburnt hydrocarbon emissions. Thomson et al from the University of Leeds modelled the fuel absorption/desorption effect in 1997 (Thomson, Radcliffe et al. 1997). Lubricant film thickness and temperature, along with engine speed were found to be very influencing on the rate of fuel absorption. Again stressing the extremities of cold start conditions, it was found that absorption and desorption rates were greatest with the thicker films produced at the colder temperatures (Thomson, Radcliffe et al. 1997).

Gamble et al, from University of Leeds, modelled piston secondary motion (Gamble, Priest et al. 2000) and lubricant transport past the piston ring pack (Gamble, Priest et al. 2003). It was found that any oil that accumulates in front of the ring, will adjust the oil film thickness ahead of the ring (Gamble, Priest et al. 2003), Figure 2-8.

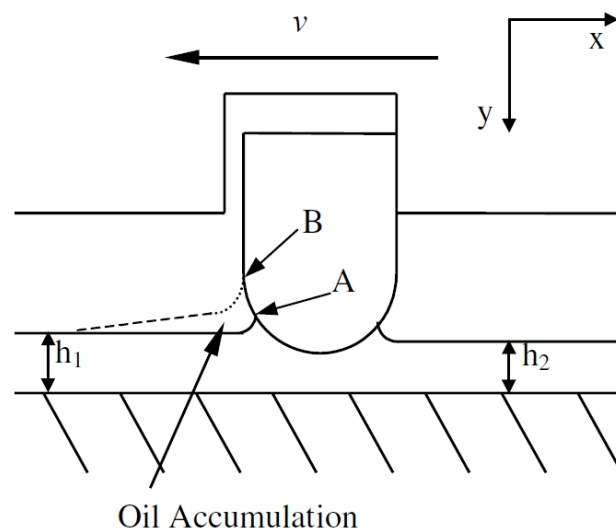


**Figure 2-8: Oil accumulating ahead of ring (Gamble, Priest et al. 2003)**

In Figure 2-8, point A is the first point of contact for the oil film on the ring and as oil accumulates ahead of the ring, the film thickness increases and contact occurs further up the ring at point B. This has implications for the hydrodynamic equations since the inlet oil film thickness is varying (Gamble, Priest et al. 2003) and is possibly the reason why piston rings experience a shift in lubrication regime in the interface during the engine cycle (Rabute and Tian 2001; Tian 2002).

From the 1990's, as technology advanced and new techniques became available, there was an upswing in experimental studies.

## **2.3 Experimental piston ring research**

Experimental piston ring research progressed simultaneously with theoretical modelling. Much research has involved piston ring friction and the investigation of lubricant consumption, which has led to the discovery of lubricant transport mechanisms past the piston rings. In the early days of ring-wall lubrication, there was doubt as to the amount of lubricant present in the ring pack during engine operation. It can be appreciated that below the oil control ring, there will be excess lubricant and any above will only be partly lubricated. Theoretical film investigation is sensitive to the assumptions, modelling theory and the boundary condition applied, and only provides an insight. This has encouraged experimental developments in measurements of lubricant film thicknesses within the piston ring and cylinder wall interface as a means to fully understand transport mechanisms.

### **2.3.1 Lubricant transport and consumptions mechanisms**

There are many factors influencing the rate of lubricant flow through the rings, from temperature and pressure to engine speed and load. It has been suggested that the piston ring lubricant flow is driven by two dynamics. Those being inertia driven, due to the movement of the piston, and gas driven; caused by gas flow through rings which depends on the position of the ring gaps (Min, Kim et al. 1998; Thirouard and Tian 2003).

The rings undergo various axial forces contributing to the lubricant flow driven by inertia. The rings are continually experiencing frictional forces and a difference in gas pressure above and below the ring (Furuhama and Hiruma 1972). Such effects allow the rings to move axially, circumferentially and twist, and it is these effects which cause concern for lubricant consumption (Bailey and Ariga 1990). The gas flow (blow-by) through the ring pack has been investigated by Ruddy et al (Ruddy, Dowson et al. 1981), and it was found from modelling, based on a large marine diesel engine, that gas flow rates are a maximum when the ring gaps are in line (Ruddy, Dowson et al. 1981). The blow-by gas carries any lubricant through the piston ring gaps, onto the piston lands, and eventually into the crankcase due to the interfacial shear stresses between the gas and the oil (Thirouard and Tian 2003). Hence the flow rate of blow-by gas influences the flow of lubricant through the ring pack.

Piston ring flutter is a major concern for lubricant consumption and this phenomenon occurs when the gas pressure is unable to balance the inertial force to hold the ring in its groove and as a consequence excessive blow-by and lubricant consumption results, due to the poor sealing ability of a fluctuating ring, which is greater than the gas flow through the ring gaps (Rabute and Tian 2001; Tian 2002). The illustration in Figure 2-9 demonstrates how the various forces ‘fight’ to balance the ring in the groove. It is this balancing which forces the rings into various dynamic motions, altering the transport mechanism.

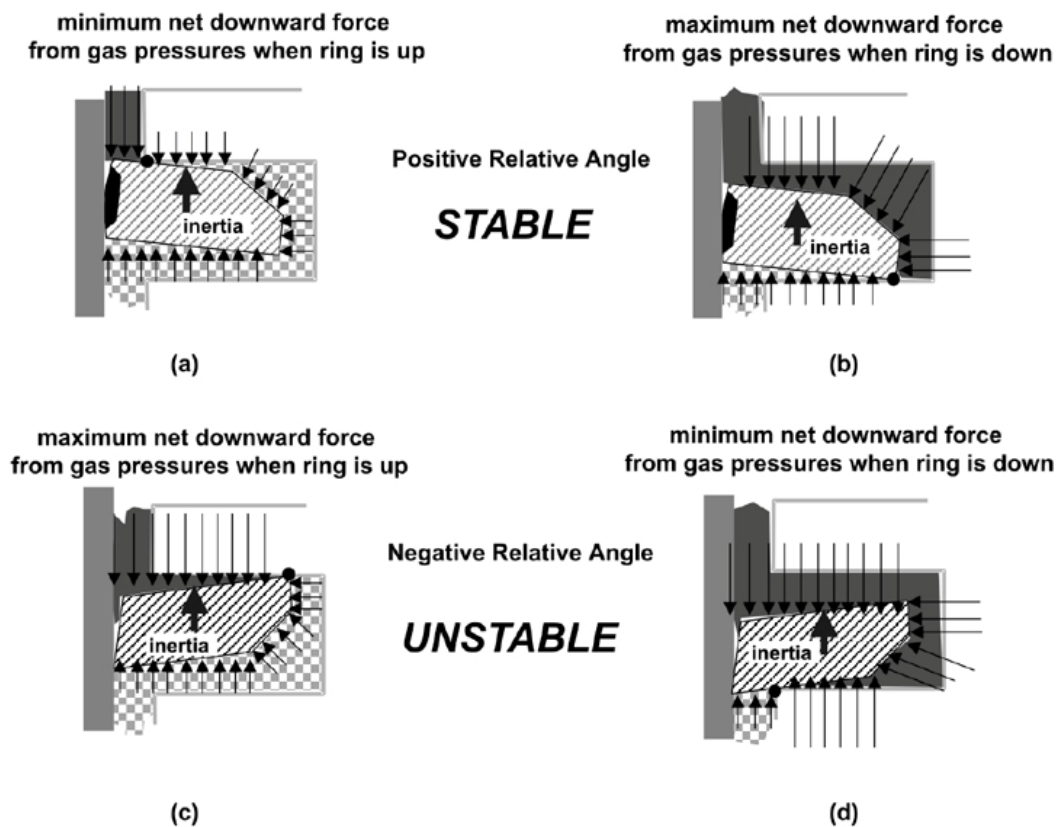
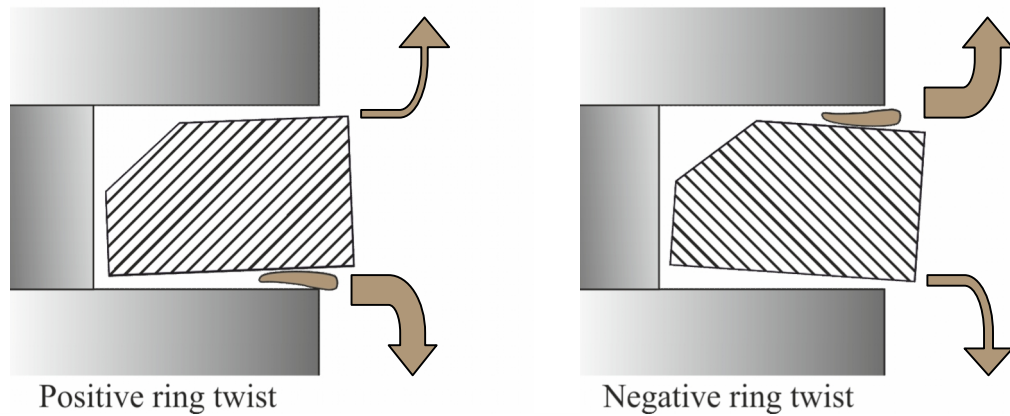


Figure 2-9: Inertia and gas forces fight to keep the ring stable (Tian 2002)

Ring twisting is also a concern for lubricant consumption since certain twisting mechanisms can squeeze lubricant in and out of the piston grooves. The schematic in Figure 2-10 demonstrates two different mechanisms of ring twisting; positive and negative, within the ring groove. It can be seen that if a positive twisting is in action, positive meaning an upward direction towards the combustion chamber, the lubricant would be squeezed out of the groove and fall into the crankcase. On the other hand if negative twist is in action the lubricant is still squeezed out of the groove, but the direction of the twist forces the lubricant

upwards towards the combustion chamber (Thirouard and Tian 2003). This also causes a concern for lubricant consumption.



**Figure 2-10: Dynamics of ring twisting cause the lubricant to squeeze out of piston groove. Reproduced from (Thirouard and Tian 2003)**

Nakashima et al, (Nakashima, Ishihara et al. 1995) investigated relative piston ring gap positions including when the piston ring gaps are out of phase to each other, Figure 2-11, and when the rings gaps are all in line, Figure 2-12. A single cylinder motored engine with a quartz liner was used, with a high speed CCD camera recording lubricant flow. From Figure 2-11, the minimum flow rate through the ring pack is observed and as expected, in Figure 2-12, the maximum flow rate through the ring pack is experienced when the ring gaps are set in line (Nakashima, Ishihara et al. 1995).

Apart from ring dynamics, piston secondary motion has an effect on oil consumption. If the piston is moving away from the cylinder wall surface, the ring sealing ability is compromised, and easier lubricant transport towards the combustion chamber can occur (Munro and Parker 1975; Shin, Tateishi et al. 1983; Gamble, Priest et al. 2000).

The flowchart in Figure 2-13 shows a diagram of the oil flows in an engine reproduced from Burnett et al (Burnett, Bull et al. 1995). It can be seen that lubricant transport in the form of a mist in the gas flow, from the crankcase to the combustion chamber, is another contributor to lubricant consumption and is caused by reverse blow-by effects.

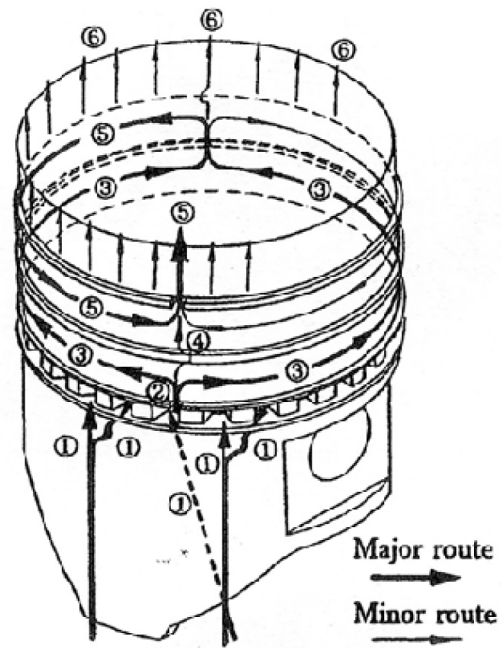


Figure 2-11: Oil Flow observed when ring gaps are all 180° out of phase with each other (Nakashima, Ishihara et al. 1995)

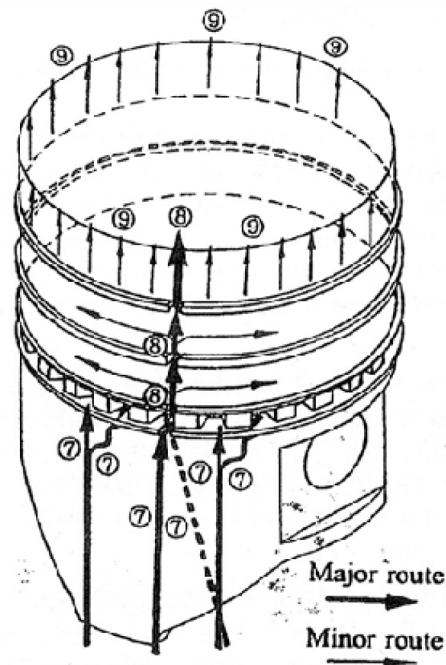
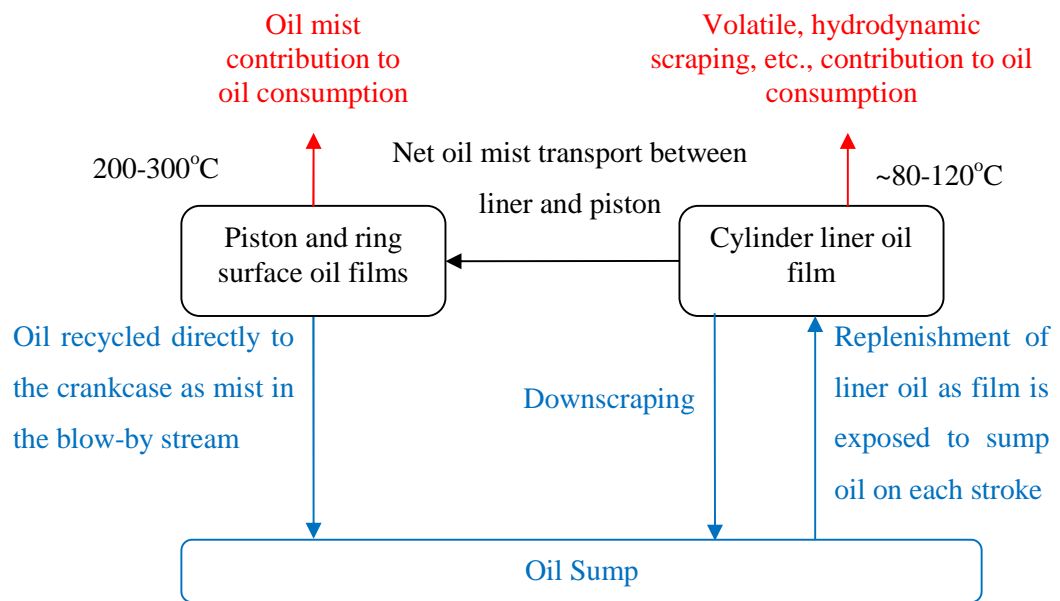


Figure 2-12: Oil Flow observed when ring gaps are all in phase (Nakashima, Ishihara et al. 1995)



**Figure 2-13: Flow of oil in an engine, reproduced from (Burnett, Bull et al. 1995)**

It is generally accepted that particulate emissions are greatly influenced by lubricant consumption (Bailey and Ariga 1990; Min, Kim et al. 1998; Thirouard and Tian 2003). Min et al. investigated lubricant consumption while using a hydrogen fuelled engine. Any carbon compounds, such as  $\text{CO}_2$ , in the exhaust were therefore assumed to come completely from the consumption of the lubricant. Min also placed radioactive isotopes in the rings and measured the ring rotation with respect to engine speed and load. One major increase of oil consumption rates into the exhaust was found to be caused by ring rotation when the top two ring gaps were in-line (zero phase angle). Accordingly, a minimum oil consumption rate was recorded when the ring gap positions were out of phase by  $180^\circ$  (Min, Kim et al. 1998; Jung and Jin 1999). In the recent years it has been difficult to determine why this occurs and much work has been undertaken to examine oil films and transport within the ring pack. It has been stated (Thirouard and Tian 2003), that it is the lubricant in the piston grooves which causes ring dynamics to be influential on the total lubricant consumption.

Bore wear and distortion can also change lubricant flow patterns. As the bore becomes more polished with worn rings, the sealing ability decreases and as a result, lubricant is able to flow past the rings more freely, as observed by McGeehan (McGeehan 1983). Engine tests were conducted on five turbocharged diesel engines, with runs lasting up to 120 hours. The influence of different oil formulations was also considered. Bore polishing is caused by crown land piston deposits which are hard and polish the bore to the point where the cross

hatch honing is removed. The polished bore and rings are more likely to scuff since lubricant retention of a polished bore is poor. This increases the lubricant consumption. McGeehan stated that bore polishing, and ultimately lubricant consumption, can be reduced providing lubricant formulations with additives to reduce piston ring deposits. Bore deformation due to high operating temperatures, causes the bore to become out-of-round. Schneider et al. (Schneider, Blossfield et al. 1993) investigated bore deformation and explicitly stated that a deformed bore affects the oil consumption rates and the rotation of the top two compression rings thereby influencing the lubricant flow. They used an open-deck 4.5 litre V8 engine and altered the level of out of roundness for one cylinder by either adjusting the clamping forces of the cylinder head, removing material from the outside of the liner to promote bore distortion and by wrapping steel bands around the outside of the liner to induce some distortion. Radioactive techniques were then used to measure the ring rotation and the amount of oil consumption simultaneously. It was found that if the cylinder bore out of roundness was up to 110  $\mu\text{m}$  of radial difference (whereby a nominal production level of 50  $\mu\text{m}$  is acceptable), not only does a significant increase in blow-by and oil consumption result, but ring rotation reduces.

The lubricant flow in an engine is complex. For complete protection the oil flow should be continual and be present in all the mechanics of the system. However this is not always the case. The piston ring pack has been observed to operate in a starved condition by Brown and Hamilton (Brown and Hamilton 1977) and this would promote high friction and scuffing wear. To reduce the potential for oil starvation it has previously been proposed, (Kovach, Tsakiris et al. 1982; Basaki, Saito et al. 2000; Seki, Nakayama et al. 2000), to reduce the oil control ring tension, thereby allowing more oil to enter the piston ring pack. However, even though this is desirable it causes an increase in oil consumption since the ring may not conform sufficiently to a bore that could be out-of-round (Kovach, Tsakiris et al. 1982; Basaki, Saito et al. 2000).

In modern engines, lubricant consumption has been greatly improved with advancing technology, such as narrower tolerances now achievable in machining and more advanced research into materials and coatings. Many modern engines in service can operate comfortably without ever needing oil top ups in-between oil drain intervals. However, in recent attempts to improve the fuel economy and reduce the harmful exhaust gases emitted from the exhaust, many manufacturers have begun to deactivate cylinders (Leone and Pozar 2001; Fujiwara, Kumagai et al. 2008). Although a very successful means of operation with reductions in engine pumping losses, there are concerns for elevated oil consumption, since a lack of compression pressure on the rings in the deactivated cylinder results in easy upward

oil flow to the combustion chamber and into the exhaust. Ma from the General Motors Company (Ma 2010), has recently investigated this. Design changes in piston ring and cylinder wall clearances, ring gaps, and drain hole sizes was recommended to improve the downward flow of the excess oil, (Ma 2010).

The oil film thickness between the piston ring and cylinder wall is of major importance when investigating lubricant transport patterns and oil availability in the ring pack. In order to validate the modelling predictions of lubricant film thickness between the ring and cylinder wall, there have been various experimental developments.

## **2.4 Lubricant film thickness measurement methods**

The three frequently used experimental techniques employed to measure the lubricant film thickness between the piston ring and the cylinder wall are electrical methods, laser induced fluorescence and more recently, ultrasound.

### **2.4.1 Electrical methods**

Electrical film thickness methods can either be conducting using electrical resistance and inductance transducers or capacitance transducers.

#### **2.4.1.1 Electrical resistance**

By electrically insulating part of the piston ring from the rest of the piston and allowing an electric current to flow from the piston ring and the cylinder wall and measuring the resistivity, it is possible to obtain information on the lubricant film thickness (Courtney-Pratt and Tudor 1946; Furuhashi and Sumi 1961; Dow, Schiele et al. 1983). The electrical resistance measured is proportional to the film thickness and a thicker film consequently produces a greater resistance. However, with such an examination of the films, a smooth plot of resistance against crank rotation was not easily observed. When the ring contacts the cylinder wall a short circuit is experienced and a complete breakdown of the films is observed at TDC and BDC where boundary lubrication results (Sherrington and Smith 1985).

#### **2.4.1.2 Inductive transducers**

The distance between the piston ring and the cylinder wall can be measured with inductive transducers to give a measurement for the lubricant film thickness present. These transducers

work on the principle of induction of a magnetic material. The separation between a wire coil and a magnetic material is dependent on the inductance (Sherrington and Smith 1985).

Wing and Saunders were one of the first to report this technique (Wing and Saunders 1972). The piston ring was made part of the armature circuit and was excited by an alternating current. Two sensors were placed in the back of the ring, on opposite sides of the piston ring, and used to monitor the distance between the back of the ring and the piston. The benefit of such a method allows a continuous oil film to be measured across the piston stroke but was found to be highly temperature sensitive and inappropriate for fired engine investigation since the transducer output is non linear and the transducer has very low thermal stability (Sherrington and Smith 1985).

### **2.4.1.3 Capacitance transducers**

One of the first reported lubricant film thickness measurements by the capacitance transducer method was achieved by Brown and Hamilton in 1978 (Brown and Hamilton 1978) at the University of Reading. Lubricant film thicknesses between 4 and 12 $\mu\text{m}$  were measured from slow motored engine speeds from 200-800 rpm with capacitance transducers mounted in the liner. Lubricant cavitation was found to disturb the signal. At Reading, Moore continued this work further (Moore and Hamilton 1978; Moore 1979; Moore 1981; Moore 1985). The lubricant film thickness between the piston ring and wall is investigated by measuring the electrical capacitance between the interface (Moore 1979), this technique is known as parallel plate capacitance. Moore stated that for thin films between 0.1  $\mu\text{m}$  and 1.0  $\mu\text{m}$  the capacitance method can be accurately calibrated using the parallel plate formula. Greater than 1.0  $\mu\text{m}$  and it is necessary to calibrate the system through other means since the fringing field of electrons diverges the signal from theory (Moore 1979). In one of his papers (Moore 1979), with transducers mounted in a cylinder liner, he found that during engine run-in the capacitance method did 'fail' since the composite surface roughness of the piston ring and liner was greater than the lubricant film thickness. The metal contact between the rings and the liner greatly disturbed the signals. However when working, the capacitors were very sensitive and had very good resolution; it was possible to measure the minimum film thickness at both the mid stroke and TDC at an engine speed of 1800 rpm with values of 2.0  $\mu\text{m}$  and 0.2  $\mu\text{m}$  respectively (Moore 1979). In 1985, Moore investigated the influence of lubricant viscosity on the minimum film thickness experienced across the four piston ring pack (Moore 1985). The same Petter AV1 diesel engine was employed with two capacitance transducers mounted near top dead centre and mid-stroke, as used in previous research papers (Brown and Hamilton 1977; Brown and Hamilton 1978; Moore and Hamilton 1978).

The engine was equipped with a switchable sump, allowing a series of lubricant samples with different viscosity grades to be examined. The major find, was that the minimum lubricant film thickness, especially at top dead centre, increases as the lubricant viscosity decreases (Moore 1985).

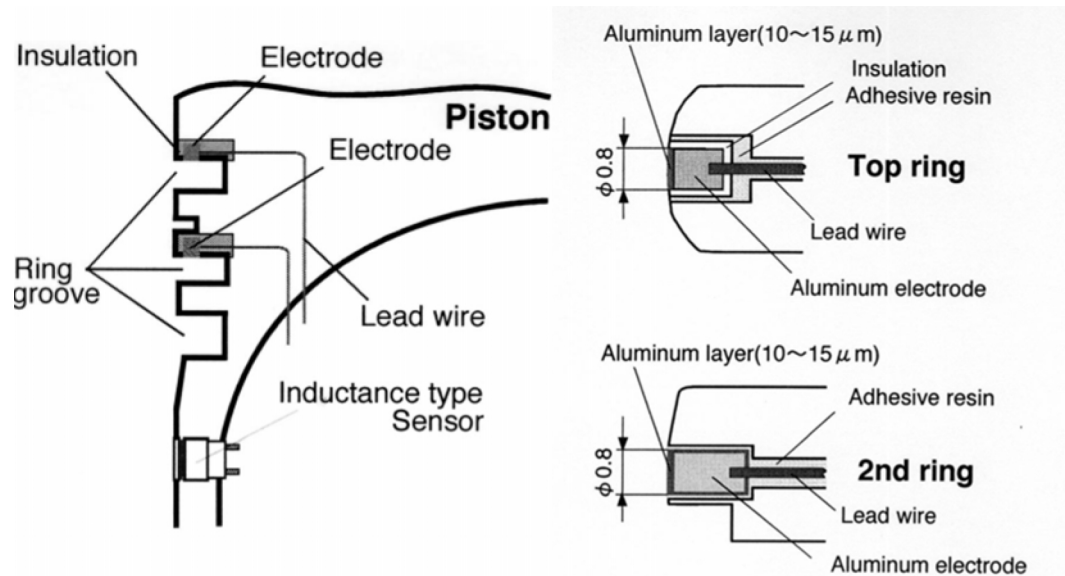


**Figure 2-14: Cross sectional view of the capacitance transducers mounted in the top and scraper ring by Takiguchi (Takiguchi, Sasaki et al. 2000)**

Shin et al. (Shin, Tateishi et al. 1983) placed transducers in the top ring of a motored diesel engine in 1983. One of their major findings was that at 1300 rpm with no load and without the oil control ring, the film thickness at the top ring increases on average by  $3 \mu\text{m}$  across the complete engine cycle, since the control action of the missing ring is not occurring. The angle of inclination of the piston ring to the cylinder wall was also found to influence piston ring lubricant profiles (Shin, Tateishi et al. 1983). A more recent paper from Takiguchi et al. (Takiguchi, Sasaki et al. 2000), saw a major advancement in placing the transducers in the rings. Takiguchi et al. followed Shin's work (Shin, Tateishi et al. 1983) and placed transducers in the running surfaces of the top and the second scraper rings as shown in Figure 2-14. This allowed the effects of the thrust and antithrust side ring dynamics to be investigated in terms of lubricant film thickness, by positioning and pinning the rings during installation. An additional inductance type sensor was installed in the piston skirt to monitor piston slap motion. The electrode wires were taken through the piston and even though this may sound extreme for small wires, the author states that the system was reliable up to 2800

rpm in their four stroke diesel engine. Film thickness measurements with respect to engine stroke were measurable and it was found that films for the top ring had the greatest difference when compared to theoretical results in the expansion stroke, Figure 2-15. Here, an increase in engine speed barely influenced the film thickness. It was found that the back pressure from the second ring on ring reversal increased the film thickness of the top ring. This was more evident with no engine loading (Takiguchi, Sasaki et al. 2000).

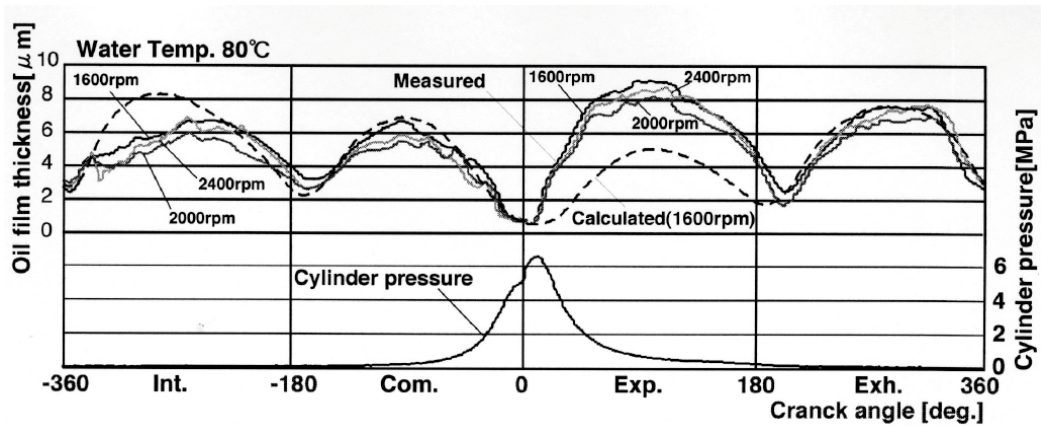


**Figure 2-15: Lubricant film thickness measurements of the top ring across all four engine strokes (Takiguchi, Sasaki et al. 2000)**

The capacitance,  $C$ , is usually expressed as:

$$C = \frac{\epsilon_s \epsilon_o S}{h_{OFT}} \quad \text{Equation 2-1}$$

Where  $\epsilon_s$  is the dielectric constant of the substance present between the parallel plate electrodes (the lubricant),  $\epsilon_o$  the vacuum dielectric constant,  $S$  the transducer surface area and  $h_{OFT}$  the oil film thickness (Shin, Tateishi et al. 1983).

In a recent paper by Söchting and Sherrington (Söchting and Sherrington 2009), investigated the effect of engine load and lubricant viscosity on the minimum oil film thickness experienced at the piston ring to cylinder wall interface. A naturally aspirated compression ignition engine mounted on a dynamometer to provide load was used. Two capacitance sensors were mounted flush to the cylinder wall and could both observe the top and second piston ring. Two different monogrades and a single multigrade lubricant were tested at four different engine loads. It was found that the use of thinner lubricants generally

provided a reduced minimum film thickness at the piston rings and the change in load had less of an effect than the change in viscosity. Similar results of the impact of engine load on oil film thickness were also observed by Tamminen et al. (Tamminen, Sandström et al. 2006) and Takiguchi et al. (Takiguchi, Sasaki et al. 2000).

Measuring lubricant film thickness with a capacitor transducer requires the dielectric constant of material it is measuring the displacement across, to be known for correct calibration. In this case the material being the lubricant. As the lubricant degrades, the dielectric constant of the lubricant changes and as a result any existing calibration would not be valid. The small transducer and consequently small electric wires do not survive for long periods, due to the harsh environment of extreme temperature and pressure. Thermal expansion of the transducer wires and the glue used to hold the wire, to either the liner or the piston, has caused reliability issues with transducers failing over short periods. During engine run-in, Moore (Moore 1979) found that the signal was very random and erratic, caused by the electrodes touching as the lubricant films were much thinner than the combined asperity heights of the ring and the cylinder liner. Shin et al. (Shin, Tateishi et al. 1983), struggled to get any signals and it was found that coating the transducers in Aluminium Oxide improved signal to noise ratio and reliability.

#### 2.4.2 Laser Induced Fluorescence (LIF) method

Laser induced fluorescence (LIF) measurement of lubricant film thicknesses between the cylinder wall and the piston ring was first conducted by Ting in 1980 (Ting 1980) with many researchers following (Hoult, Lux et al. 1988; Dearlove and Cheng 1995; Inagaki, Saito et al. 1997; Sanda, Murakami et al. 1997; Arcoumanis, Duszynski et al. 1998; Arcoumanis, Duszynski et al. 1998; Casey 1998; Takiguchi, Nakayama et al. 1998; Seki, Nakayama et al. 2000; Taylor and Evans 2004; Yilmaz, Tian et al. 2004; Baba, Suzuki et al. 2007; Ohsawa, Kiyama et al. 2011) and also on connecting rod bearings (Nakayama, Morio et al. 2003). The principle uses laser light which absorbs in oil that has been dosed with a fluorescent dye. The oil fluoresces a different wavelength to the carrier signal and this return beam is converted into a voltage signal by using photomultiplier tubes. The signal can be read into a computer for recording. The intensity of the signal is related to the film thickness (Hoult, Lux et al. 1988; Takiguchi, Nakayama et al. 1998). Baba et al (Baba, Suzuki et al. 2007) produced an equation, Equation 2-2, which represents the intensity  $I$  of the fluorescence.

$$I = I_o K(\lambda) F(T, \lambda) ch_{OFT}$$

**Equation 2-2**

Where  $I_o$  is the initial intensity of laser source,  $c$  is dye concentration,  $h_{OFT}$  is oil film thickness,  $K(\lambda)$  and  $F(T, \lambda)$  are constants relating to wavelength of the source and temperature  $T$  respectively. As can be seen from Equation 2-2, the fluorescence intensity is influenced by the temperature, the film thickness and the dye concentration (Baba, Suzuki et al. 2007). These conditions and their effects are discussed in detail in a Chapter 3.

The success of LIF lies in the calibration. In the past, researchers have etched grooves of known depths in the piston skirt as a means of calibration, as Seki et al. (Seki, Nakayama et al. 2000) did, but Dearlove suggested that this method is ineffective since the grooves will wear as the piston skirt will eventually wear with piston slap dynamics (Dearlove and Cheng 1995). Other researchers (Hoult, Lux et al. 1988; Takiguchi, Nakayama et al. 1998; Baba, Suzuki et al. 2007) have used lubricant samples of known film thicknesses statically to gain calibration of the system. Figure 2-16 shows an LIF optics system mounted in the liner of an engine as used by Yilmaz et al (Yilmaz, Tian et al. 2004). Many researchers use similar optical arrangements. As can be seen from the schematic, the return signal is different to the carrier signal due to the shift in wavelength as caused by the fluorescence, known as Stokes Shift and this is discussed in detail in Chapter 3.

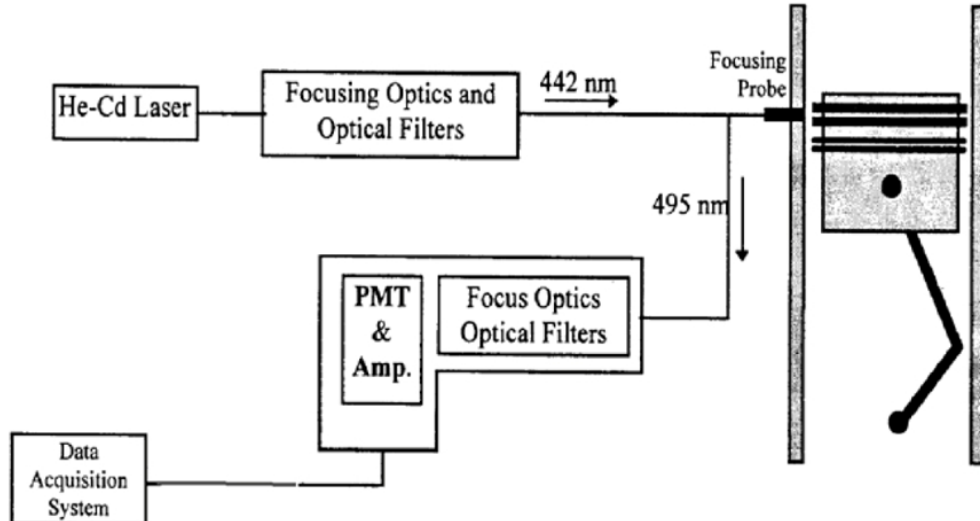


**Figure 2-16: LIF method through the liner as used by Yilmaz (Yilmaz, Tian et al. 2004)**

Initially, LIF was used as a means to achieve film thickness measurements (Ting 1980; Hoult, Lux et al. 1988; Inagaki, Saito et al. 1997) but it was clearly seen that the system has the potential to investigate lubricant transport within the ring pack. The common system of shining a laser beam through the liner was criticised (Casey 1998; Takiguchi, Sasaki et al.

2000; Thirouard and Tian 2003) for only providing information at one point and not valuable information about the oil film variation for the entire piston ring – cylinder wall interface, like the capacitance method was capable of doing when transducers were mounted in the ring (Shin, Tateishi et al. 1983; Takiguchi, Sasaki et al. 2000). This has led to the introduction of multipoint LIF investigations, whereby multiple LIF probes were used at various positions on the cylinder liner to improve the understanding of the oil film profiles radially around the piston (Arcoumanis, Duszynski et al. 1998; Nakayama, Seki et al. 1998; Takiguchi, Nakayama et al. 1998). The benefit of this outweighs the additional cost in extra probes and photomultiplier tubes, as Takiguchi et al. found that a considerable amount of oil is supplied to the oil control ring at TDC for completion of the compression and exhaust strokes on the thrust side of the cylinder liner, and only at the end of the exhaust stroke on the anti-thrust side.

Further improvements in multipoint LIF have seen a two dimensional LIF system being developed at Massachusetts Institute of Technology, USA by Thirouard et al. (Thirouard, Tian et al. 1998; Thirouard and Tian 2003). They used a single cylinder diesel Kubota engine with a quartz window, with a viewing area of 20 mm long and 8 mm wide, installed in the liner for initial LIF system development, and also a gasoline Peugeot single cylinder research engine, with a slightly larger viewing window, to investigate modern gasoline engine operating conditions. The window was used to observe the fluorescing lubricant when laser light was absorbed by the doped oil, coupled with a CCD camera system to inspect and record the lubricant transport (Thirouard, Tian et al. 1998; Thirouard and Tian 2003), as shown schematically in Figure 2-17. It was observed that lubricant flows on the piston lands both axially and circumferentially. Axial flow was influenced by piston inertia force, and circumferential flow was seen to be influenced by blow-by gases which ‘carry’ the lubricant from one piston land to the next via the piston ring gaps. One of the more interesting findings was that lubricant breaks down into a mist in the ring gaps which was never discovered before. The lubricant was found to entrain into one of the top two ring gaps with the gas flow and continues to flow with gas stream. Any droplets exiting the gaps can transfer to either the cylinder wall or the piston lands. The gas flow and velocity dictates the fate of disposition of the droplets. This process was difficult to detect with single point LIF since it was believed that the dye concentration in the mist was too low to be detected than if in liquid state. Figure 2-18 shows an illustration of what is believed to occur in the ring gaps (Thirouard and Tian 2003). LIF has also been used with Particle Image Velocimetry (PIV) recently (Baba, Suzuki et al. 2007; Kato, Fujita et al. 2009) to investigate the lubricant velocity and lubricant film thickness, when experiencing different operating conditions.

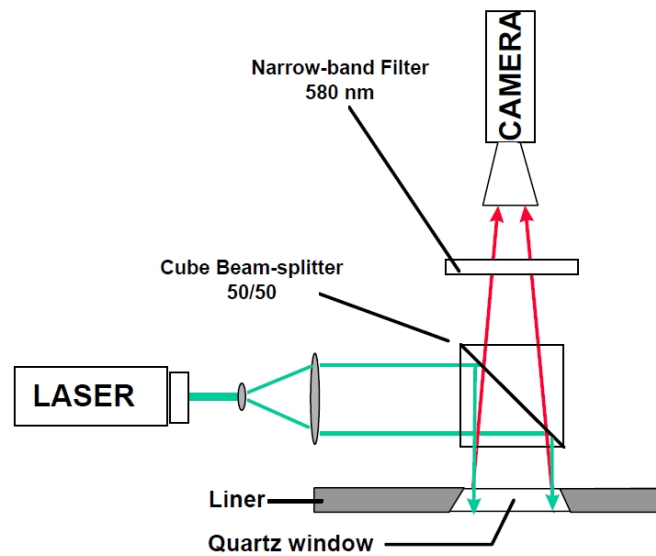


Figure 2-17: 2D LIF system as used by Thirouard (Thirouard, Tian et al. 1998)

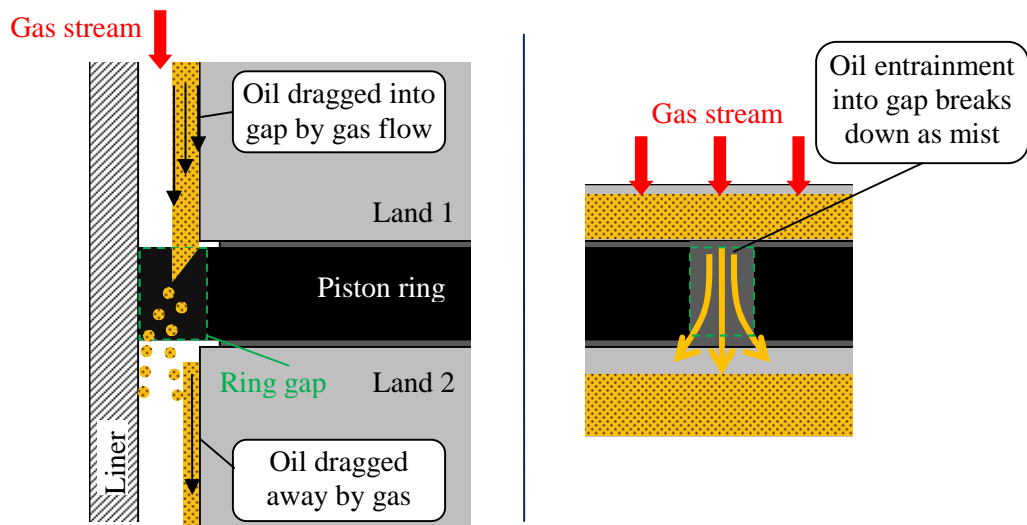
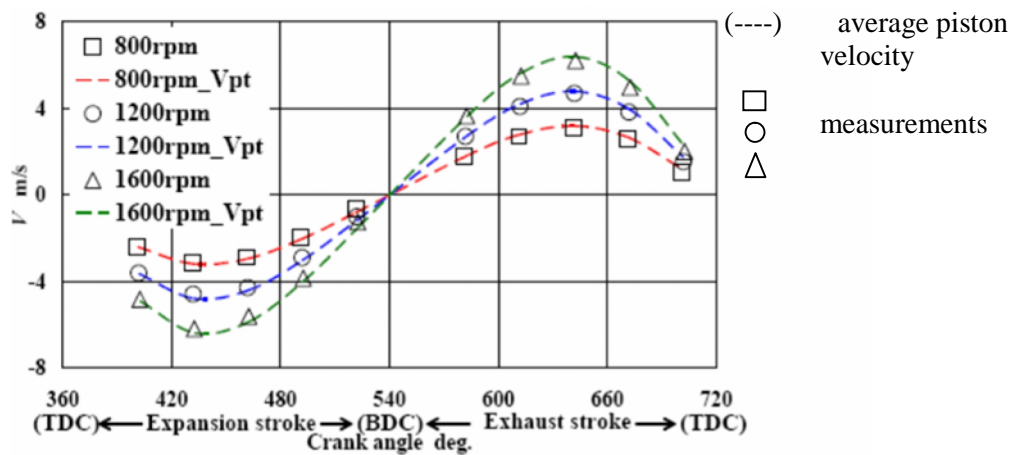


Figure 2-18: Oil misting due to blow-by gases in the ring gaps. Adapted from Thirouard and Tian (Thirouard and Tian 2003)

PIV for lubricant flow investigation is a fairly new concept, and is based on visualisation with results in velocity vectors to examine the oil speed and direction behaviour (Baba, Suzuki et al. 2007). Usually PIV requires tracer particles, so that the velocity has a reference, but in an operating engine these particles would cause abrasive wear. Instead Baba et al. found that the oil film illuminated by LIF, in a quartz cylinder equipped motored engine, was

constant during a small time period allowing artificial vectors to be introduced to a known time frame for oil flow velocity measurements. Baba et al. found that the oil velocity is close to the theoretical piston speed, Figure 2-19 and that any difference occurs just after BDC when the oil film exhibits a small time delay. It was also noted in another test that at the same engine speed the oil film velocity is greater in a motored engine state than when fired. When fired, the LIF data is disturbed by the combustion event (Baba, Suzuki et al. 2007) and this could be causing anomalies in fired results. Clearly PIV coupled with LIF for oil film velocity measurements, is still in its infancy and requires further investigation.



**Figure 2-19: Comparison of oil film velocity by PIV with average piston speed  $V_{pt}$  at various engine speeds (Baba, Suzuki et al. 2007)**

LIF as well as capacitance film thickness measurements do have their limitations. They both cannot cope with lubricant cavitation and as a result anomalies are recorded.

### 2.4.3 Ultrasound method

Recently, a novel method of using ultrasonic frequency to measure the lubricant film thicknesses has been attempted at the University of Sheffield (Harper, Dwyer-Joyce et al. 2005; Zhang, Drinkwater et al. 2005; Dwyer-Joyce, Green et al. 2006; Avan, Mills et al. 2010; Gasni, Wan Ibrahim et al. 2011; Mills, Avan et al. 2013).

The method involves transmitting and reflecting ultrasonic pulses. If there is a film present between two solids, an ultrasonic pulse, directed at the film, will reflect from it. The signal of the reflected pulse is proportional to the stiffness of the film. The film thickness can be

determined from the stiffness providing the acoustic characteristics of the film medium are known (Harper, Dwyer-Joyce et al. 2005).

When investigating lubricant films between the piston ring – cylinder wall interface, this method uses an ultrasonic transducer attached to the outside of the liner, Figure 2-20. The transducer continuously pulses and any reflected pulses, that bounce off the piston as it passes, are recorded along with the incident pulses.

The principle of this process is described below, (Dwyer-Joyce, Green et al. 2006).

The reflection coefficient,  $R_c$ , based on the proportion that is reflected, is related to the stiffness of the layer between the interface,  $k$ , governed by:

$$R_c = \frac{1}{\sqrt{1 + \left(\frac{2k}{\tilde{S}_z}\right)^2}} \quad \text{Equation 2-3}$$

Where  $\omega$  is the angular frequency and  $z$  is the acoustic impedance of the material either side of the layer. This equation is true when the acoustic impedance of the surfaces in the interface are the same and when the ultrasonic wavelength is greater than the film thickness. The stiffness of the lubricant layer of thickness,  $h_{OFT}$ , between an interface is given by:

$$k = \frac{B}{h_{OFT}} \quad \text{Equation 2-4}$$

Where  $B$  is the bulk modulus of the lubricant. Knowing that the speed of sound,  $c_s$ , is governed by the density,  $\rho$ , and the bulk modulus by:

$$c_s = \sqrt{\frac{B}{\rho}} \quad \text{Equation 2-5}$$

Then, combining Equation 2-4 and Equation 2-5:

$$k = \frac{\rho c_s^2}{h_{OFT}} \quad \text{Equation 2-6}$$

Combining Equation 2-3 and Equation 2-6 it is possible to derive the following equation in terms of the lubricant film thickness:

$$h_{OFT} = \frac{2 \dots c_s^2}{\xi_z} \sqrt{\frac{R_c^2}{1 - R_c^2}} \quad \text{Equation 2-7}$$

The technique is capable of measuring thin films in the region between 2 and 21  $\mu\text{m}$  (Dwyer-Joyce, Green et al. 2006) which is respectable when compared to capacitance and LIF techniques. Through strict calibration even thinner films between 0.5-1.3 $\mu\text{m}$  have been reported (Zhang, Drinkwater et al. 2005). Figure 2-21 shows an example of the lubricant film thickness of the piston ring to cylinder wall interface of a motored engine speed of 840 rpm taken from a recent paper (Avan, Mills et al. 2010). The distance on the scale refers to the distance up and down the piston.

Another recent paper from Sheffield University (Avan, Mills et al. 2011), saw a positive step forward with an investigation into simultaneous piston ring – cylinder liner friction and oil film thickness measurement. The test was conducted using a Plint TE77 high frequency reciprocating tribometer with a part of a piston ring and a cylinder liner as the specimens. A series of eight ultrasonic transducers were mounted in an array underneath the liner specimen, and any incident and reflected ultrasonic signals were recorded to provide information of the lubricant film thickness. The speed and load was increased independently to investigate the effects of these with two lubricant samples of different viscosities. It was found that with loads ranging from 40 – 180 N, boundary lubrication was taking place. As the load was increased, the friction coefficient remained constant as the film thickness reduced. However, as the speed was increased, the oil entrainment speed increased causing the oil film thickness to increase and consequently the friction coefficient to reduce (Avan, Mills et al. 2011).

The ultrasonic method relies on the stiffness of the lubricant being known, similar to the dielectric constant of the lubricant being a requirement for capacitance transducers. These rely on the lubricant being isotropic, as they are bulk parameters. There is some argument that the stiffness of the lubricant, and hence the bulk modulus and the dielectric, would change during operation when ring dynamics are considered and at the dead centres where ring reversal takes place and piston frictional forces are greater. The technique can however detect some cavitation of the lubricant, since the method can detect lubricant and air (cavitation). The reflection can only take place off either the piston ring, for film thickness measurements, or air, for cavitation investigation, it cannot however, measure both cavitation and lubricant film thickness (Avan, Spencer et al. 2013).

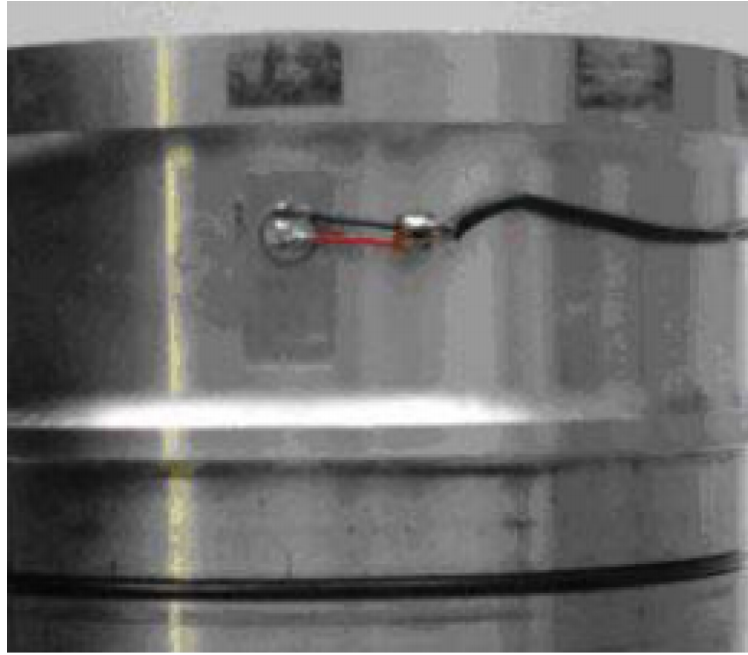


Figure 2-20: Ultrasonic transducer mounted to outside of liner (Dwyer-Joyce, Green et al. 2006)

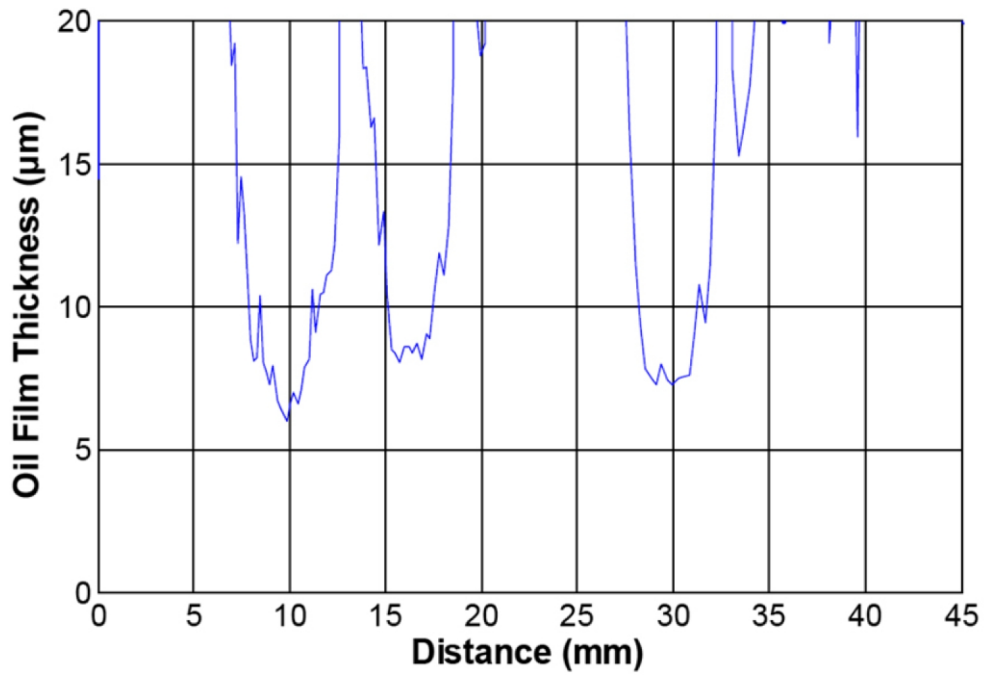


Figure 2-21: Typical OFT measurement of the piston ring – liner interface using ultrasound at a motored engine speed of 840 rpm (Avan, Mills et al. 2010).

#### 2.4.4 Summary of the measured film thicknesses in the literature

A summary of the lubricant film thicknesses measured between the piston ring and cylinder wall by some researchers in the past is presented in Table 2-1. This information is based on what engine type and speeds, engine operating condition; either fired or motored, and the type of film thickness measurement technique that was employed. Those with a ‘\*’ are an approximate range deduced from the graphs in the relevant journal papers.

Reference	Method	Engine Type	Engine Operation	Engine Speed (rpm)	OFT range ( $\mu\text{m}$ )
(Söchting and Sherrington 2009)	Capacitance	Diesel	Fired	2000	4.0-12.0
(Radcliffe 1993)	Capacitance	Gasoline	Motored	1000	1.6-5.8
(Brown and Hamilton 1978)	Capacitance	Diesel	Motored	200-800	5.0-13.0*
(Moore 1985)	Capacitance	Diesel	Motored	1000	0.9-2.0
(Dhar, Agarwal et al. 2009)	Capacitance	Diesel	Motored	1300-1400	0.2-8.2
(Seki, Nakayama et al. 2000)	LIF	Diesel	Fired	1500-2000	0.5-4.0
(Taylor and Evans 2004)	LIF	Diesel	Fired	1000	0.9-4.7
(Takiguchi, Nakayama et al. 1998)	LIF	Diesel	Fired	2000	0.6-3.5
(Avan, Mills et al. 2010)	Ultrasound	Diesel	Motored	840	6.0-8.0*

**Table 2-1: A summary of the lubricant film thickness as measured at the piston ring through various experimental techniques and conditions by previous researchers**

From Table 2-1, the first striking piece of information is that lubricant film thickness measurements have rarely been conducted on gasoline engines, and as a result the tested engine speeds are low. Many commercially available diesel engines now have the technology to have higher speeds approaching those of gasoline engines. The fact that diesel engines have been considered the choice for film thickness measurements by researchers, could be due to the fact that diesel engines generally have a larger access area for probes than in gasoline engines.

The three lubricant film thickness techniques have very similar film thickness measurement ranges, with the exception of ultrasound which is developing rapidly. All methods do however, require a strict calibration procedure to ensure the film thickness measurements are within order. Capacitance and LIF have similar oil film thickness measurement range. The ultrasound measurements currently have a much narrower range but is a newer technique being developed. Sherrington (Sherrington 2011) has suggested that film thickness methods in general will continue to be used for research and development purposes and as technology advances, the possibility of providing an online piston ring oil film thickness measurement with feedback control, to optimise the lubricant flow to the ring pack, looks promising.

For this research, LIF was chosen over the other film thickness methods since there is a possibility to combine a future idea of measuring the chemical composition of the lubricant, through the same optical observation window, using infrared absorption techniques thereby improving the understanding of piston ring lubrication during service.

## 2.5 Summary

In the introductory chapter and this literature review chapter, an overview of the technology and importance of piston ring research for reciprocating internal combustion engines has been made. This has included:

- the operation of the internal combustion engine and the role of the piston ring pack
- the development, design and coating considerations of the piston rings
- a brief account of engine lubrication, degradation and common detection and sampling methods
- a literature review of theoretical piston ring research
- a literature review of experimental piston ring research including specific research related to lubricant transport and consumption mechanisms, with the benefits and the different methods of measuring the lubricant film thickness within the piston ring – cylinder wall interface

The literature review shows that there is a need to understand the tribology of the piston ring pack. There has been much research on modelling of piston ring to cylinder wall lubrication which discusses fully flooded, starved and elastohydrodynamic operating conditions, with experimental research proving initial theories and predictions

It can be seen how the state of the lubricant within the piston ring pack plays an important role in mechanical energy losses. There is little detailed knowledge of how the lubricant

degrades with time. This is primarily by oxidation, which affects the tribological behaviour within the piston ring pack, which in turn impacts fuel economy and exhaust emissions. Knowledge of the lubricant film thickness between the piston rings and the cylinder wall is fundamental to our understanding of engine tribology.

One of the major issues in the automotive industry is that there is no clear indication yet of when a lubricant requires renewal based on the condition of the lubricant. The manufacturers base their oil drain intervals on experience with engine oils that meet the international specifications be they European (e.g. ACEA) or American (e.g. ILSAC GF-5)

This project is aimed at bridging that gap between lubricant performance and lubricant degradation.

The project objectives were outlined in the first chapter. This project will make use of laser induced fluorescence (LIF) as a means to investigate the lubricant film profile in two gasoline engines; a bench top motored rig and a research engine based on a production engine, as the lubricant changes composition in terms of chemical degradation and viscosity change when in service. The influence of extracting lubricant from the TRZ of the piston ring pack can also be assessed and measured when simultaneously measuring lubricant film thickness and extracting TRZ lubricant samples. The LIF system also has the scope to be coupled with in-situ chemical analysis using infrared spectroscopy to provide lubricant film thickness and lubricant quality information in the future.

# **Chapter 3 Development of a Laser Induced Fluorescence Technique on a Motored Engine**

The design and manufacture of a laser induced fluorescence (LIF) apparatus to measure the lubricant film thickness within the piston ring - cylinder wall interface is described in this chapter. This chapter also introduces the first engine, a Volkswagen (VW) horizontally opposed motored engine, used for the development of the LIF system.

The VW engine has been used in the past for piston ring lubricant film thickness and friction measurements (Radcliffe 1993; Thomson 1996). For this research, its primary use was to aid development of the LIF imaging system since it only offers motored operation before a final move to the Ricardo Hydra for fired engine investigation. The VW engine underwent numerous modifications which are outlined in this chapter. Laser fluorescence principle theory is introduced along with the design considerations for the optical system. Extensive calibration, and the variables that influence the fluorescence signal, was also conducted with various calibration ideas proposed and tested as outlined in this chapter.

## **3.1 VW horizontal piston motored engine**

### **3.1.1 Specifications and previous OFT work on engine**

The LIF system was developed and tested on a motored engine since this is an intermediate step between a test rig and a fired engine. As an additional benefit, the motored engine allowed good control over the environment and is excellent for test development. The motored engine, Figure 3-1, was designed and commissioned by Radcliffe in 1993 for his doctorate, which investigated lubricant film thickness and friction simultaneously in a piston ring assembly (Radcliffe 1993). In an attempt to keep manufacturing costs low, Radcliffe decided to use as many OEM engine components as possible. A 1970cc VW Type 4 horizontally opposed gasoline engine, with engine code CU, was acquired. The engine originally had four cylinders of 94 mm bore diameter and 71 mm stroke, but for research

purposes, the crankshaft was reduced in length to only allow two cylinders to be motored. One of the cylinders housed the standard VW piston assembly specification setup, whilst the

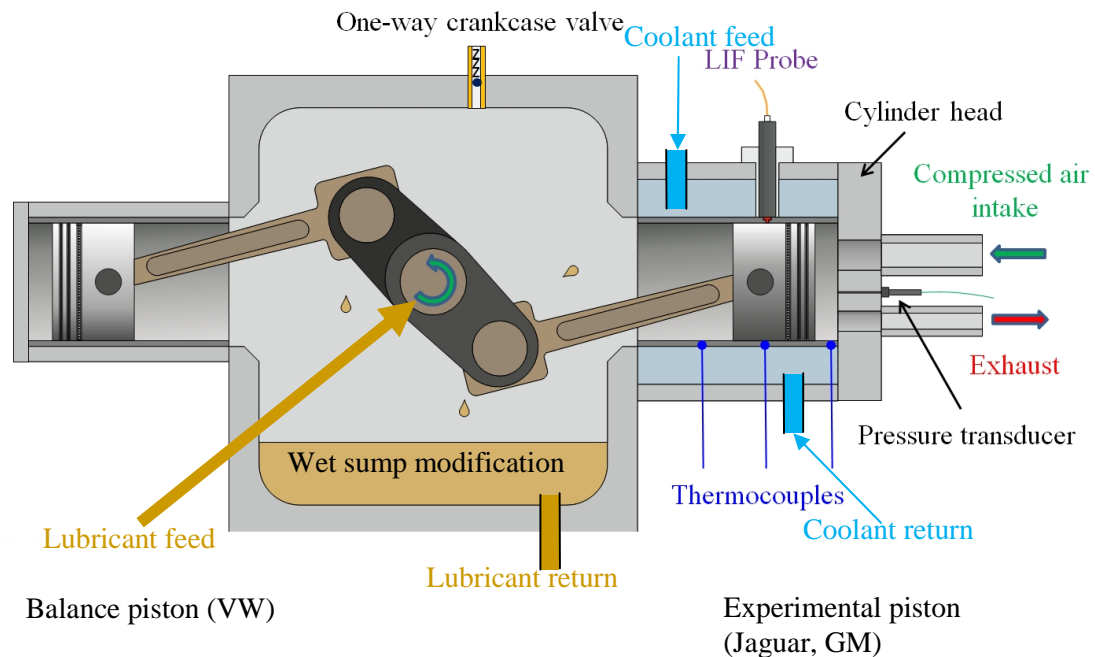


**Figure 3-1: A schematic of the modified motored engine used for the development of the LIF system**

other cylinder was initially adapted for a smaller diameter Jaguar V12 piston assembly with a new 90 mm diameter bore cylinder liner. The small end bush of the connecting rod only required a slight ream to accept the Jaguar piston. This adapted cylinder was used for the experimental investigations and the change to a Jaguar piston was motivated by a project sponsorship from Jaguar Cars Limited (Radcliffe 1993). The work continued with Thomson who added thermocouples to include liner temperature profiles along with the film thickness and friction results (Thomson 1996). The Jaguar piston and cylinder liner were replaced by the same diameter GM piston, with 86mm diameter, as used in the Ricardo Hydra engine and a new liner at a later date, but no documentation exists of the change. In all cases, the heavier VW piston was turned at the crown to be equally balanced by mass to the test piston.

The instrumented piston side incorporates a floating liner which is rigidly attached at the lower end to three Kistler 9311A force transducers, which are fed in parallel into a Kistler 5011 charge amplifier. The top of the liner is not attached rigidly, but is fixed in place with a 102 micron shim in-between the cylinder head and the liner, coloured in red in Figure 3-2.

The shim forms a seal between the cylinder head and the barrel, and hence the coolant, but also has been designed so that only a small force is exerted on the liner. This allows the liner to react entirely to the piston ring pack friction in the axial direction, which is measured by the force transducers and is known as a force balance seal. This has been used by researchers in the past when instrumenting floating cylinder liners (Furuhashi and Sasaki 1983; Parker, Adams et al. 1989). More about the engine can be found in Radcliffe's thesis (Radcliffe 1993).

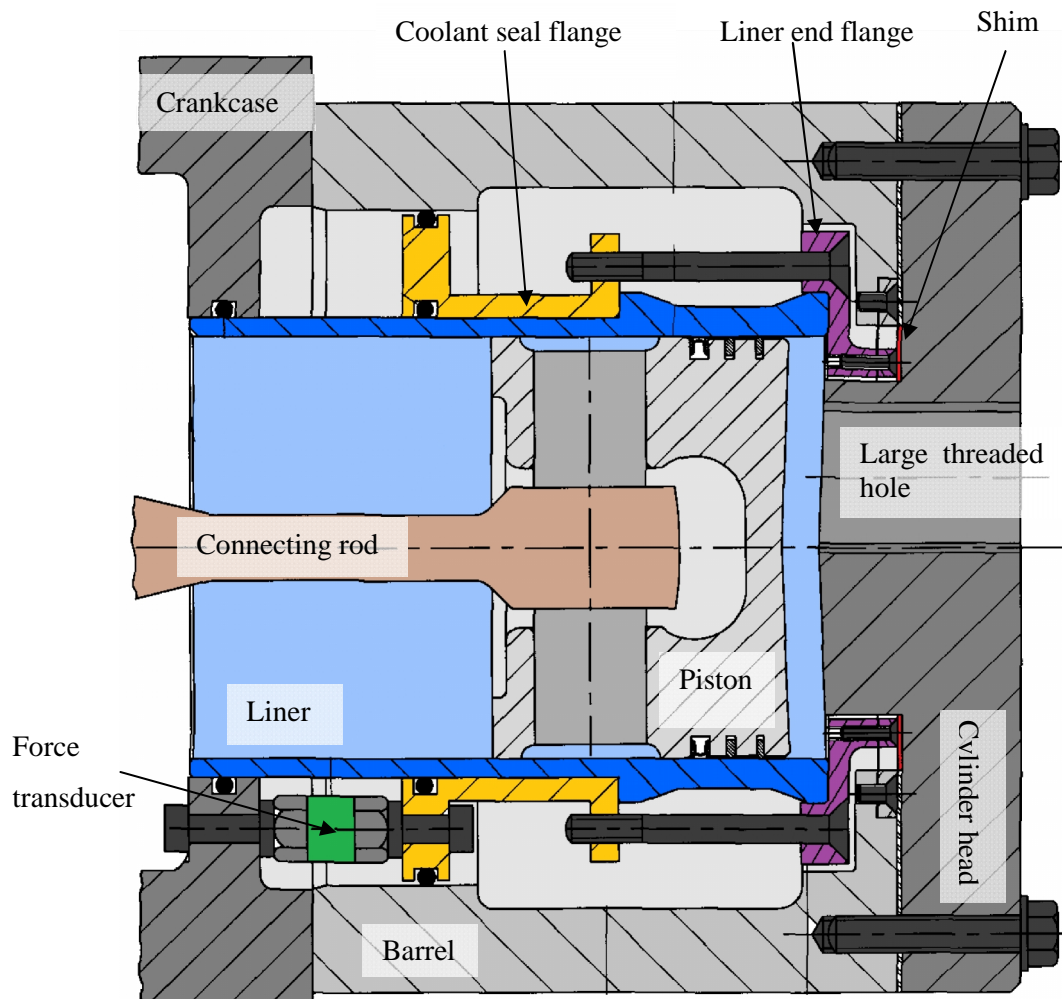


**Figure 3-2: A cross section of the experimental cylinder. Adapted from (Radcliffe 1993)**

The crankshaft is driven by a Hainsworth Speedranger 2.2 kW, direct current motor, via a pulley belt system and sits on a platform below the engine. The maximum speed of the engine was originally in excess of 3000 rpm, but was altered because of the poor starting torque of the motor. It was found that if the piston rested at either near TDC or BDC after its

previous run, the lower piston speeds at these positions relied on higher starting torques than the motor was specified for, to turn the engine. The engine can be run with or without a cylinder head (no compression pressure), and using a head caused this problem to be even worse. To rectify this problem, the pulley on the crankshaft and the motor spindle was swapped to allow for a speed reducing setup. This provided increased starting torques but with the penalty of a now lower maximum engine speed of 1450 rpm.

During the on-going development of the LIF system, many modifications to the engine were made in an attempt to improve the engine either for the benefit of the LIF system or the engine itself. The next sections describe in detail the modifications to the crankcase breather system, cylinder compression pressures and method of supplying the coolant and lubricant.

### **3.1.2 Modifications to lubricant and coolant supply**

In the original configuration, the engine lubricant was a dry sump setup, and was used to lubricate the mechanical components and also act as a coolant in the barrel for the instrumented cylinder. A Haake 10 litre heated oil bath, which was situated on the floor, had an internal thermostat controller and an internal pump to supply lubricant coolant to the experimental barrel, and an additional Baldor direct current 29 hp oil pump was used to provide a high flow of lubricant to the two crankshaft bearings, into the connecting rod big ends and spray towards the piston assembly. The feed and return pipes for the engine oil pump were placed directly into the heated oil bath. Oil flow to the engine bearings was pressurised via a hydraulic pressure regulator and oil flowed through a high efficiency Pall oil filter. The oil pressure was indicated via a pressure gauge and the oil returned back to the bath under gravity. Lubricant was used as the coolant as opposed to antifreeze since it could be used as a coolant to remove heat from the piston assembly, be heated to provide temperature controlled analysis of the piston assembly and it is a rust inhibitor. The original system itself was perfect for the motored engine. However, since there is a large lubricant sump volume, it was expensive to dope a large amount of lubricant for fluorescence investigation with fluorescent dye. The smallest lubricant bath available was only 5 litres but this did not have an internal pump and could not be used for the coolant. So, a change in the lubricant supply system was required.

The heated bath was to remain as the supply for the coolant to the barrel. The crankcase volume is approximately 7.5 litres and is therefore large enough to contain two litres of test oil to lubricate the internals without affecting the displacement volume of the engine. So, the system was changed from a dry to a wet sump system, modification as shown in Figure 3-1.

This also allowed the lubricant, originally used for the barrel coolant and that for the engine internals, to be separate and different, and thereby allowing the sump test oil to be doped in much smaller quantities. During this change, it was also noted that the coolant seal flange that secures the liner in place and fits inside the barrel providing a seal of the coolant from the crankcase, coloured in yellow in Figure 3-2, had sections removed where an o-ring would seat, and as a result the coolant was not sealed from the crankcase. The flange, originally designed by Radcliffe (Radcliffe 1993), was modified by Thomson for passing liner thermocouples to a cut-out on the side face of the barrel (Thomson 1996). To rectify this, a new flange was turned from mild steel to the original specification as designed by Radcliffe. There was now a seal between the coolant jacket and the crankcase and a wet sump system could now be implemented. The two separate pipes in the bath; oil feed and return, were removed from the bath and connected with a straight connector and jubilee clips, thereby removing the use of the heated bath as a dry sump for engine lubrication. Two litres of test lubricant was then poured into the crankcase from the case cover. The initial test saw the lubricant aerate as air was being drawn in from an open loop. Originally, there was an additional lubricant drain on the cover for the balance piston which returned excess oil in the crankcase breather system to the lubricant sump, mentioned in Section 3.1.3 below. During engine operation, air was drawn in from the crankcase breather and caused the oil to aerate. On inspection, the balance piston had the crown removed for balance purposes, as mentioned in Section 3.1.3 below, and hence did not require any means of a breather since the piston was just moving. The drain was capped off and the engine was now operating with a wet sump system without the oil aerating.

### **3.1.3 Modifications to crankcase breather system**

Radcliffe experienced numerous issues regarding the crankcase breather system (Radcliffe 1993). As both pistons come to BDC together and the crankcase volume is small, the frictional measurements suffered due to pressure fluctuations in the crankcase. Various attempts to provide a breather system that would not pressurise the crankcase and dampen the pressure fluctuations were tried and tested. The purpose of a crankcase breather system is first to allow air into and out of the crankcase and as a secondary effect, separate any oil mist. Radcliff designed a system consisting of 50 mm diameter PVC plumbing piping which allowed air to flow between the crankcase and the combustion chamber of the non-instrumented piston, Figure 3-3. The piping was also open to the atmosphere with a gauze used as an air filter to prevent dust from entering the engine. Radcliffe found that the system worked well in terms of the cyclic variation in pressure, but suffered from large amounts of

oil misting in the long pipe connections which would eventually end up in the atmosphere. The piping system was also found to be choked at the higher speeds possibly due to the small diameter piping. To correct this, a large 25 litre drum was placed above the crankcase in an attempt dampen the cyclic variation and minimise the effect of choking. The drum was sealed and any oil collected in the drum could be drained back into the sump (Radcliffe 1993).

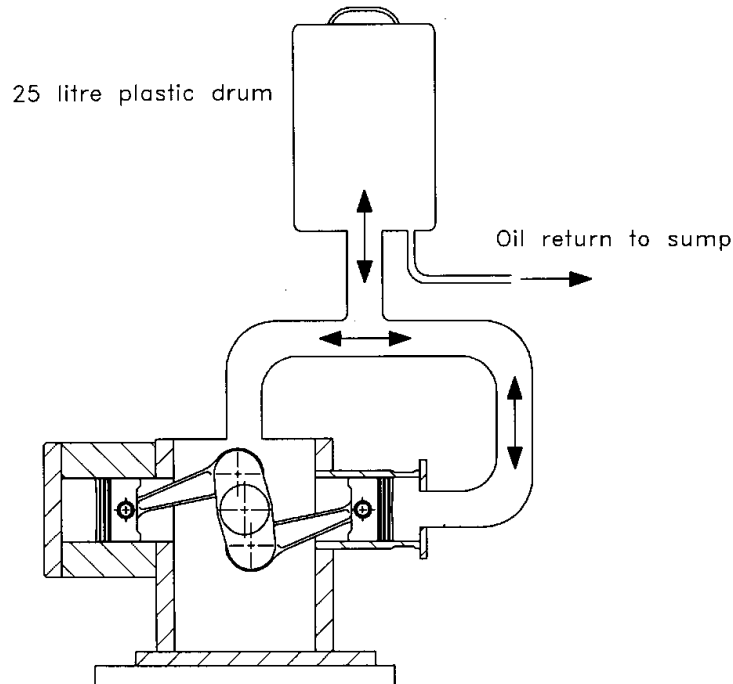


**Figure 3-3 : Original crankcase breather system (Radcliffe 1993)**

When this project commenced, the pipe work was only remaining on the engine and required replacing as some of the pipes were cracked. Since the fittings on the crankcase cover and the end cover on the balance fitting were designed to accept 50mm inner diameter, the same size of hydraulic pipe system was used. There was no way of suspending a similar large container from the ceiling so instead a 1.2 m long pipe of 50 mm diameter was used instead, which was placed above the crankcase, and an aftermarket vehicle air filter was placed on top. The system worked well and did not require any additional oil drain as the oil would simply flow back down the pipe into the crankcase. However, since the crankcase had a large 50 mm diameter opening, it was found that approximately 0.5 litres of oil was getting trapped in the pipe system during engine operation and took some time to drain back into the crankcase after engine shutdown. As mentioned in the above Section 3.1.2, the lubricant supply system originally served a dual purpose; one to provide lubricant to the mechanicals

of the engine and two, to act as a coolant for the instrumented piston where compression took place. On the original 10 litre lubricant supply system, 0.5 litres of lubricant trapped in the pipe work was not an issue. When the system was changed to a wet sump application, it was found that the oil pressure to the bearings was reduced at higher engine speeds due to a lack of oil in the 2 litre sump system. As a result, a rethink on the crankcase breather was required.

There was no need to balance the air flow between the piston, in the non-instrumented cylinder, and the crankcase since the piston crown had been removed for balance purposes. So this meant that the air in the crankcase and on the instrumented piston side required exhausting to prevent the crankcase from pressurising. In modern engines, as a means of blow-by gas contribution to emissions, positive crankcase ventilation (PCV) systems are used. A PCV system vents blow-by gasses that escape past the piston assembly into the crankcase back into the intake system to be reused as opposed to the atmosphere, thereby reducing harmful emissions. Various attempts were made to implement such a system on the motored rig. In the initial attempt, a ¼" BSP Martonair non return valve was fitted on the crankcase top cover which expelled air into a 3/8" diameter PTFE tubing straight into a ½" BSP Martonair non return valve fitted to the cylinder head. It was found that air was pulsating back and forth in the PTFE tubing during engine operation, as an oil droplet was seen to be 'stuck' in one position in the tube. The tube eventually burst due to excessive heating and the idea was scrapped. The biggest problem was the cylinder head. There was insufficient room to use a larger fitting, and hence larger tubing, since the head was occupied by a Kistler 601 pressure transducer and a large bolt to adjust the compression ratio and hence compression pressure. It was decided to keep the non-return valve on the crankcase cover and expel the air to a separate large 5 litre container which was then vented to the extraction system. The crankcase experienced a lower pressure when the pistons headed towards TDC thereby allowing the oil to remain in the bottom of the sump rather than as a mist in the crankcase and retain oil pressure at the bearings. A pressure gauge was later fitted to the crankcase to determine if the crankcase pressurised and a fluctuation of 5 psi in pressure was observed. The same collection container was later used as the exhaust for the instrumented cylinder as mention in the next section.

### **3.1.4 Modifications to cylinder pressure**

For basic engine simulation a motored engine is highly recommended over a fired engine, since an expensive engine control system and toxic exhaust extraction system is not required. However, attaining similar engine operating conditions is far more challenging with motored

engines. In particular, having high cylinder peak pressures is extremely difficult since there is no combustion to enhance cylinder pressures. It was always desirable to have higher cylinder pressures for the LIF system so that film thickness profiles resemble those of a fired engine. Radcliffe used a 1/2" BSP Martonair non return valve for the inlet which had a cracking pressure of 16 bar.

The cylinder head was fitted with a large bolt which extended into the chamber, of which when loosened, reduced the cylinder compression ratio (cr), due to the increase in the clearance volume, and as a result provided a means of reducing the peak pressure from a maximum of 16 bar. The bolt needed to be secure when the desired compression ratio was set so that the bolt did not come loose with engine vibration and hence alter the ratio during engine operation. A set of three spacers of different lengths providing a means to secure the bolt, Figure 3-4, and allowing for 3 different compression ratios of 7.4:1, 9.4:1 and 11.6:1, were made. Peak cylinders pressures of 9, 13 and 16 bar respectively were now possible at 1200 rpm, whereas before Radcliffe would achieve 16 bar at engine speeds around 3000 rpm (Radcliffe 1993). Even though there were now three different engine loading operations, it was inconvenient to constantly change spacers and something more variable was considered.

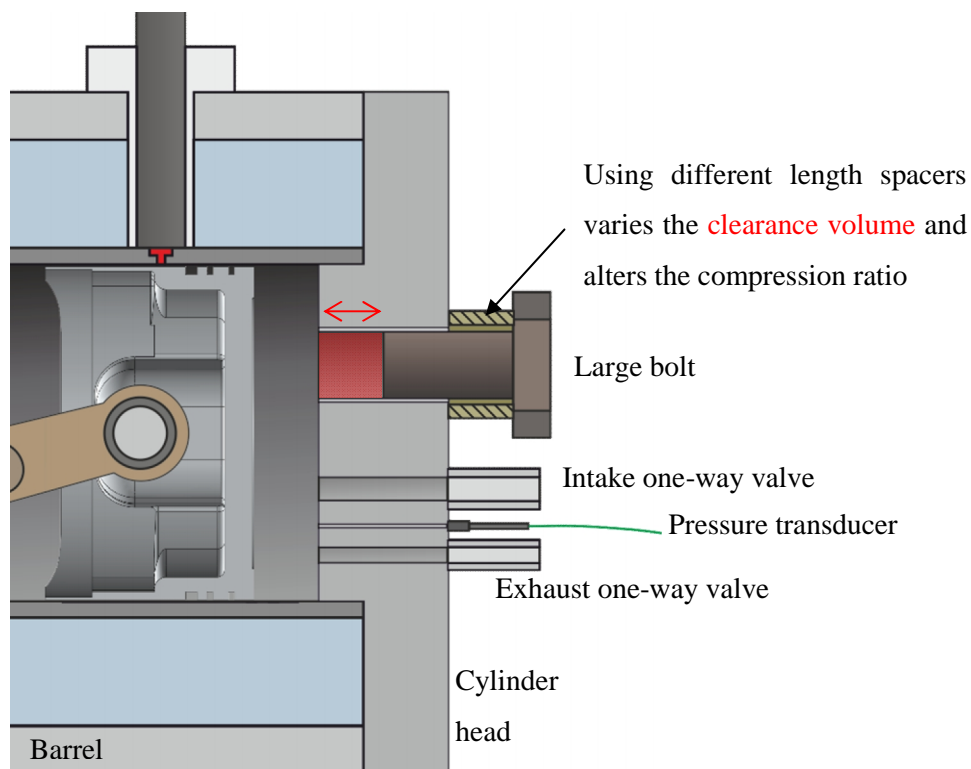


**Figure 3-4: Schematic of how compression ratio of cylinder was adapted**

A pneumatic airline, with a maximum pressure of 10 bar, was used to provide a means of forced induction and increase cylinder peak pressures. The airline was connected to a Norgren air pressure regulator to reduce and vary the flow rate of the incoming air. A ½” BSP schrader valve was fitted to the non-return valve on the inlet on the cylinder head and the pressure regulator connected to this permanently. It was now possible to vary peak cylinder pressures and increase them above 16 bar. A maximum of 1.5 bar of forced induction, at 1200 rpm, provided a cylinder peak pressure in excess of 25 bar. At these peak pressures the drive became unstable and either reduced in speed or the motor shut down. As a result of this, the engine peak pressure was capped at 22 bar throughout this research to remain below the maximum load capacity of the motor. A summary of the variation of peak cylinder pressure with and without forced induction and the use of 3 different spacers, thereby altering the compression ratio, at varying engine speeds is shown in Table 3-1, Table 3-2 and Table 3-3. A schematic of the engine system complete with the LIF probe and the compressed airline intake is shown in Figure 3-1.

Speed (rpm)	With Forced Induction (bar)	Without Forced Induction (bar)
500	17	13
800	18.5	14.8
1000	19.3	15.4
1200	20.2	15.7

**Table 3-1: Variation of peak cylinder pressures with and without forced induction at 11.6:1 cr**

Speed (rpm)	With Forced Induction (bar)	Without Forced Induction (bar)
500	14.8	10.8
800	16.9	11.5
1000	17.8	12.3
1200	18.1	12.6

**Table 3-2: Variation of peak cylinder pressures with and without forced induction at 9.4:1 cr**

Speed (rpm)	With Forced Induction (bar)	Without Forced Induction (bar)
500	13.7	8.3
800	15.1	8.8
1000	15.8	9.1
1200	16.4	9.2

**Table 3-3: Variation of peak cylinder pressures with and without forced induction at 7.4:1 cr**

## 3.2 Laser induced fluorescence (LIF)

### 3.2.1 Fluorescence principles

Fluorescence is a effect used to identify specific components within chemical and biological bodies. It can provide a wide base of information of a part which may seem difficult to identify with the naked eye. Dyes and stains are generally used as these have a fluorescent component allowing specific molecules to be detected with surprising sensitivity and selectivity.

Depending on the dye, some electrons have the capability of being excited to higher internal energy states through absorption of light energy. These molecules are unstable at this higher internal energy state and decay resulting in light being emitted. This activity is known as fluorescence and those molecules with the ability to fluoresce are known as fluorophores. The principles of this process are described below, (Hauglan 2005).

Fluorescence is a three stage process as shown schematically in Figure 3-5 below.

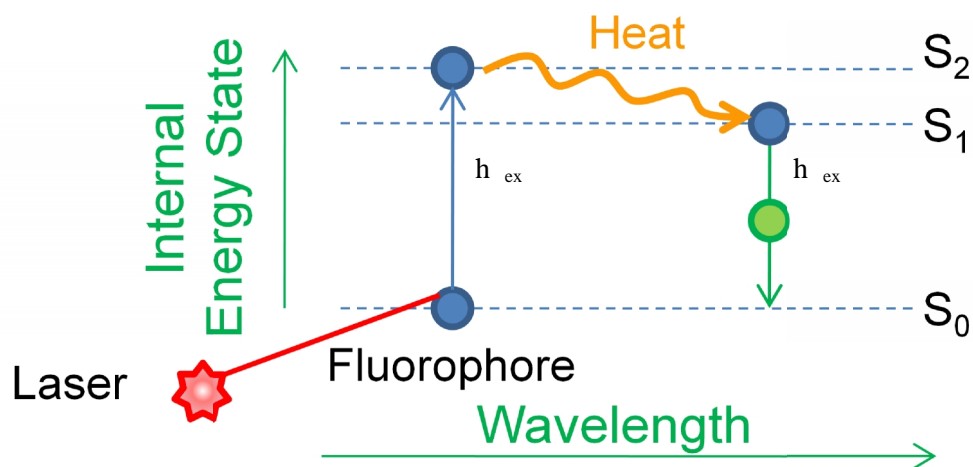


Figure 3-5: Diagram illustrating fluorescence process (Hauglan 2005)

Stage 1: Excitation - At the energy ground state,  $S_0$ , the fluorophore is stable and does not fluoresce. When a photon (light) of energy,  $h_{ex}$ , (where  $h$  is the Planks constant, and  $\nu$  is the frequency) from an external source such as that from a laser or incandescent lamp strikes the fluorophore it is absorbed exciting the molecule to a higher state,  $S_2$ .

Stage 2: Excited-state lifetime - The fluorophore undergoes a multiple number of interactions within its molecular environment and can also exhibit multiple excited levels depending on the energy and frequency of the external source. At these excited levels the fluorophore is unstable and decays to a lower energy level,  $S_1$ , by releasing some heat energy to become semi-stable. The length of time the fluorophore is in excited states is known as the excited lifetime and typically lasts for 1-10 nanoseconds.

Stage 3: Fluorescence emission - Next the fluorophore molecule returns to the ground state from the semi-stable state. As it does this a photon of energy,  $h\nu_{em}$ , is emitted and released as light. The energy of the photon is lower than that of the photon provided from the external source and as a result the wavelength of the emitted light is longer. This provides the inherent colour change in light emitted to that which it is exposed to.

In summary:

$$E = h \nu_{ex} = S_2 - S_1 \quad \text{Equation 3-1}$$

$$h \nu_{em} = S_1 - S_0 \quad \text{Equation 3-2}$$

$$S_1 - S_0 < S_2 - S_1 \quad \text{Equation 3-3}$$

Hence,

$$\nu_{em} < \nu_{ex} \quad \text{Equation 3-4}$$

Since,

$$\lambda = \frac{c}{\nu} \quad \text{Equation 3-5}$$

where  $\lambda$  is the wavelength and  $c$  is the wavespeed and is constant, then,

$$\lambda_{em} > \lambda_{ex} \quad \text{Equation 3-6}$$

Since the fluorophore is capable of returning to its initial ground state it is capable of absorbing light energy yet again and repeating the entire process generating multiple signals from the same molecule. This is an ideal situation and in reality increased duration of exposure and intensity of the external source to the fluorophore would result in diminishing fluorescence since the structure of the molecule changes prohibiting its ability to fluoresce. This effect is known as photobleaching.

### 3.2.2 Stokes shift

As mentioned earlier the emitted fluorescence signal is of a longer wavelength than the one absorbed as Equation 3-6. The energy difference between the two ( $h\nu_{EX} - h\nu_{Em}$ ) is known as the Stokes Shift (Hauglan 2005) as can be seen in Figure 3-6.

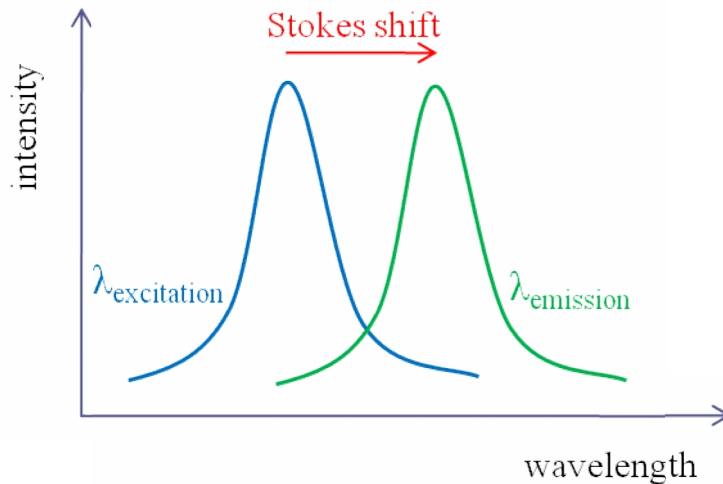


**Figure 3-6: Illustration of Stokes Shift theory**

The magnitude of the Stokes Shift is fundamental to the sensitivity of the fluorescence emission since it allows the photons emitted to be isolated from the excitation photons (Hauglan 2005) allowing easier detection.

In summary, the spectra excited and emitted contains important information for detection analysis using the fluorophore appropriately and effectively.

### 3.3 LIF system

This research continues the development of the LIF system from an undergraduate student, Rahimiardali (Rahimiardali 2008), who initially set the system out but did not manage to complete the system and achieve a film thickness measurement from the piston assembly. His original design included an optical arrangement of coloured filters, a 600  $\mu\text{m}$  core fibre optic cable and a collimator probe tube of 16mm diameter and housing two planoconvex lenses of 10mm diameter. The collimator tube sat in-between the fibre optic and a sapphire window in the cylinder liner, and provided a means of collecting all diverging light from the end of the fibre optic, making it parallel before focussing the light into the window for examination. The optical arrangement was attached to the laser head and included room for

two photomultiplier tubes (PMT), photon counting detectors, to measure both incoming laser (PMT 1) and returning fluorescence light (PMT 2), but was incorrectly designed and only allowed detection of the fluorescence return signal, as shown in Figure 3-7. A new optical system with new PMTs was designed for this research. Rahimiardali's collimator probe and the fibre optic cable were redesigned following problems with sealing the collimator probe from the coolant jacket on the motored engine and alignment issues with the sapphire window in the liner.

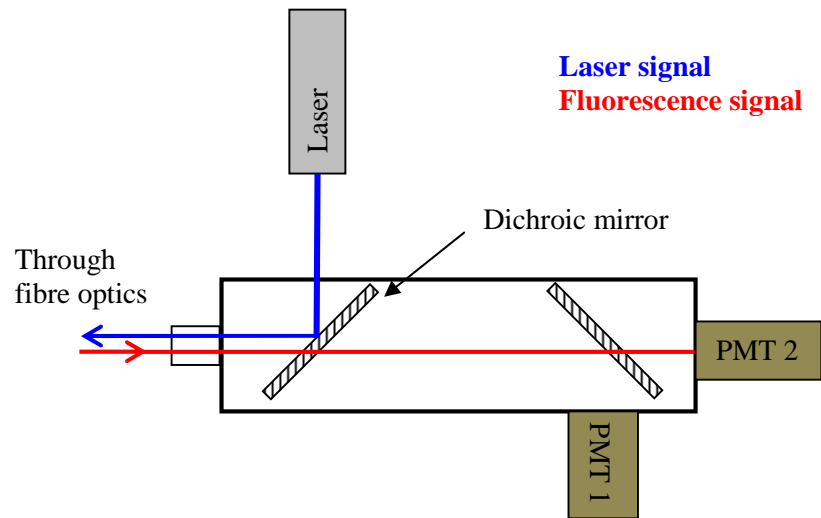


**Figure 3-7: A schematic of the original optics arrangement as used by Rahimiardali (Rahimiardali 2008)**

The probe system was always situated at piston mid-stroke since this is where the thickest lubricant films would be expected because the piston speed is about its maximum. The probe system was capable of examining the complete piston ring pack as it passed the window in the liner in both directions. At TDC, the oil behaviour on the piston skirt could also be observed.

### 3.3.1 Laser system and optical arrangement

A Melles Griot Argon-Ion Series 543 continuous laser was available. It had an adjustable wavelength range from 465 – 514 nm along with a variable laser power output from 125 to 250mW. The laser head is connected to a Melles Griot Series 400 power supply and heat extraction system. Pyrromethene 567A dye was the fluorophore chosen which has a hydrocarbon chemical structure and absorbs 488 nm laser emission well and fluoresces at a peak wavelength of 543 nm giving a substantial stokes shift (55 nm). The peak fluorescence

also worked well with the transmission spectrum of the dichroic mirror with transmission rates of approximately 94% at 543 nm.

For laser transmittance to the engine and fluorescence signal separation, a bespoke light tight enclosed optical system was designed using off the shelf parts from Thorlabs, Inc which was attached to the laser head source. The original fibre optic cable was used to transmit and collect laser and fluorescence signals to and from a sapphire window, which provides the optical access to the piston assembly, in the cylinder liner. The original available system consisted of a 10 mm diameter collimator probe and a 600  $\mu\text{m}$  single mode fibre optic cable. The schematic in Figure 3-8 illustrates the optical system and the parts inventory is provided in the Appendix A1.

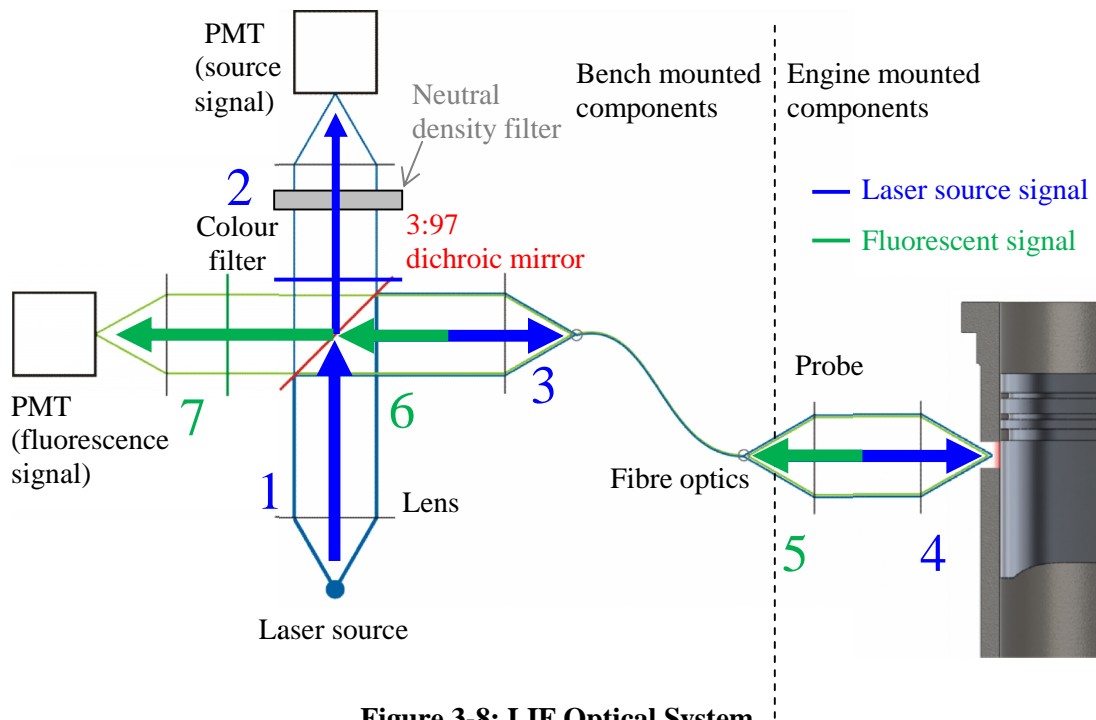


**Figure 3-8: LIF Optical System**

As can be seen from the schematic in Figure 3-8, the optics is split between those that are bench mounted and those that are engine mounted. An air-sprung optics bench was used to provide a vibration free optics arrangement with minimal environmental disturbance. From the laser emission (488 nm) (1), the beam is split at the centre of the optics at an ideal reflectivity-transmission ratio of 97:3 so the majority of the light is used in the engine for absorption and a small amount of light transmits through the mirror, a blue filter, a biconvex lens and finally into a PMT (2), so that the incoming laser source signal is recorded. Since this PMT just observes continuous strength laser light, a neutral density filter of optical

density 2.0, which reduces the intensity of the incident light to 1% of the original, was placed in front of the PMT to reduce the laser intensity and prevent premature burnout of the PMT. The reflected laser light travelled past a biconvex lens which focused the light through a multi-mode fibre optic cable with a 600  $\mu\text{m}$  core diameter (3). This cable was eventually changed to a smaller core diameter of 105  $\mu\text{m}$ , to improve the signal to noise ratio. The fibre optic screws into a collimator probe mounted in the engine, which houses two plano-convex lenses, with the flat side of each lens facing away from each other as illustrated Figure 3-8, and provides a means of collecting laser light and making it parallel before refocusing it to its destination whether that be the laser light into the engine or the fluorescence return into the fibre optics (4, 5). The initial collimator probe had spacers in between the lenses to set the desired focal length, as shown in Figure 3-9 below. The return fluorescence (543 nm) (6) is outside the operable range of the dichroic mirror and hence transmits through the mirror, at a reflectivity-transmission ratio of 6:94, through a green filter, through a biconvex lens and finally into an additional PMT to measure the fluorescence intensity (7).

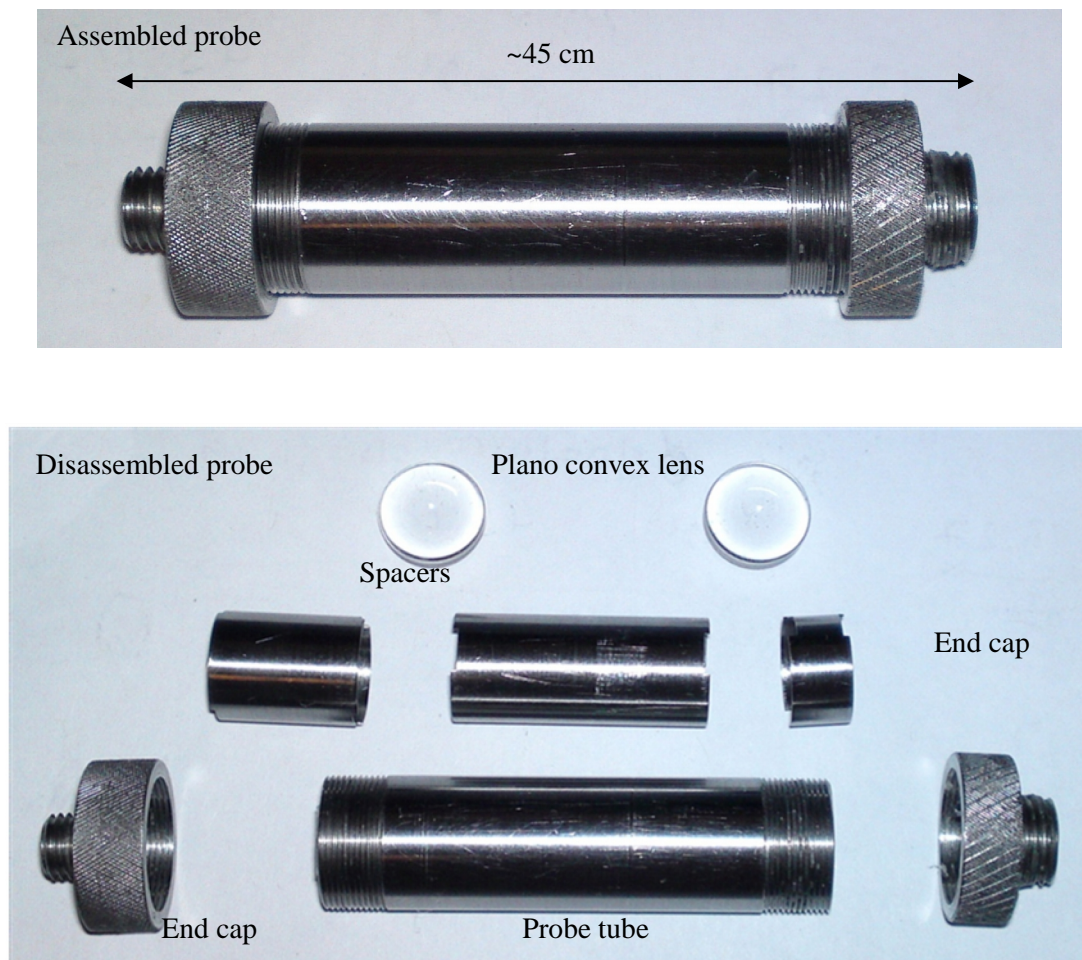


**Figure 3-9: Original complete assembled collimator probe and dismantled probe**

There were continuous problems with sealing the probe designed by Rahimiardali from the coolant jacket, as the probe was mounted in a matching thread machined into the cylinder liner, and coolant would leak into the threads of the probe cap ends and the space between the probe and the cylinder liner. It was not a simple case of increasing the tightening torque of the probe to the liner, since the probe would touch the window surface and damage it. Paper gaskets were made in an attempt to improve the seal of the probe at the cylinder liner interface and this proved successful, Modification 1 in Figure 3-10. However, the seal on the probe cap end threads was still problematic. The small access window in the barrel to fit the probe in place meant adding any silicone sealer was difficult. Even if a seal could be placed, it would not prevent eventual leakage as the seal would come loose due to engine vibration. Additionally, the thread length available in the liner, to allow the probe caps to screw as mentioned later, was small and sufficient sealant could not be added. In an attempt to improve the seal, a ‘crush bush’ sleeve, Modification 2 in Figure 3-10 that would slide over the probe and fit between the cap ends was turned from aluminium. The sleeve was manufactured to be slightly greater in length than the distance between the cap ends, when the probe was assembled, so that the sleeve would crush and provide a tight seal. This proved successful for a short period of time.

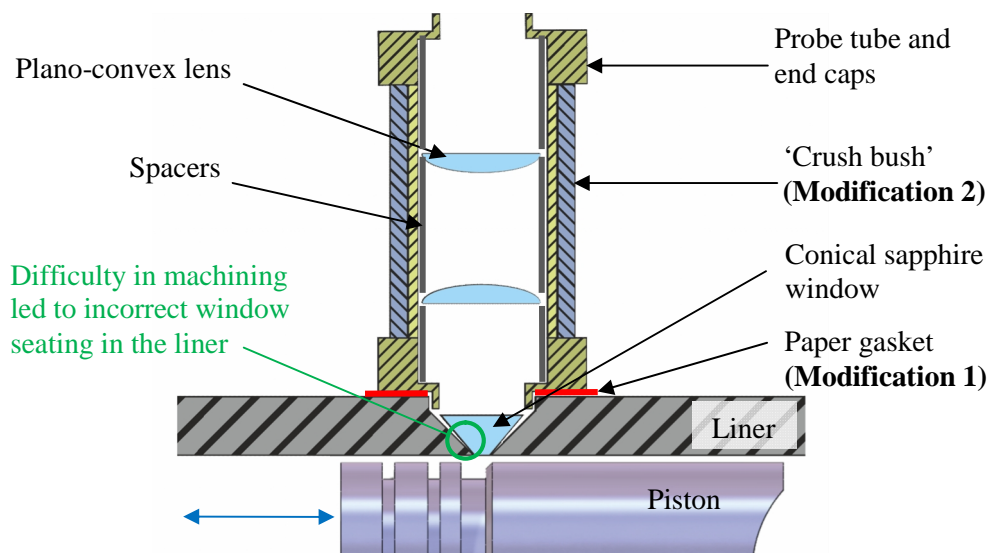


**Figure 3-10 : Illustration of crush bush sealing and conical window seating in the liner**

The original design of the sapphire window was of a conical shape 3.06mm thick with a major diameter of 7.11 mm and a minor diameter of 1.00 mm. The window was inserted into a 45° taper that was machined in the liner and allowed the window to theoretically fit flush of

the liner inner surface, as shown in Figure 3-10. The taper did provide difficulty in aligning the window square to the inner liner surface as machining a 45° taper on a cylindrical surface to an acceptable tolerance is extremely difficult, and a misaligned window would always allow the test lubricant to leak through. What would appear to be a perfectly aligned window in the liner was not always the case. When a profilometry scan with a Taylsurf profilometer was conducted, Figure 3-11, it can be clearly seen that the window was not aligned. A continuous streak of leaking windows, misalignment and coolant leaking into the collimator probe, led to a complete change of the probe and window shape.

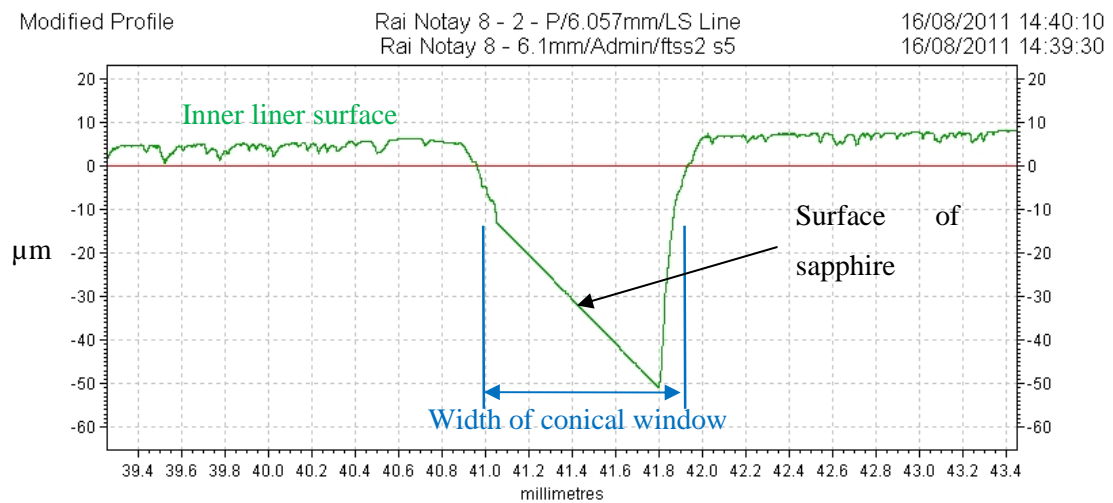


**Figure 3-11: Talysurf profile of the misaligned conical window in the liner**

### 3.3.2 New collimator probe and window design

Repeated failure of the original collimator probe and the window in the cylinder liner, as designed by Rahimiardali (Rahimiardali 2008), suggested a new approach to this part of the system was required. There was now an opportunity to improve the signal to noise ratio.

Rahimiardali's collimator probe was manufactured in-house from mild steel and although having the convenience of a bespoke system, it has some inherent flaws. Firstly, a degree of adjustability of the probe system is required to satisfy any focal lengths of the lenses used since manufacturing tolerances are finite and secondly achieving surfaces with low reflectance and matt black colouring is required to prevent any scattering of light and increase the signal to noise ratio. The original probe had spacers between the lenses and the length of the spacers dictated the position of the focal point of the lenses on the sapphire window in the liner. The optimum position of the focal point should lie just on the inner

surface of the window in the liner to accurately measure the OFT between the cylinder liner (where the inner surface of the window should be flush) and the piston ring. It was found upon measurement of the focal length that the spacers set the focal point approximately 0.2mm before the window surface. This reduced the signal to noise ratio dramatically.

A collimator probe system consisting of parts from Comar Instruments was purchased and mountings required to use the parts on the motored engine were designed around this new probe. The probe was anodised black which is best for the prevention of light scattering from internal reflection. The probe is a simple collection of tubes of different lengths with an internal fine threaded bore and allows optical lenses to sit square inside when lens retaining rings with external threads are used. This provides the dynamic feature of the probe allowing focal points to be adjusted according to application. A new sapphire window was designed and sent for manufacture at Yorlab, Figure 3-12. Sapphire material was retained and chosen over alternative optical materials since it has a similar thermal expansion as cast iron, the liner material. The window was a step design so that it could sit flat to a surface milled in the liner preventing any misalignment issues. The new window has increased area of adhesion over the previous conical design allowing for a more reliable seal with adhesive, without being excessively large and altering the natural engine operating condition. It had a 2 mm diameter liner optical access. A schematic of the window in the liner and the collimator probe is shown in Figure 3-12. The technical drawing of the window is in the Appendix B1.

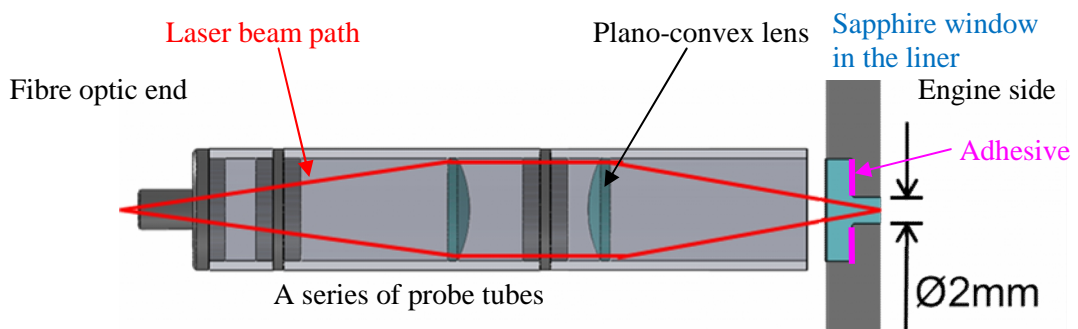


**Figure 3-12: New dynamic collimator probe and step window design**

One of the major drawbacks of the previous probe system was that coolant would eventually leak into the probe system and cover the lenses. The wall thickness of the liner was originally 5mm and when a 3 mm thick conical window was used, only approximately 2 mm thick material was left for a thread to accept the probe end caps. For the new probe system, it was decided to design and manufacture a liner with a larger wall thickness. The wall

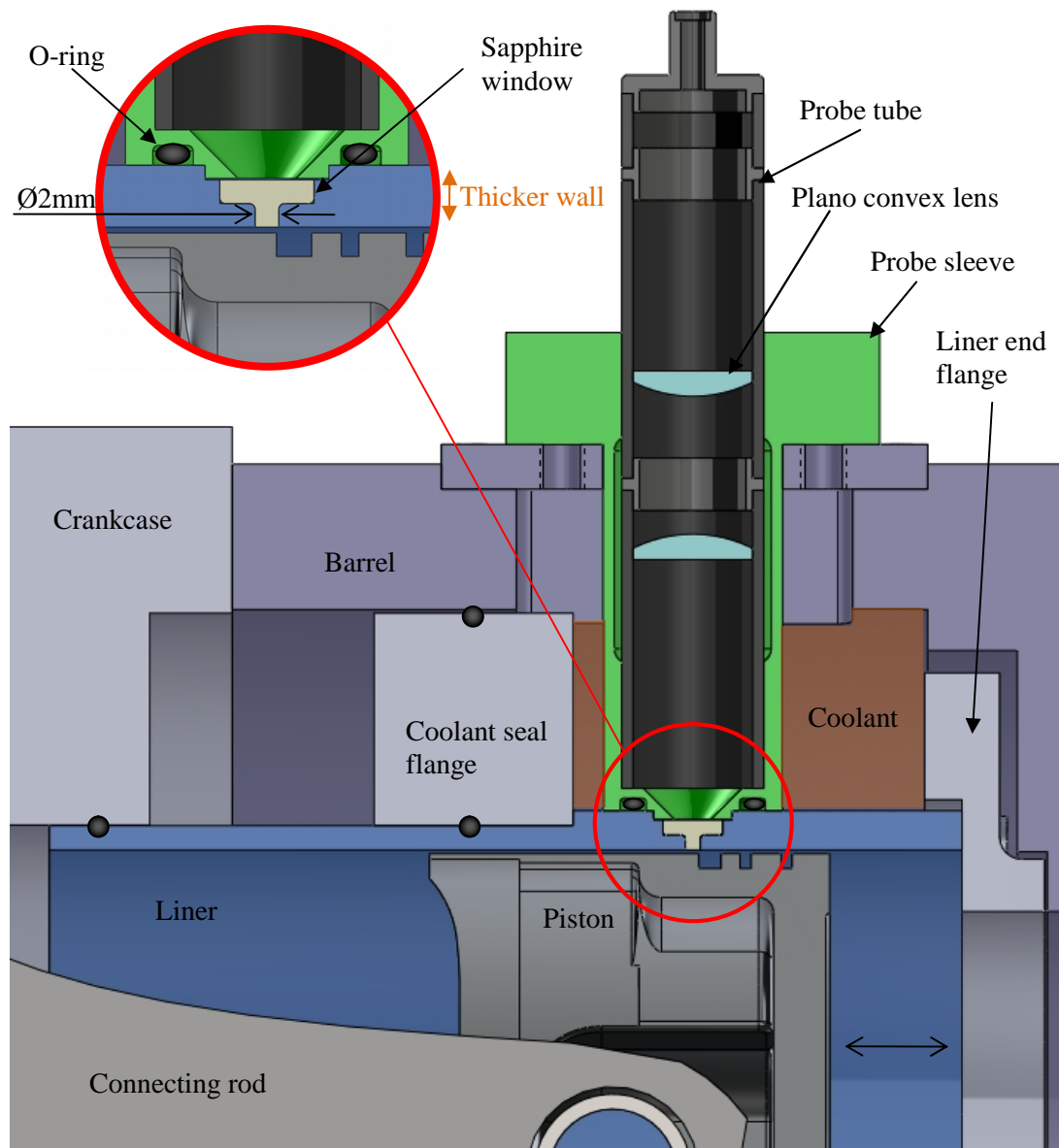


**Figure 3-13: A schematic of the new optical probe setup on the motored engine**

thickness was turned to 7 mm as this was the maximum thickness that could fit through the flange plate holding the top of the liner in place. On the original system, the threads on the probe caps and the one in the liner to accept the probe would continuously allow coolant to leak through, so to prevent any leaking with threads it was decided to design a system which did not make use of any threads to hold the probe to the liner. Instead, a sleeve was designed and turned from aluminium which would accept the probe and protect it from the coolant by fitting in-between the liner to the outside of the motored engine barrel. The liner had a flat machined on the outside edge on the thrust plane, where optical examination took place, so

that the sleeve could house an o-ring seal to seal the whole system, window and probe, from the coolant. The complete optical arrangement can be seen in Figure 3-13 and technical drawings of the system are in Appendix B2 and Appendix B3. The sleeve had been turned to include an edge which sat in a section milled in the liner where the window was, which helped with alignment but did restrain the floating liner. As a result, no piston assembly friction measurement was possible on the motored engine. An M3 grub screw held the probe in position. The biggest advantage the sleeve had over the previous method of screwing a probe into the liner, was that the collimator probe could be removed from the engine without disassembling the engine components or draining the coolant. The sleeve worked well and there were no reported cases of leaks. A similar strategy was employed on the Hydra engine, as discussed in Chapter 5.

The new probe was slightly larger in diameter, 16 mm internal bore, and as a result the original plano-convex lenses of 10 mm diameter could not be used, so new lenses were purchased. There was a need to improve the signal to noise ratio, and one of the drawbacks of the original system was that the fibre optic had a core diameter of 600  $\mu\text{m}$ . This implies that at the focal point of the lenses, the focus point will only be a minimum of 600  $\mu\text{m}$  in diameter too, and as the piston ring was 1.5 mm thick, the signal to noise was greatly convoluted. Convolution being an effect whereby an image is distorted due to wide aperture, the aperture here being the diameter of the focal point as dictated by the lenses and ultimately the fibre core diameter. By reducing the core diameter of the fibre optic, the convolution effect can be reduced and a more accurate profile of the piston ring can be captured. An example of optical convolution and reducing it with aperture is shown in Figure 3-14. It can be seen that by reducing the fibre core aperture, an improvement in the signal profile is gained. However, by reducing the core diameter, the amount of light transfer is less and as a result the signal is reduced so there is a trade-off. For this particular reason, a fibre optic cable with a 105  $\mu\text{m}$  was purchased. The new fibre optic cable had a numerical aperture, which dictates the maximum divergence angle or acceptance angle, suitable for the focal length of the plano-convex lens such that all the diverging light from the end of the fibre optic would be transferred through the lenses without any light internally reflecting and causing light scattering inside the probe tube. Since the new probe tube was threaded on the inside it was possible to set the focal point of the laser to suit the system. The focal point of the laser was set to the inner surface of the liner, therefore the surface of the window which interacts with the oil film, so that the oil film across the window to the piston ring could be measured.

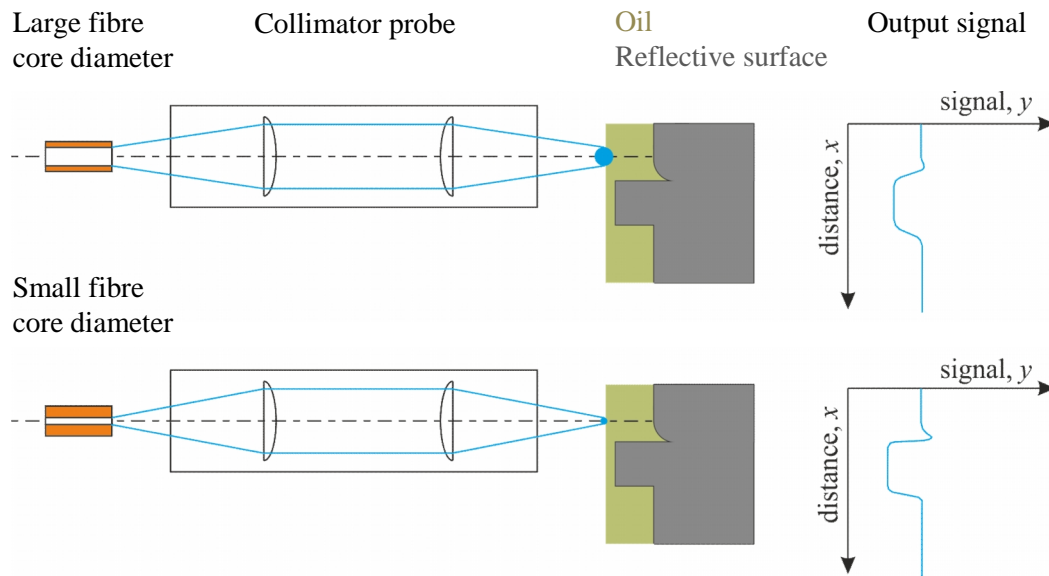


**Figure 3-14: Illustrating the importance of fibre optic aperture on optical convolution**

### 3.4 LIF Calibration

To gain an understanding of the fluorescence signals from the PMT, it was necessary to calibrate the signal with known lubricant film thicknesses. Different techniques were employed to calibrate the signals statically and after much deliberation a purpose built calibration system was built. By chance, during initial calibration runs, it was found that the reflectivity of the surface used as the calibration standard was extremely important. Inagaki et al. (Inagaki, Saito et al. 1997) used reference blocks which have known depths etched in the surface for calibration, Nakayama et. al and Takiguchi et al. (Takiguchi, Nakayama et al. 1998; Nakayama, Morio et al. 2003) have both calibrated their system using a known film thickness squished between two plates containing slip gauges, and Arcoumanis et al. (Arcoumanis, Duszynski et al. 1998; Arcoumanis, Duszynski et al. 1998) mounted the end of their fibre optic in the anvil of a high resolution micrometer which had an oil film squished in-between. However, it is very rare to see researchers consider the material and the material surface reflectivity which should in fact be similar to that of a piston ring. Since the point of interest is the lubricant films experienced at the piston rings, the reflective surface should be of similar material and surface roughness as the piston ring for accurate calibration. Ultimately, an actual piston ring taken from a running engine was used as the reflective surface.

An investigation into the effects of temperature and dye concentration on fluorescence efficiency, that being the ability of the fluorophore fluorescing when absorbing laser emission, was undertaken. Since the project is concerned with lubricant degradation, the sample transparency for light transmission, the opacity, was also investigated.

### 3.4.1 Lubricant film thickness calibration methods

The PMT used for the fluorescence imaging requires calibration with known lubricant film thicknesses so that the lubricant profiles obtained from the engine can be understood. Static calibration is usually performed outside the engine environment and dynamic calibration on the engine during operation. Placing grooves of known thicknesses etched on the piston, generally on the piston skirt, is one method of dynamic calibration and it is possible to obtain a value for the PMT output as the groove in the piston passes the optical window in the cylinder wall. Seki et al (Seki, Nakayama et al. 2000) and Dearlove and Cheng (Dearlove and Cheng 1995) both attempted this method but Dearlove and Cheng found that the grooves would eventually wear out causing concern for correct calibration. This author also believes that it cannot be assumed that the interface between the piston skirt and the cylinder wall is completely filled with lubricant for this type of calibration method to be valid.

However, as an initial attempt to understand the developing LIF system, a piston was placed in the lathe and four grooves of increasing depths were turned into the skirt surface, Figure 3-15, followed by a surface profile scan using a Taylor Hobson Talysurf profilometer machine, Figure 3-16.

4 grooves in piston skirt of increasing depths

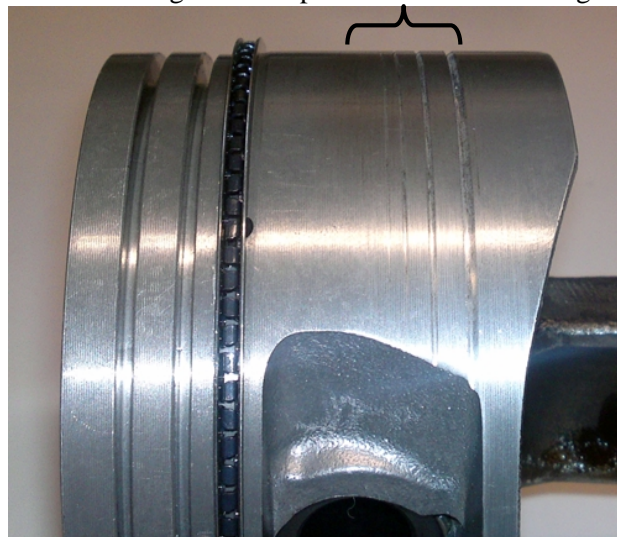


**Figure 3-15: Four grooves turned into the piston skirt for dynamic calibration**

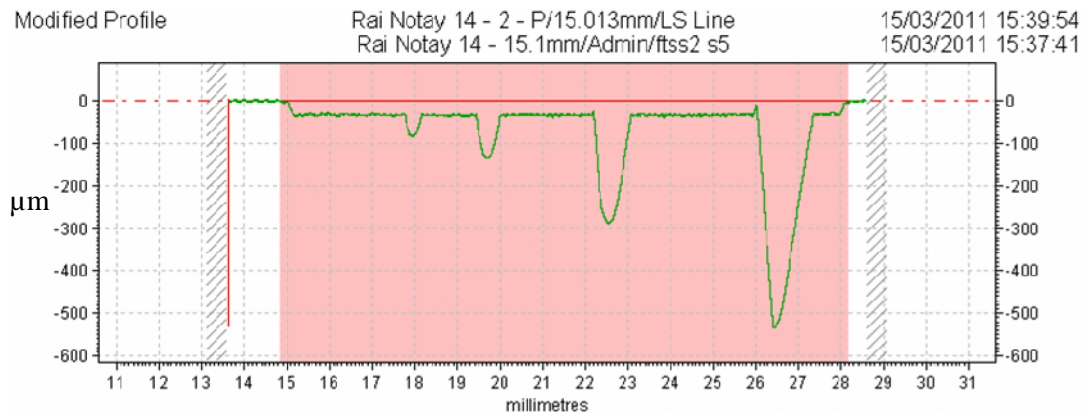


**Figure 3-16: Surface profile scan of the four grooves on the piston skirt**

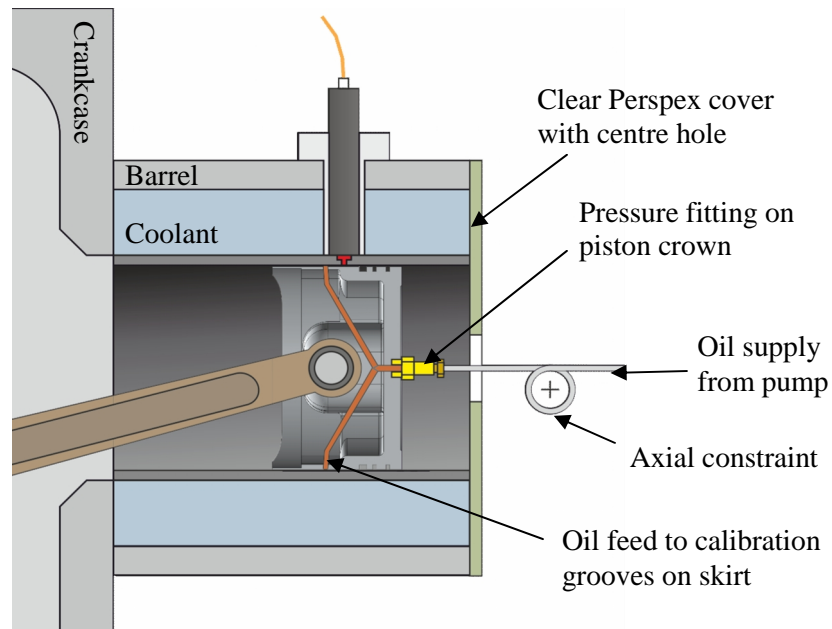


**Figure 3-17: Oil feed to calibration grooves on skirt to prevent local lubricant cavitation**

As can be seen from the surface profile scan, Figure 3-16, the smallest depth that could be turned on the skirt was a groove of approximately  $70\mu\text{m}$  and in reality for an operating engine this would be too thick a film to be present under the piston rings. Unfortunately, even though grooves were present on the skirt, they could not be detected on the oscilloscope as the piston passed the probe doubting fully flooded lubrication was taking place on the skirt. In an attempt to allow for fully flooded lubrication on the piston skirt, lubricant was fed onto the skirt from the oil pump via a pressure fitting place on the piston crown. Lubricant

flowed to the underside of the skirt, through a hole drilled through the skirt, via a copper pipe which was attached to the underneath of the crown. A PTFE pipe was attached to the fitting on top of the crown and an axial constraint on the outside of the engine controlled the position pipe due to the rapid piston motion, Figure 3-17. The cylinder head was replaced with a clear Perspex cover with a centre hole to provide clearance for the fitting on the crown and for observation. The engine speed was limited to 200 rpm since above the speed the PTFE pipe would fail at the constraint due to fatigue. Although the additional oil feed provided fully flooded lubricant operation, the oil feed hole was in direct sight of the LIF probe. As a result, the LIF signals were found to be saturated and it was beginning to get even more difficult to distinguish the grooves. So, an alternative idea was required and it was decided to attempt calibration statically.

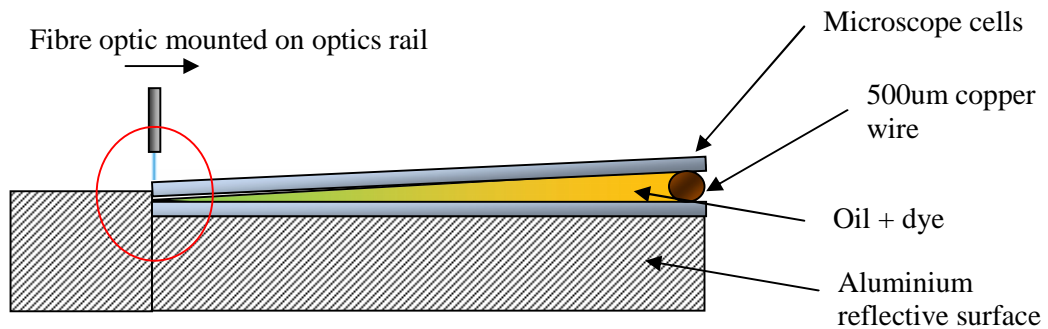


**Figure 3-18: An attempt at fluorescence calibration using an increasing oil film thickness trapped between two microscope cells**

Another attempt at calibration saw an increasing oil film between two microscope slides which was created by a wedge between the two slides. A copper wire of 500 µm diameter was placed at one end of the slides to create the wedge effect between the slides. A similar method was employed by Baba et al. (Baba, Suzuki et al. 2007) and Kato et al. (Kato, Fujita et al. 2009). The slides were placed on an aluminium block to provide a reflective surface.

The calibration piece was placed upon an adjustable height stage and the end of the fibre optic was mounted on an optics rail. The fibre optic could slide along the optics rail and by using a dial gauge it was possible to measure the displacement of the fibre optic. The system is shown in Figure 3-18 and a typical result is shown in Figure 3-19. Although it was possible to achieve an accurate calibration coefficient the design failed at elevated temperature since the copper wire would expand. So the film thickness would vary with temperature and as a result an alternative solution was required. Another reason why this

idea was not taken further, was that the microscope slides introduced additional reflectivity and stray light which influenced the output and hence the calibration coefficient. It is also apparent that there is a slight 'bump' in the calibration line of Figure 3-19 which was found to be caused by the light focusing on the slide edge as the fibre optic scanned across the cell surface. It was decided that the best way forward was to keep any static calibration very similar to the probe in the liner.

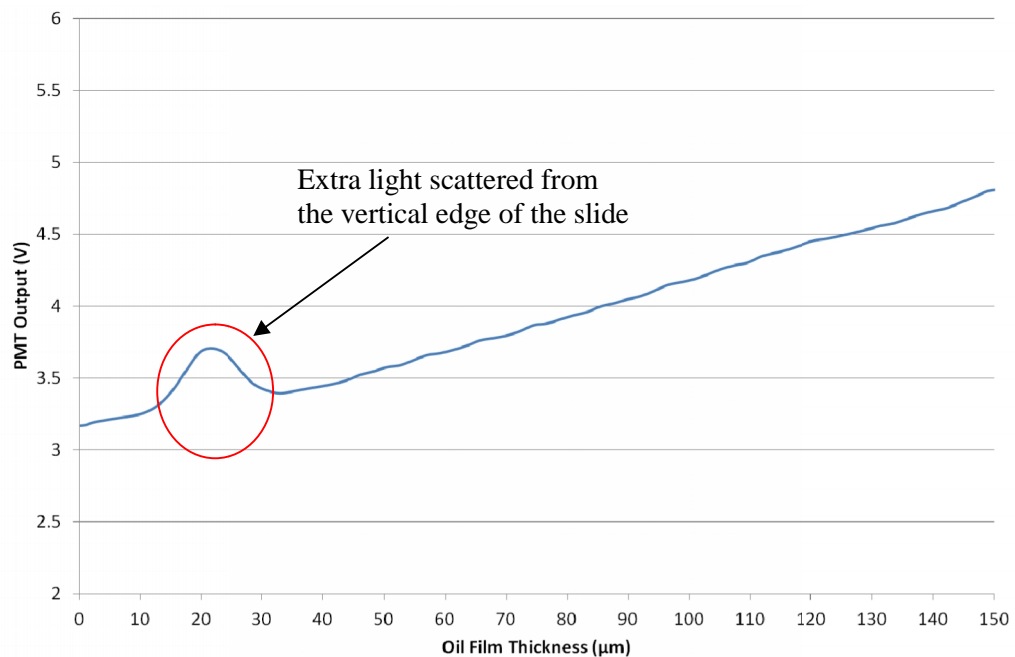


**Figure 3-19: Typical calibration graph obtained from the wedged cells**

This included variables such as focal length distance to the point of interest; in an engine this is the piston ring, on the calibration setup it is the reflective piece, the use of the same collimator probe as used in the engine, same reflective object to measure any static oil films against the piston ring in the engine, same method of light transfer to the point of interest; meaning if the laser light exits the probe and passes just a sapphire window which forms one of the interfaces of the oil film (the other being the piston ring) then the light should pass the same window in the calibration setup and nothing else. Taking the variables into consideration and controlling them allowed a static calibration setup to be designed and manufactured, Figure 3-20.

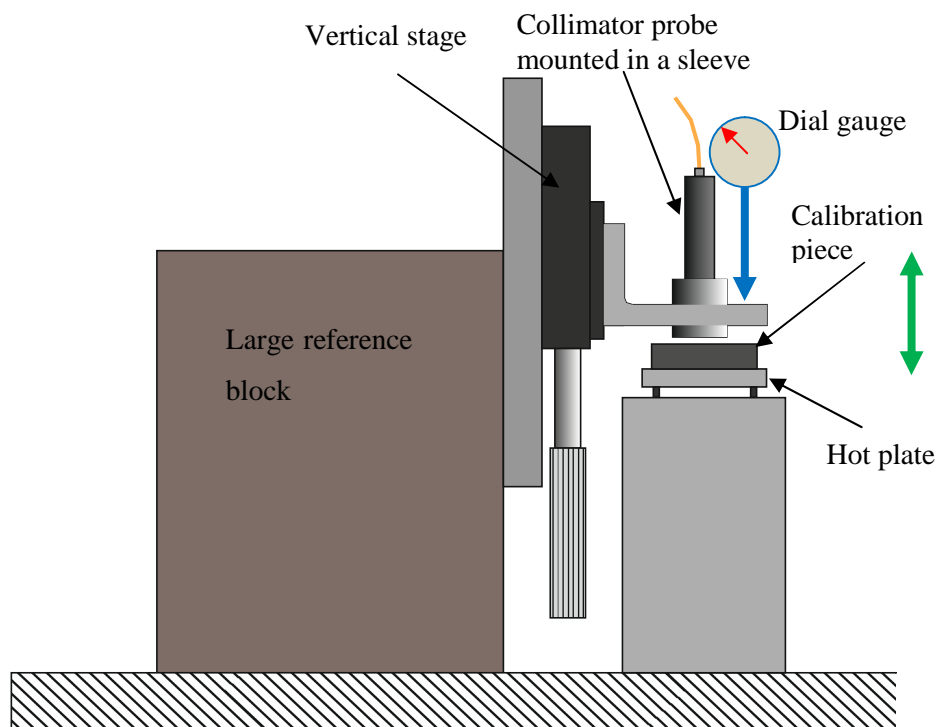


**Figure 3-20: Calibration setup designed and manufactured**

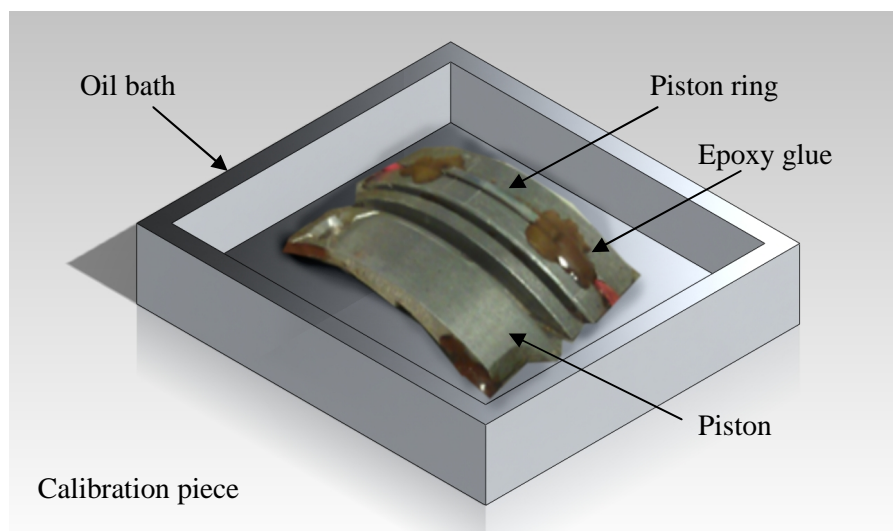


**Figure 3-21: Part of a piston and piston ring which was initially used as the reflective surface for calibration**

As can be seen from the schematic in Figure 3-20, a vertical stage was clamped to the side of a large reference block and the collimator probe was made part of the stage by using a sleeve in which the probe could be mounted. The sleeve also housed a spare sapphire window of the

same shape as the window in Figure 3-13. The sleeve was machined from aluminium. Similar tolerances that were used for the liner, where the window was to mount, were employed so that the focal point of the laser was in the same position as used in the engine, which was the window surface that interacts with the oil. A calibration piece, Figure 3-21, was situated underneath the sleeve. The calibration piece was simply an oil bath which contained part of a piston ring mounted into a slice of a spare piston, and a K type thermocouple to measure oil temperature. The ring piece was used as the reflective surface and test lubricant was poured into the bath for calibration. The probe sleeve, which was mounted on the vertical stage, would move back and forth from the piston ring and the lubricant across the piston ring and the sapphire window was measured as the film thickness. Initially a plunger type dial gauge with a resolution of 2  $\mu\text{m}$  was attached to the vertical stage to monitor the height and thereby the film thickness between the piston ring and the window. It was often difficult to locate the crest of the ring, to ensure no lubricant would be present between the ring and the window, and as a result the ring was later changed to an equivalent flat chromium piece. The dial gauge was later found to have stick slip on the plunger and was replaced with a linear variable differential transformer (LVDT) with a resolution of 0.25  $\mu\text{m}$ . The calibration piece was placed on top of an aluminium hot plate which contained a 400 W ceramic heater element of 6mm diameter and 100mm length, and this was controlled by a separate heater control box. The hot plate was mounted on an aluminium block so that the calibration piece was at the correct height for the vertical stage.

The use of the hot plate allowed lubricants to be tested against temperature and not just oil quality, i.e. oil degradation phase. It was not an issue if the calibration piece expanded due to an increase in temperature since it was possible to re-zero the dial gauge once the temperature was stable. The calibration system was the first of its kind and the repeatability up to film thicknesses of approximately 100  $\mu\text{m}$  was found to be  $\pm 0.5 \mu\text{m}$ . Any examination above 100  $\mu\text{m}$  and the repeatability changed to  $\pm 1 \mu\text{m}$  which was found to be caused by backlash in the micrometer screw of the vertical stage. Since lubricant films greater than 100  $\mu\text{m}$  in the piston ring pack are rare, the system was deemed appropriate for LIF calibration.

A description of the calibration procedure for a test lubricant follows below, with a selection of some of the calibration tests of the oil samples used in this research in Appendix C:

- a) Add lubricant sample to be calibrated to the oil bath
- b) Set hot plate to desired test temperature for calibration and allow to lubricant to thermally stabilise for approximately 30 minutes

- c) Lower the stage to its lowest position using the micrometer, thereby allowing the probe sleeve and hence optical window to sit on the reflective piece under its own weight
- d) Check fluorescence return signal and record
- e) Remove probe from sleeve and position flat against a similar reflective piece outside the calibration rig and record fluorescence signal return
- f) Check and compare both readings, they should be equal indicating no fluorescence emission is occurring from the contact between the window and the reflective piece, hence no measurable lubricant film present. If not, adjust the oil bath position underneath the sleeve and recheck
- g) Once satisfied, begin calibration using calibration program and the LVDT as described in Chapter 7. Adjust stage height and alter the film thickness between the window and the reflective piece. Record film thicknesses against PMT output using the program.
- h) For next test sample to be calibrated, remove existing sample and clean components using suitable solvent (e.g. Heptane or Acetone) and repeat above steps.

### 3.4.2 Temperature effects

The quantum efficiency, that being the rate of electron production from photons when striking the fluorophore, depends upon the viscosity and temperature of the lubricant. A dye molecule strikes a lubricant molecule and this is how the dependency arises. The Debye – Einstein equation predicts the collision rate,  $k_c$ , given as Equation 3-7 below (Parker 1968; Hoult, Lux et al. 1988).

$$k_c = (8RT/\eta) \quad \text{Equation 3-7}$$

Where  $R$  is the gas constant,  $T$  absolute temperature and  $\eta$  viscosity.

The Stern – Volmer equation governs the change in quantum efficiency shown as Equation 3-8 (Parker 1968).

$$F_q^0 / F_q - 1 = k_c \tau_0 [Q] \quad \text{Equation 3-8}$$

Where  $F_q^0$  is unquenched fluorescent efficiency (background fluorescence),  $F_q$  is actual fluorescent efficiency,  $\tau_0$  the lifetime of the excited fluorophore (about  $10^{-3}$  nanoseconds

(Parker 1968)) and  $[Q]$  the concentration of the quenching lubricant molecules (Hoult, Lux et al. 1988).

From Equation 3-7 and Equation 3-8 it can be seen that as the temperature increases molecular interactions increase, reducing the lubricant viscosity and degrading the signal (Hoult, Lux et al. 1988).

### 3.4.3 Dye concentration

Some samples can fluoresce naturally, they contain intrinsic fluorophores, whereas others require a doping agent (dye) and are said to contain extrinsic fluorophores (Lakowicz 2006). All test engine lubricants used were of the Group 3 lubricant type which are highly refined lubricants with a higher base oil quality and so do not contain any intrinsic fluorophores and require a doping agent to provide the fluorescence. There are many doping agents available for a wide range of fluorescent imaging applications and laser systems. The correct doping agent is based on the amount of absorption of the laser emission wavelength. A major requirement for the correct dye for the application was that the dye had to be completely soluble in the lubricant sample without any additional catalyst to improve the solubility and without affecting the natural operating performance of the lubricant.

The concentration of the dye was determined mathematically by taking into account the maximum path length, i.e. the thickest films to be observed.

Lubricant films under the top compression ring can be as large as 20  $\mu\text{m}$ . If we consider that the maximum film we will observe is 20  $\mu\text{m}$ , then we will only be able to observe films up to 20  $\mu\text{m}$  and nothing greater since the dye concentration will be optimum up to this thickness. As a result, the maximum film thickness to be observed across the ring pack, i.e. the maximum optical path length, was assumed to be 200  $\mu\text{m}$ . This would allow the film thickness up to 200  $\mu\text{m}$  to be clearly identified. So this maximum thickness was taken as the path length  $b$  (in cm) in the Beer-Lambert law, as defined by Equation 3-9.

$$A = \nu bc$$

**Equation 3-9**

Where  $A$  is the absorptivity (defined by the absorption curve of the laser wavelength emission when using fluorescence dye),  $\nu$  the molar extinction coefficient (litres/mole cm) and  $c$  the molar concentration (mole/litre). As per the specification in Appendix D, the maximum absorption of the laser excitation at 488 nm in Pyrromethene 567A is  $A = 0.16$ ,  $\nu = 8.4 \times 10^5$  and the molecular weight is 374.32

The concentration for a path length of 200  $\mu\text{m}$  is given as:

$$c = \frac{0.16}{(8.4 \times 10^5 \times 0.020)}$$

$$c = 9.52 \times 10^{-5} \text{ mole/litre}$$

$$\begin{aligned} c(\text{weight}) &= 9.52 \times 10^{-5} \text{ mole/l} \times 374.32 \text{ g/mole} \\ &= \underline{35.6 \text{ mg/litre}} \end{aligned}$$

So, 35 mg/litre of dye was used as the doping concentration. This was acceptable for fresh lubricant with excellent results of films being measured from near zero to easily up to 200  $\mu\text{m}$ . For degraded samples, it was necessary to add more dye up to concentration rates of 100 mg/litre. Even then, because of the high sample opacity, as mentioned in the next section, the maximum measurable films were the general order of 50  $\mu\text{m}$  thick, which was still acceptable for examination under the piston rings. Figure 3-22 shows an example of why dye concentration is important. Two test lubricants, as used in the Chapter 4, one a fresh fully formulated lubricant and the same lubricant but which had degraded. The fresh lubricant contains the prescribed 35 mg/litre of dye whereas the degraded lubricant contains 100 mg/litre. Even though the degraded lubricant contains more dye, the fluorescence efficiency is poorer due to the weaker absorption of the laser in the sample.

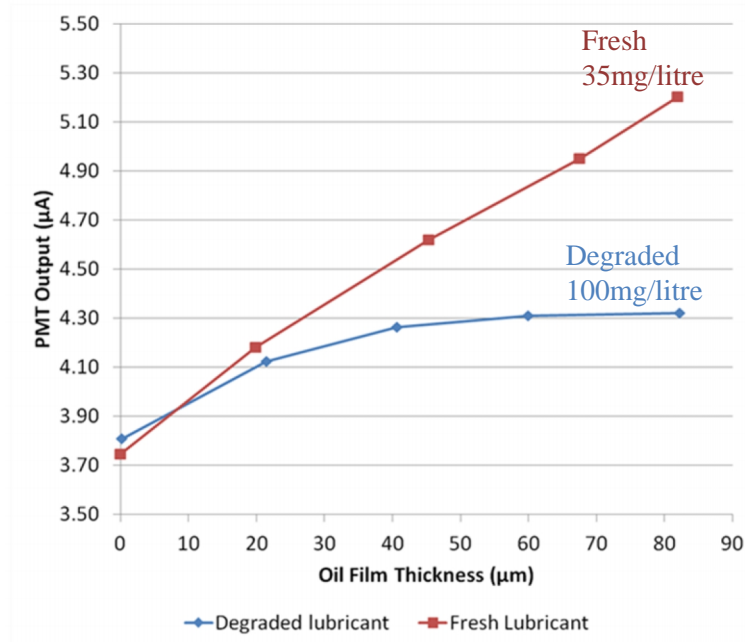


**Figure 3-22: Increased level of dye concentration is required for degraded lubricants**

### 3.4.4 Sample opacity

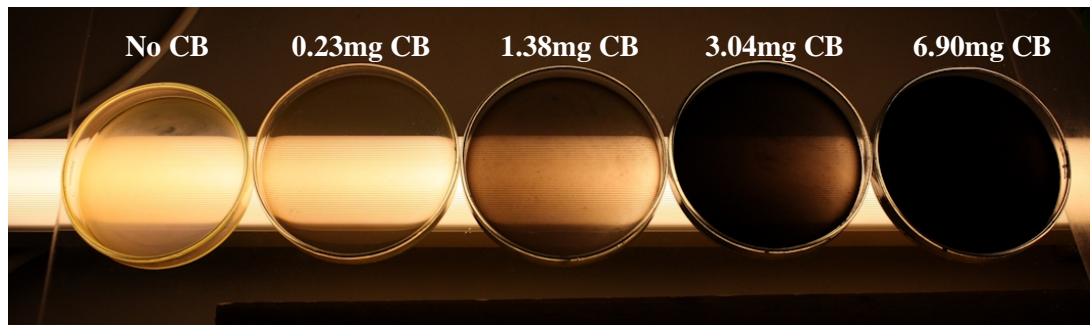


**Figure 3-23: Contamination with carbon black (CB) influences the sample opacity**

One of the interesting findings of this research was that the opacity of the lubricant plays a big part in the fluorescence signal return. The opacity is defined as the optical transparency in terms of how easy an optical beam is capable of passing through a medium. The stronger the opacity, the less transparent the medium and hence the poorer transmission. In the past when researchers have used LIF as a means of lubricant film thickness measurements, fresh lubricant, which is generally a clear light tan colour, has been used. As a result, since the opacity of the lubricants used was acceptable for laser transmission, lower powered lasers could be used and laser absorption was not an issue. In this research with degraded lubricants, which are generally black in colour caused by carbon deposit contamination and the oxidation process itself which produces darker coloured components (Hammond 2003), the opacity cannot be ignored. As a means to investigate the effect of the opacity further, Monarch 280 carbon black powder with a typical particle size of 41 nm and a density of 146 kg/m<sup>3</sup> acquired from Cabot Corporation, data sheet in Appendix E, was used to tone fresh lubricant samples that had been equally doped with dye. Carbon black powder was used as it has been shown to have similar molecular structure and aggregate size when compared with soot (Ruot, Faure et al. 2000). Fresh Shell XHVI 8.2 base oil with 1% detergent and dispersant, with lubricant specification in Appendix F2, was doped with 75 mg/litre of dye. Sample quantities were limited to 2 ml in volume and placed in a petri dish with increasing levels of carbon black (CB) concentration. Figure 3-23 illustrates the influence of carbon black contamination in terms of sample opacity when each sample was placed on a light box. It can be seen that as the concentration of carbon black increases, the opacity reduces and hence the light transmission becomes weaker. Figure 3-24 shows the importance of opacity when the samples are calibrated. The abrupt change in the calibration coefficient at around 10  $\mu\text{m}$  is caused by backlash in the calibration setup as discussed earlier in this chapter.

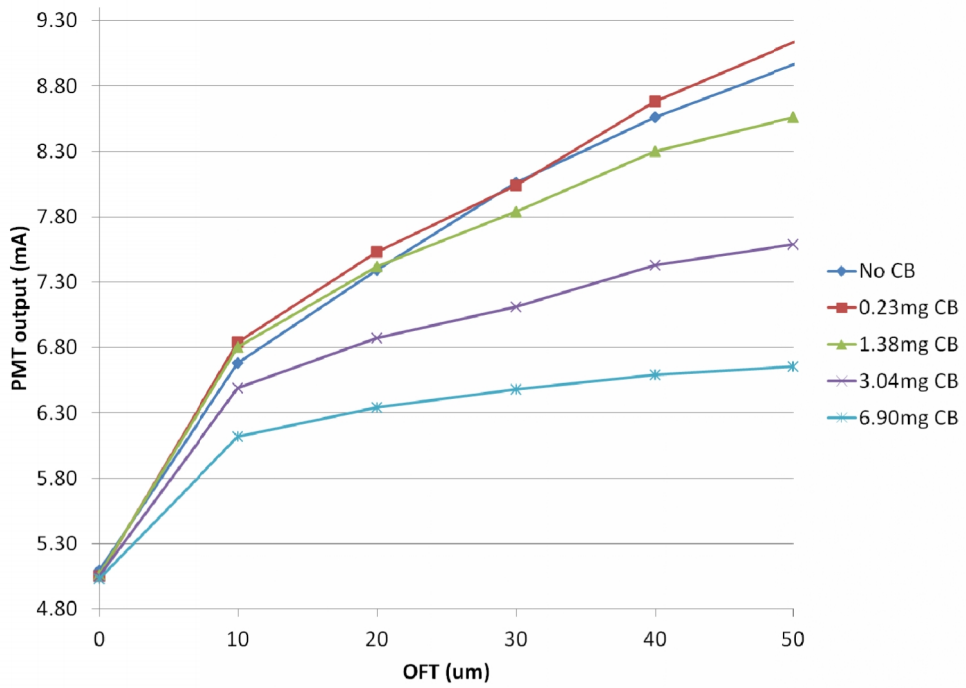


**Figure 3-24: The importance of opacity becomes apparent when the samples are calibrated**

### 3.4.5 Surface reflectivity

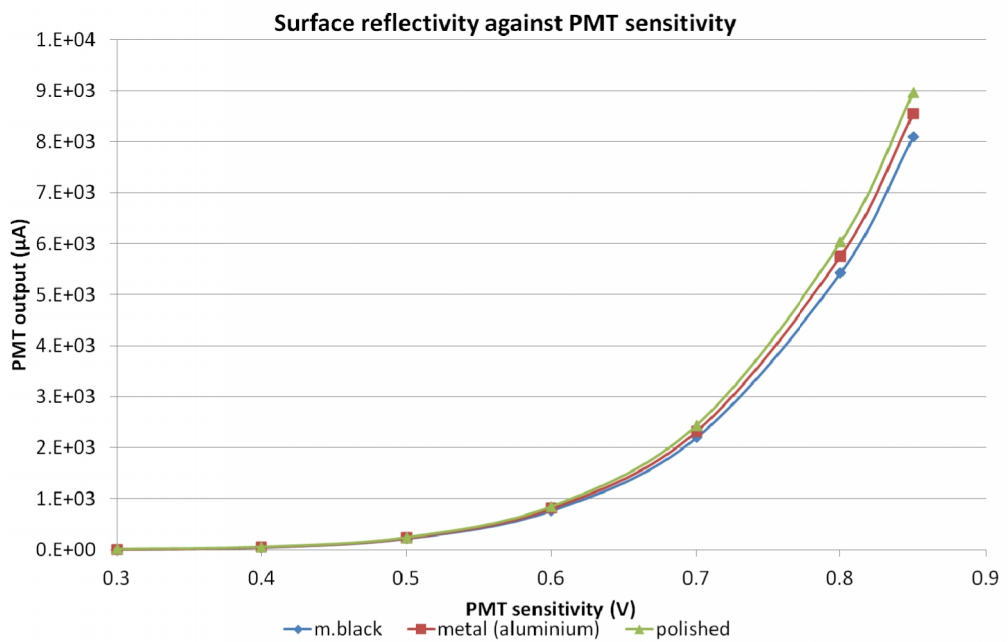


**Figure 3-25: Influence of surface reflectivity when PMT sensitivity is increased**

Another important factor when considering the fluorescence signal return is the choice of the reflectivity of the material used at the point of examination for the signal to return back through the fibre optic cable. The fluorescence emission of the molecule is the same in all directions, but that fluorescence which is moving away from the probe window is reflected back to the sensor and the amount of reflection depends heavily on the reflectivity of the surface. The sensitivity of the PMT would also contribute to the output and the sensitivity to the material surface finish. To investigate the effect of the material surface reflectivity, three aluminium strips were used which had different surface finishes; one painted matt black, one polished to a mirror finish and one left with the standard received aluminium finish. The fibre optic probe was placed above each material piece, so that the focal point was on the surface, and the return signal was measured. No lubricant sample or any sample doped with dye was placed on the pieces, they were left bare to just examine the reflectivity. The PMT control sensitivity voltage was increased and the PMT output was recorded, Figure 3-25. The PMT sensitivity voltage is just purely the gain. It can be seen, as expected, that as the PMT sensitivity is increased the influence of the surface reflectivity becomes more significant. This is interesting as during long engine operation periods, components such as piston rings generally become polished and hence the surface reflectivity would change. Therefore, it is wise to keep the PMT sensitivity suitable for the application without introducing the effects of dark current, that being the small current that flows through the PMT diodes even when no light is entering the PMT module. From the graph in Figure 3-25, it can be seen that a maximum sensitivity voltage of 0.6 V gives sufficient sensitivity to minimise differences due to surface reflectivity and having enough sensitivity to actually detect fluorescence of small lubricant films. It was therefore decided to keep the PMT sensitivity at 0.6 V for the duration of this research.

### 3.5 Summary

A technique to measure the lubricant film thickness experienced between the piston ring and the cylinder liner interface was developed on a motored engine. The engine required extensive modification for the purposes of this research and a sound technical skill on engineering optics and design was gained.

Fluorescence principles and the influence of sample temperature and opacity, fluorescent dye concentration and the material surface reflectivity on fluorescence efficiency was also considered. The original LIF probing system was found to cause repeated sealing issues, coolant leakage and window seating misalignment in the cylinder liner. As a result a new optics probe, fibre optic cable and sapphire observation window developed and provided a

better signal to noise ratio than before. Various calibration ideas were tried and tested, but failure of these for the applicability of the research resulted in the design and manufacture of a purpose built calibration system. The calibration system allowed test lubricant samples to be calibrated against temperature and the measurement of the temperature dependence on the fluorescence efficiency, and the oil quality. In the next chapter a discussion on the testing procedure employed and results from the motored engine are made.

# **Chapter 4 Implementation and Results of Testing on the Motored Engine**

A set of tests to investigate the influence of lubricant degradation on the lubricant film thickness experienced under the piston rings was undertaken and is described in this chapter. An implementation of the tests, a description of the tests themselves, the results, discussion and finally the conclusions are presented. Gasoline lubricant samples were acquired from customer vehicles at the Mercedes Benz (MB) leasing firm in Leeds, UK, along with a single diesel lubricant sample provided by Southwest Research Institute (SwRI), Texas, USA. All MB lubricant samples were of the same multigrade type with differences only in the vehicles they were extracted from and the service interval. The diesel engine lubricant was a post-test reference test lubricant of a monograde type. Engine testing included the effects of engine speed, load and cylinder peak pressure.

The results show significant differences in OFT profiles of the piston ring pack when the lubricant quality changes with degradation, which would have an impact on the tribological performance of the piston ring pack.

## **4.1 Implementation**

A LIF imaging system complete with laser optics, collimator probe and fibre optic was designed and developed for lubricant film thickness measurements of a reciprocating motored engine as described in Chapter 3. The new measurement system was implemented and initial motored engine OFT results demonstrated the potential of this system.

### **4.1.1 Setting the focal point of lenses**

The collimator probe was housed in an aluminium sleeve, which protected the probe from any coolant leak as the laser light in the probe passed from the outside of the engine, through the barrel where coolant flows, and into the sapphire window in the cylinder liner. The sleeve was manufactured with tolerances in the order of  $\pm 0.2$  mm to keep manufacturing costs low and, since the focal point of the lenses in the probe can be adjusted and set to the

desired position, the manufacturing tolerances did not need to be any finer. The laser light is focussed in the engine and maximum laser absorption occurs at this point. The optimum position of the focal point, for highest signal to noise ratio for measuring the lubricant film across the interface between the window and the piston ring, is on the inside window surface. The inside window surface of the sapphire window was locked in place flush with the cylinder liner.

The probe tube had an internal thread and it was possible to move the position of the lenses in the tube to alter the position of the focal point. A depth gauge was used to first determine the accuracy of the sleeve machining to the technical drawing, Appendix B3, and also how far down the probe tube the lenses sat. The focal length of the lenses was 13.6 mm. From the internal depth of the sleeve, it was possible to determine how far down the tube the lenses needed to be to achieve the optimum position of the focal point. A couple of retaining rings with external threads inside the tube retain and position the lenses at the desired distance.

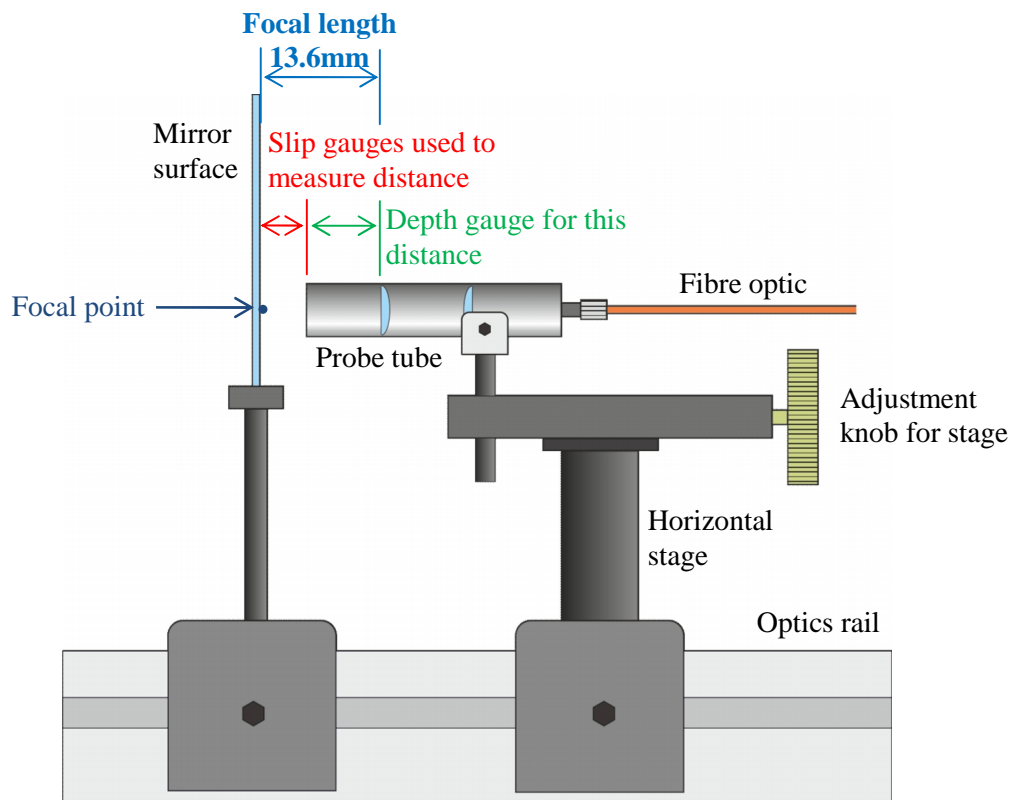
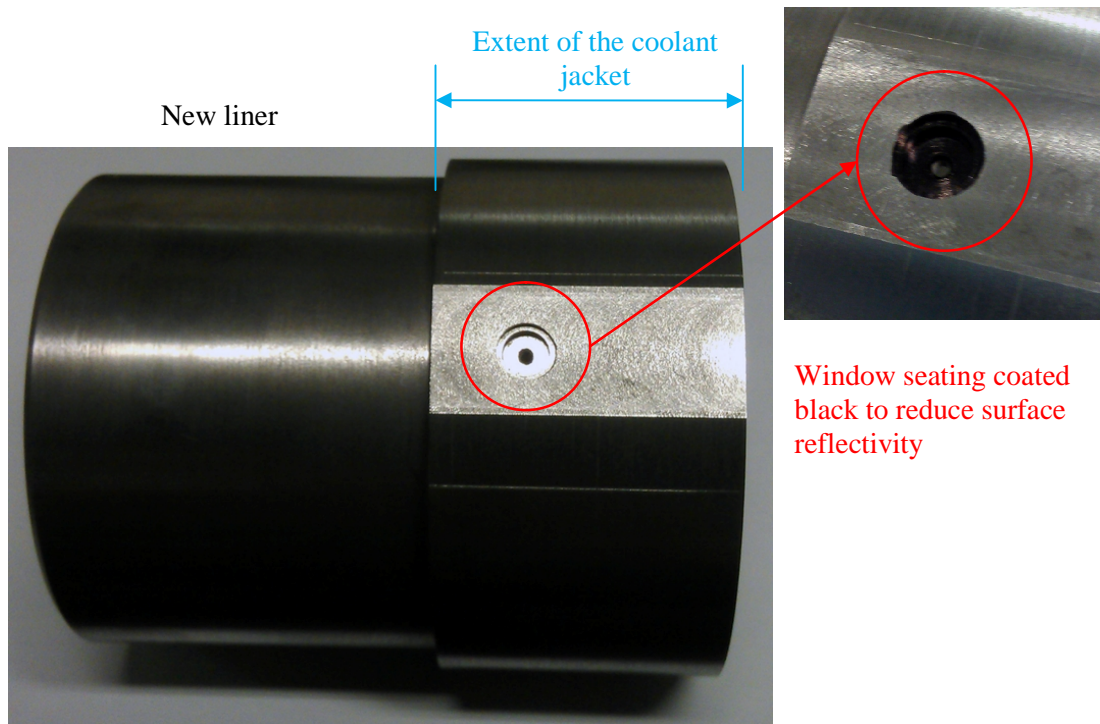


Figure 4-1: Illustration of the position of the focal point of the lenses

Figure 4-1 shows the system to accurately measure the focal point of the lenses. The probe tube was aimed at a mirror and the reflected laser emission light passed back through the lens. The reflected laser emission beam intensity was measured using the fluorescence signal PMT and removing the green colour filter in front of the PMT to allow the reflected blue emission to be monitored. An optical rail was used to mount an optics mirror and mount the collimator probe to a horizontal stage. The probe was moved back and forth from the stationary mirror and the output of the PMT was monitored on an oscilloscope. The focal point was determined at the maximum PMT signal output and the distance between the end of the probe tube and the mirror was measured using slip gauges, along with the measurements of how far down the tube the lenses sat. The combined distance calculation gives the focal length. Measuring and altering the focal point position this way was the most accurate since the output of the PMT was monitored. The focal point is not an infinitesimal point, but is determined by the fibre core diameter, the smaller the core diameter the narrower the focal point. In this research, the focal point was approximately  $105\ \mu\text{m}$  in diameter similar to the core diameter of the fibre used. The resolution of the apparatus to measure the correct focal point was found to be approximately  $\pm 50\ \mu\text{m}$ .



**Figure 4-2: The reflectivity of the window seating surface was reduced to minimise the effects of stray light**

### **4.1.2 Black coating of window seat**

During engine and LIF probe assembly, it was noted that the window seating in the new liner, which had an increased wall thickness to accommodate the new probe, as mentioned in Chapter 3, was machined to a high degree of accuracy to fit the window and this caused a concern for light scattering as the surface was left highly reflective. Taking the collimator probe tube, which is anodised matt black, as a standard example, it was decided to colour the window seating in the liner black. A black marker was used as opposed to coating it with a spray paint of the same colour since the tolerance for the window seat was already tight. It was found that the coating was not easily rubbed off and more than adequate to reduce the surface reflectivity for the optical examination, Figure 4-2.

### **4.1.3 Piston rings**

For the development of the LIF system, the ring pack remained to standard specification and comprised of:

- Grey cast iron top compression ring which is phosphated with chrome rolled inlay and a barrel face
- An grey cast iron taper faced Napier style scraper ring
- A three piece oil control ring with chrome plated steel rails

### **4.1.4 Cylinder liner thermocouples**

As the fluorescence efficiency is influenced by the lubricant temperature, Chapter 3, thermocouples were added to the cylinder liner to examine the temperature distribution. Three blind holes of 2 mm diameter were drilled into the outside surface of the liner approximately to a depth of 1 mm from the inner liner surface to prevent break through. Holes were drilled at either near TDC, mid-stroke and BDC. The TDC thermocouple had to be placed 5 mm from the top liner edge otherwise the wiring interfered with the liner seal flange. K-type thermocouple wire was used and glued into the holes with epoxy glue, Figure 4-3. An additional thermocouple was placed in the barrel to monitor coolant temperatures. All four thermocouple wires were taken outside the engine through a plate attached to the barrel which also served as a location for the LIF probe sleeve, Figure 4-3. The thermocouples and the probe sleeve were sealed, to prevent coolant leaks, using clear silicone sealer. The same silicon sealer plus an additional paper gasket were used to seal the

barrel to the crankcase. The four thermocouples were then wired into the National Instruments hardware for data acquisition as described in Chapter 7.

An example temperature trace of the motored engine at 1000 rpm with 10 bar peak cylinder pressure is presented in Figure 4-4. The coolant jacket only extends to just below the mid-stroke position on the liner (see Figure 4-2), hence the BDC thermocouple measures the highest temperature regardless of speed and pressure as there is no cooling. The TDC thermocouple wire was found to have eventually interfered with the liner flange seal and a small cut in the wire meant that the flange temperatures were measured instead of TDC liner temperatures. Since the mid-stroke temperatures were most important, for calibration of the LIF signal, the TDC wire was not replaced as a complete engine strip down was required and the testing continued.

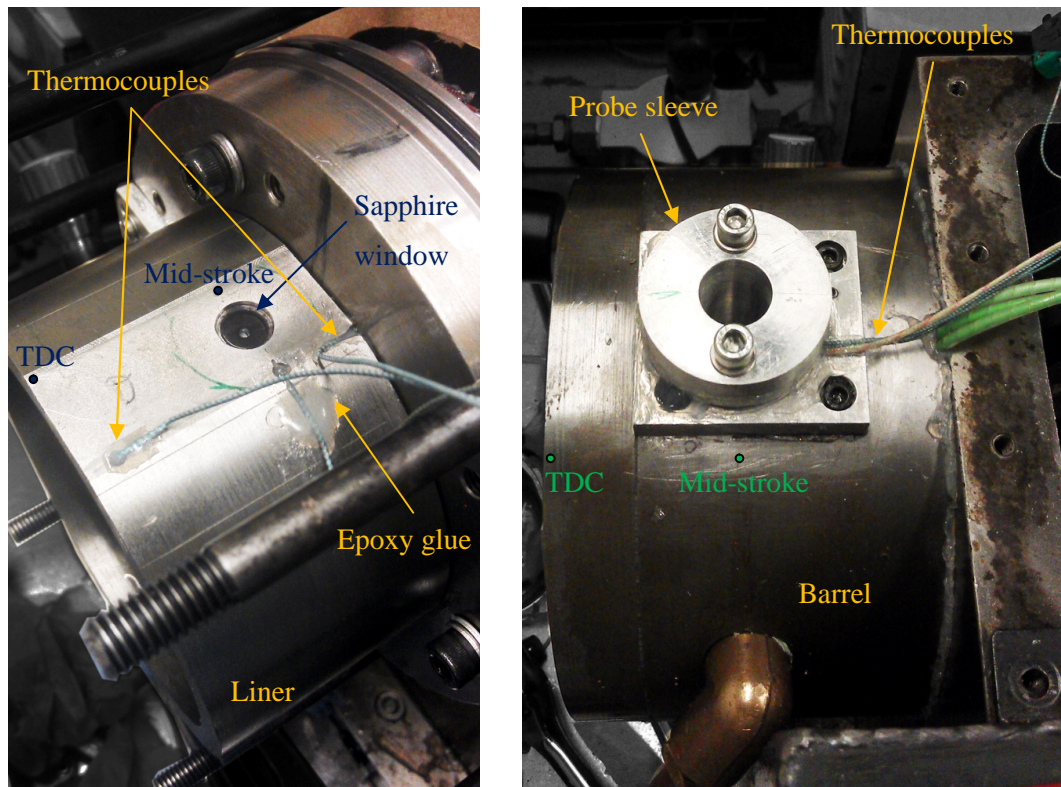


**Figure 4-3: Thermocouples used to monitor cylinder liner temperatures**

#### **4.1.5 Installation of the optical encoder and engine TDC position**

A Series 85 hollow shaft optical encoder from Hohner Automation Limited was used to determine the crank angle position of the engine and to act as the sample clock for the data acquisition system. This particular encoder produces 720 pulses per revolution along with a single TTL (transistor-transistor logic) reference signal once every revolution. The single

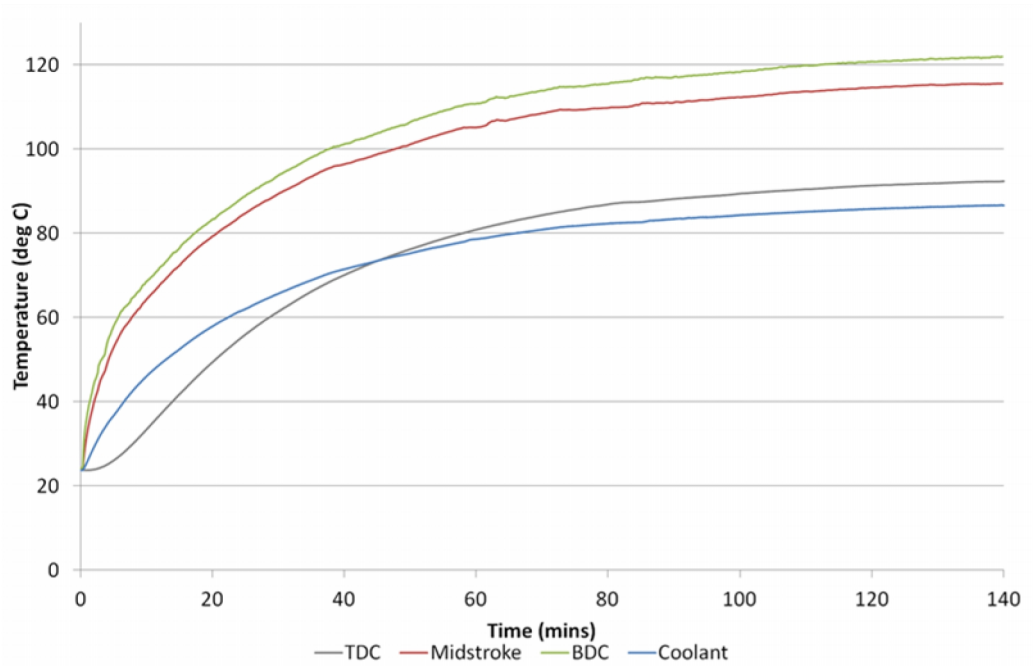


**Figure 4-4: Liner temperature trace at 1000 rpm and 10 bar cylinder peak pressure**

reference signal was used to monitor the TDC position of the piston. This type of encoder is known as a quadrature encoder since there are two output channels, A and B, which are  $90^\circ$  out of phase and are used to determine the direction of rotation. The additional benefit of this, is that during data acquisition the rising and falling edges of both channels are recorded allowing four times the resolution of the encoder, therefore allowing an impressive  $0.125^\circ$  resolution of crank angle. The shaft encoder was attached using grub screws to the tail end of the crankshaft which extended out of the crankcase through an oil seal.

A plunger type dial gauge, with a resolution of  $2\ \mu\text{m}$ , was used to help determine the TDC position of the piston in the cylinder liner. An initial estimate was made by manually setting the piston at approximately TDC and aligning and setting the encoder reference line pulse at TDC. The piston itself moves very little with crankshaft angle near TDC position, approximately up to  $10^\circ$  either side of TDC, so the piston displacement measurement was taken at least at  $20^\circ$  either side of TDC. The crankshaft was rotated before TDC (BTDC) to a deflection of 2mm on the dial gauge and the encoder angle was recorded. The crankshaft was then rotated anticlockwise toward BDC and then back to TDC, so now after TDC (ATDC), and the encoder angle was noted for the same plunger deflection. Measurement either side of TDC allowed the difference between the angles to be calculated allowing the encoder to be adjusted to the correct piston TDC position. This procedure was repeated at different angles

to improve the accuracy of the TDC position. An estimated accuracy of  $\pm 0.125^\circ$  crank angle was achieved. To reduce any systematic error, measurement was performed on both sides of TDC (Eriksson 1998).

#### 4.1.6 Cylinder head pressure transducer

As mentioned in Chapter 3, a Kistler 601 dynamic piezo-electric pressure transducer was used to monitor the peak cylinder pressures and this was connected to a Kistler 5011 charge amplifier. The voltage output from the charge amplifier was sampled and recorded on one of the channels on the data acquisition system.

Piezoelectric sensors are very sensitive and measure compressive load. They require no external power source, but are very prone to leakage, hence cannot be used to measure a static load or pressure as they have very small time constants (Taylor 1997) whereby eventually the signal decays to 'zero' for a constant load, so a drift in the signal is often seen. As a result they are often used with charge amplifiers to control the time constant for dynamic cyclic measurement, like cylinder pressure measurements, and the 'zero' is actually a floating zero which is an average of the value being measured (Radcliffe 1993). A known procedure to calibrate pressure transducers is to use a hydraulic dead weight tester (DWT) machine. Weights are added to a hydraulic line system with the pressure sensor part of the line and this provides an accurate calibration of the sensor. This is a perfect application for static pressure sensors, known as piezoresistive sensors, but not for dynamic sensors. It must also be noted at this stage that dynamic pressure transducers will always drift towards zero during constant loads. For cylinder pressure measurements there will always be a drift of the zero which needs to be post corrected.

As a means to calibrate the dynamic 601 sensor, a static Kistler 4045 pressure transducer was calibrated on a small DWT and then used to aid calibration of the 601 sensor. If both pressure transducers experience the same pressure load at the same time, then since the 4045 sensor is calibrated, the 601 can also be calibrated. A bespoke four way pressure splitter block was connected to a nitrogen gas bottle which provided regulated gas pressure up to 25 bar. Both pressure sensors, the un-calibrated 601 and the calibrated 4045, were connected to either port of the block and the final port had a gate valve attached to release the pressure, Figure 4-5. The maximum pressure rating for the 4045 is 100 bar, whereas for the 601 it is 25bar. Repeated tests were performed with repeats within 1% error of each and with confidence levels of 1.00. It was found that the sensitivity of both pressure transducers was linear in response up to the measured 25 bar, Figure 4-6. The difference in the gradients for

both sensor calibrations is caused by the specific transducer sensitivity setting required for each sensor on the charge amplifier as dictated by the manufacturer.

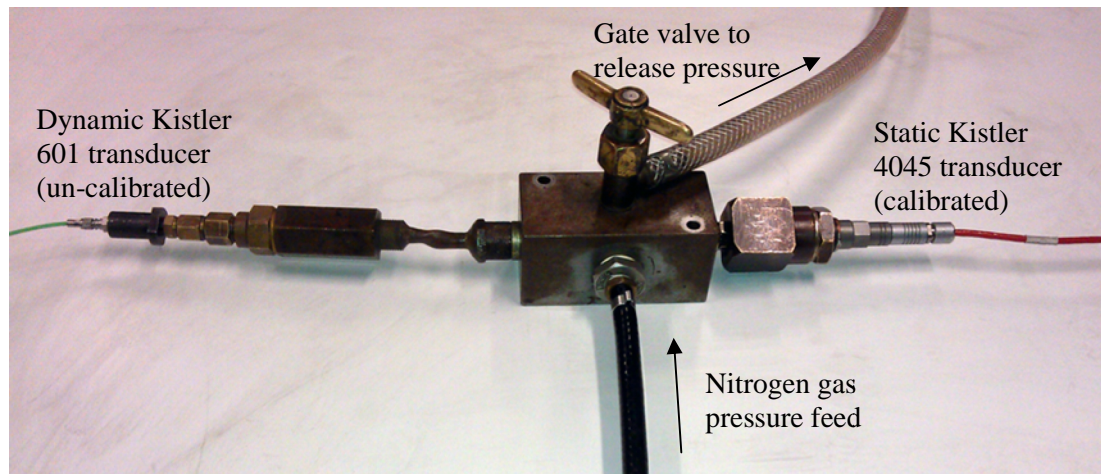


**Figure 4-5: Four-way pressure splitter used to help calibrate Kistler 601 pressure transducer**

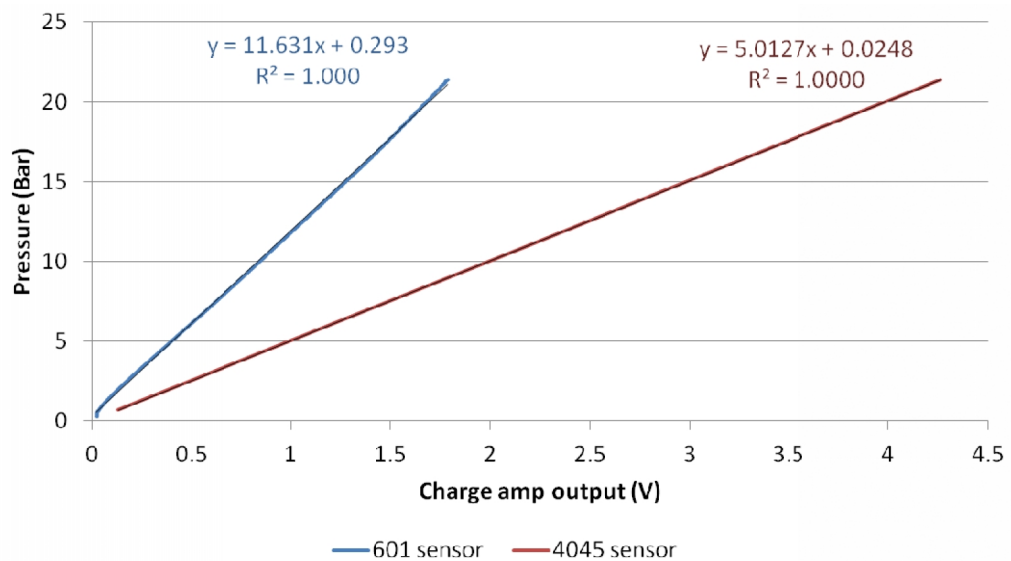


**Figure 4-6: Calibration graphs for pressure transducer sensors 601 and 4045**

As mentioned earlier, cylinder pressure measurements with a dynamic transducer need to be post corrected to adjust for the zero drift in the signal. This can be clearly seen in Figure 4-7 which shows the cylinder pressure traces of both the uncorrected and corrected zero. To correct for this offset, it was assumed that after the intake stroke, at BDC, the one-way valve

on the cylinder head would open to equalise the pressure to the minimum, assumed to be atmospheric. This is similar to the method described by Radcliffe (1993).

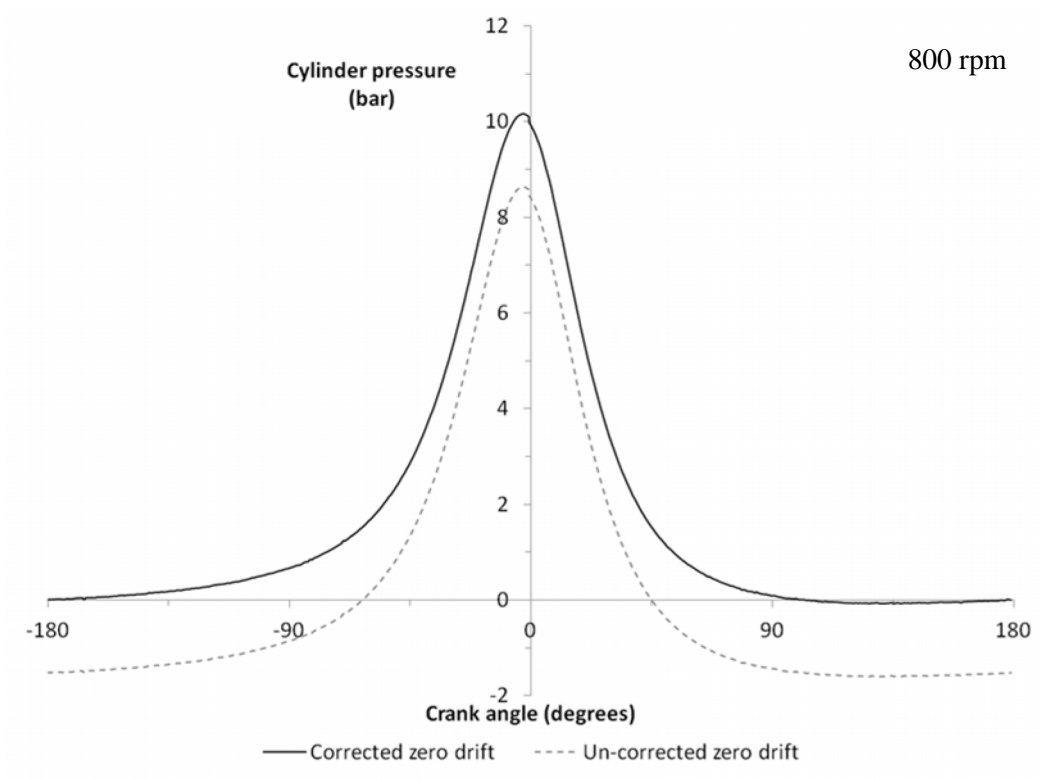


**Figure 4-7: Motored engine cylinder pressure measurement showing correction applied for pressure drift**

## 4.2 Engine Lubricant samples

Since this research was interested in the influence of lubricant degradation on piston ring – cylinder wall lubricant film thicknesses, five degraded gasoline multigrade lubricant samples were acquired from Mercedes Benz (MB) Leasing in Leeds, UK and a single degraded diesel monograde lubricant sample from Southwest Research Institute (SwRI) Texas, USA. The lubricant samples from MB were from customer vehicles acquired during lubricant drain service intervals and were from a wide range of vehicles. An additional fresh lubricant sample of the same type as the gasoline samples was also acquired. The diesel sample from SwRI was an API end-of-test lubricant sample removed from a Caterpillar 1Y73 diesel engine when tested for the requirements of the lubricant standards API CF and API CF-2. These standards test for lubricant effectiveness in preventing ring sticking and

ring/piston/liner scuffing, and a complete test lasts 120 hours (ASTM D4485). A list of the lubricants, their grade and service interval is presented as Table 4-1.

Lubricant	Description	SAE Grade	Oil Type	Service Interval
A	MB Fresh/Castrol Edge SLX Professional Longtec	0W-30	Gasoline	Fresh lubricant sample
B	2005 MB A170 Auto	0W-30	Gasoline	5470 miles
C	2009 CLK200 Kompressor	0W-30	Gasoline	9156 miles
D	Reference test oil (API CF/CF2)	40	Diesel	120 hours
E	2010 MB C180 CGi	0W-30	Gasoline	9722 miles
F	2009 CLK200 Kompressor	0W-30	Gasoline	8463 miles
G	2000 C320 V6	0W-30	Gasoline	8362 miles

**Table 4-1: A list of the lubricants acquired for the investigation of piston ring to cylinder wall film thickness measurements**

#### 4.2.1 Lubricant chemical analysis

The lubricants in Table 4-1 were analysed to examine the state of degradation by FTIR spectroscopy using a Perkin Elmer S100 Series FTIR. For the MB samples, a scan was taken of the fresh lubricant (Sample A), with the complete spectra with known compound absorption peaks presented as Figure 4-8. The region below  $1200\text{ cm}^{-1}$  is known as the fingerprint region of the spectra where exact identification of compounds is difficult since an overlap of different compound absorption peaks occurs. For this research, the focus was carbonyl oxidation which absorbs infrared between  $1800$  and  $1650\text{ cm}^{-1}$ . The spectra of all samples showing the carbonyl oxidation peak is presented in Figure 4-9. It can be clearly seen from the spectra that there is an increase in the nitration, from combustion products, and carbonyl oxidation when compared to the fresh Sample A. For clarity, the diesel sample, Sample D, has also been included to demonstrate the universality of FTIR infrared spectroscopy. A repeat sample scan was performed on the fresh sample A and was found to be within 1% of the first scan. Overlaying the fresh lubricant sample and degraded lubricant sample on the same spectrum provides quick identification of lubricant chemical changes and has been attempted by researchers in the past (Coates and Setti 1983; Powell and Compton 1993)

By comparing the area underneath the oxidation region of each degraded sample to the same area of the fresh lubricant, it is possible to provide some quantification to the increase in degradation as caused by oxidation. This is assuming that the fresh sample has not oxidised. The data in Table 4-2 shows the percentage increase in oxidation for each of the degraded gasoline samples. This method of investigating the absorption intensity increase as a means of providing some information on the percentage change of an absorption peak has been performed in the past by Coates and Setti (Coates and Setti 1986).

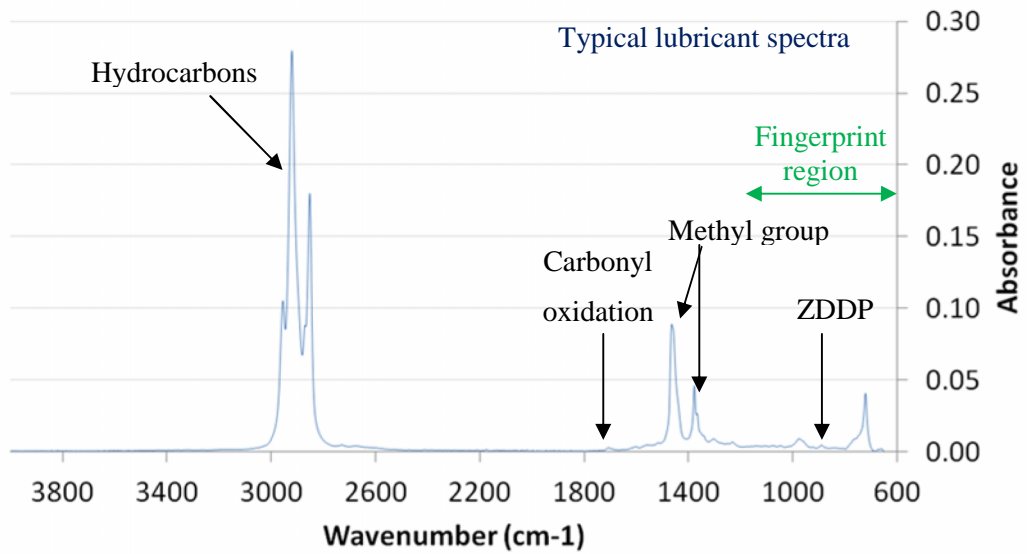


**Figure 4-8: FTIR spectra of Sample A showing most common absorbance peaks**

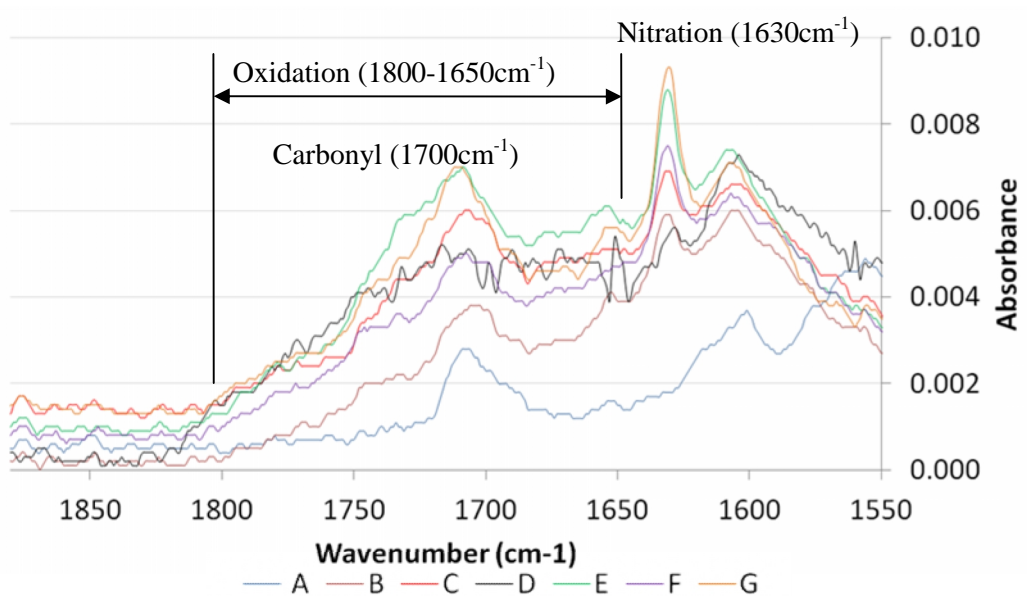


**Figure 4-9: FTIR spectra of oxidation and nitration absorption for all samples**

Lubricant	% Increase in oxidation (1800-1650cm-1)
B	81
C	219
E	272
F	168
G	246

**Table 4-2: Percentage area increase in the oxidation region of the gasoline lubricant samples when compared to the fresh sample**

From Table 4-2, it can be seen that there is an increase in oxidation across all lubricant samples. To investigate the samples further, the lubricant viscosity was also measured.

#### 4.2.2 Lubricant viscosity analysis

The viscosity of the lubricant changes as the lubricant degrades, which in turn should influence the lubricant film thickness experienced at the piston rings. As a result, the viscosity of the lubricant is equally as important as the changes in lubricant chemistry through degradation.

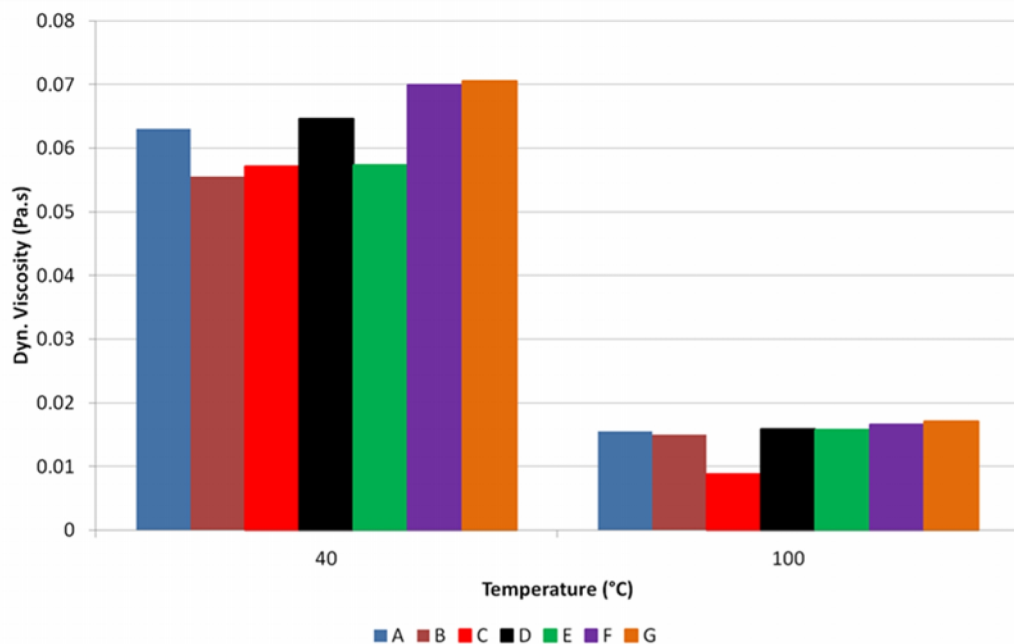


**Figure 4-10: Dynamic viscosity of all samples at 40°C and 100°C**

The viscosity of the lubricant samples was measured with a Malvern Kinexus Pro rheometer using a cone on plate arrangement at shear rates from  $1 \text{ s}^{-1}$  to  $1000 \text{ s}^{-1}$  and temperatures increasing in  $20^\circ\text{C}$  intervals from  $20^\circ\text{C}$  to  $120^\circ\text{C}$ . A repeat of the fresh sample, A, was conducted and at the higher temperatures was found to be within 1% of the initial viscosity scan. For clarity, only results at  $40^\circ\text{C}$  and  $100^\circ\text{C}$  are shown in Figure 4-10. As expected, as the temperature increases, the viscosity of the lubricant decreases. The area of interest is at the higher temperatures, those above  $80^\circ\text{C}$  which is similar to the temperatures to be experienced by the lubricant in the piston ring pack of the motored engine. The largest viscosity change is shown by Sample C but all other gasoline samples were found to have similar viscosity at the higher temperatures.

Since at this stage there was a lack of variation in sample viscosity and in chemical degradation, for the purpose of this research, the first four samples in the list in Table 4-1 were chosen and used in the motored engine for testing. Those samples were 3 gasoline samples; Sample A, B, C and the single diesel sample, Sample D. To improve the clarity of the written communication, Samples A, B, C and D are now known as Samples A (MB fresh), B (MB medium size car), C (MB sports car) and D (diesel) respectively for the rest of this study. These samples underwent further viscosity analysis at high temperature and high shear rates.

Modern lubricants are specified in terms of high temperature and high shear (HTHS) viscosity stability since modern engines operate at high temperatures and speeds. Therefore, it was necessary to investigate the change in HTHS viscosity values due to lubricant degradation and compare with values quoted by lubricant manufacturers. Manufacturer quoted HTHS viscosity values are performed at a temperature of  $150^\circ\text{C}$  and a shear rate of  $1.0 \times 10^6 \text{ s}^{-1}$  following the ASTM D4683 standard (ASTM D4683-10). The test samples A, B, C and D were analysed with a PCS Ultra shear viscometer machine at high shear rates from  $1.0 \times 10^6$  to  $1.0 \times 10^7 \text{ s}^{-1}$  at temperatures 80, 100, 120 and  $150^\circ\text{C}$ . These results are displayed in Figure 4-11. It must be noted that Sample D, diesel sample, failed to produce any results on the viscometer at higher shear rates above  $5.0 \times 10^6 \text{ s}^{-1}$  since the torque with this lubricant exceeded the maximum measurable by the machine at a temperature of  $80^\circ\text{C}$ .

From Figure 4-11, it can be clearly seen that all samples undergo a decrease in viscosity as the temperature increases. The multigrade lubricants suffer from shear thinning at all temperatures since they contain polymer viscosity index improver additives, whereas the monograde diesel lubricant is shear stable. The minimum HTHS viscosity at  $150^\circ\text{C}$  and  $1.0 \times 10^6 \text{ s}^{-1}$  in the lubricant specification is noted and it can be seen that as the lubricant

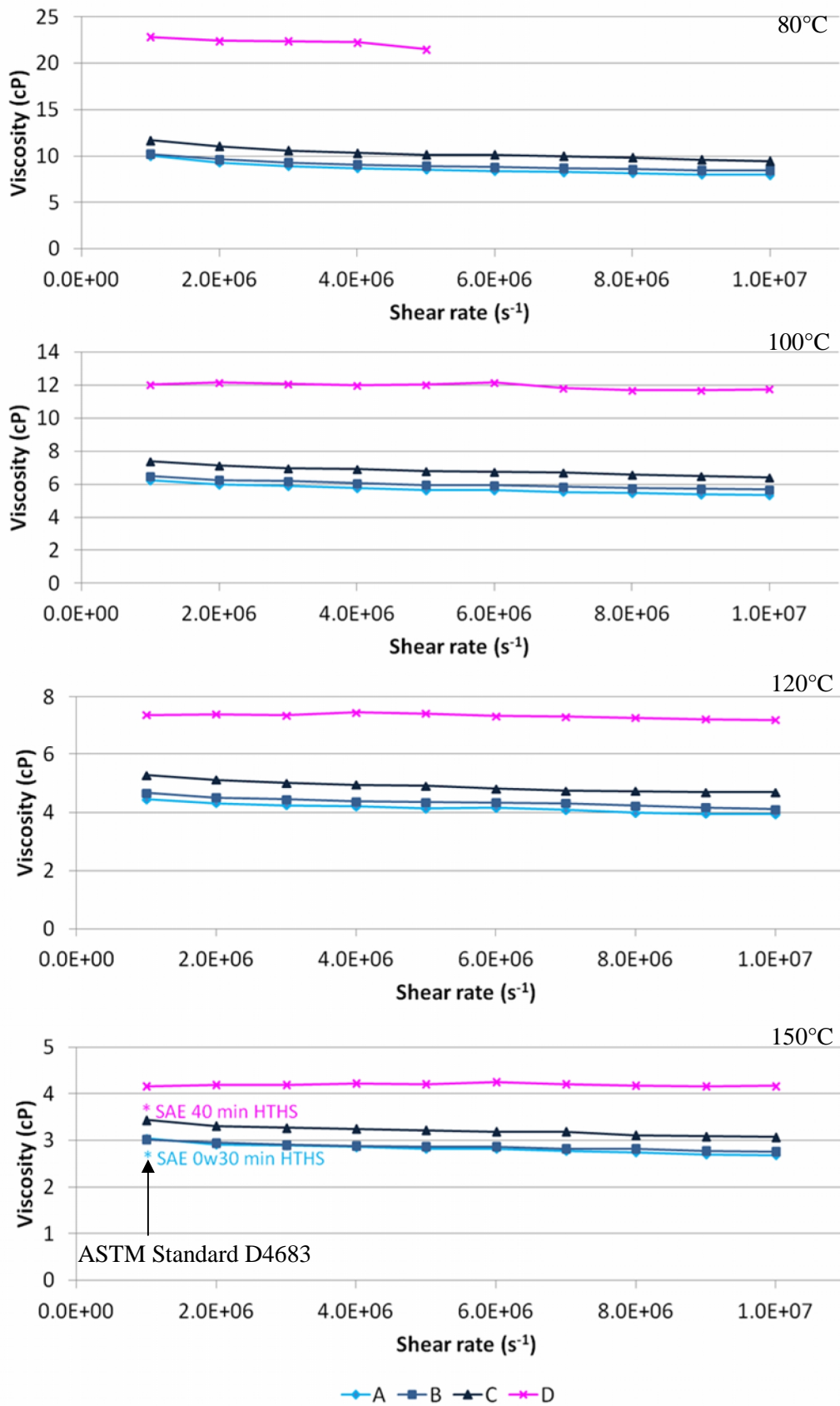


Figure 4-11: HTHS viscosity at increasing temperature for Samples A, B, C and D

degrades, through service, an increase in viscosity occurs at the higher shear rates.

### 4.3 Testing and test matrix

Four lubricant samples were selected, A (MB fresh), B (MB medium size car), C (MB sports car) and D (diesel), and these were tested at three different engine speeds, 800, 1000 and 1200 rpm, at four different cylinder peak pressures, 4, 10, 16 and 22 bar and four different mid-stroke temperatures, 80, 100, 120 and 150°C. The heated bath used for the coolant supply and the increase in cylinder pressure were used collectively to help increase the temperature of the barrel and hence the liner and piston assembly to achieve the higher temperatures desired. However, higher temperatures were not achievable at lower peak cylinder pressures, so lower peak cylinder pressure tests were not conducted at the higher temperatures.

For each test, a single parameter was changed, either the temperature, the speed or the cylinder pressure whilst the other two were kept constant. Tests were conducted in this simple manner to gain an appreciation of the effect of the individual engine parameters on the piston ring lubricant film thickness, but admittedly were unable to statically examine parameter interaction. Once the engine was at the test operating condition, the engine was operated for an additional 30 minutes to ensure that the temperature of the engine was stabilised before data acquisition for the fluorescence investigation commenced. The data acquisition of the fluorescing lubricant only took approximately a couple of seconds which provided a data file of the piston ring film thickness profiles per a number of engine cycles. To check for repeatability, test numbers were selected at random and repeated once. Once the test matrix was completed for one lubricant the next test lubricant was employed after a double lubricant flush and drain. During the lubricant change procedure, the test lubricant was drained from the engine, 2 litres of a fresh lubricant of the same kind was poured into the engine sump and the engine operated with this lubricant for approximately one hour at 1200 rpm engine speed and at 16 bar cylinder peak pressure. This lubricant was then drained and the 2 litres of the test lubricant was used to flush the engine of the previous lubricant at the same engine flushing operating conditions, until finally this was drained and 2 litres more of a fresh batch of the test lubricant was poured into the sump ready for examination. At each lubricant drain, a new oil filter was used. Performing the oil flush in this manner reduced the likelihood of cross contamination of lubricant occurred.

The test matrix used for the fresh lubricant, Sample A, is presented in Figure 4-12.

Speed (rpm)	800 rpm	1000 rpm	1200 rpm	800 rpm	1000 rpm	1200 rpm						
Test	1	2	3	4	5	6						
Mid-stroke Temp (°C)	80	80	80	100	100	100						
Pressure (bar)	4	4	4	4	4	4						
Oil Sample	A	A	A	A	A	A						
Speed (rpm)	800 rpm	1000 rpm	1200 rpm	800 rpm	1000 rpm	1200 rpm	800 rpm	1000 rpm	1200 rpm			
Test	7	8	9	10	11	12	13	14	15			
Mid-stroke Temp (°C)	80	80	80	100	100	100	120	120	120			
Pressure (bar)	10	10	10	10	10	10	10	10	10			
Oil Sample	A	A	A	A	A	A	A	A	A			
Speed (rpm)	800 rpm	1000 rpm	1200 rpm	800 rpm	1000 rpm	1200 rpm	800 rpm	1000 rpm	1200 rpm	800 rpm	1000 rpm	1200 rpm
Test	16	17	18	19	20	21	22	23	24	25	26	27
Mid-stroke Temp (°C)	80	80	80	100	100	100	120	120	120	150	150	150
Pressure (bar)	16	16	16	16	16	16	16	16	16	16	16	16
Oil Sample	A	A	A	A	A	A	A	A	A	A	A	A
Speed (rpm)	800 rpm	1000 rpm	1200 rpm	800 rpm	1000 rpm	1200 rpm	800 rpm	1000 rpm	1200 rpm	800 rpm	1000 rpm	1200 rpm
Test	28	29	30	31	32	33	34	35	36	37	38	39
Mid-stroke Temp (°C)	80	80	80	100	100	100	120	120	120	150	150	150
Pressure (bar)	22	22	22	22	22	22	22	22	22	22	22	22
Oil Sample	A	A	A	A	A	A	A	A	A	A	A	A

**Figure 4-12: Motored engine test matrix for test lubricant Sample A**

#### 4.4 Results and Discussion

The piston rings were removed from the engine once testing was completed and profiles of the three piston rings were taken using a Talysurf 120L profilometer. It was decided to perform a profilometric scan of the rings before and after engine testing so that any profile changes could be observed, thereby providing some evidence if the LIF profiles were to change during engine testing as a result of ring wear. The piston, complete with rings, was mounted in a Perspex piece that allowed the rings to be under tension whilst a scan was taken, Figure 4-13. This Perspex mount was developed and used by Priest (Priest 1996) and the same measurement technique as defined by him was used for this research. Using the Perspex mount, the profiles were measured at three locations circumferentially, Figure 4-14. A 2  $\mu\text{m}$  diamond tipped stylus was used. The piston was first placed square to the stylus and the ring profile was measured. The scan often had to be repeated to allow a full profile of the piston ring running race to be obtained. The profiles were outputted to a computer for analysis. To improve the clarity of the written communication, the profiles of the new, Figure 4-15, and used, Figure 4-16, piston rings are presented in this section.

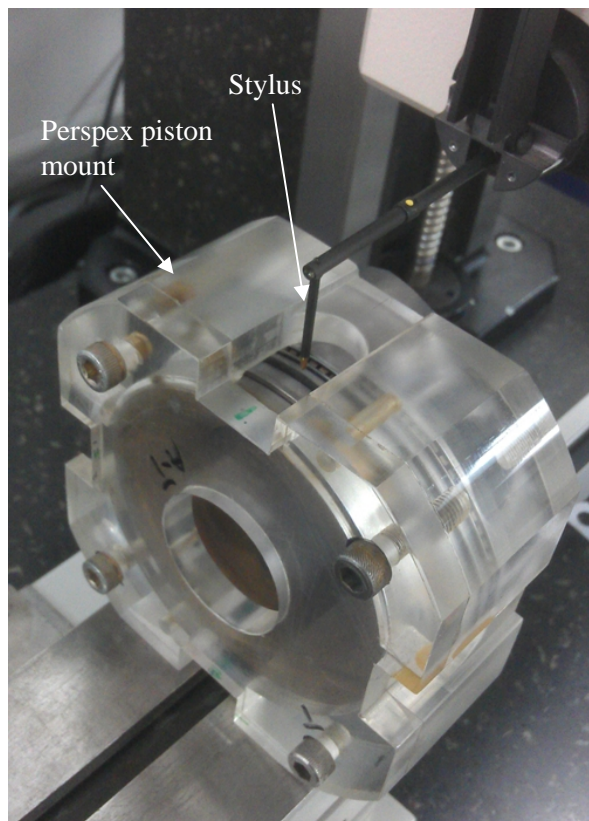


**Figure 4-13: Perspex piece used to mount the piston and allow the rings to be in tension ready for a profilometric scan. As used by Priest (Priest 1996)**

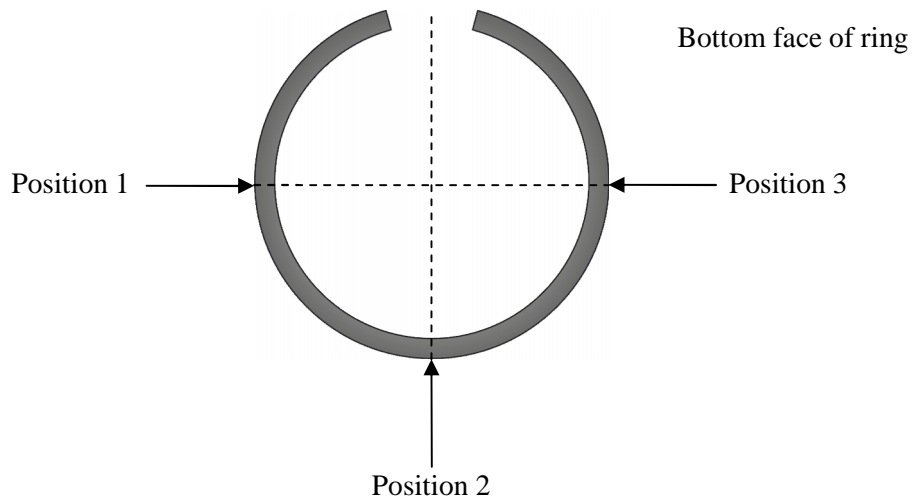


Figure 4-14: Three measurement locations taken on the piston rings

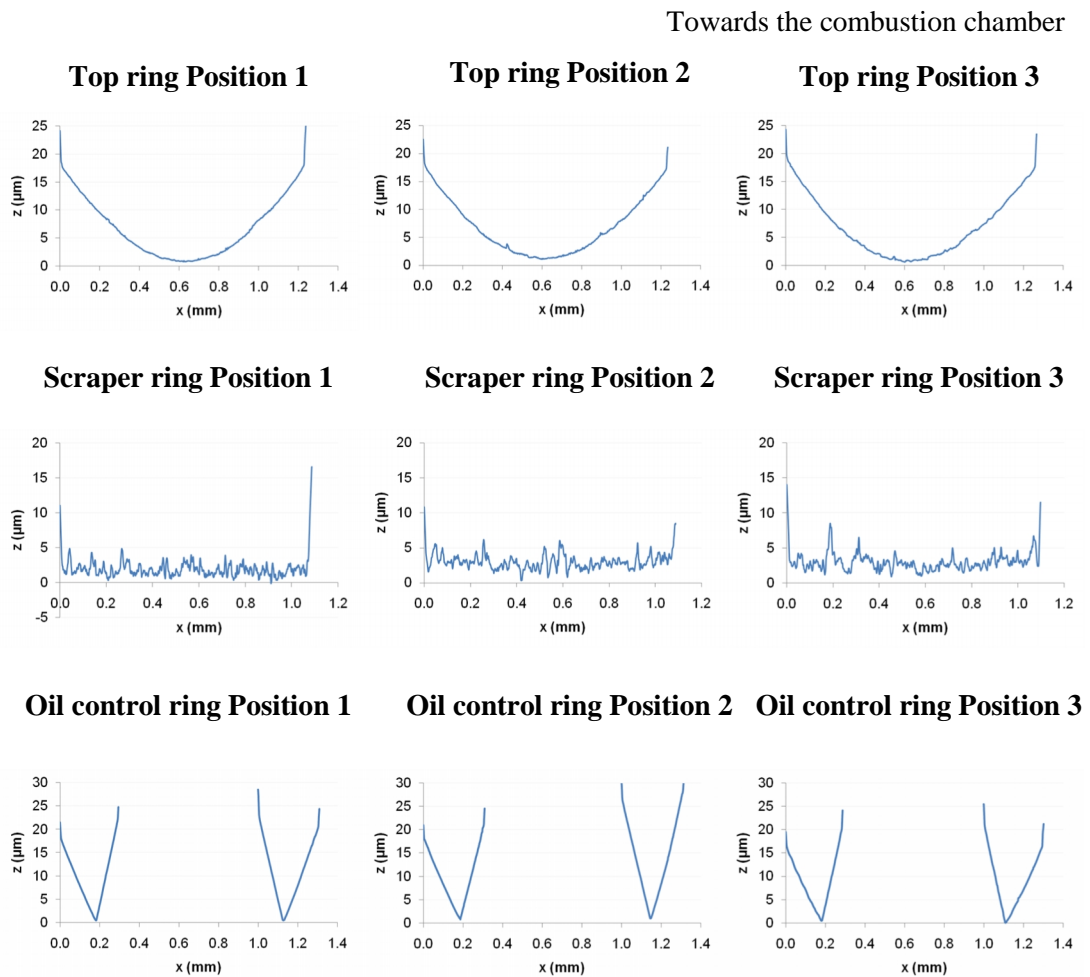
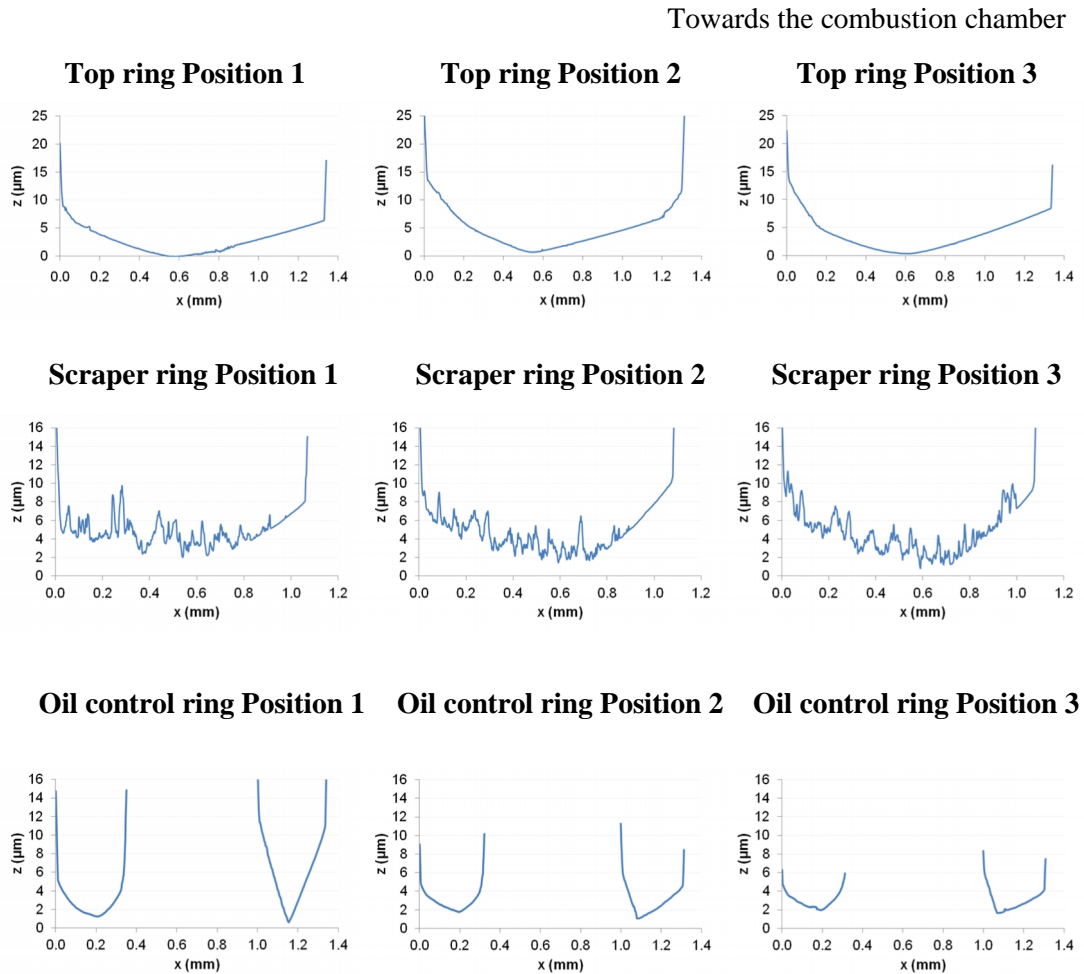


Figure 4-15: Before engine testing new piston ring profiles



**Figure 4-16: End of test (EOT) used piston ring profiles**

The running face of the top compression ring and the scraper rings show a small smooth wear pattern on the bottom tip of the both rings suggesting some running-in wear has taken place, Figure 4-16. It must be noted for the second ring, a Napier ring, the profilometry scan is a scan of the running face of the piston ring and does not include the inherent notch, which is characteristic of its design and benefits the lubricant scraping action. It was decided to just take a scan of the running face since there was a possibility that the stylus would be damaged if the scan trace extended over the full ring face. Both rails of the oil control ring seem to be quite sharp in the profile. This is possibly caused by flanking of the stylus either side of the rail. As a result, it is difficult to comment on the wear profile of the oil control ring.

To understand the film thickness profiles obtained from the engine during operation on a first occasion, in Figure 4-17 a typical LIF profile of OFT against engine crank angle during

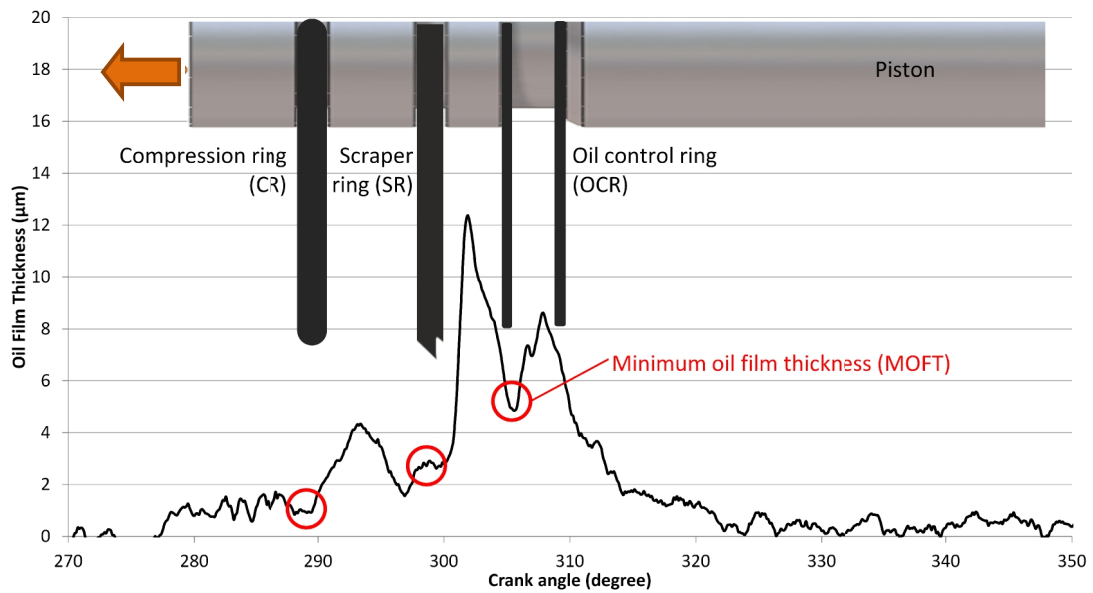


**Figure 4-17: Typical LIF profile with the piston rings superimposed (compression stroke), Sample A at 120°C, 800rpm and 22 bar peak cylinder pressure**

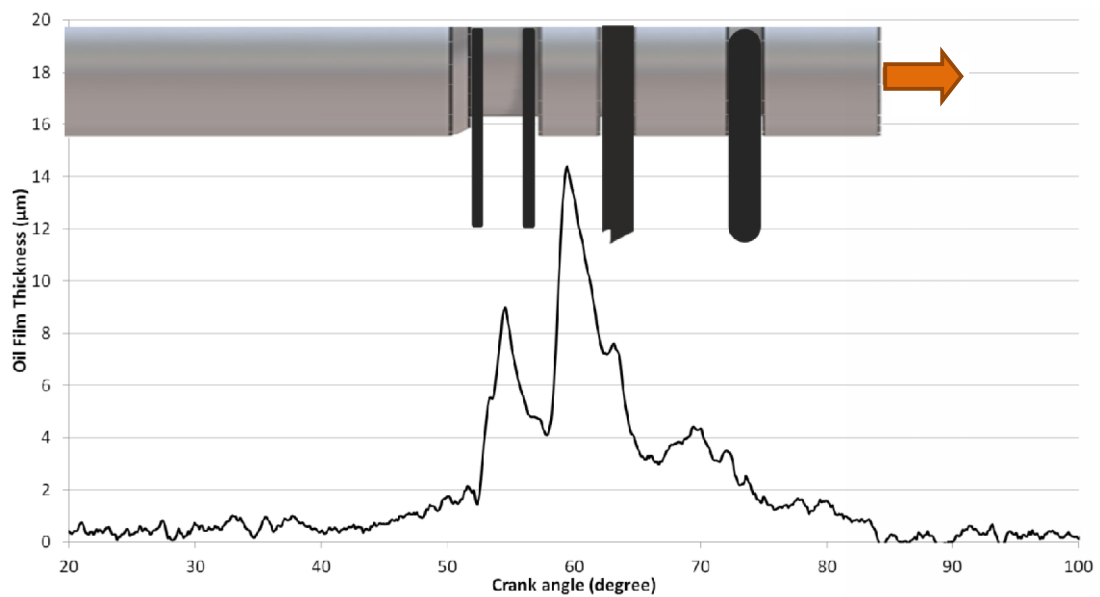


**Figure 4-18: LIF profile on intake stroke shows a mirror like image to the compression stroke profile. Sample A at 120°C, 800rpm and 22 bar peak cylinder pressure**

the compression stroke is presented. A schematic of the piston and piston rings has been added to help demonstrate their position in the profile. The position of the piston and the piston rings on the following figures has been accurately determined using Solidworks computer aided design software. This result refers to the fresh gasoline lubricant, Sample A,

at 800rpm, 120°C mid-stroke probe temperature and at 22 bar peak cylinder pressure. It must be noted that although a single profile of oil is observed across the piston ring pack, between the piston rings the LIF signal will combine any lubricant on the piston lands and lubricant on the cylinder wall (i.e. the optical window) since the technique is two dimensional. For this reason the focus of this research are the films observed under the piston ring, that is the minimum oil film thickness (MOFT). Also the MOFT at the oil control ring (OCR) was taken as the film experienced under the upper oil control rail since the bottom flank of the ring groove had an inherent chamfer which sometimes created a reservoir for local oil films that saturated the film under the lower control ring making exact identification of the MOFT under this rail difficult.

During engine testing, it was found that operating at such high pressures did cause the gaskets to fail prematurely. Initially, the engine was sealed with silicone sealer to prevent the oil contaminating the coolant and preventing coolant leaks. But since high compression pressures were now possible, with the forced induction setup, silicone sealer was found to burst at the interface between the shim and the barrel, causing a loss of cylinder pressure and the coolant oil to aerate. As a result, orange Hermetite Instant Gasket, used for cylinder head sealing, was used with great success.

All LIF results obtained from the motored engine were averaged over 10 complete engine cycles and the standard deviation was found to be 0.7  $\mu\text{m}$  at the piston rings. The standard error was found to be 0.22  $\mu\text{m}$  over the 10 engine cycles. An explanation of this and further data filtering is discussed in Chapter 7. Repeatability was also tested by repeating measurements and the results fell within the repeatability of the initial measurements.

The intake stroke for the same engine operating conditions, Figure 4-18, has an almost mirror image of the profile for the compression stroke, Figure 4-17. The compression stroke does however show a slightly lower film under the second ring suggesting that the increase in cylinder pressure, as the piston moves towards TDC, is pushing the ring harder against the liner thereby squeezing the lubricant out from under the ring. However, since inter-ring gas pressures were not recorded, this can only be assumed to be an effect on the lubricant film thickness. Also, the Reynolds boundary condition predicts thicker films on the downstroke than the upstroke part of the cycle as investigated by Richardson and Borman (Richardson and Borman 1992).

In Figure 4-19 and Figure 4-20, a summary is presented of the effect of engine temperature on the MOFT experienced at the piston rings at engine operating conditions of 800rpm speed

and 22 bar peak cylinder pressure for all test lubricants during the compression stroke. The first noticeable effect that becomes apparent is that regardless of lubricant quality or

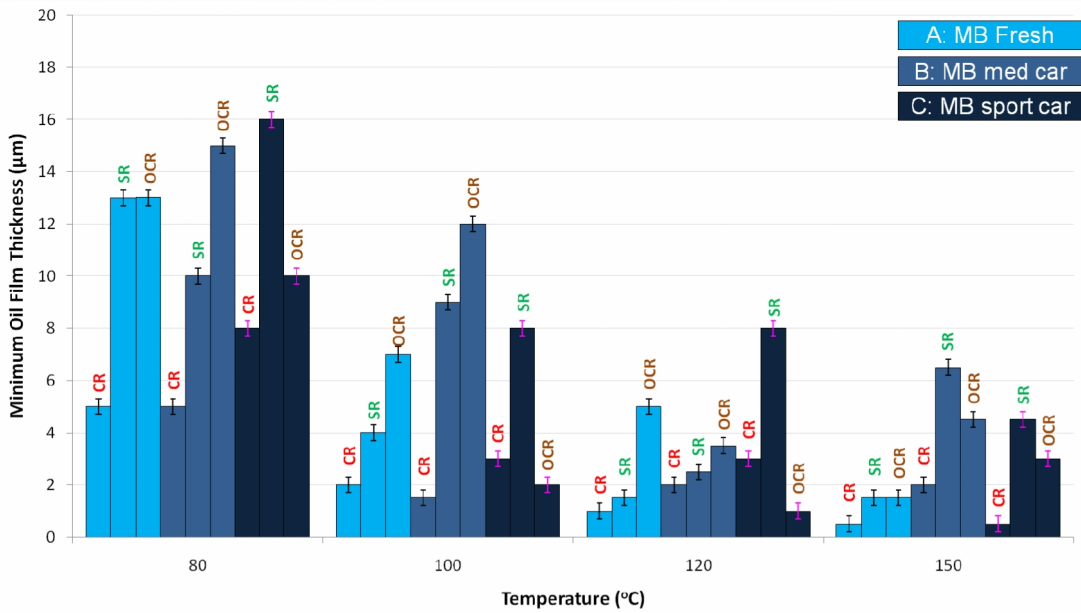


**Figure 4-19: The effect of lubricant temperature on MOFT across the complete piston ring pack for the MB gasoline lubricant samples at 800 rpm and 22 bar pressure**

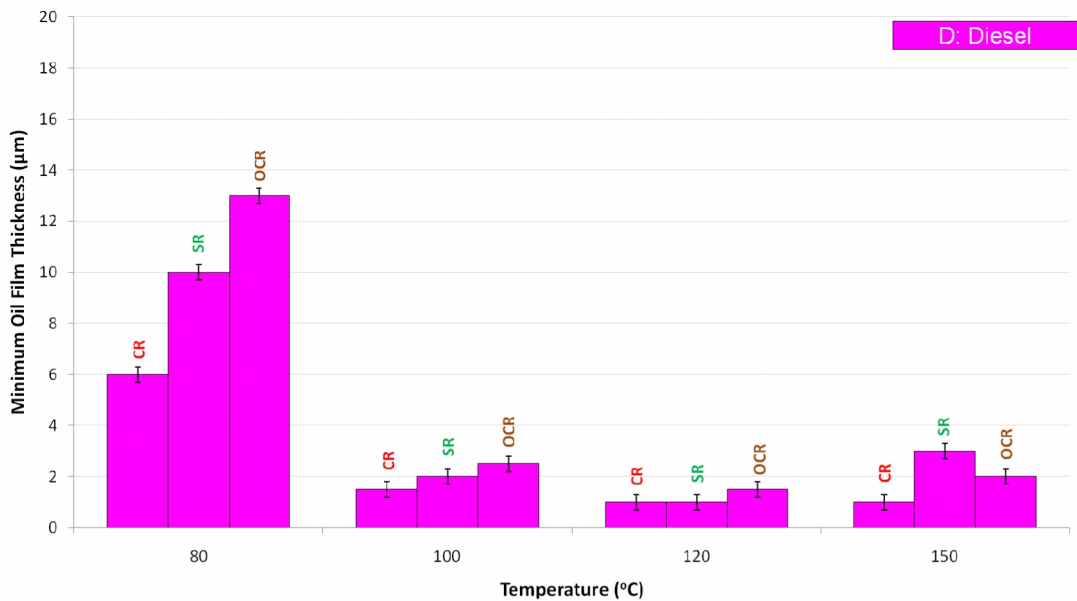


**Figure 4-20: The effect of lubricant temperature on MOFT across the complete piston ring pack for the SwRI diesel lubricant sample at 800 rpm and 22 bar pressure**

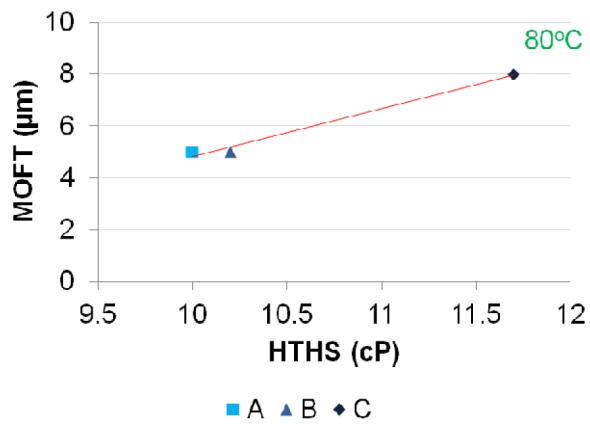


Figure 4-21: Compression ring MOFT vs HTHS viscosity, 80 °C, 800 rpm and 22 bar pressure

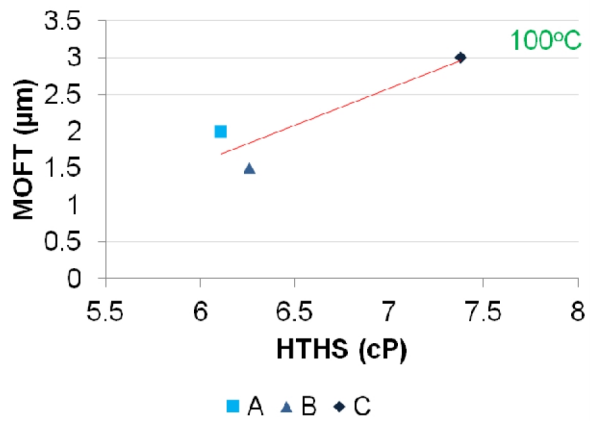


Figure 4-22: Compression ring MOFT vs HTHS viscosity, 100 °C, 800 rpm and 22 bar pressure

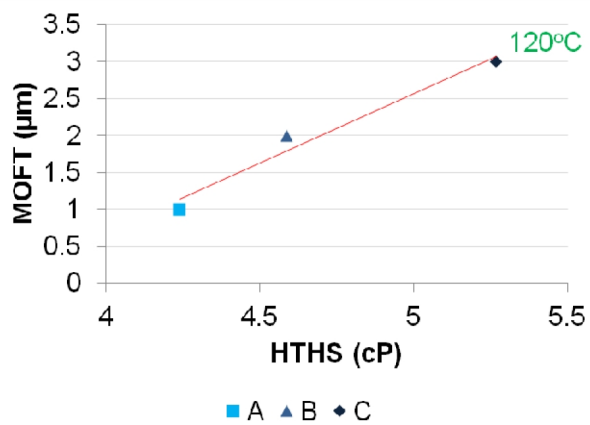


Figure 4-23: Compression ring MOFT vs HTHS viscosity, 120 °C, 800 rpm and 22 bar pressure

lubricant type, the film thickness reduces across the complete ring pack as the temperature increases. This is obviously caused by the lubricant viscosity decreasing with temperature.

Using the data from these results, it was possible to calculate the instantaneous shear rate of the lubricant and hence the instantaneous HTHS viscosity at the mid-stroke position and plot this against the MOFT for the film thicknesses at the compression ring for each gasoline lubricant. Results of the MOFT against the HTHS viscosity values at temperatures 80°C, 100°C and 120°C are presented as Figure 4-21, Figure 4-22 and Figure 4-23 respectively. We can see that the viscosity of the gasoline type lubricants decrease by approximately 50% between 80°C and 100°C whereas the decrease in viscosity between 100°C and 120°C is much smaller. As a result, we see a larger reduction in lubricant film thickness between 80°C and 100°C. Sample C, which is the most degraded gasoline sample, tends to have a greater film thickness than the Sample A, which is the fresh equivalent, see Figure 4-19. Sample C has a greater HTHS viscosity than Sample A and this increase in viscosity is the reason why the film thickness is larger. Sample B, the second most degraded gasoline sample, has very similar profiles to Sample A and is consistent with the HTHS viscosity values being very similar. It can be seen that up to 120°C, lubricant degradation is important especially under the compression ring as it can be seen that there is a clear indication that a degraded lubricant presents thicker films under this ring but as temperatures increase above 120°C the effect becomes negligible. The diesel lubricant, Sample D, (see Figure 4-20) almost immediately experiences a lower MOFT as the temperatures increase above 80°C, but after does not show as much change as the gasoline lubricant did. Strangely, the diesel lubricant was expected to retain thicker piston ring lubricant films as temperature increased much better than the gasoline lubricants since it is a SAE 40 monograde lubricant with a greater viscosity than the gasoline lubricants, but instead it presented reduced films above 80°C. This actually correlates well with the behaviour of Sample D observed in the HTHS viscosity results (see Figure 4-11) as an increase in the test from 80°C to 100°C saw a greater decrease in the viscosity than anything above 100°C.

The effect of cylinder peak pressure on the MOFT at the piston rings at 800 rpm and 120°C mid-stroke temperature during the compression stroke is illustrated in Figure 4-24 for the gasoline lubricants and in Figure 4-25 for the diesel lubricant. From Figure 4-24, it can be seen that as the compression pressure is increased, the rings are pushed harder into the cylinder liner and the film thickness is observed to reduce but only very slightly. The gasoline lubricant which is most degraded, Sample C, presents a larger film thickness across the entire piston ring pack than Sample A throughout the test. Strangely, the diesel lubricant (see Figure 4-25) does not seem to be affected by the increase in the cylinder pressure as the

films under the top two rings per pressure increase are small and similar. A possible cause is that the higher viscosity of the lubricant, when compared to the gasoline lubricants, is affecting the oil flow into and out of the ring pack. An opposite effect of the use of lower

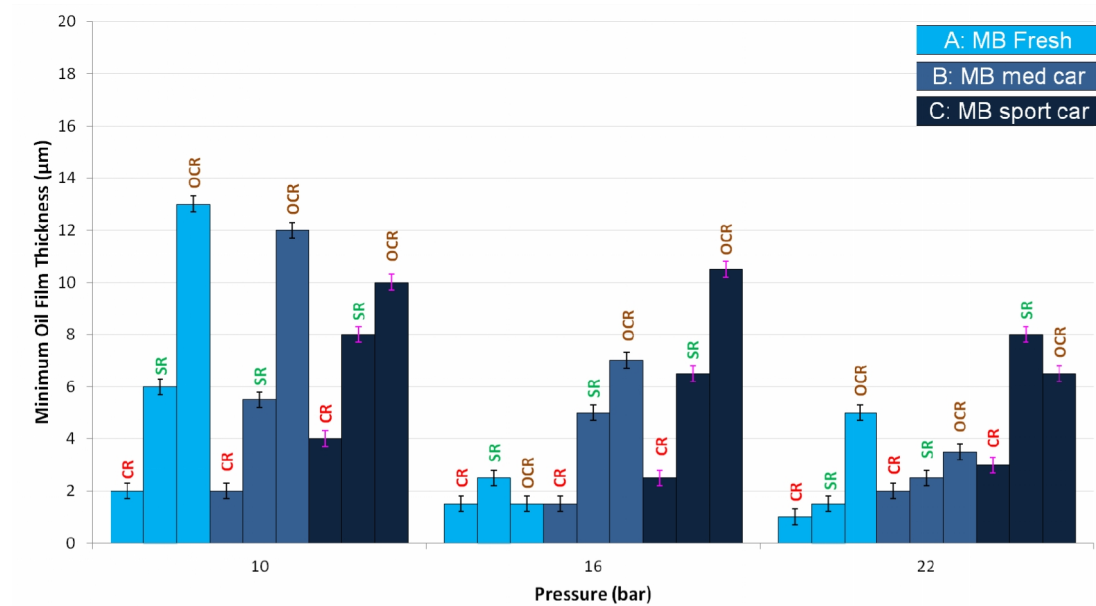


**Figure 4-24: The effect of cylinder peak pressure on the piston ring pack MOFT for the MB gasoline lubricant samples at 800 rpm and 120°C**

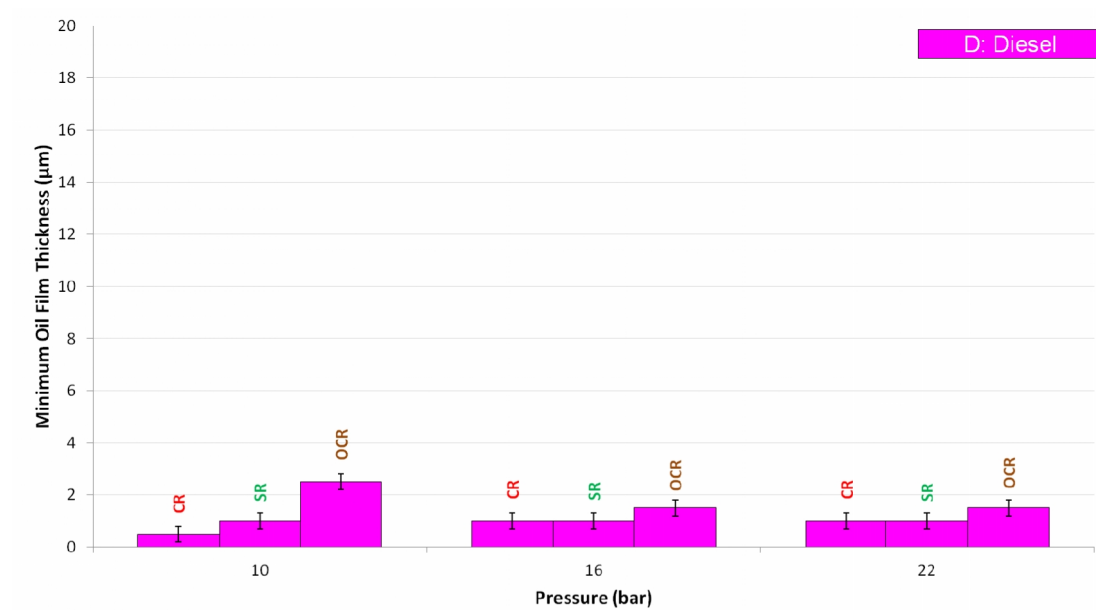


**Figure 4-25: The effect of cylinder peak pressure on the piston ring pack MOFT for the SwRI diesel lubricant sample at 800 rpm and 120°C**

viscosity lubricants was that a thicker lubricant film has been measured at TDC in a diesel engine (Moore 1985).

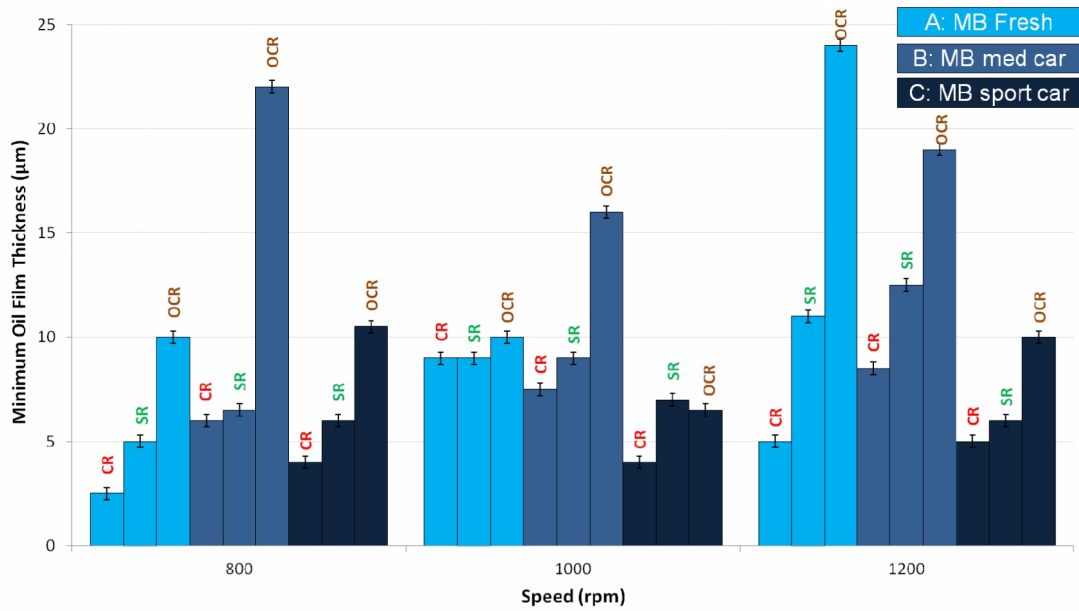


**Figure 4-26: The effect of engine speed on the piston ring pack MOFT for the MB gasoline lubricant samples at 16 bar cylinder pressure and 100°C**

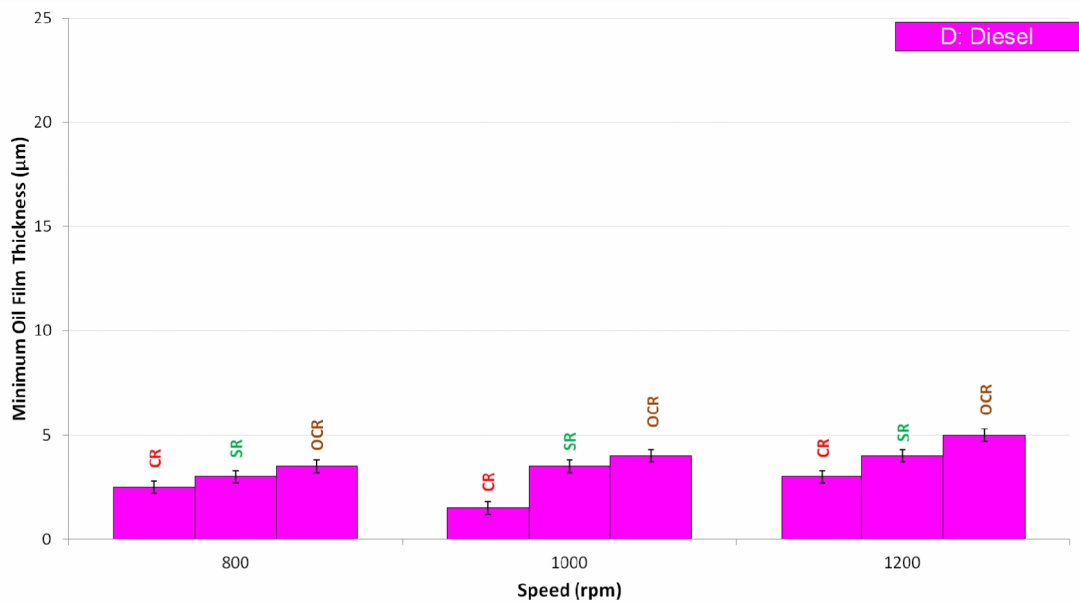


**Figure 4-27: The effect of engine speed on the piston ring pack MOFT for the SwRI diesel lubricant sample at 16 bar cylinder pressure and 100°C**

The effect of engine speed on the MOFT at the piston rings at 16 bar peak cylinder pressure and 100°C mid-stroke temperature is illustrated in Figure 4-26 for the gasoline lubricant samples and in Figure 4-27 for the single diesel lubricant sample. It can be seen that as the engine speed increases, the MOFT, especially at the bottom two piston rings, increases. The crankshaft speeds are greater and the rate of the oil squirt onto the liner, from the crankshaft and connecting rod, will also be greater thereby contributing to the increase in oil availability in the piston ring pack. The diesel sample (see Figure 4-27) does present similar trends to the gasoline lubricants when the engine speed increases. Additionally, the Reynolds boundary condition predicts thicker films under the piston rings as the engine speed increases (Richardson and Borman 1992). However, again the greater lubricant viscosity is affecting the flow of the lubricant in and out of the ring pack and this could be the reason why the diesel lubricant does not follow the trend as proficiently as the gasoline lubricants. However, it must be stated that without measuring the oil flow rate through the ring pack simultaneously, this can only be considered as a hypothesis. Admittedly, the small range in engine speed does not provide much variation in the piston ring pack MOFT when considering the influence of the lubricant degradation.

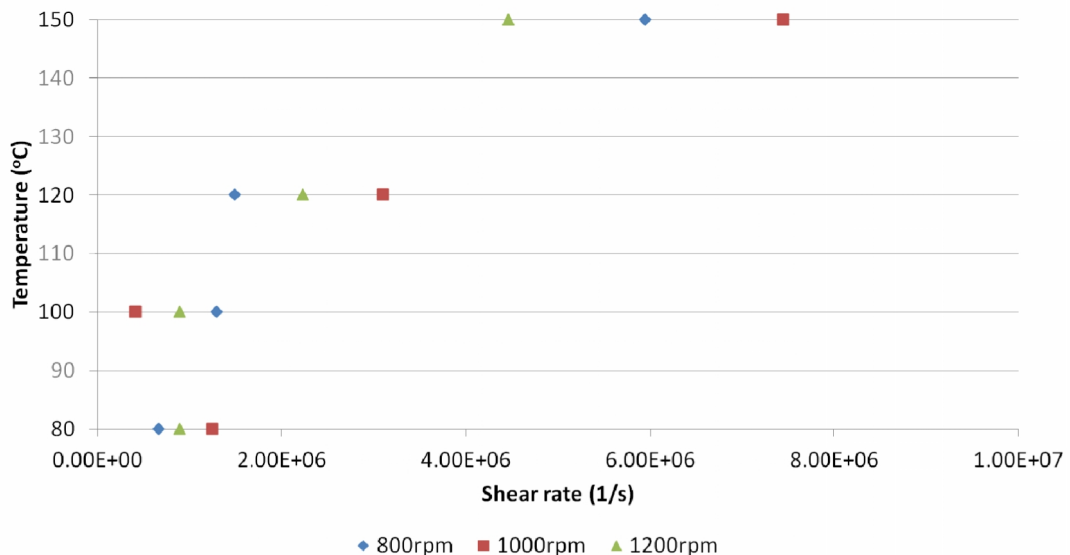


**Figure 4-28: The influence of temperature and engine speed on Sample A lubricant shear rate at 16 bar peak cylinder pressure**

Since the film thickness is measured at the piston ring and from calculations of the piston speed at mid-stroke, it is possible to determine the shear rate of the lubricant between the

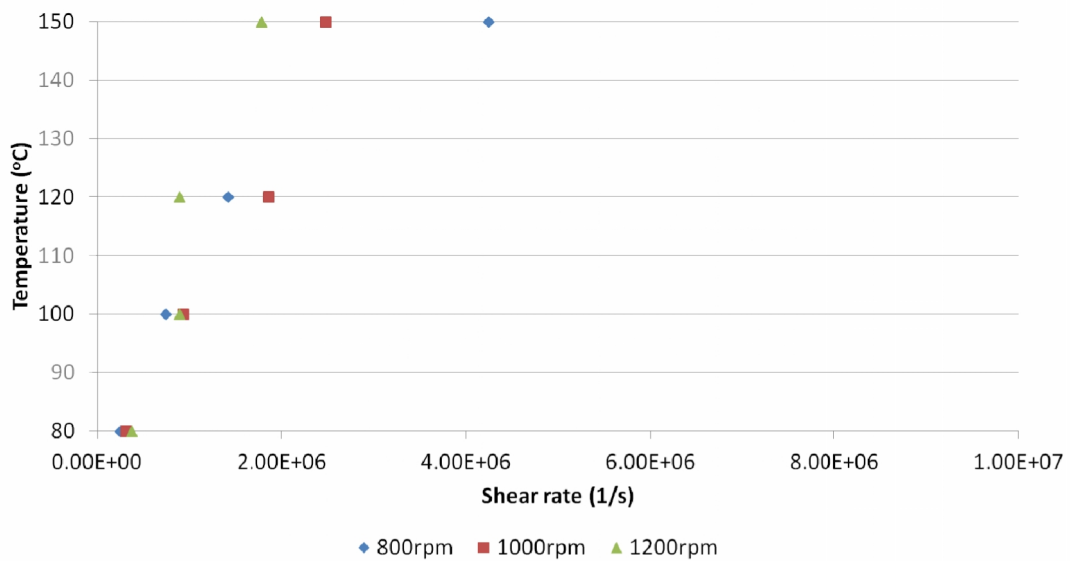


**Figure 4-29: The influence of temperature and engine speed on Sample C lubricant shear rate at 16 bar peak cylinder pressure**

piston ring and the cylinder wall. The shear rate as a function of temperature and speed for a peak cylinder pressure of 16 bar is presented in Figure 4-28 for Sample A and Figure 4-29 for Sample C. Immediately it can be seen that the temperature is a major contributor to the shear rate the lubricant experiences since the viscosity of the lubricant decreases with temperature, which in turn minimises the film thickness at the piston ring for a given engine speed. Since Sample C has a larger viscosity than the fresh Sample A, the overall maximum shear rate for any given temperature or engine speed for the former is much less than Sample A. It must also be noted that regardless of the fact that the shear rate for the fresh lubricant is much greater than the degraded lubricant, permanent viscosity loss does not occur since there is a lack of energy to completely break the polymer bonds during operation (Mortier, Fox et al. 2009). Additionally, as engine speed increases for a given temperature, the film thickness is greater, as discussed earlier, and as a result the shear rate reduces with the increasing film thickness.

#### 4.4.1 End of test (EOT) components

During the first set of tests, a sudden large accumulation of lubricant occurred at the second ring position. The cylinder head, barrel and liner of the engine were removed and upon inspection it was found that the second piston ring was broken and this was replaced and testing continued. No visible damage to the engine liner or the piston and the piston

assembly was observed. This was also a good time to investigate the engine and check for any issues.

Photos of the engine liner were taken at the end of engine testing on the thrust side, Figure 4-30, and the anti-thrust side, Figure 4-31, of the liner. Again on both surfaces no visible damage to the liner was observed, proving the LIF probing system caused no physical damage to the natural operating condition of the engine.

The cylinder head was removed. It was observed that on the piston crown there was residue from where the temperatures were high enough to cause the lighter compounds in the lubricant to evaporate leaving the heavier compounds adhering to the piston crown. This can be clearly seen in Figure 4-30, Figure 4-31 and Figure 4-32. Also, Figure 4-32, shows how the probe sleeve fits into the barrel to allow the probe optical examination without interfering with the coolant jacket, which was a concern as mentioned in Chapter 3.



**Figure 4-30: Thrust side of cylinder liner at EOT**



**Figure 4-31: Anti-thrust side of cylinder liner at EOT**

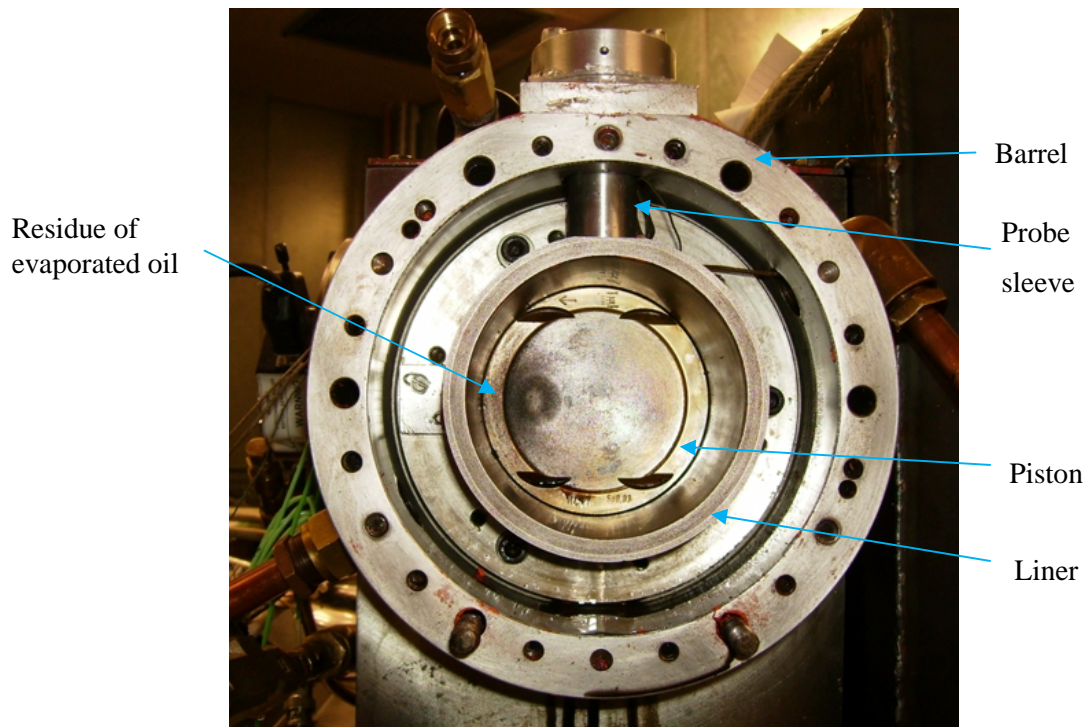


**Figure 4-32: Cross section of engine without cylinder head showing the piston crown deposits**

## 4.5 Conclusions

A LIF system has been developed to investigate the piston ring to cylinder wall lubricant film thickness for a range of engine operating conditions and also a wide range of engine lubricants. The novelty in the system is that film thickness profiles of even degraded engine lubricants can be investigated with very good spatial resolution. The results were obtained from a motored gasoline engine and the following conclusions can be drawn:

- the LIF system is universal in that lubricant film thickness profiles of different types of engine lubricants with varying degradation and viscosity grades can be investigated.
- the lubricant film thickness profiles of the intake and compression strokes were almost identical in shape. The compression stroke did however, present lower film thickness under the piston rings due to the increase in cylinder pressure as the piston came towards TDC.

- increasing the mid-stroke, and hence lubricant, temperatures saw the lubricant viscosity decrease, which in turn reduced the MOFT at the piston rings. This was true regardless of lubricant type, grade or even quality in terms of degradation phase.
- a reduction in cylinder peak pressure reduces the overall effectiveness of the piston ring sealing of the top two rings and increased the MOFT at the ring pack.
- more lubricant is available on the cylinder liner and hence the piston ring pack, since a greater rate of oil throw from the crankshaft and connecting rod occurs at higher speeds, thereby increasing the piston ring MOFT.
- HTHS viscosity results correlated very well with the lubricant profiles and the MOFT values. It was also found that an increase in engine speed reduced the lubricant shear rate since the film thickness increased but an increase in mid-stroke temperatures had the an opposite effect and the lubricant shear rate increased for any given engine speed.
- the shear rate of the degraded lubricants, which had a greater increase in viscosity, were generally found to present lower shear rates regardless of engine operating condition than an equivalent fresh lubricant of a lower viscosity.
- generally, a fresh gasoline engine lubricant was seen to have a lower MOFT under the top two piston rings than an equivalent degraded lubricant regardless of engine operating condition.

# **Chapter 5 Development and Testing of a LIF System on a Ricardo Hydra Fired Test Engine**

The LIF system had been implemented successfully on the motored engine and much of the initial development problems had been resolved. It was now time to move on to the fired Hydra engine work to confirm some of the initial motored engine results and to test the system at higher engine speeds and loads.

A complete move of the LIF system to the Hydra engine was made and to facilitate this, additional parts had to be designed and machined. All bench mounted optics were transferrable, but new components were required for fitting to the engine. The design strategy followed the success of the system on the motored engine with a new probe sleeve being machined. A spare unfinished Hydra barrel was available and this was machined to accommodate the new probe sleeve and hence, the LIF collimator probe.

The engine lubricants acquired from Mercedes Benz and used for testing purposes in Chapter 4, were also used as test lubricants in the Hydra engine. Engine testing included the effects of engine speed and load. These results are presented and discussed in this chapter.

## **5.1 Ricardo Hydra gasoline single cylinder engine**

The Ricardo Hydra is a gasoline single cylinder engine designed primarily for research purposes by Ricardo Consulting Engineers Limited. This engine has already been proven to be a successful engine for tribology research and many publications have been drawn from it, such as (Stark, Wilkinson et al. 2004; Mufti and Priest 2005; Lee, Priest et al. 2006; Mufti, Priest et al. 2006; Mufti and Priest 2009). It is a naturally aspirated gasoline indirect injected engine based on a quarter of a commercially available 1998 cc in-line 4 cylinder General Motors engine introduced in 1988. The engine uses a production piston (AE reference 24024) and an equivalent production piston ring pack set (AE reference R23490). It was equipped with a single 86 mm bore wet liner housed in a barrel allowing for liquid cooling. The parent engine had a metal bore and no separate cylinder liner. As a result, the cylinder liner for this engine was turned from cast iron and machined in-house. The stroke length was

86 mm and the compression ratio in this configuration was 10.5:1 with a displacement of 499.5 cc. The engine has dual overhead camshafts and had four valves per cylinder; two inlet valves and two exhaust valves. The flywheel is directly connected to a dynamometer which can provide motoring operation and absorb torque under fired conditions. It can be operated fired up to 5000 rpm, which was software limited, and with a maximum torque output of 36 Nm. The engine uses a dual lubricant supply such that the crankshaft and the piston assembly can be lubricated with a separate lubricant to the valvetrain. This allows high quality lubricant to lubricate the valvetrain whilst simpler formulations for test purposes can be used to lubricate the bottom end without causing premature wear of the valvetrain. The cylinder liner is lubricated via a splash feed from the crankshaft rotation coupled with a connecting rod squirt action. This cylinder liner lubricant supply setup is exact to the parent engine system. A CP Engineering control system, using Cadet V14 software, was used to electronically control the engine and the dynamometer in terms of ignition advance, injection squirt rates, desired engine speed and load. A Horiba Automotive Emissions Analyser, model MEXA-554JE, was used to analyse the exhaust emissions and determine whether the charge mixture is stoichiometric, and provide quantitative information on the CO, CO<sub>2</sub> and the unburnt hydrocarbons. The CP Engineering control system is defined further in Chapter 7 and the Ricardo Hydra engine specifications are presented in Appendix G.

## **5.2 Implementation of the LIF system on the Hydra**

### **5.2.1 Design and manufacture of Hydra barrel**

The use of the probe sleeve to allow the collimator probe to be removed from the engine and be sealed from the coolant jacket was a successful design idea that was used on the motored engine. A similar sleeve was also required for the Hydra engine.

The Hydra engine was equipped with a barrel that accepted a single wet cylinder liner and retained coolant that flowed in and out of the barrel, for heat removal, similar to the barrel on the motored engine. The barrel was an original specification made from cast iron. A spare unfinished barrel was available at the start of this project which was machined from mild steel and it was decided to use this as a means to provide optical access to the liner. This barrel required drilling and tapping to accept the cylinder head bolts, and also required the coolant drain and supply holes for the cylinder head.

Since there was a spare square barrel available, it was decided that any machining of the barrel should take into account the possibility of expanding the current single point LIF

probe in the future to a multipoint system with additional probes. It was also desirable to have a system where the probe could be removed from the engine and to have a barrel that could be easily instrumented without the need for a tedious engine disassembly. The design of the Hydra engine restricts any access to the front of the barrel, because of the timing belt, but there is access to the barrel on the left (thrust side), right (anti-thrust side) and back (flywheel side) of the engine. It was decided to remove sections from these three sides of the barrel to allow access to the cylinder liner in the centre. The illustration in Figure 5-1 shows the modified Hydra barrel. The sections coloured in green are the sections that were machined and removed for access to the cylinder liner, which was positioned in the orange section. The blue face on top is the face the cylinder head fixes to with a gasket in-between.

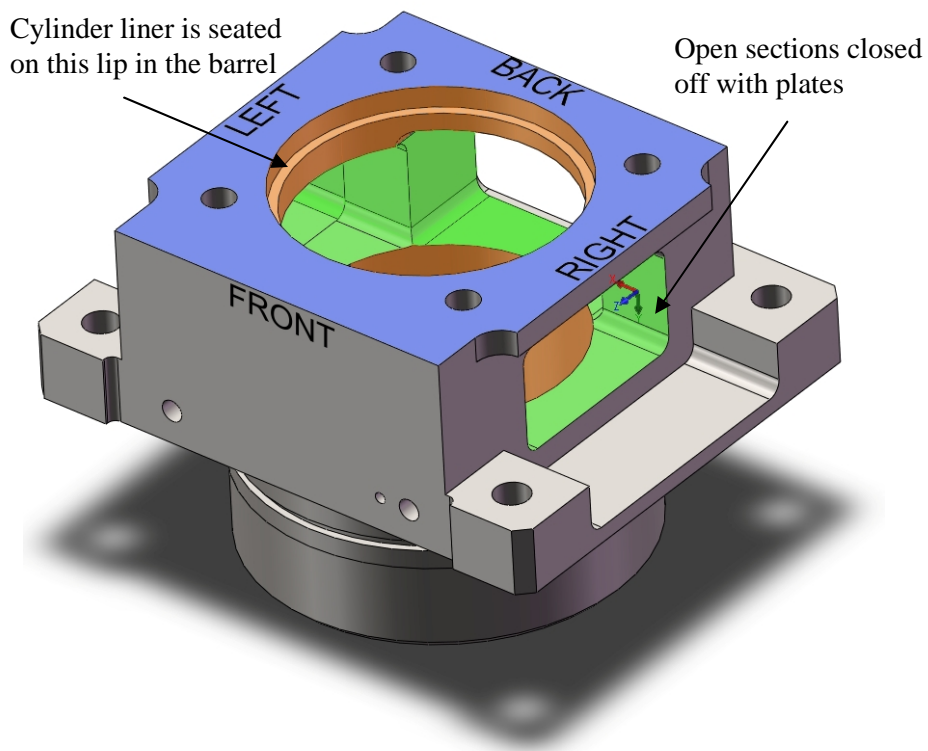


**Figure 5-1: Illustration of modified Hydra barrel**

By opening the side sections on the barrel, an improvement to the access of the external surface of the cylinder liner was made. This in turn improved liner instrumentation installation and eased the routing for any liner oil sampling pipes. Each side section required a 10 mm thick mild steel plate slightly larger than the open section to cap off the section and contain the coolant. Each plate was held in place with an array of M5 screws. To prevent coolant leaks, paper gaskets were placed between these plates and the barrel. An additional

benefit of using plates, was that should there be a need to instrument the barrel with other sensors or even sampling tubes, the plate could be changed and no further modifications to the barrel would be required. This has a greater advantage over the original cast iron barrel whereby any modifications for the installation of instrumentation devices would be permanent.

The original barrel has the coolant intake on the thrust side and the coolant outlet on the anti-thrust side of the cylinder head. Since it was desired to have the LIF probe on the thrust side, a barbed hose tail was turned from mild steel and welded on the plate on the flywheel side to accept the coolant pipe allowing coolant to enter the barrel from this side, Figure 5-2.

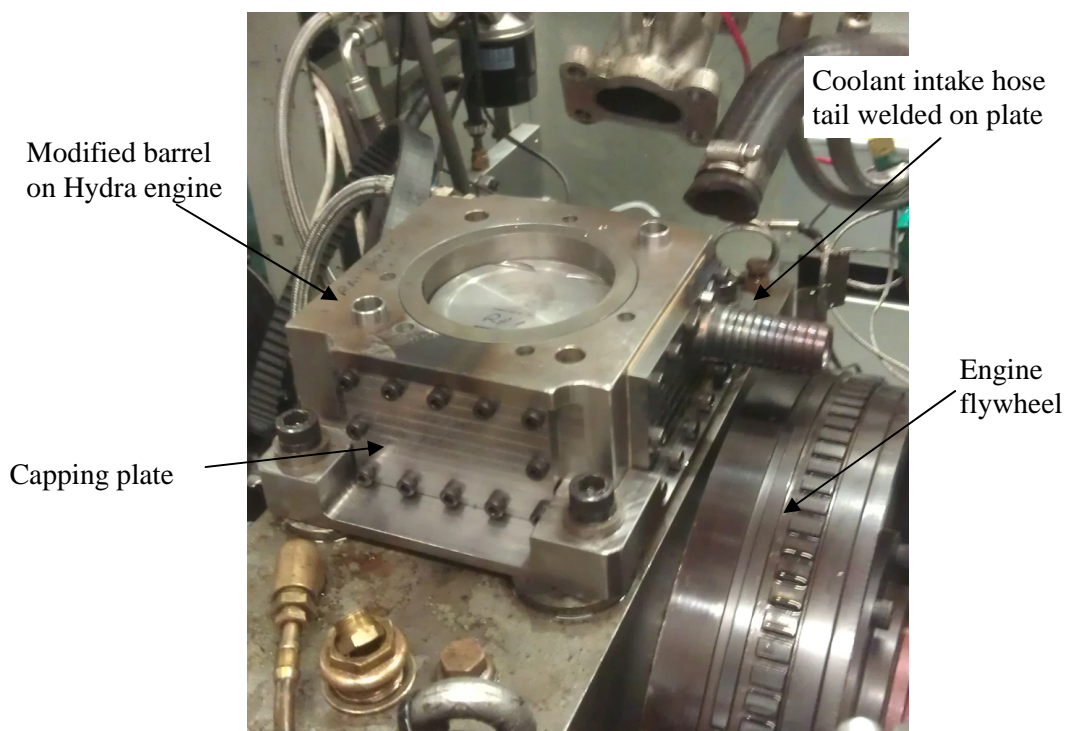


**Figure 5-2: A picture of the coolant intake re-positioned on the engine flywheel side**

Similar to the system implemented on the motored engine, a liner with a thicker wall was machined and used to help improve the fixing of the window and the probe sleeve to the liner. The liner had a wall thickness of 9.5 mm as opposed to the original 5.0 mm. The thicker wall of the liner was only present from just below the TDC and extended to just below the mid-stroke position. The larger wall thickness meant that it was not physically possible for the liner to fit into the bore of the barrel since the extra material interfered with the lip at the top of the barrel, which seats the liner in the barrel, and can be seen in Figure

5-1. So, it was decided to remove the extra wall thickness of the liner, but retain it at the probe position. Since future expansion was the focus, the material was retained at three sections circumferentially around the liner, at the thrust, anti-thrust and flywheel side of the engine, Figure 5-3. These sections were at 90° to each other and were machined flat. Consequently, three sections from the barrel lip at the same positions were also removed to allow this liner to be inserted. This allowed the liner to be inserted and aligned correctly every time during subsequent engine disassembly and assembly, since the liner could only be inserted in one way.

A probe sleeve was machined from aluminium, similar to the sleeve as designed and manufactured for the motored engine. This sleeve was fitted from the outside and attached to the plate on the thrust side. The setup, complete with the liner in the barrel and the probe sleeve attached, can be seen in the illustration in Figure 5-4. A groove in the bottom of the sleeve held an o-ring between the sleeve and the liner to seal the sleeve and the window from the coolant, as can be seen in the schematic in Figure 5-5. The probe position was at mid-stroke and on the thrust side to remain consistent with the setup on the motored engine. The same sapphire window, as used in the motored engine, was also mounted in the cylinder liner for the Hydra engine. The same practice of colouring the window seating black, as for the motored engine in Chapter 4, was also implemented on this liner.

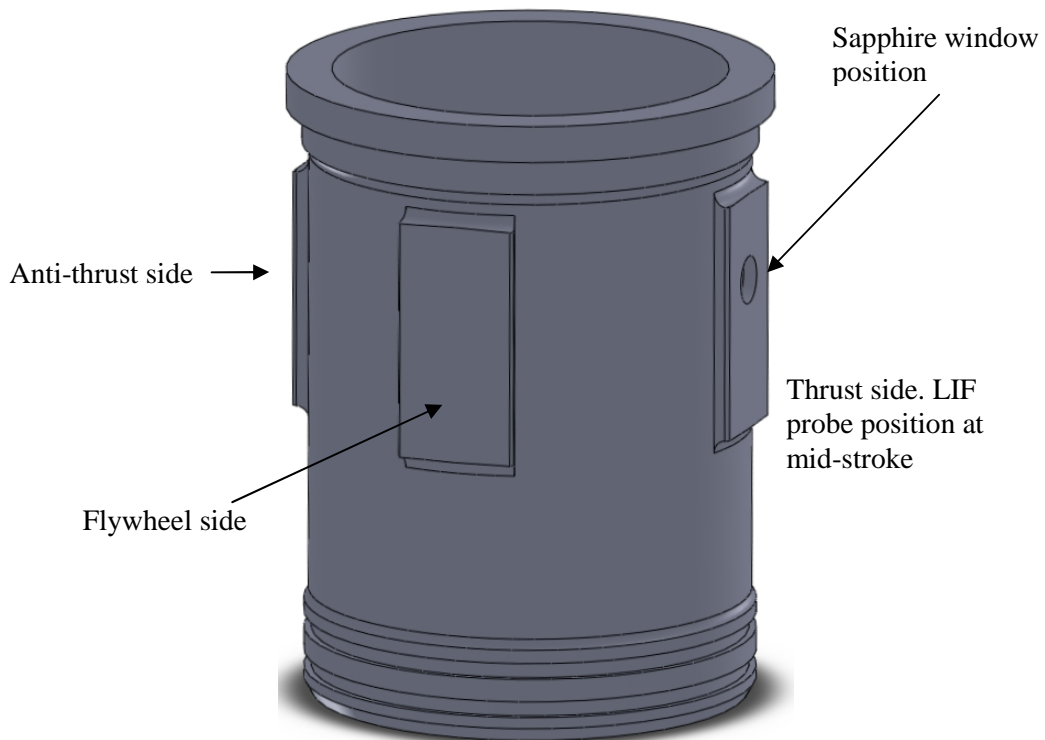


**Figure 5-3: Modified cylinder liner with extra material at 3 locations**

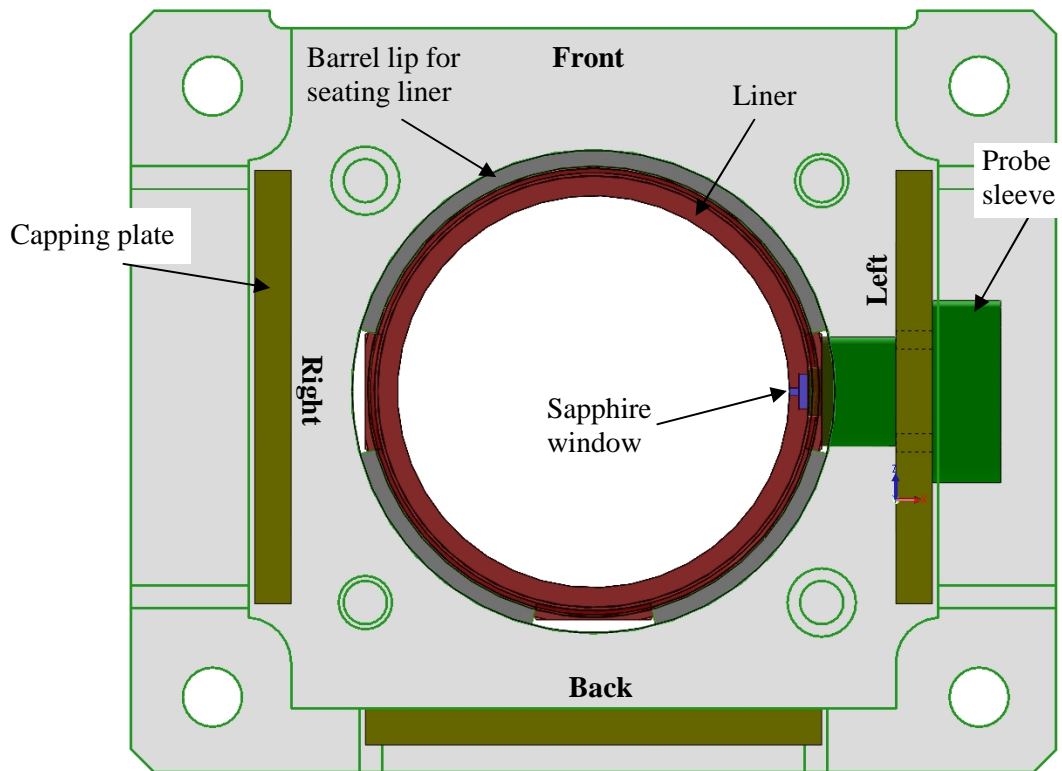


Figure 5-4: The top view of the barrel complete with liner and probe sleeve

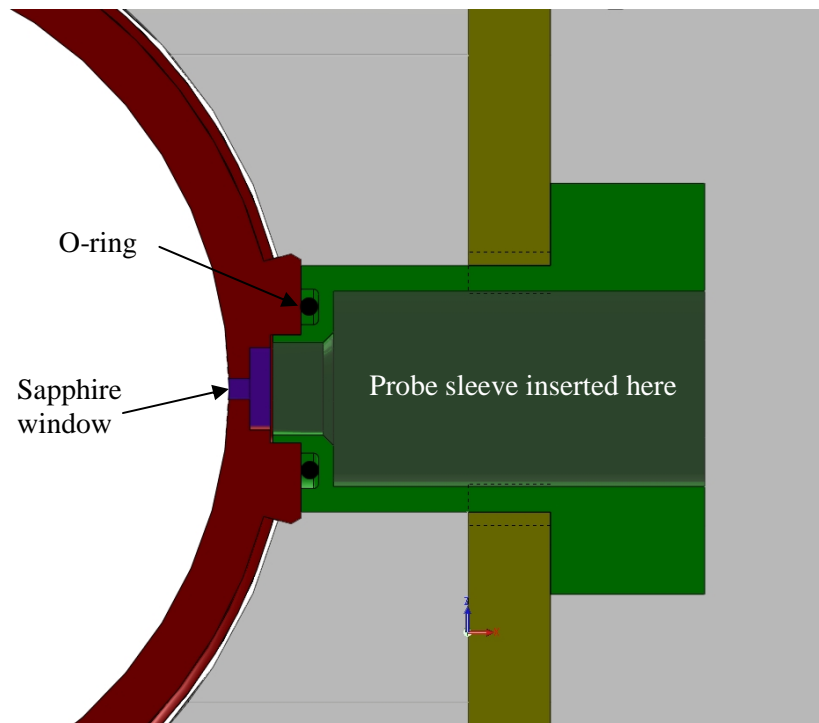


Figure 5-5: A cross sectional view of the interface between the liner and the probe sleeve

### 5.2.2 Cylinder liner thermocouples and mid-stroke sampling tube

As in the motored engine, three thermocouples were located in the cylinder liner to measure the temperature distribution. The data obtained from these was used in the calibration of the LIF signal from the test lubricant. Three blind holes of 2 mm diameter were drilled into the outside surface of the liner approximately to a depth of 1 mm below the running surface on the thrust side. A hole was drilled at near TDC, mid-stroke and BDC. K-type thermocouple wire was used and held in position with epoxy glue. All three thermocouple wires were taken outside the engine through the same capping plate as used for the LIF probe sleeve. The thermocouples and probe sleeve were sealed with silicone sealant to prevent coolant leaks. These thermocouple wires were then wired into National Instruments hardware for data acquisition as described in Chapter 7.

Since the range of temperatures at the mid-stroke position for the probe for the Hydra engine was unknown, it was decided to first measure and record the temperatures for various engine speeds and loads. The engine was stabilised at each test condition for an hour and at an air fuel ratio (AFR) of 14.7:1. This temperature data is shown in a graph as Figure 5-6.

To sample lubricant from the mid-stroke for post test analysis, a sample hole of 0.5 mm was drilled into the cylinder liner at this position. This hole was opened up to accept a M3 screw thread so that a hose tail fitting could be inserted that could accept a sample tube. A Polytetrafluoroethylene (PTFE) sample tube of 1.5 mm inner diameter was used and this was fitted over the hose tail. For additional sealing ability, silicone sealer was applied liberally on the fitting. The tube exited the barrel to the outside through a combination of brass fittings mounted on the same plate as used for the thermocouples and the probe sleeve, Figure 5-7. The tube passed through to a vial where the sample was collected and any blow-by gases that had passed through the tube were extracted from the vial and exhausted. During testing, it was possible to collect approximately 20 ml of sample every 8 hours and a faster rate of collection was observed at the higher engine speeds. It was found during testing that the sample tube would come loose and the sample began to contaminate the coolant, since the tube passed through the water jacket, and it was often required to reseal the tube. It was found that orange Hermetite instant gasket sealer was best to seal the tube on the hose tail of the fitting in the liner but for additional strength a small metal piece was crimped over the tube end to secure it to the hose tail fitting. This modification worked well with no contamination of engine coolant.

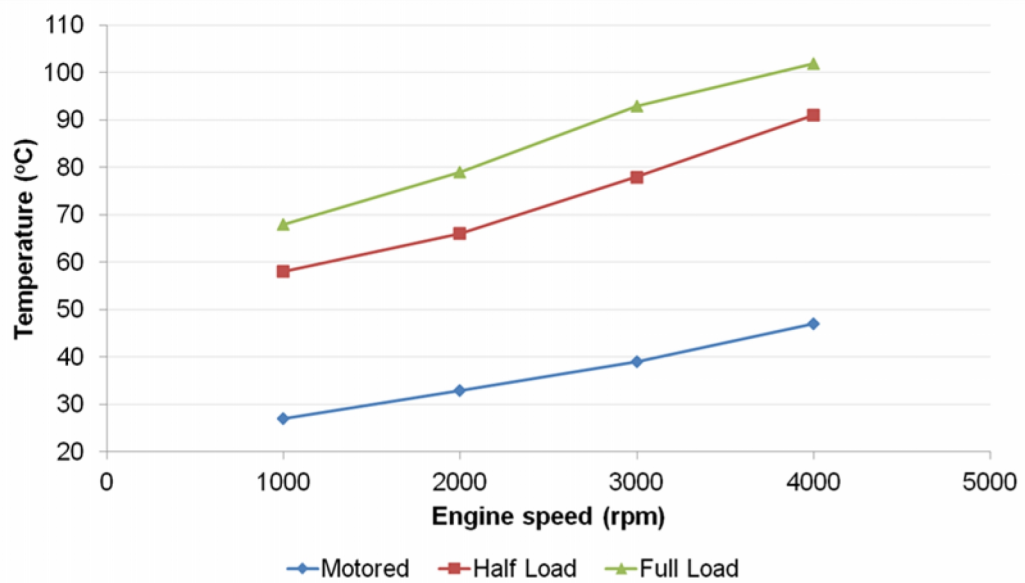


Figure 5-6: Mid-stroke liner temperatures for various engine speeds and loads

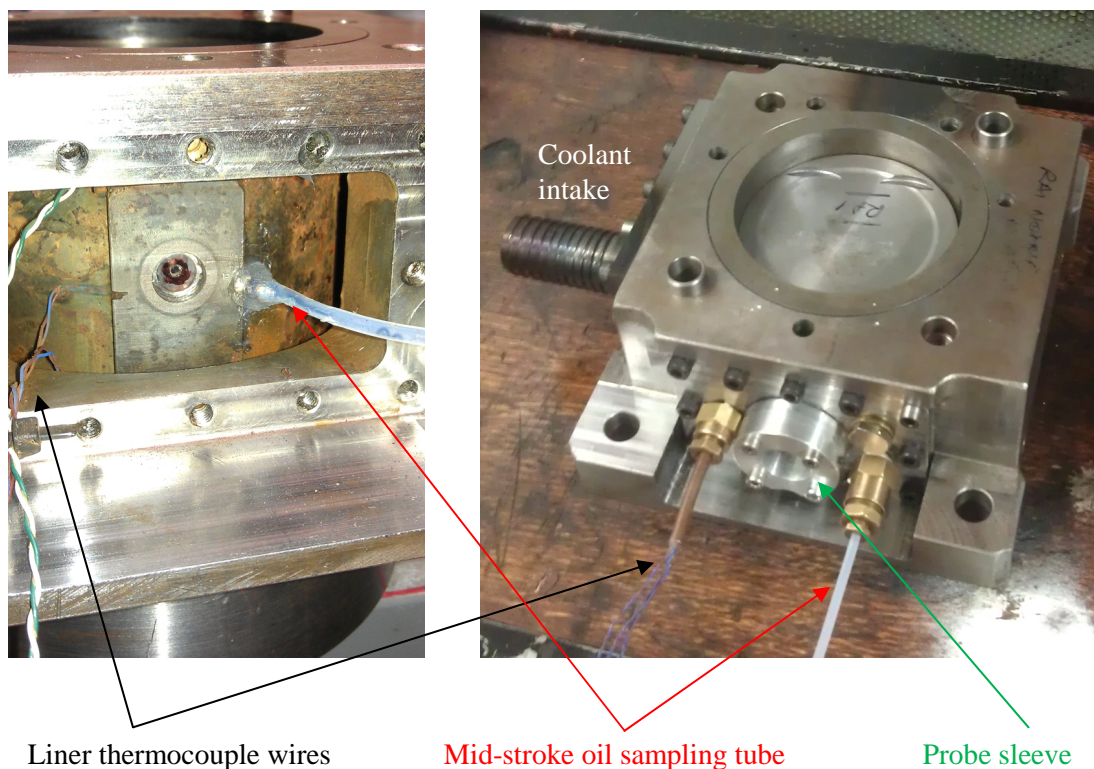


Figure 5-7: Mid-stroke sampling tube and thermocouple wires on the thrust side as the probe

### 5.2.3 Piston rings and running-in

Prior to any engine testing, a new piston complete with the same piston ring pack as used on the motored engine and described in section 4.1.3, was run-in against the new cylinder liner which had the window inserted. Running-in took place with a fresh fully formulated lubricant of SAE 5W30 grade. The running-in procedure used is detailed in Table 5-1.

Test Number	Speed (rpm)	Load (% of max)	Test Period (hours)
1	1500	50	6
2	2000	50	6
3	2000	100	10

Table 5-1: Running-in test procedure

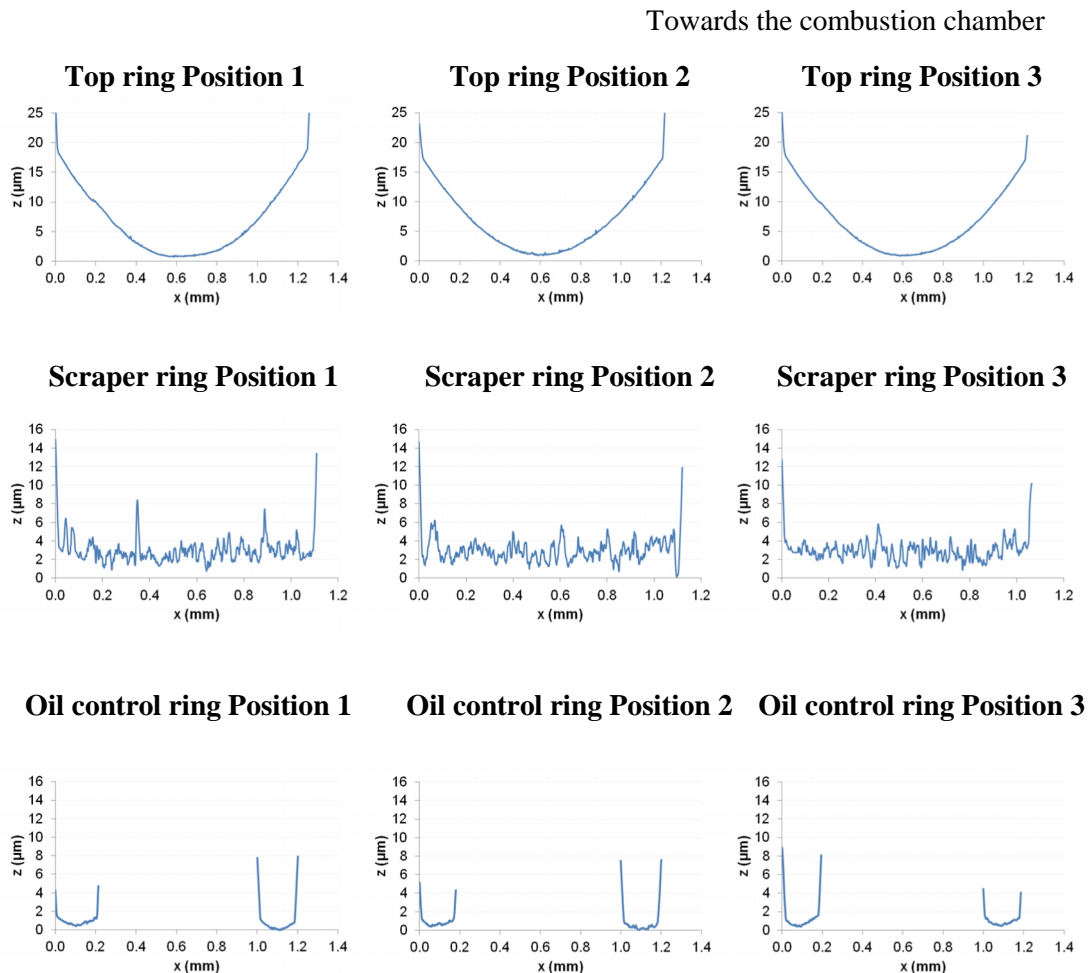
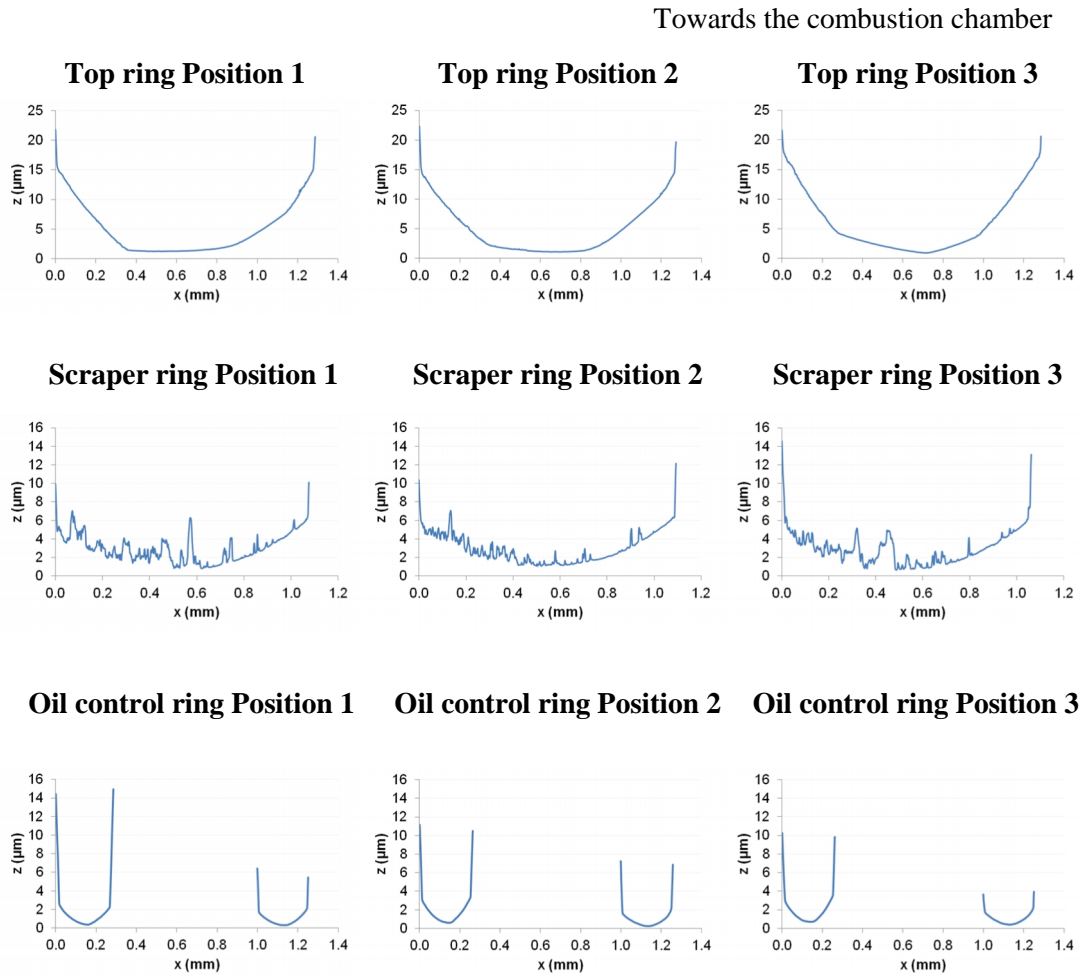


Figure 5-8: Piston ring profiles before engine run-in



**Figure 5-9: Piston ring profiles after engine run-in**

The piston was removed from the engine and surface profile scans were taken of the piston ring pack before and after engine run-in. The piston rings show some wear has occurred during engine run-in when comparing the profiles from before testing, Figure 5-8, and after testing, Figure 5-9. The rings were measured at the same three locations as for the motored engine in Section 4.4.1. The barrel shaped top ring has a flat wear profile on the face which has run-in against the liner. The second ring also has some wear just on the tip of the bottom edge of the ring. The two rails, upper and lower, of the oil control ring appear to have become more barrel shaped and the profile is much smoother with less peaks and valleys.

A 3D profile analysis of the window in the liner was taken, Figure 5-10. A 16 mm<sup>2</sup> area scan of the window in the liner was taken with a profile measurement taken approximately every 0.001 mm in the direction of piston motion and a spacing of 0.075 mm in the circumferential

direction. It can be seen from the 3D scan, that the window surface was flush and level with the surface of the liner after engine run-in. A single 2D scan was extracted from the 3D scan, Figure 5-10, in the direction of the piston motion (A), Figure 5-11, and the circumferential direction (B), Figure 5-12. Both single profile scans show that the window was flush to the running surface of the liner in all directions at the centre point. This was ideal since the laser emission was at the centre point. Additionally the window surface caused no damage to the liner or the piston ring as can be confirmed in the piston ring profiles before, Figure 5-8, and after run-in, Figure 5-9, and also in the EOT pictures of the liner and piston in a later section.

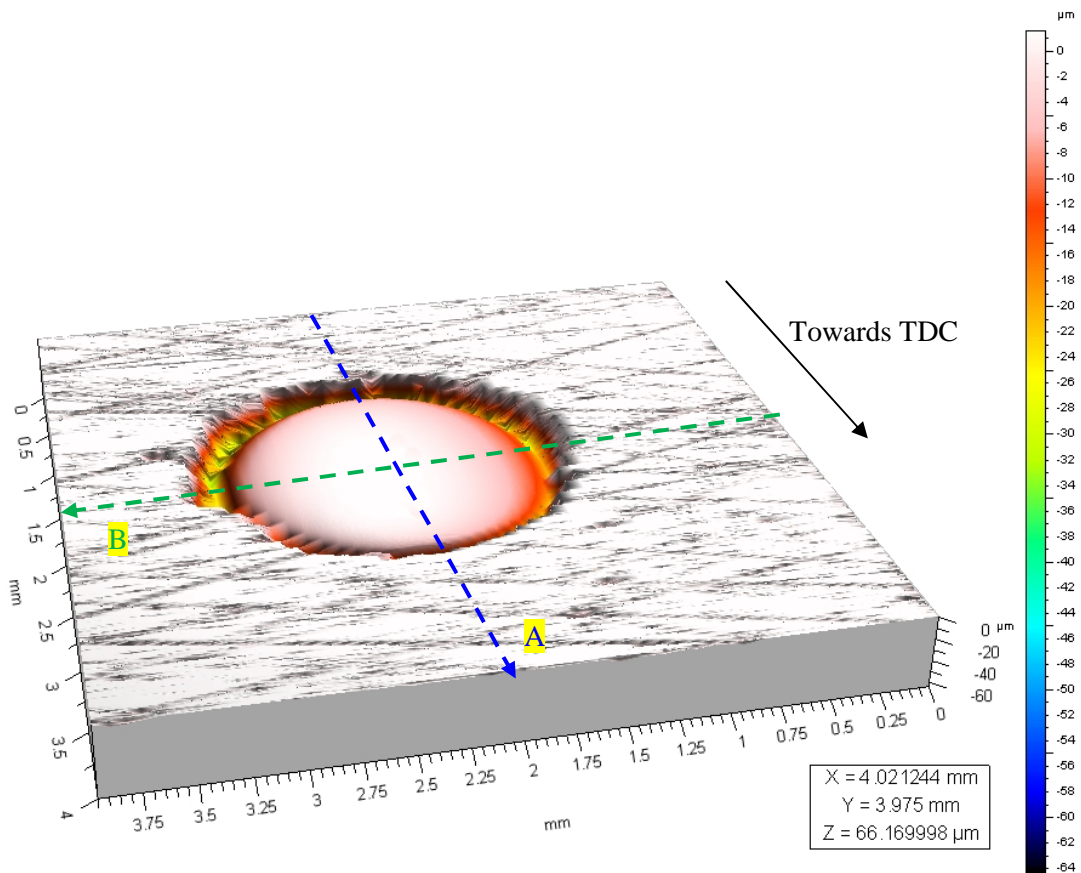


**Figure 5-10: A 3D scan of the Hydra liner shows the window is flush with the running surface**

#### 5.2.4 Engine lubricant samples

The same gasoline lubricant samples as used in the motored engine for testing, Sample A (fresh lubricant), Sample B (MB medium sized car) and Sample C (MB sports car), were used in the Hydra engine for testing purposes. The monograde diesel lubricant, Sample D as

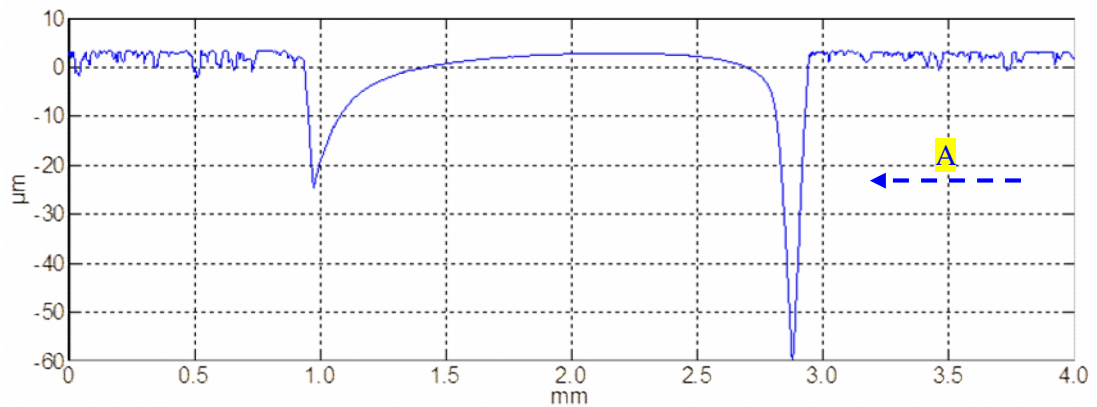


**Figure 5-11: A 2D profile scan of the window in the liner in the direction of the piston motion**

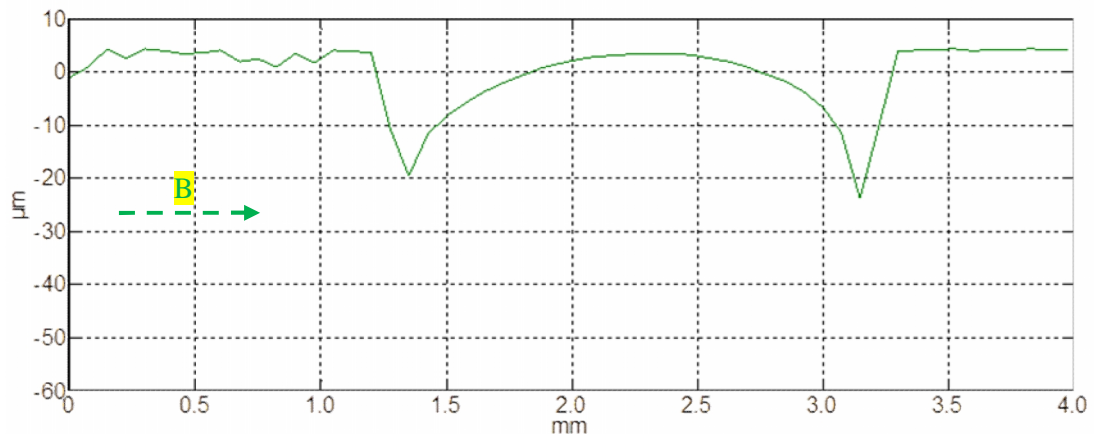


**Figure 5-12: A 2D profile scan of the window in the liner in the circumferential direction**

used in the motored engine, was not used in the Hydra engine because there were concerns that this lubricant would provide inadequate component protection during fired engine operation.

### 5.3 Testing and test matrix

Three lubricant samples were used on the Hydra engine to investigate the influence of lubricant degradation on the minimum lubricant film thickness experienced by the piston ring. The lubricants were tested at four different engine speeds, 1000 rpm, 2000 rpm, 3000 rpm and 4000 rpm and three different engine loads of 0% (motored), 50% and 100% of

maximum torque. The engine was operated under fired conditions at an AFR of 14.7:1. The AFR was measured from the exhaust gases using a Horiba MEXA-554JE Automotive Emission Analyser.

Once the engine was at the test operating condition, it was run for 30 minutes to ensure the engine was stabilised before the data acquisition commenced. A ‘snapshot’ of the piston ring oil film thickness profiles was taken once the engine was stabilised. To check for repeatability, a random selection of test conditions was repeated. Once the test matrix was completed for one lubricant the next test lubricant was employed after a double lubricant flush and drain. This was similar to the method employed on the motored engine with a new oil filter used at each lubricant drain.

The test matrix used for the fresh lubricant, Sample A, is presented in Table 5-2. A similar test matrix was used for the two other lubricant samples; Sample B and Sample C.

Speed (rpm)	1000	2000	3000	4000
Test Number	1	2	3	4
Load (% of max. torque)	0	0	0	0
Test Oil	Sample A	Sample A	Sample A	Sample A

Speed (rpm)	1000	2000	3000	4000
Test Number	5	6	7	8
Load (% of max. torque)	50	50	50	50
Test Oil	Sample A	Sample A	Sample A	Sample A

Speed (rpm)	1000	2000	3000	4000
Test Number	9	10	11	12
Load (% of max. torque)	100	100	100	100
Test Oil	Sample A	Sample A	Sample A	Sample A

**Table 5-2: Hydra engine test matrix for test lubricant Sample A**

## 5.4 Results and Discussion

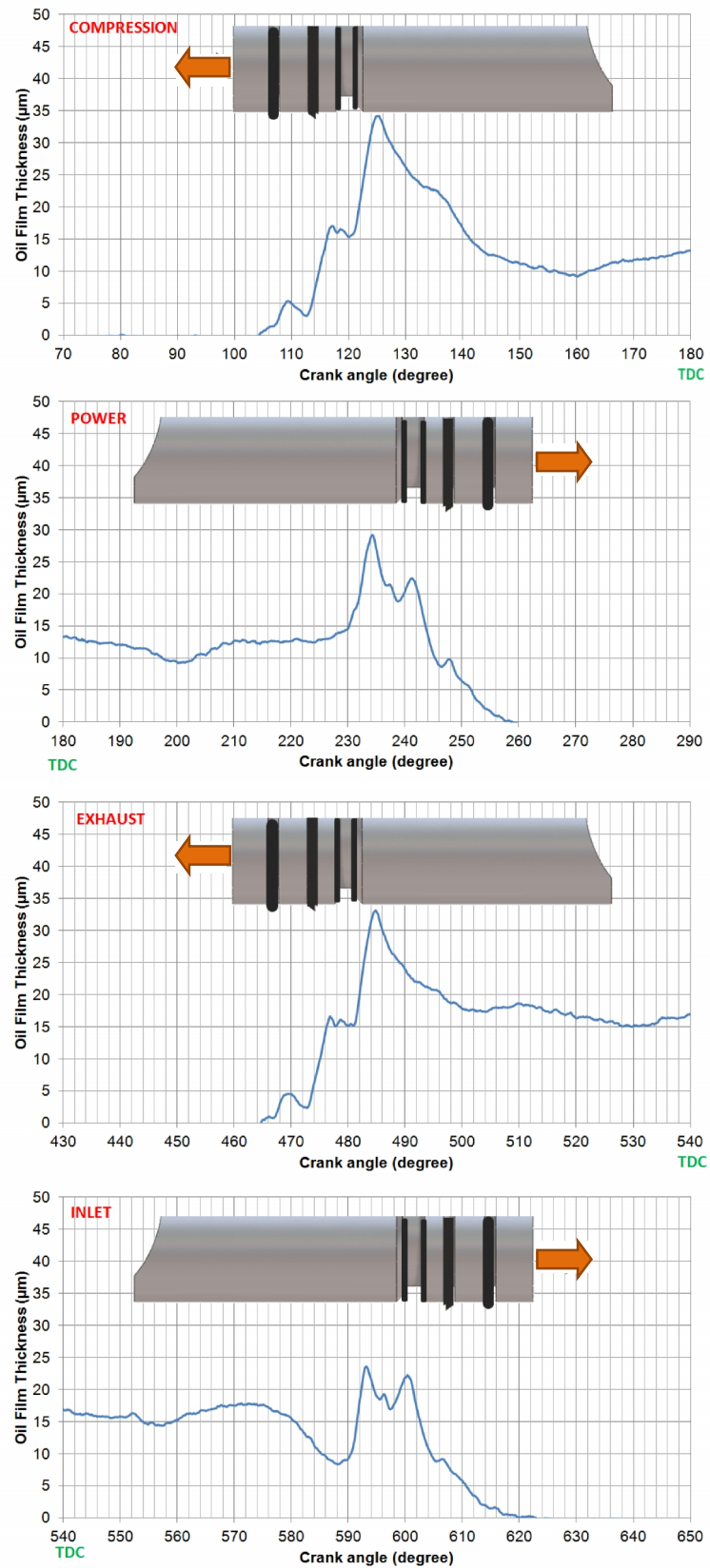


Figure 5-13: Typical 4 stroke LIF profile for Sample A at 1000 rpm, 50 % load, 60 °C

With the addition of two extra strokes, the power and exhaust strokes, it was now possible to observe the variation of the lubricant film thickness profiles across a complete 4 stroke gasoline engine cycle. The profiles presented in Figure 5-13 refers to the result obtained with the engine operating on the fresh lubricant, Sample A, at 1000 rpm and firing at 50% load. The position of the piston rings and the piston direction are superimposed on the figure. The position of the piston and the piston rings on the following figures has been accurately determined using Solidworks computer aided design software. Almost immediately from the profile traces, it can be seen that the piston direction greatly influences the complete oil film thickness profile. The profile between the piston downstrokes is clearly different to the profile on the piston upstrokes. The skirt profiles are interesting too. The cylinder pressure of the compression and power strokes is greater than the cylinder pressures of the inlet and exhaust and as a result a lower film thickness profile is measured on the skirt. It is however difficult to conclude whether the film measured here or even between the piston rings, on the lands, corresponds to the film between the piston and the cylinder liner since the technique is two dimensional and only strengthens the viewpoint of just using the piston ring MOFT results.

It must be noted at this point that the results were averaged over 50 complete engine cycles and the standard deviation was found to be  $0.7 \mu\text{m}$  at the piston rings. The standard error was found to be an impressive  $0.10 \mu\text{m}$  over the 50 engine cycles, with an explanation of this provided in Chapter 7. Repeatability was also established by repeating random test conditions and the results fell within the repeatability of the initial measurements. Due to the scale of the following results, the error of  $0.1 \mu\text{m}$  is not displayed on the figures. Also all temperature recordings here were at the mid-stroke probe position.

Figure 5-14 displays the piston ring MOFT results when the engine is operating at a motored speed of 1000 rpm. The mid-stroke temperature was measured to be  $30 \text{ }^\circ\text{C}$  during steady operating conditions. Figure 5-15 displays the piston ring MOFT results of Figure 5-13 where the engine was operating fired at 1000 rpm and 50% load. The mid-stroke temperature was measured here to be  $60 \text{ }^\circ\text{C}$ . By comparing the two figures, Figure 5-14 and Figure 5-15, it can be seen that the firing action does reduce the MOFT experienced by the piston ring pack substantially. This is expected since the cylinder pressures during the latter would contribute to the lower films along with the increase in cylinder temperatures as combustion takes place. The same was observed for a combination of different engine speeds and operating conditions. The films measured at the compression ring for the compression and exhaust stroke remain consistently small whether the engine is firing or motoring.

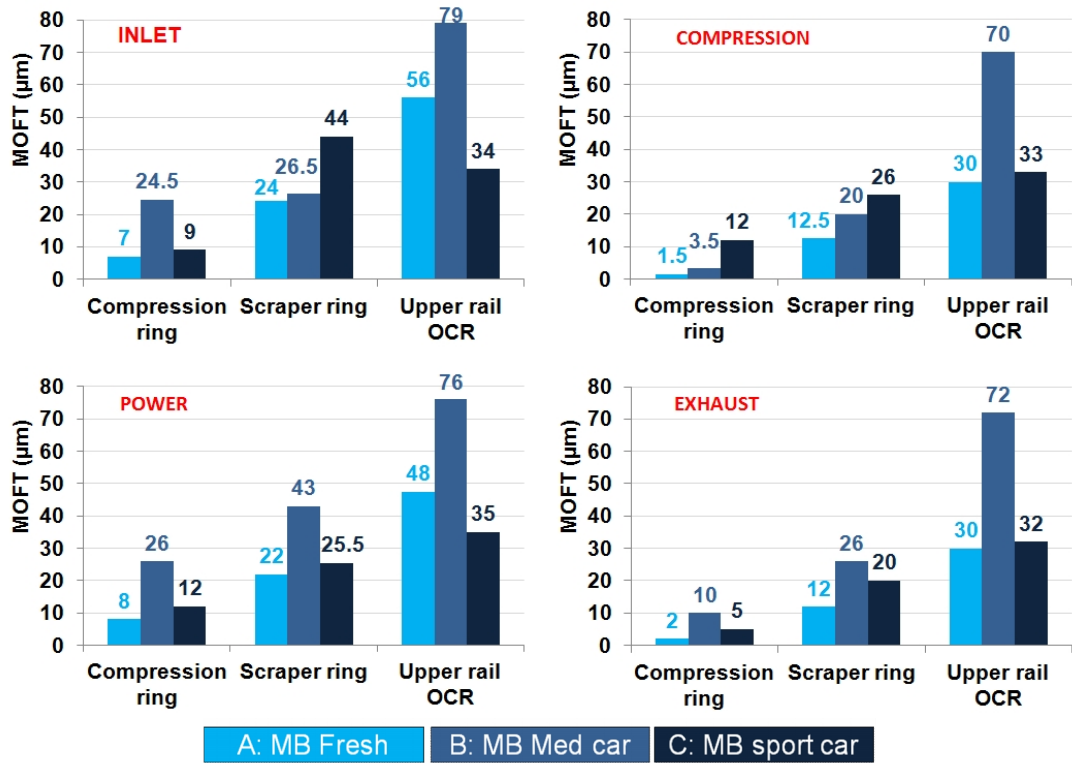


Figure 5-14: Piston ring MOFT at 1000rpm, no load (motoring), 30 °C

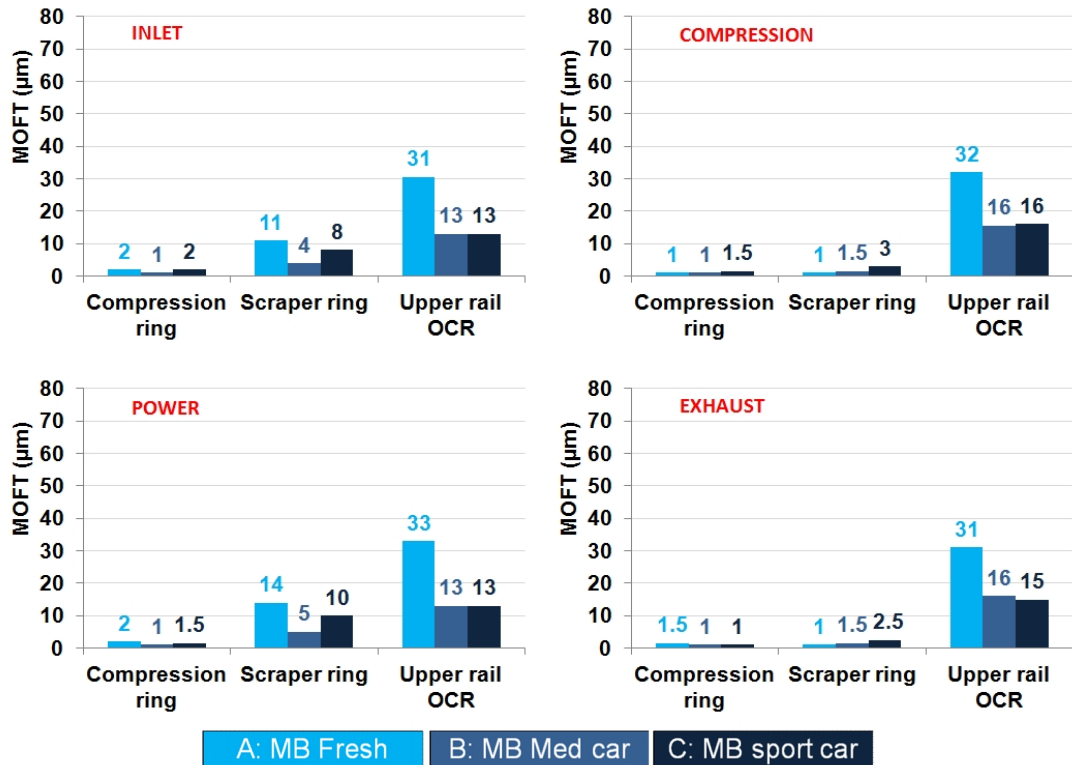


Figure 5-15: Piston ring MOFT at 1000rpm, 50% load (firing), 60 °C

It is now possible to observe the difference between the upstroke and downstroke on the piston ring MOFT. The lubricant films during the upstrokes are generally thinner than the lubricant films during the downstrokes and this is fairly evident regardless of whether the engine is firing or motoring. The second ring is of a Napier type ring and this performs at its best at scraping excess lubricant from the cylinder wall on the downstroke. As a result, during firing operation on the downstroke there is an accumulation of lubricant at the inlet to the second ring and hence a larger film thickness is observed here on the inlet and power strokes than either the compression or the exhaust strokes. In fact, on the upstrokes, the films observed at the second ring are similar to those at the compression ring. Here lubricant starvation is occurring because as the piston moves upwards towards TDC, the lubricant supply offered to the second ring is that from the compression ring which, was originally starved, and hence the second ring is starved of lubricant also. The top compression ring continues to remain operating in a starved condition throughout the complete engine cycle at this test condition.

In terms of investigating the effect of lubricant degradation across the complete engine cycle, during motored operation, the films for the fresh lubricant, Sample A, present lower films when compared to the most degraded lubricant, Sample C. However, under fired conditions Sample A presents a thicker film under the ring pack than the degraded samples during the inlet and power strokes. Sample A has the lower HTHS viscosity value than any of the other degraded lubricants and the lower lubricant viscosity is possibly allowing for a better lubricant flow into the ring pack, hence a greater film is observed at the scraper and oil control rings. However, as mentioned earlier, since the lubricant flow is not directly measured, this can only be assumed. However, the compression ring profiles are similar in thickness regardless of the quality of the lubricant or the stroke.

The piston ring MOFT results presented in Figure 5-16 show the effect of increasing the engine speed at maximum load. Since there was a lack of substantial variation between the two downstrokes; the intake and power stroke and also between the two upstrokes; the compression and exhaust stroke, only the compression and power stroke data is presented. It can be seen from the figure that as the engine speed is increased, a greater film thickness is generally experienced across the piston ring pack. As the engine speed increases, the crankshaft rotational speed increases and the rate of lubricant throw from the crankshaft bearings and the connecting rod is greater. Additionally, there is also a greater rate of piston inertial, gas effects and ring pumping. A combination of these would result to more lubricant available on the cylinder wall for lubrication and hence thicker films under the rings. So, it is acceptable to state that at the lower engine speeds, oil availability is critical.

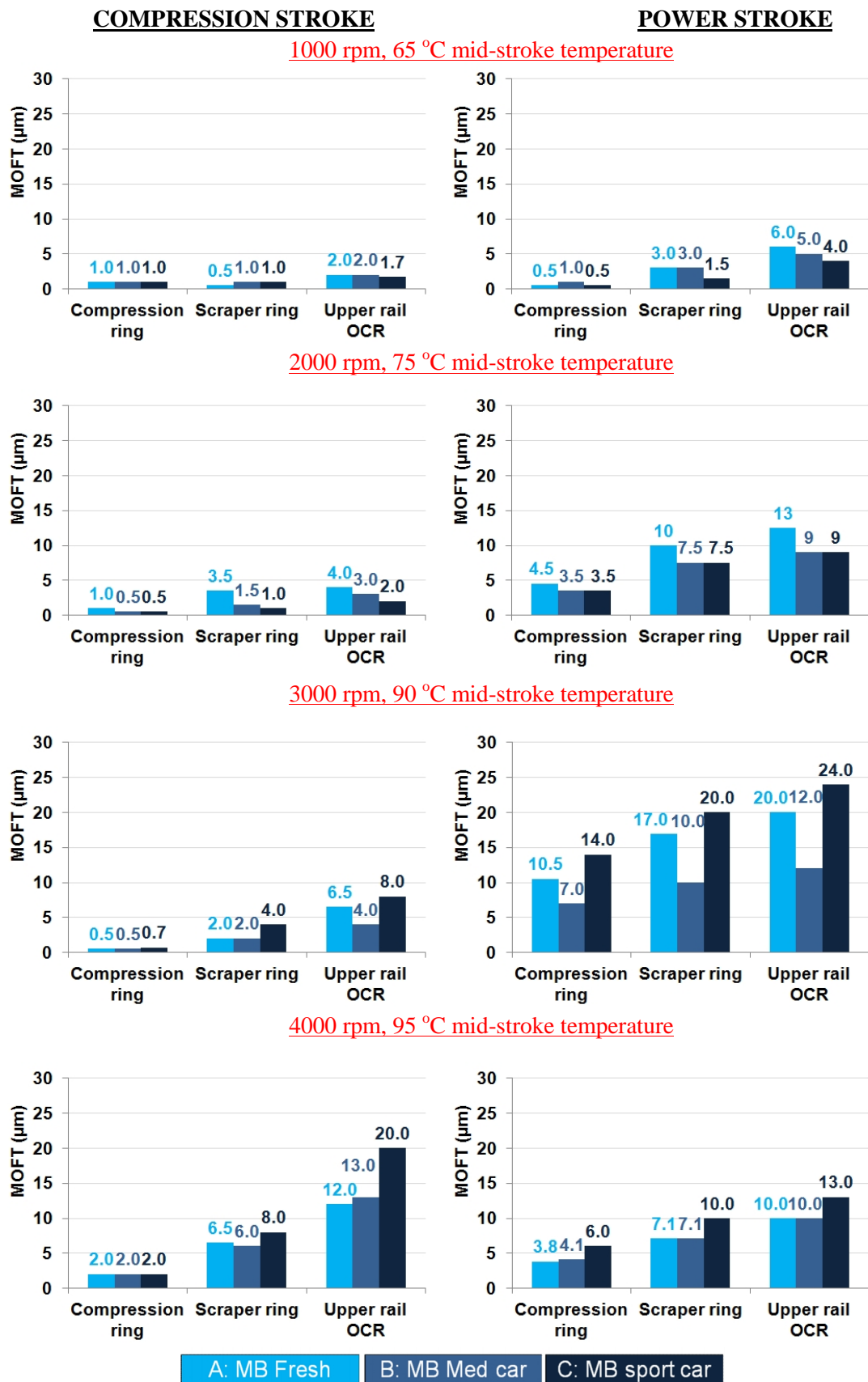


Figure 5-16: The effect of engine speed at maximum load on piston ring MOFT

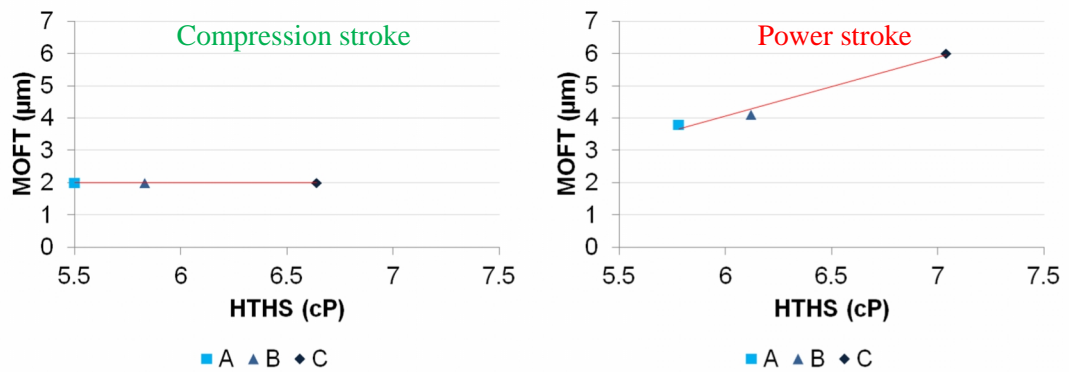


Figure 5-17: MOFT vs. HTHS viscosity – compression ring, 4000rpm, 100% load, 95 °C

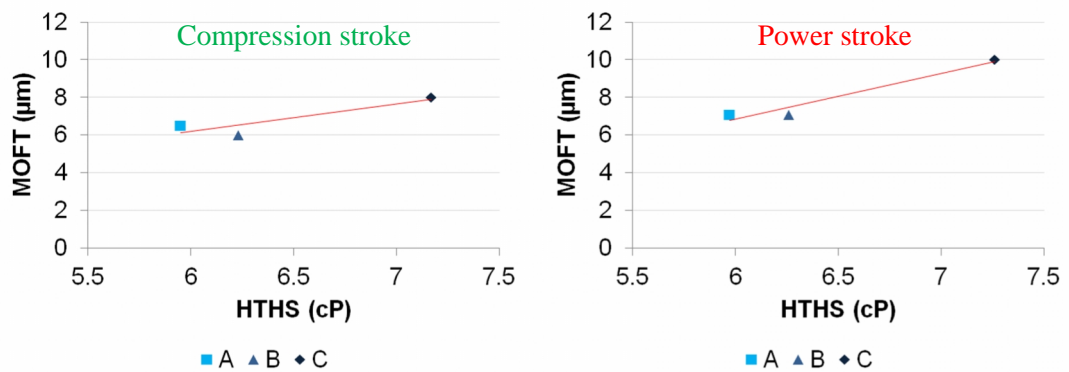


Figure 5-18: MOFT vs. HTHS viscosity – scraper ring, 4000rpm, 100% load, 95 °C

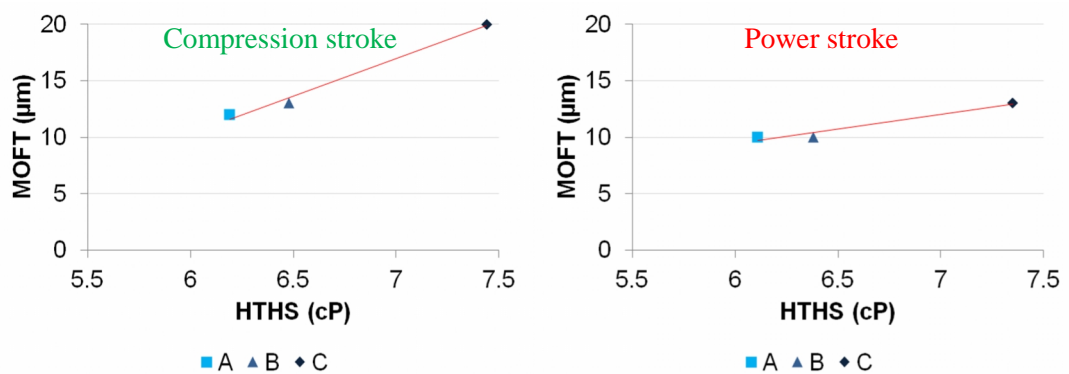


Figure 5-19: MOFT vs. HTHS viscosity – oil control ring, 4000rpm, 100% load, 95 °C

The film thickness increases as the engine speed increases on the compression stroke whereas on the power stroke there is a reversal in this trend at 4000 rpm. It is not known why exactly this occurs, other than the increase in chamber pressures has contributed to a lower lubricant viscosity and hence a lower piston ring MOFT. However, as the speed increases the

influence of the lubricant degradation becomes more apparent. The most degraded lubricant, Sample C, shows consistently higher film thickness profiles as the speed increases. Here the HTHS viscosity of the lubricant is appreciably more and therefore it is acceptable to state that at the higher engine speeds, the lubricant viscosity and hence lubricant degradation is more dominant. Sample B, being of a similar HTHS viscosity as Sample A, is also showing less difference at the highest test engine speed emphasising the fact that the viscosity of the lubricant is more dominant at the higher engine speeds.

Using the HTHS viscosity data measured for each test lubricant (See Section 4.2.2), it was possible to plot results of the instantaneous measured piston ring MOFT against the instantaneous HTHS viscosity value. The results of the test condition at 4000 rpm and 100 % load for the compression, scraper and oil control rings is presented as Figure 5-17, Figure 5-18 and Figure 5-19 respectively. The shear rate was determined based on the measured MOFT and the mean piston speed at mid-stroke and this was used to estimate the instantaneous HTHS viscosity value using linear interpolation of the measured HTHS viscosity results. This test condition was chosen since the mid-stroke liner temperature, 95 °C, was the closest to the measured HTHS viscosity temperature of 100 °C. It can be seen from the results, that there is very good correlation between the measured piston ring MOFT and the HTHS viscosity value. Generally, the higher HTHS viscosity lubricant, Sample C, is presented the greatest film thickness than either Sample A or B at the rings, which is regardless of test engine stroke.

The data presented in Figure 5-20 shows the influence of increasing the engine load on the piston ring MOFT during the power stroke at 1000 and 3000 rpm. It can be seen that as the torque output is increased, cylinder temperatures increase along with a greater reduction in the film thickness than experienced with a decrease in engine speed alone. Also, as the fired engine speed increases the film thickness increases and this increase is not reduced as the load increases. As the motored engine speed increases, the film thickness for Sample A increases across the entire ring pack as expected. But, the results for Sample B and C do not lie on the same trend and produce thinner films at the bottom two rings as the speed changes. Additionally, the influence of lubricant degradation only becomes apparent at higher engine speeds and the maximum loads as otherwise the highly degraded Sample C provides smaller films across the entire ring pack than the fresh Sample A. This suggests that at the extremities, high temperature and high cylinder (pressure) loading, and high engine speeds, the lubricant viscosity is dominant.

**POWER STROKE**

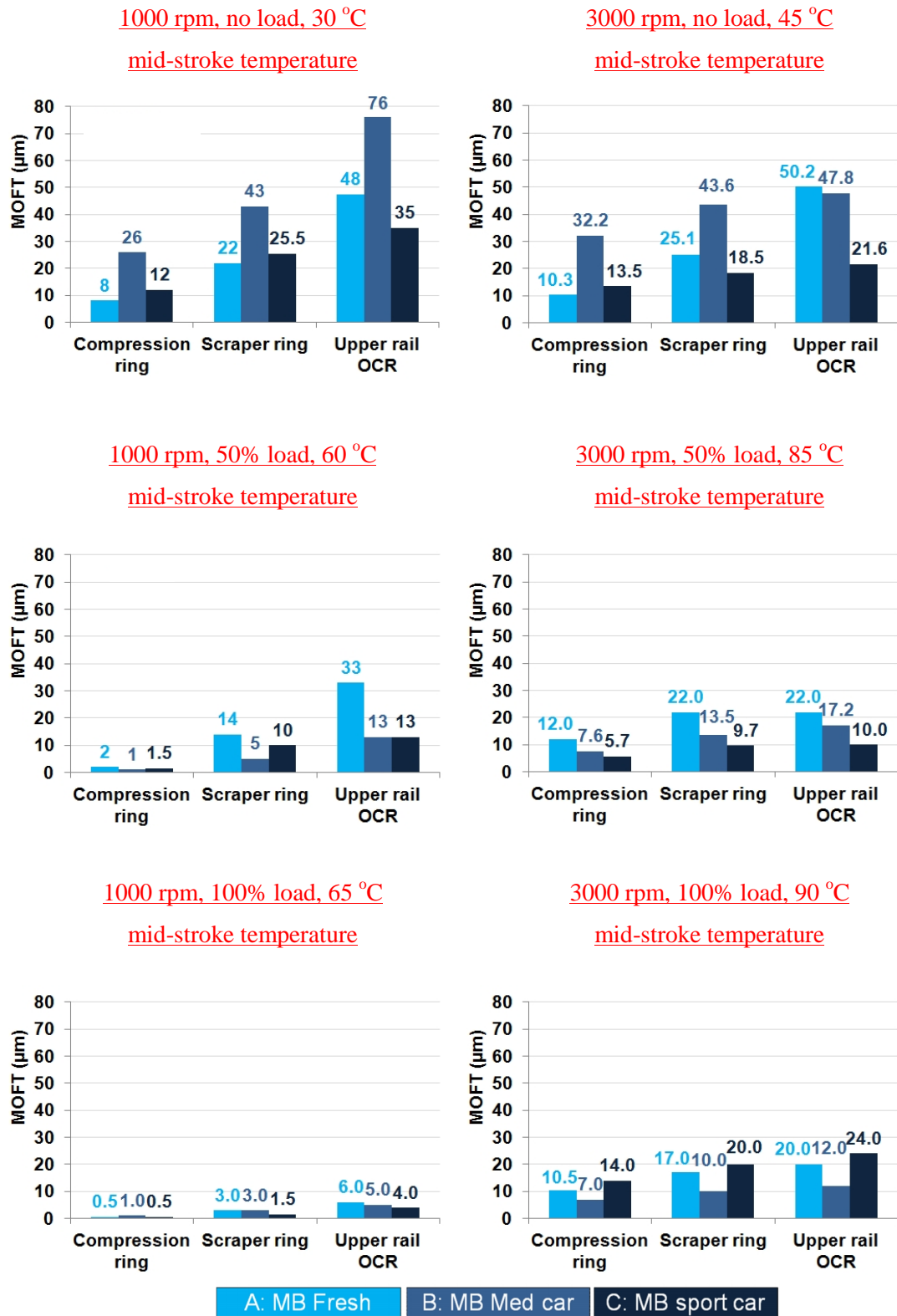


**Figure 5-20: The effect of engine load on piston ring MOFT at engine speeds of 1000 and 3000 rpm**

The shear rate as a function of engine speed and load for Sample A during the compression and power strokes is displayed in Figure 5 21 and Figure 5 23 respectively and for Sample C

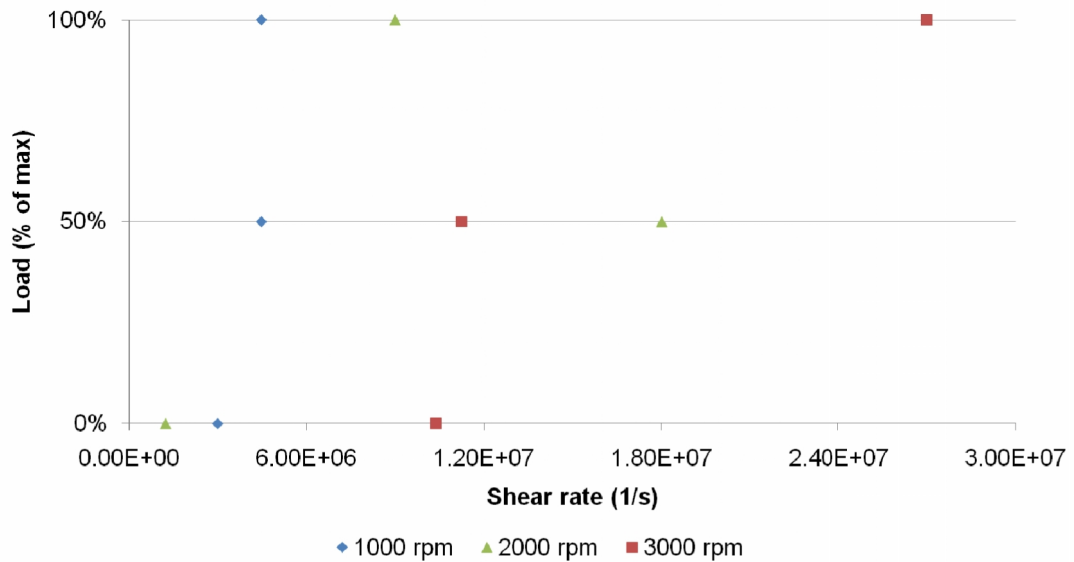


**Figure 5-21: The influence of engine load and engine speed on Sample A lubricant shear rate during the compression stroke**

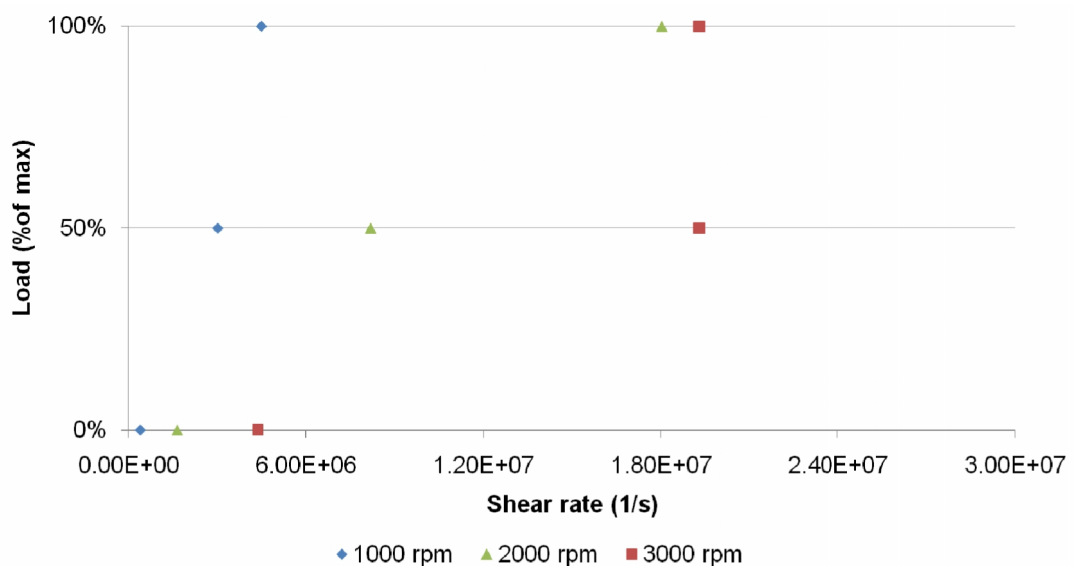


**Figure 5-22: The influence of engine load and engine speed on Sample C lubricant shear rate during the compression stroke**

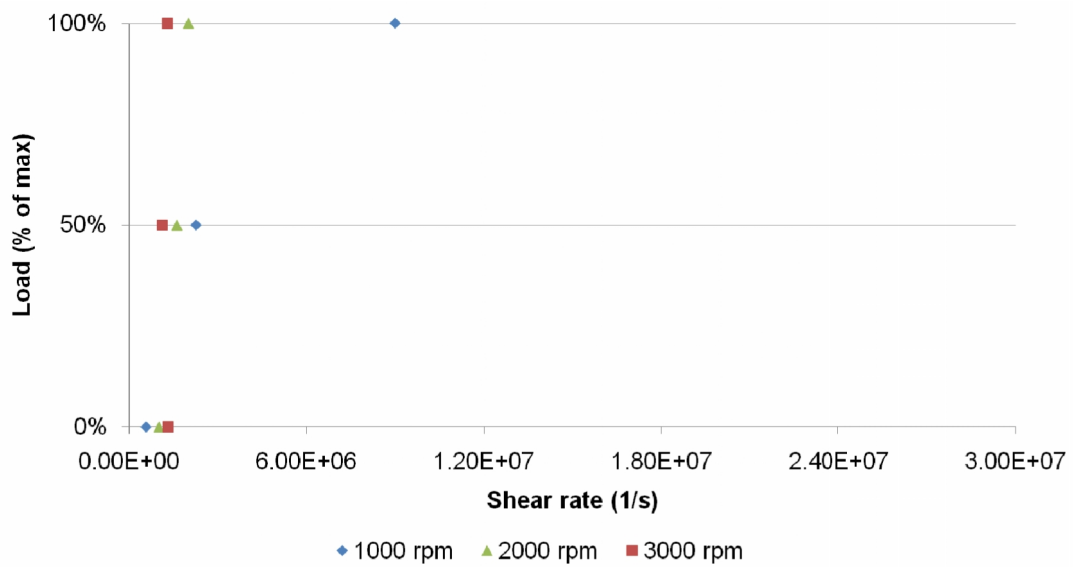


**Figure 5-23: The influence of engine load and engine speed on Sample A lubricant shear rate during the power stroke**

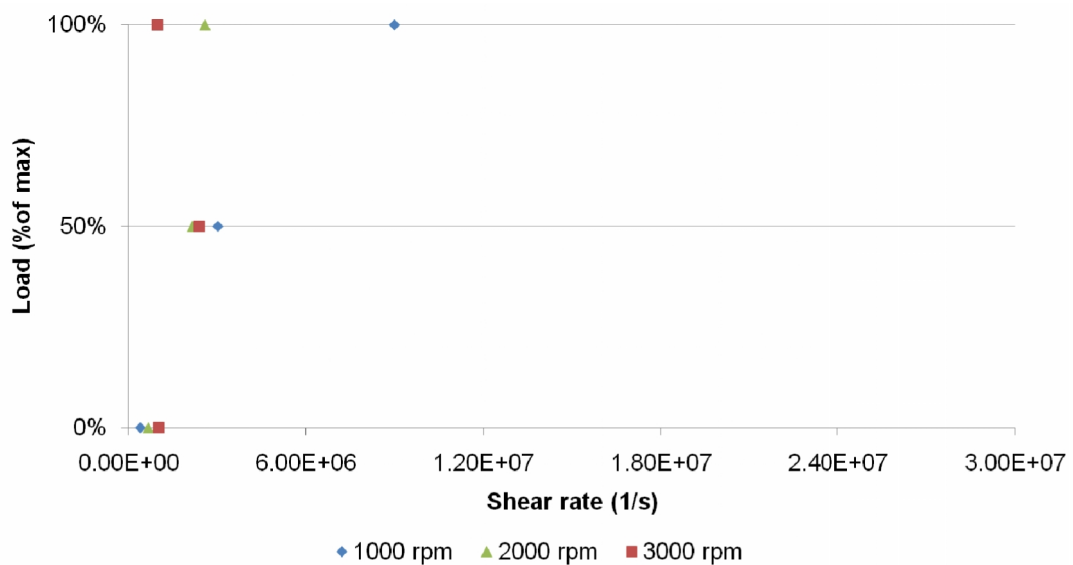


**Figure 5-24: The influence of engine load and engine speed on Sample C lubricant shear rate during the power stroke**

for the two strokes in Figure 5-22 and Figure 5-24. There is a large variation in the shear rate regardless of engine speed or load between the two strokes. Due to the smaller films measured during the compression stroke and together with high piston sliding speeds, the

shear rate begins to become much greater than those experienced during the power stroke. This is true for all lubricants tested. This shows the lubricant undergoes a cyclical variation in shearing during operation at a constant engine speed or load. In terms of the influence of lubricant degradation on the outcome of the lubricant shearing, the greater HTHS viscosity of Sample C is proving beneficial since a larger film is retained under the ring at higher engine speeds and loads which in turn experiences a lower shear rate than the fresh Sample A. It must be noted at this point, that the duration and high shear rates are still not enough to completely deform the polymer bonds and cause permanent viscosity loss (Mortier, Fox et al. 2009).

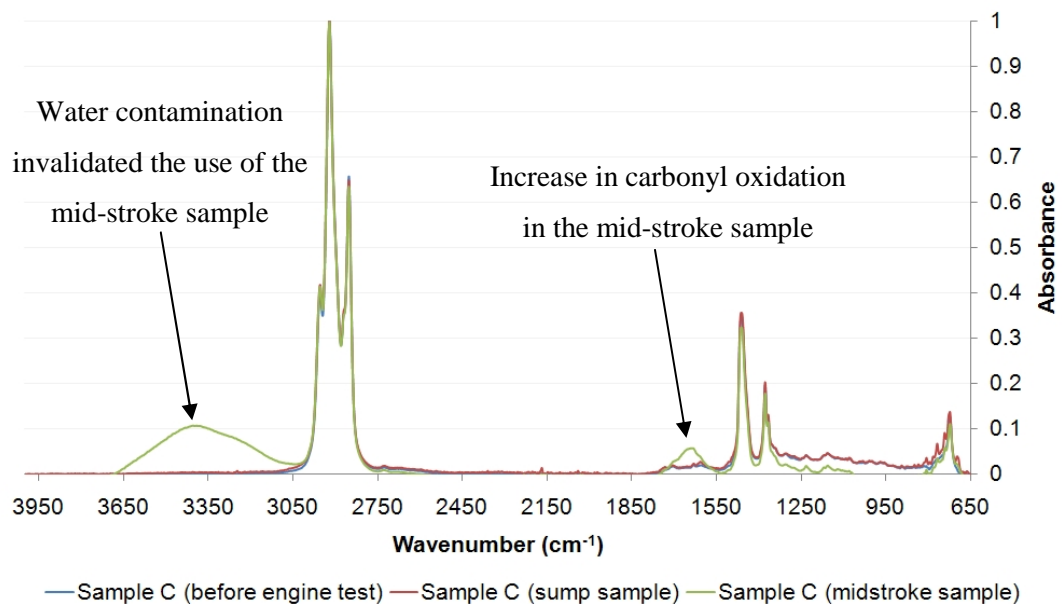


**Figure 5-25: FTIR spectra of lubricant Sample C; before engine testing, mid-stroke and sump samples**

It was proposed to extract lubricant samples from the mid-stroke position and provision was made (see Figure 5-7). However, during firing operation a beige sample was beginning to collect in the vial which was found to be an emulsion of water in oil, due to the combustion process, and as a result no sample collected from the mid-stroke was used for post analysis. Although this sample appeared to have an increase in the carbonyl oxidation when compared to the sump sample, as can be seen from the FTIR spectra presented as Figure 5-25, the excess water rendered the sample useless for fluorescence calibration. It was believed that water was extracted from the liner as a vapour down the tube and carried with the blow-by

and oil mist, and condensed in the vial. However, since there was no triggering of sample collection from this point as the piston passed and was continually sampling during engine operation, what would be collected could be regarded as being none representative of piston mid-stroke lubricant sample. As a result, samples were extracted from the sump after each test condition and used for calibration purposes to help provide information on the film thicknesses for that particular test condition.

During firing, noise was being recorded by the PMT during the start of the ignition pulse for the excitation for the spark plug, see Figure 5-26. The noise was, however, only small with a maximum peak signal voltage output of approximately 6 mV and only lasted approximately 2 ms every ignition cycle. The noise did not affect the results of the fluorescence intensities, since the value was small and was removed by the post filtering process. It has been included here for completeness.

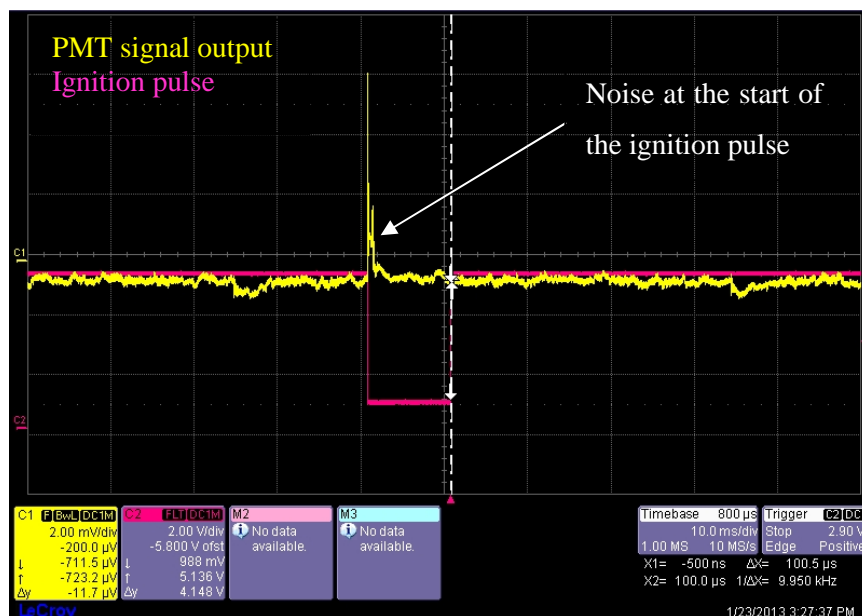
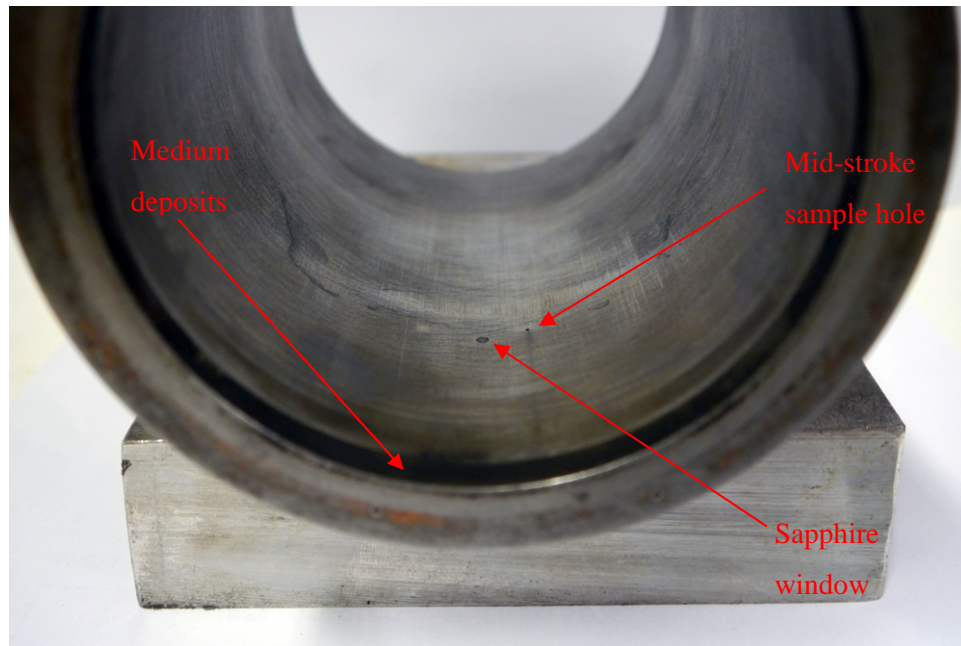


Figure 5-26: Spark plug noise at the start of ignition as observed on the oscilloscope

#### 5.4.1 EOT components

Photos of the engine cylinder liner were taken after the LIF engine testing was completed. A picture of the thrust, Figure 5-27, and anti-thrust, Figure 5-29, side of the cylinder liner was taken. Both images show some light deposits around the TDC just above top ring reversal position. Both sides of the liner show some introduction of medium deposits adhering to the surface. There is also a light varnish colour to the liner, which is present along the full length

of the bore. The thrust side of the piston shows some light - medium deposits on the top two lands, Figure 5-28, whereas the anti-thrust side shows only very light deposits and a varnish appearance, Figure 5-30. The images correspond well to the cylinder liner EOT images which show similar light deposits above the top ring reversal. The piston did not contain any excessive carbon deposits within the ring grooves and the rings were not stuck in position when the piston was removed from the cylinder liner.



**Figure 5-27: Thrust side of EOT cylinder liner**



**Figure 5-28: Thrust side of EOT piston**

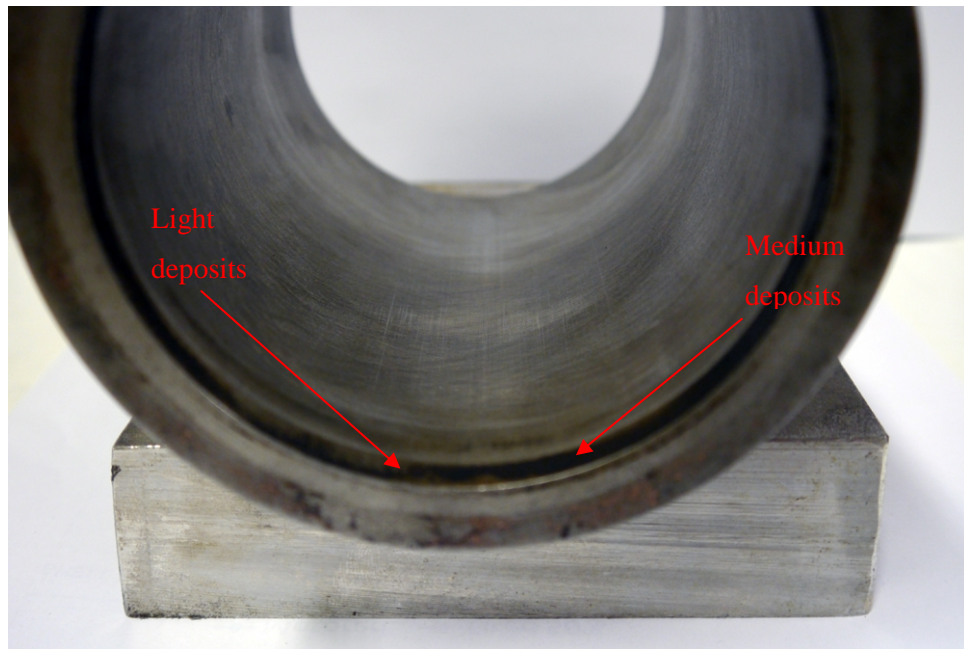


**Figure 5-29: Anti-thrust side of EOT cylinder liner**



**Figure 5-30: Anti-thrust side of EOT piston**

As a final observation, an optical prism was placed on the liner surface just above the sapphire window. This allowed a clear high resolution picture to be taken of the window, the sample hole and the surrounding area, Figure 5-31. It can be clearly seen that the cross hatch honing pattern of the liner is still present and no damage or polishing to the liner has

occurred around the window and the sample hole. It is therefore safe to assume that the window and the sample hole did not affect the natural operating condition of the engine.

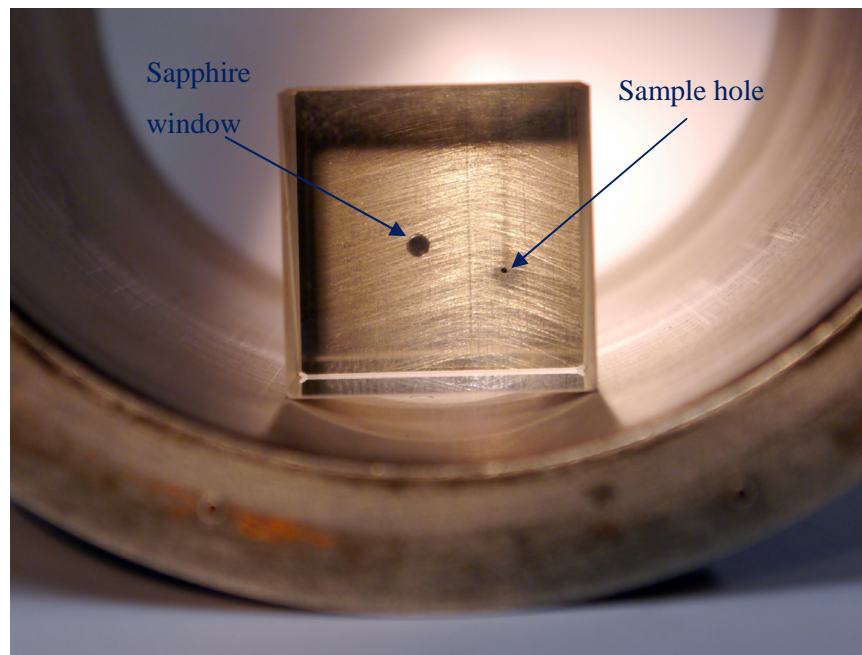


**Figure 5-31: The use of a prism to observe the area around the window in the liner**

## 5.5 Conclusions

The LIF system has been developed further in a fired gasoline engine to investigate the influence of lubricant degradation on the piston ring to cylinder wall lubricant film thickness. A wide range of operating conditions were tested with a selection of degraded lubricants as used on the motored engine. The results were obtained from the Ricardo Hydra gasoline engine and the following conclusions can be drawn:

- The film thickness of a degraded lubricant can still be measured even during fired engine operation with results that have very good spatial resolution.
- An instantaneous lubricant scan of all four engine strokes showed that there is a difference between the measured lubricant film thicknesses which depends on the direction of the piston motion and it was found that the ring profiles were the main cause of this. This was different to the two stroke profiles taken from the motored engine which were almost mirror images of each other.

- Thinner lubricant films were observed on the compression and the exhaust strokes for the top two rings than for the intake and power strokes. This occurs during both firing and motoring operation. It is believed lubricant starvation is occurring as the piston moves upwards towards TDC since the lubricant supply offered to the second ring is that from the compression ring which, was originally starved, and hence the second ring was starved of lubricant also.
- The introduction of firing, and hence increased cylinder pressure and temperature, reduces the film thickness of the lubricant under the rings. A continuous increase in engine loading reduces the film thickness further regardless of engine speed. A similar effect was observed on the motored engine where an increase in the cylinder pressure reduced the piston ring MOFT.
- At the slower engine speeds, the rate of lubricant throw from the crankshaft and the connecting rod is much less than at higher speeds. As a result, at slower engine speeds the availability of lubricant is less and hence the film thickness in the ring pack is smaller. However, as the engine speed increases a greater availability of lubricant on the cylinder liner contributes to a higher film thickness. Additionally, there is a greater rate of inertial, gas effects and ring pumping which would contribute to more lubricant availability in the piston ring pack. This is true regardless of lubricant quality.
- At the higher engine speeds, the high temperature high shear rate viscosity of the lubricant, was found to be more dominant in influencing the extent of thicker piston ring MOFT than the engine speed. This was also true for the results obtained from the motored engine.
- Due to the change in the lubricant film thickness per engine stroke, it was found that the lubricant shear rate also changes even during constant engine operation. In the compression stroke, an excessive amount of shearing was found to occur at high engine speeds and loads.
- Generally, the HTHS viscosity values of the test lubricants correlated well with the measured piston ring MOFT. Again this was true for the results obtained from the motored engine.

# **Chapter 6 Piston Ring Pack Lubricant Residence Times and the Influence of Top Ring Zone Sampling on Piston Ring Lubricant Film Thickness**

The flow of the lubricant has been shown to be highly influential on the gas flow and the piston inertial effects in an operating engine, as discussed in Chapter 2. The lubricant in the piston ring pack is more degraded than the lubricant in the sump since it interacts with the combustion gases and experiences higher temperatures and pressures. Additionally, the lubricant in the ring pack is of a much smaller volume than the bulk lubricant in the sump. The lubricant residence time is therefore important in determining the flow of lubricant through the ring pack and the replenishment of the lubricant in the ring pack, which both govern the extent to which the lubricant in the sump becomes degraded (Yasutomi, Maeda et al. 1981a; Lee, Stark et al. 2004).

In previous chapters, the lubricant film thickness was measured using a laser induced fluorescence technique. Since the technique examines the fluorescence intensity, it is possible to further the method to investigate the lubricant flow through the ring pack. This technique was applied to the Ricardo Hydra engine and compared to previous ring pack residence time results by other researchers.

A twin switchable sump system was setup that allowed the lubricant supply to the crankshaft bearings and the piston assembly to be changed during engine operation. By using two lubricant sumps with one of the lubricants doped with fluorescent dye, it was possible to measure the time required for the new lubricant to displace the old lubricant in the interface between the ring pack and the cylinder wall when the supply was changed over. Two fresh lubricants with different viscosities were tested and the results are presented and discussed in this chapter.

Additionally, lubricant has been sampled from the piston top ring zone in the past and it was not entirely certain the extent to which sampling lubricant in this manner affected the

distribution of the lubricant in the ring pack, if at all. An investigation into this was made with the LIF technique and is also discussed in this chapter.

## 6.1 Previous Studies of Piston Ring Pack Residence Time

Both Stark et al. (Stark, Gamble et al. 2005) and Lee (Lee 2006) measured the residence time of the lubricant in the ring pack of the Hydra engine using lubricant which had a certain concentration a hydrocarbon marker. By sampling lubricant from the top ring zone (TRZ) at the same time, it was possible to determine the ring pack residence time by analysing the concentration of the marker in the TRZ lubricant samples. Stark et al. used 2 litres of lubricant which was mixed with a hexadecane marker at 5% concentration (v/v) and after the engine was operating stably for 30 minutes, a further 2 litres of test lubricant containing 5% hexadecane (v/v) and 5% octadecane was added. The test lubricant used was Shell Extra High Viscosity (XHVI) 8.2 base lubricant. Lubricant samples were extracted from the TRZ over a 90 minute period at an increasing sample collection interval from 5 seconds to 10 minutes. By comparing the hexadecane marker to the octadecane marker in the TRZ sample, it was possible to express the octadecane marker as a percentage of the 5% concentration in the sump. The marker in the TRZ sample was compared to the marker in the sump sample. Knowing the time between sample extractions, it was possible to provide an estimate for the ring pack residence time, which is the time required to displace the degraded lubricant volume in the piston ring pack with an equivalent volume from the sump. The marker concentration in the samples was measured using gas chromatography (GC) and those markers were chosen since they could be detected by GC in very small quantities in a lubricant and are less prone to oxidation than the base lubricant, since they contain no tertiary C-H bonds (Mortier, Fox et al. 2009).

This approach of monitoring a marker in the lubricant has been tried and tested before. Saville et al. (Saville, Gainey et al. 1988) monitored a marker in the lubricant to measure the residence time in a Caterpillar single cylinder diesel engine and found a time period of 3 minutes at an engine speed of 1200 rpm. Stark et al. measured the residence time of the lubricant for the Ricardo Hydra engine operating at 1500 rpm and 50% load to be 60 seconds ( $\pm 15$  seconds). This is 3 times faster than the result obtained on the diesel engine. Stark et al. suggested that the difference could be caused by the smaller lubricant volume in the ring pack area when compared to the larger piston of the diesel engine and also the fact that diesel engines operate at higher compression pressures making lubricant flow through the ring pack more difficult (Stark, Gamble et al. 2005). Lee (Lee 2006) followed the same approach as Stark et al. on the Hydra engine with the same test lubricant and marker but tested over a

wider range of engine speeds, loads and lubricants, and measured residence time of the order of minutes on the same engine. His results are summarised in Table 6-1. Results from the method include the residence time of the lubricant sample in the TRZ tube and it is believed that a longer tube length would reduce the sample collection rate in the bottle and increase the estimate of the ring pack residence time. But, since the sample residence time in the tube was not measured, this can only be hypothesised. As a result this method is considered an indirect approach to measuring the piston ring pack residence time.

		Engine Speed (rpm)		
		1000	1500	2000
Engine Load (% of max)	33		6.0	
	50	9.0	5.5	7.5
	75		4.0	

**Table 6-1: Piston ring pack residence times (in minutes) over a wide range of engine operating conditions (error  $\pm 1.0$  min) as measured by Lee (Lee 2006)**

## 6.2 Using the LIF Technique to Measure Piston Ring Pack Residence Time

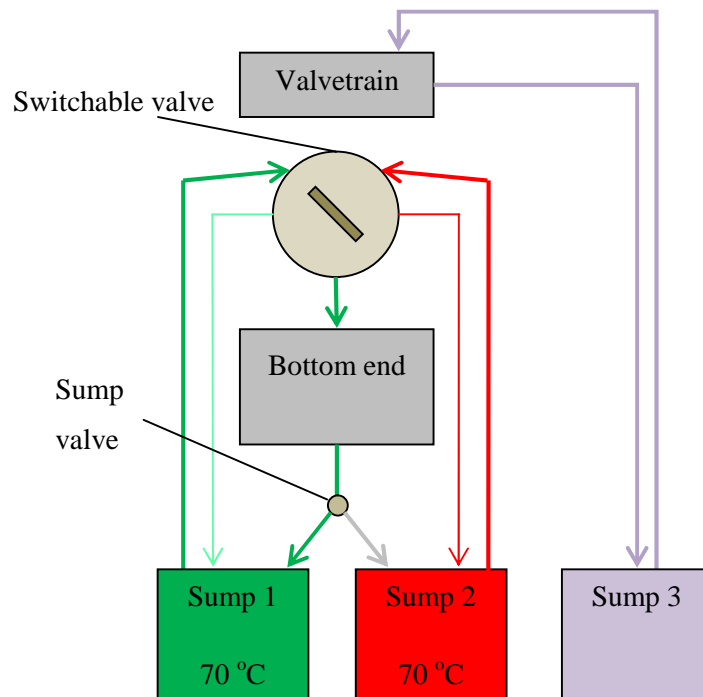


**Figure 6-1: A flow diagram of the complete engine lubricant supply**

A more direct method to measure the piston ring pack residence time is to use the LIF system as a tracer technique to monitor the flow of the lubricant through the ring pack. The Hydra engine has a two sump lubricant supply system, one for the bottom end (crankshaft and piston assembly) via the crankshaft bearings and one for the valvetrain. This allows the bottom end of the engine to be operated on the test lubricant, but the valvetrain on standard high quality lubricant (Lee 2006). By using a twin sump switchable supply system for the bottom end with the same test lubricant but with one of the lubricants doped with fluorescent dye, it was possible to monitor the flow of the lubricant through the ring pack when the supply was changed over.

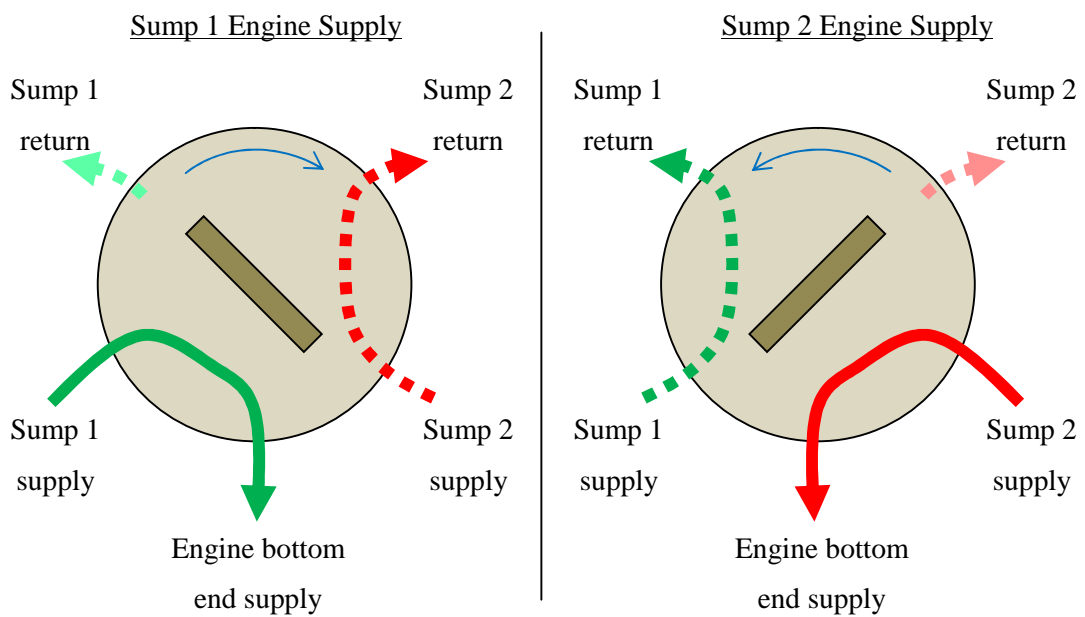


**Figure 6-2: An illustration of the oil flow for the switchable valve**

Lee (Lee 2006) designed and manufactured a switch that would allow the lubricant supply to the bottom end to be switched instantaneously without any transfer of air pockets to the crankshaft bearings. The valve was fitted to the oil inlet on the crankcase for the bottom end and used two supply and two return pipes. Both oil supplies were continuously pumped to the valve to continuously prime the system and prevent any air pockets. One sump was supplied as the bottom end lubricant, whilst the other oil supply was returned back to its sump of origin. The supply to the bottom end changed once the switch was moved from position one to position two. This is shown in the engine oil flow diagram, Figure 6-1. There was also a valve on the engine lubricant drain to switch the lubricant return from the bottom end to either be wasted or return to the sump of origin. So, in total 3 sumps were used; two

for the switchable valve for bottom end lubricant supply and the other for the valvetrain lubrication. As a result 3 oil pumps, which were the same, were used with separate oil filters. The diagram in Figure 6-2 details the oil flow diagram through the switch.

This switchable supply system was used to change the supply of lubricant to the engine. The lubricants used in the sumps were the same fresh lubricant, but in Sump 2 Pyrromethene 567A dye was added in quantities of approximately 35 mg/l and this was used as the tracer lubricant. The dye concentration was similar to the concentration used in fresh lubricants in the previous chapters and was known to provide excellent PMT signal strength under a wide range of engine operating conditions. The engine was operated on Sump 1 until the engine was operating steadily and then the supply was switched to Sump 2 and the lubricant exiting from the engine was then wasted to prevent cross contamination. Once a measurement was recorded, the lubricant outflow to waste was switched back to recirculating flow.

### 6.2.1 Implementation on the Hydra Engine

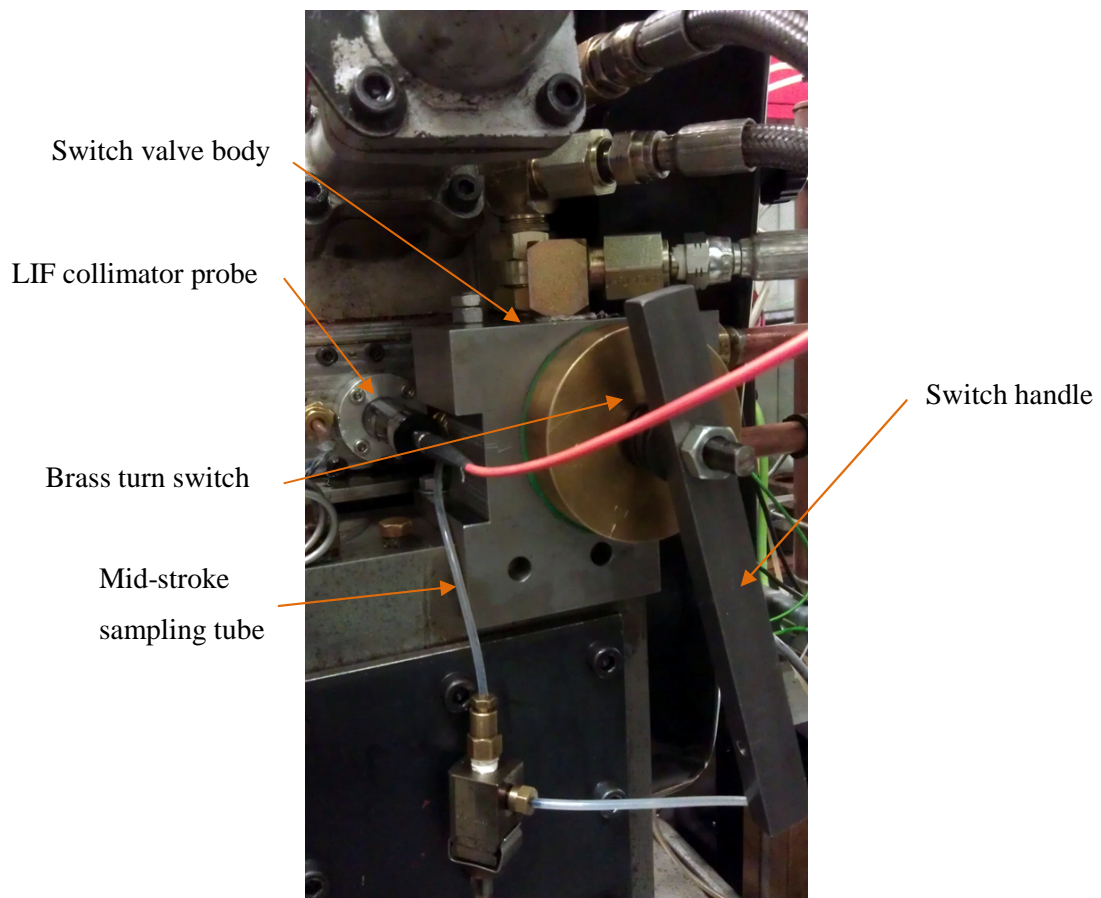


Figure 6-3: Lubricant supply switch valve on Hydra engine with LIF collimator probe

The same lubricant supply switch valve as used by Lee (Lee 2006) was used in this project. This switch was mounted on top of the Hydra crankcase where the oil gallery feed was and plumbed between the oil pumps and the oil gallery. The PTFE gasket used between the brass turn switch and the body of the switch was replaced and a new o-ring was used between the interface of the body to the oil gallery on the engine. Upon installation, it was found that the block of the switch valve interfered with both the LIF collimator probe and the mid-stroke sampling tube. As a result, part of this block was machined to provide clearance for both the probe and the sampling tube, as can be seen in the picture in Figure 6-3. It was always difficult to turn the switch since a high preload was required on the switch part of the valve in order to seal the system and prevent cross contamination. The supply change over needed to be swift during engine operation to prevent a sudden loss of lubricant to the crankshaft bearings, so an improvement here was required. A spindle, which was used to turn the switch, runs through the body of the switch. The spindle was threaded at one end. This was held in position with a series of spring washers tightened by a single M10 nut with a handle to turn the spindle. The spindle, machined from mild steel, was turned against the mild steel body of the switch. To reduce the force required to turn the spindle, a series of PTFE washers was placed between the spindle shaft and the switch body. Additionally, a larger handle was machined from mild steel which also included a 1 metre long extension bar so that the switch could be turned without the operator being close to the running engine.

## **6.2.2 Temperature Controlled Lubricant Sumps**

The sumps used for the supply to the bottom end of the engine were temperature controlled units with an internal stirring mechanism. To prevent thermal shock to the engine, the sumps were both maintained via an internal thermostat at a constant temperature of 70 °C, low enough to prevent significant lubricant degradation occurring. This method followed on from the exact same technique as Stark et al. (Stark, Gamble et al. 2005) and Lee (Lee 2006). The photograph in Figure 6-4 details the complete setup on the Ricardo Hydra engine.

## **6.2.3 Engine Lubricant Samples**

This part of the research was concerned with investigating the ring pack residence time on the Hydra engine and so it was not necessary to use degraded lubricant samples. Instead two fresh lubricant samples were used. One was the same lubricant sample as used by Stark et al. and Lee which was XHVI 8.2 base lubricant with 1% detergent and dispersant to maintain piston cleanliness. The second test lubricant used was Shell Helix HX7 AG 5W30 which is a fully formulated commercially available lubricant. Both lubricants were used from fresh and

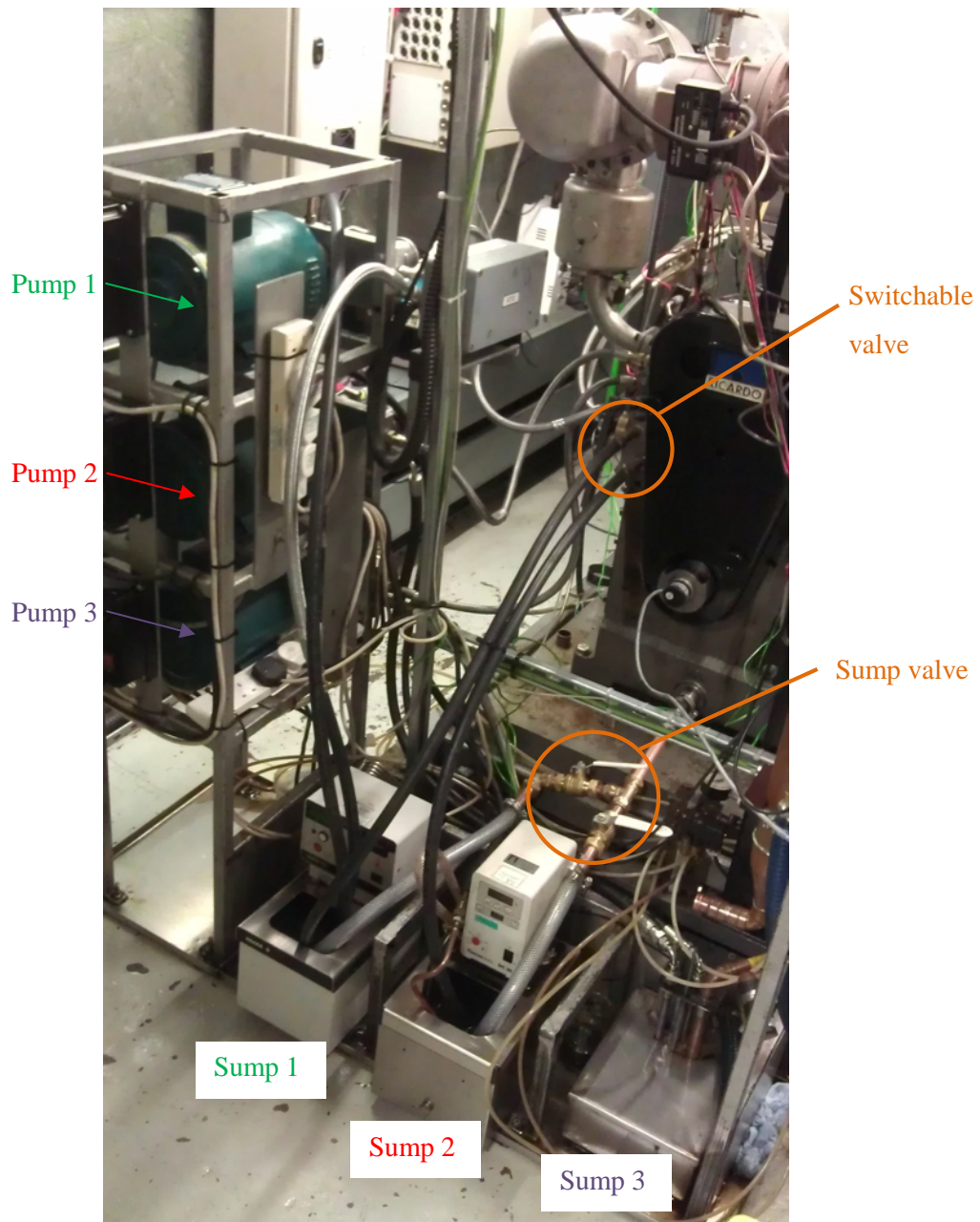


Figure 6-4: Ricardo Hydra engine equipped with 3 sump lubricant supply

	Shell XHVI 8.2, 1% detergent and dispersant	Shell Helix HX7 AG 5W30
Kinematic viscosity 40 °C (cSt)	48.0	69.5
Kinematic viscosity 100 °C (cSt)	8.3	11.7

Table 6-2: Test oil kinematic viscosity specification

mixed accordingly with the dye. The two test lubricants were used to gain appreciation of the influence of lubricant viscosity on the residence times. Table 6-2 summarises the kinematic viscosities of the two test lubricants and the complete oil specification is provided in Appendix F2 and Appendix F3.

### 6.3 Using the LIF Technique to Investigate the Influence of TRZ Sampling on Piston Ring Pack Lubrication

The TRZ sampling system, Figure 6-5, as designed by Notay (Notay 2008) and described in Chapter 2 was used in this research. The sample pipe had a miniature gate valve in-line so that the sampling could be stopped and started to investigate the resulting changes, if any, in the LIF profiles between the piston ring and cylinder wall. Since it was only a concern to investigate the sampling effects on the piston ring pack film lubricant film thickness, only one test lubricant was used and Shell Helix HX7 AG 5W30 was chosen.

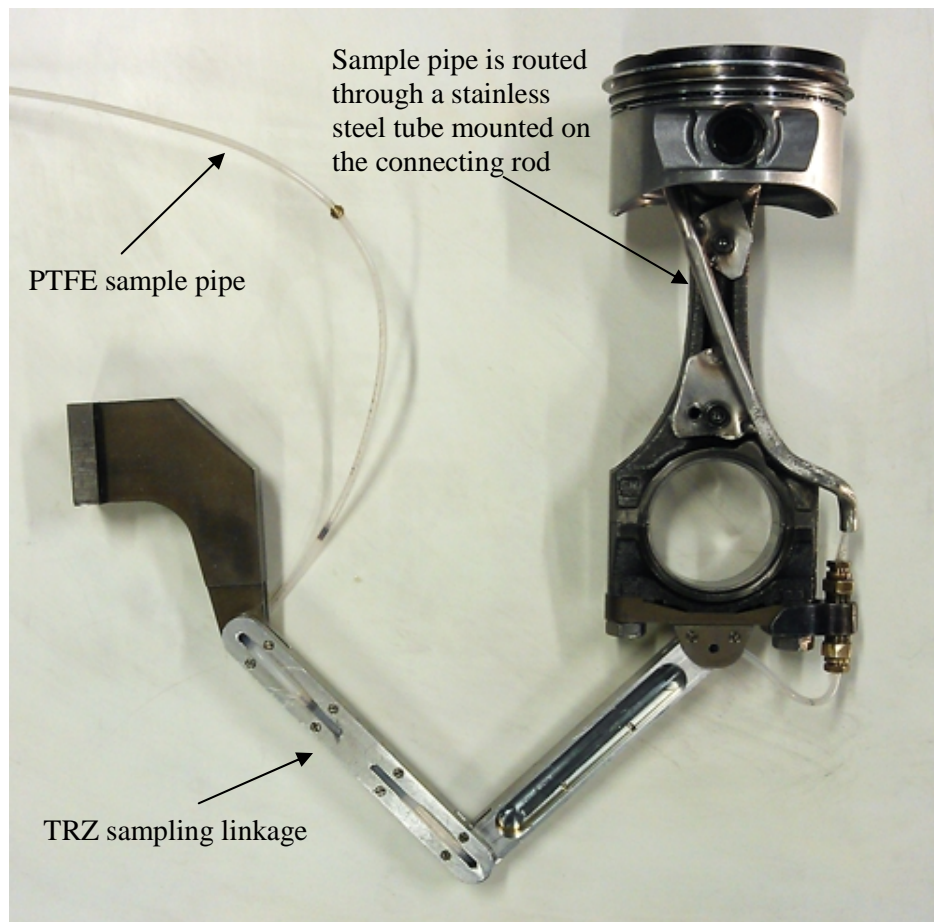


Figure 6-5: TRZ sampling linkage complete with sample pipe, connecting rod and piston assembly

## 6.4 Testing and Test Matrix

The test matrix for the piston ring pack residence time investigation is summarised in Table 6-3 and the test matrix as used to investigate TRZ sampling is summarised in Table 6-4. The orange shaded area in Table 6-3 shows the engine operating range as tested by Lee (Lee 2006) when he conducted his investigation. All residence time tests were repeated at least once, but the tests at 1500 rpm and 50% load were repeated twice to check for repeatability. Once the piston ring pack residence time test matrix was completed for one lubricant, the next test lubricant was employed after a double lubricant flush and drain. This was similar to the method as employed for the tests in Chapter 4 and 5, with a new oil filter used at each lubricant drain.

For the TRZ sampling investigation, only the engine condition at 1500 rpm and 50 % load was repeated once. From previous LIF testing, it was already known that the piston ring MOFTs observed during motored engine operation tend to be large and hence any TRZ sampling during this operation is less likely to be detrimental to the oil availability of the rings than during fired operation. As a result, the testing focus was with fired engine operation, but to improve the trend for engine load investigation, a single motored engine test at 1500 rpm was conducted.

A scan was taken when TRZ sampling commenced, with the sampling valve open, after which the sampling valve was closed to prevent further sampling. The engine was then operated for approximately one minute ( $\pm 10$  seconds) before a final LIF scan of the ring pack was taken for post comparison. A minute was chosen based on the ring pack residence time results being less than a minute for any given test condition. Each test condition was repeated at least once with the condition at 1500 rpm and 50% load repeated twice with the results falling within the repeatability of the experiments.

The piston ring MOFT was taken as a means to investigate the influence of the TRZ sampling on the ring pack oil availability.

In all experiments, the engine was run for an hour to allow stable temperature operation and ensure consistency between tests and maximise repeatability. During all fired test conditions, the air fuel ratio was maintained at  $16:1 \pm 0.1$ , which was consistent with Lee, see (Lee 2006).

		Engine Load (% of max)				
		0% (motored)	33%	50%	75%	100%
Engine Speed (rpm)	1000	XX		XX		
	1500	XX	XX	XXX	XX	X
	2000	XX		XX		
	3000	XX		X		

**Table 6-3: Test matrix to investigate piston ring pack residence time (X denotes test point, area shaded in orange is test range as investigated by Lee 2006)**

		Engine Load (% of max)		
		0%	50%	100%
Engine Speed (rpm)	1000		X	
	1500	X	XX	X
	2000		X	
	3000		X	

**Table 6-4: Test matrix to investigate the effect of TRZ sampling on piston ring pack lubrication (X denotes test point)**

### 6.5 Method Used to Measure Piston Ring Pack Residence Time

A LeCroy WaveSurfer Oscilloscope with a maximum sampling frequency of 400 MHz was used to monitor the output from the fluorescence PMT and observe the oil film thickness trends as the engine operated. Once the engine reached steady test temperature conditions, the supply of lubricant was switched over using the valve. The engine was operated on fresh lubricant without dye (Sump 1) and then switched to the equivalent lubricant which had been doped with dye (Sump 2). A stopwatch was used to measure the time taken from changing the lubricant supply to the oil film thickness profiles becoming stable on the oscilloscope. The stabilisation of the fluorescence output was taken when the film thickness profile was within 10% output per each power stroke profile.

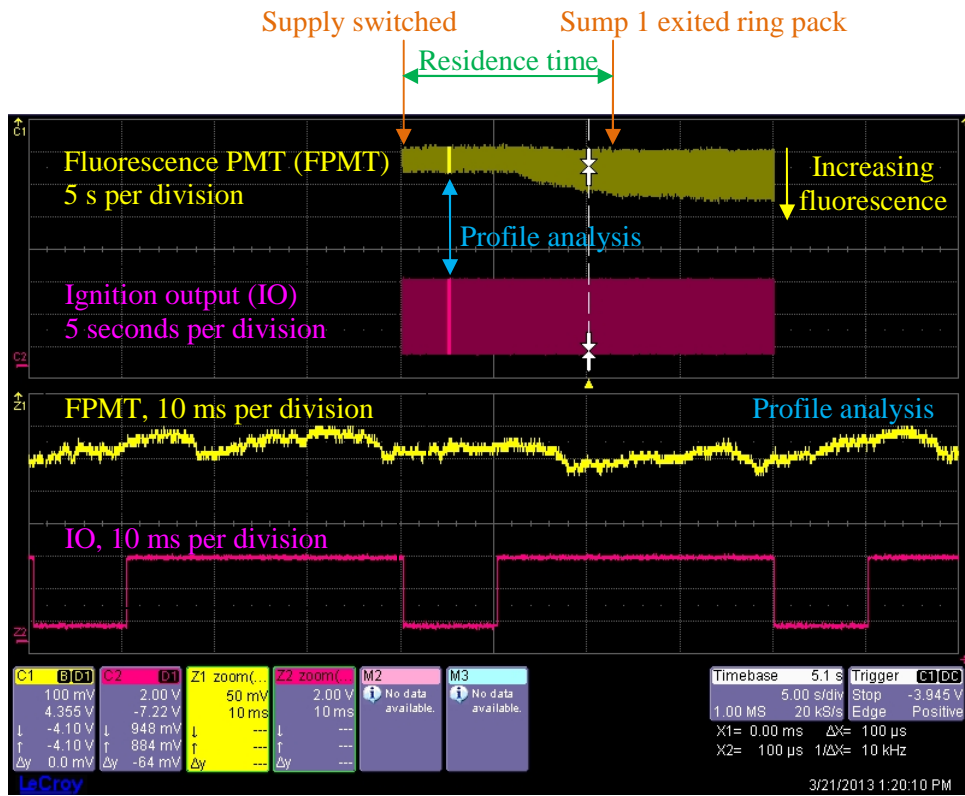


Figure 6-6: Oscilloscope image of fluorescence and ignition during the switch of lubricant supply at 3000 rpm and 50 % load

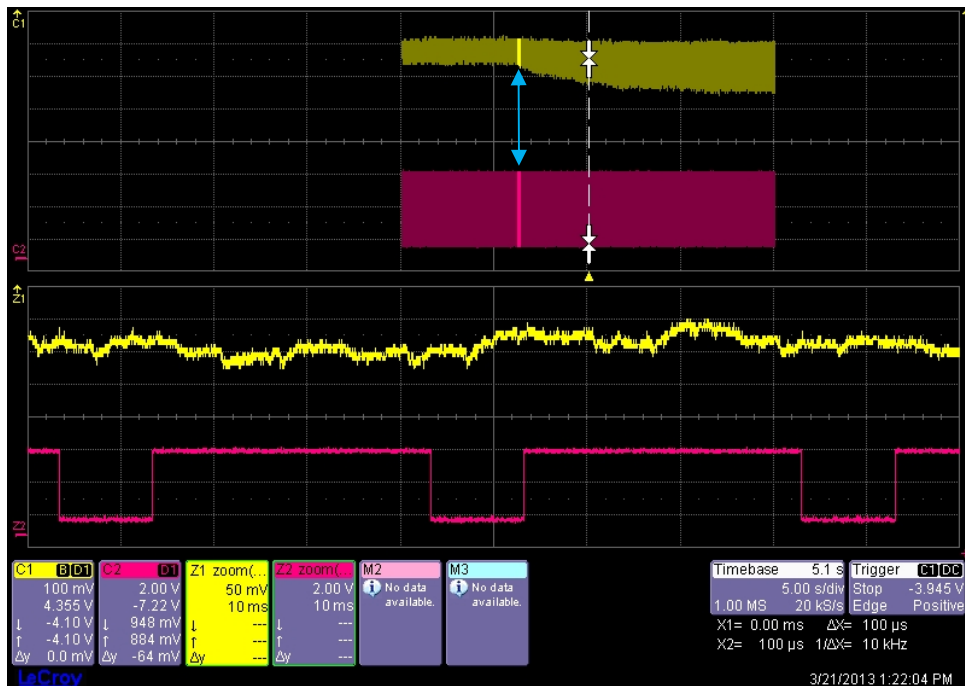
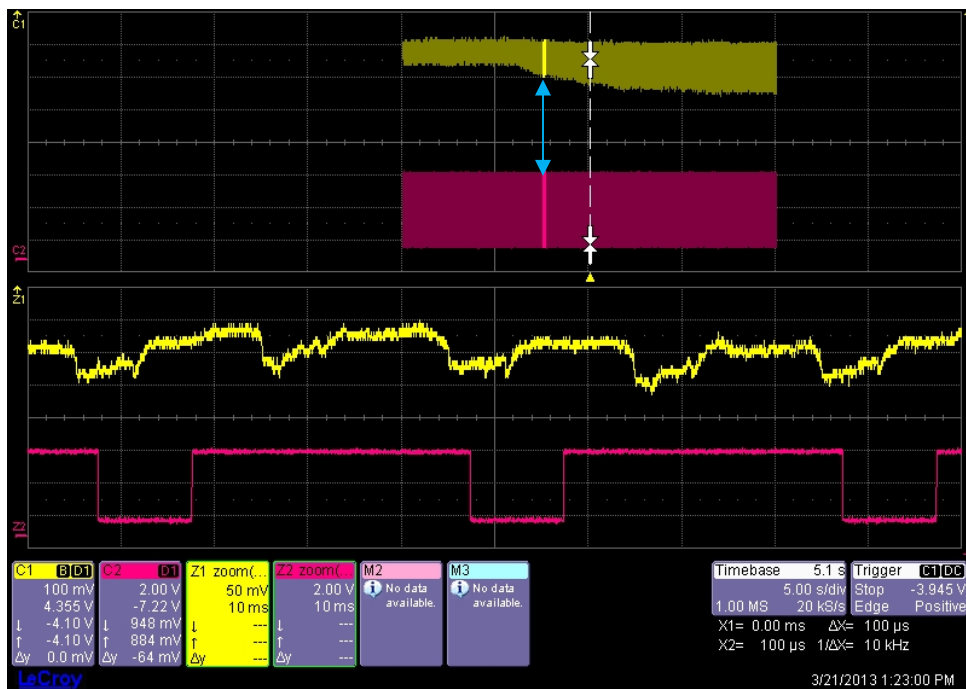
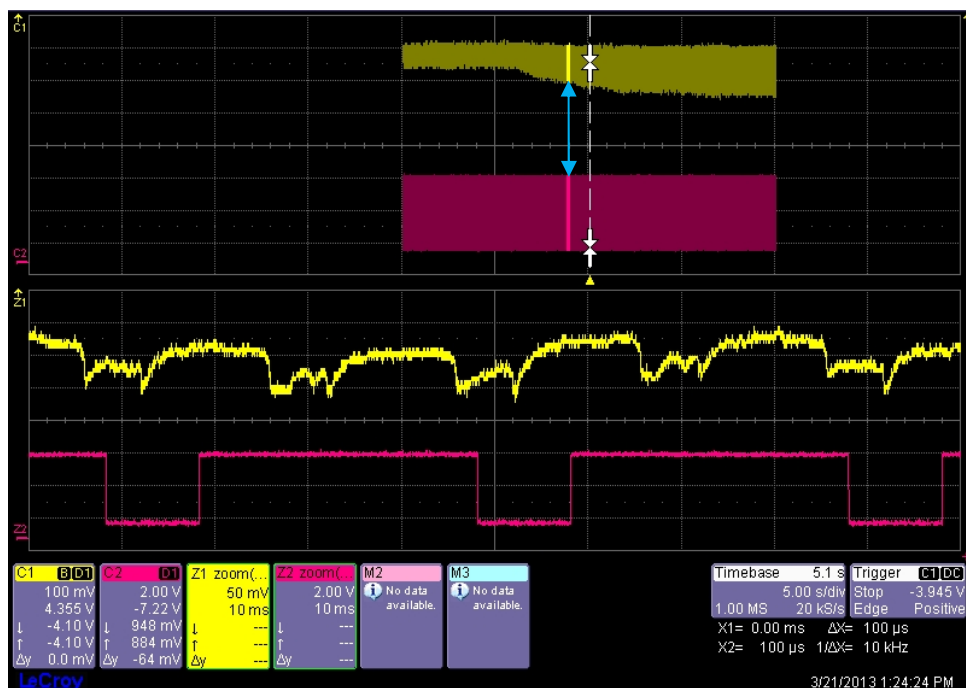


Figure 6-7: Oscilloscope image of fluorescence and ignition at the start of Sump 2 lubricant entering the piston ring pack at 3000 rpm and 50 % load



**Figure 6-8: Oscilloscope image of fluorescence and ignition with increasing concentration of Sump 2 lubricant at 3000 rpm and 50 % load**



**Figure 6-9: Oscilloscope image of fluorescence and ignition with further increase in concentration of Sump 2 lubricant at 3000 rpm and 50 % load**

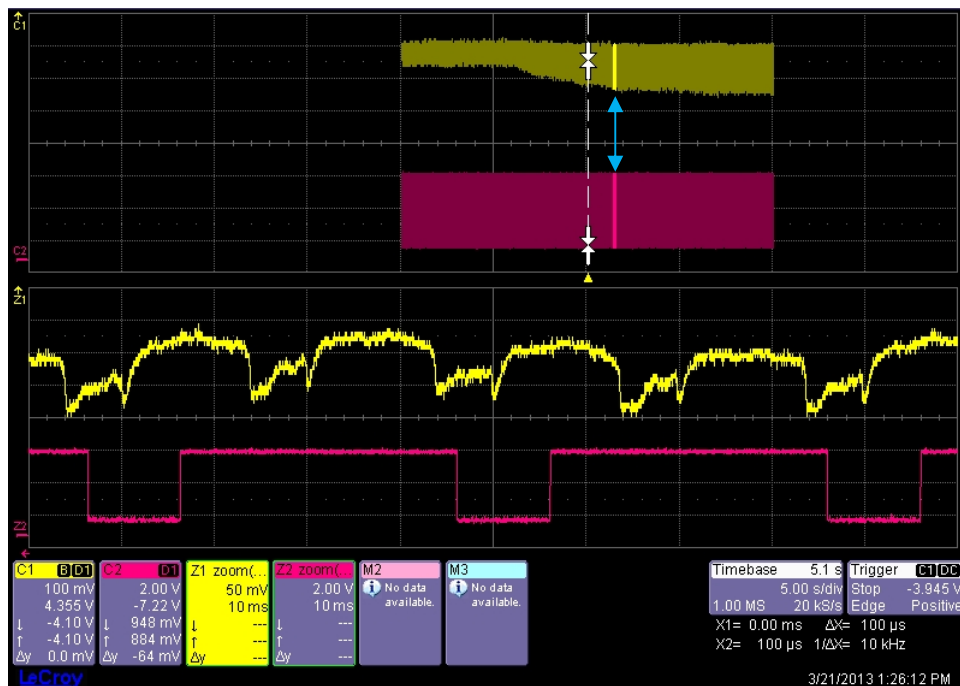


**Figure 6-10: Oscilloscope image of fluorescence and ignition once all Sump 1 lubricant has been displaced from the piston ring pack at 3000 rpm and 50 % load**

Taking the test condition at 3000 rpm and 50% load for the HX7 5W30 lubricant as an example, it was possible to record the output of the fluorescence PMTs using the LeCroy WaveSurfer Oscilloscope. The oscilloscope screenshots in Figure 6-6, Figure 6-7, Figure 6-8, Figure 6-9 and Figure 6-10 show the introduction and increasing concentration of the Sump 2 lubricant through the ring pack at this test condition. This provided a quick insight into the increase in the fluorescence signal as the concentration of the Sump 2 lubricant increased through the ring pack. The fluorescence signal was recorded via the oscilloscope as soon as the switch of the lubricant supply from Sump 1 to Sump 2 was made. Once the fluorescence signal of the ring pack stabilised, this was taken as the point at which the Sump 1 lubricant had fully exited the ring pack and all that was flowing through was the Sump 2 lubricant. The time between starting the oscilloscope recording and the point at which the Sump 1 lubricant had exited the ring pack was taken as the ring pack residence time. The fluorescence signal output increases with time indicating an increase in the concentration of the dyed lubricant (Sump 2 lubricant), and hence a decrease in the concentration of the non dyed lubricant (Sump 1 lubricant) until the fluorescence signal stabilises approximately 11.5 seconds later. By using the viewing the signal on smaller time divisions, it was possible to measure this residence time from the oscilloscope as can be seen in the scan, Figure 6-6.

This indicates that the ring pack is completely operating on the Sump 2 lubricant after this time. This was the method used to measure the ring pack residence time for all engine test conditions.

The time was measured with the lubricant supply switched from Sump 1 to Sump 2 and Sump 2 to Sump 1, so that the time taken for the dyed lubricant to enter and exit the ring pack was measured respectively. It was found that it took longer for the dyed lubricant to exit the ring pack and a greater replenishment of Sump 1 lubricant was required to completely remove any trace of dyed lubricant.

Once the lubricant supply was changed at the switch valve, the sump valve was also switched and the lubricant was drained into a separate third sump to be wasted. It was decided this was the best method to employ to prevent cross contamination of the lubricants.

## 6.6 Results and Discussion

### 6.6.1 Piston Ring Pack Residence Time

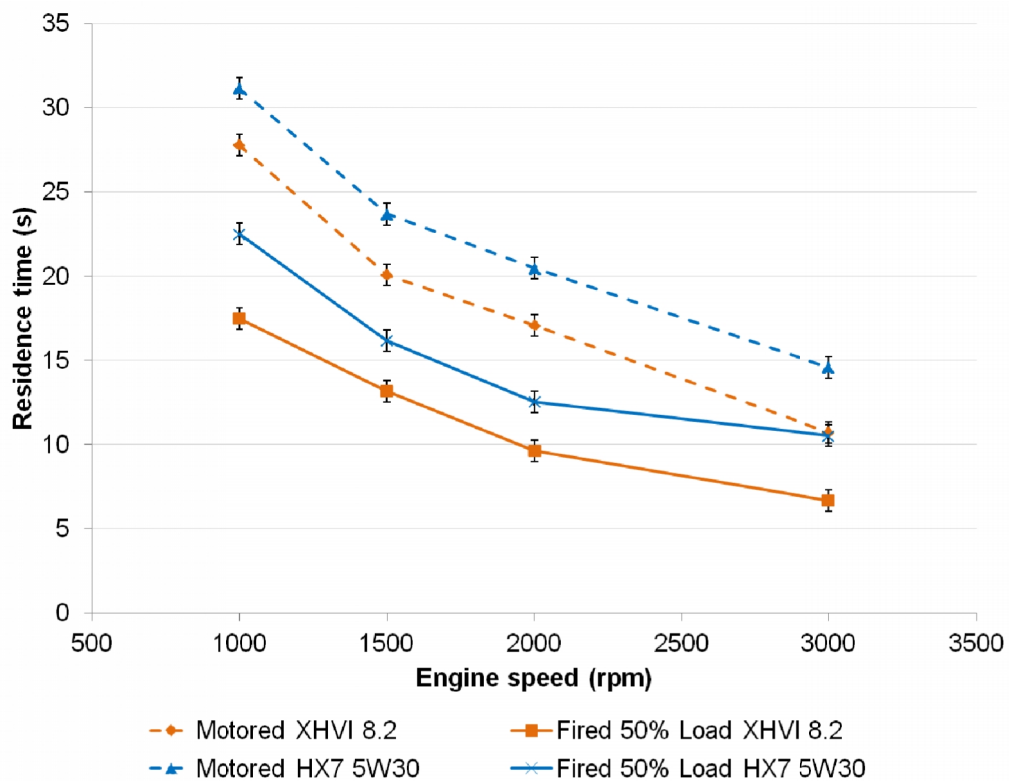
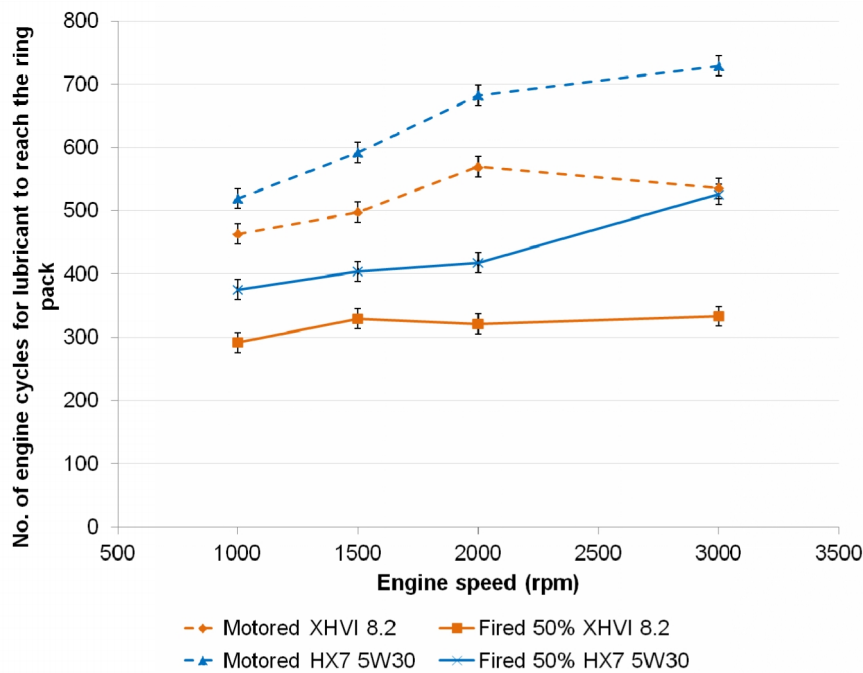


Figure 6-11: Piston ring pack residence time for lubricant supply switch from Sump 1 to Sump 2

Both test lubricants were tested at different speeds under different operating conditions. In the ring pack residence time results for the lubricant switch from Sump 1 to Sump 2, Figure 6-11, there is a clear difference between engine operating conditions regardless of test lubricant. During motored engine operation, the residence time for the lubricant is much greater than for the fired engine operation. Here it can be observed that the influence of cylinder pressure and greater cylinder temperatures during fired operation improves the rate of oil flow through the ring pack. The increased cylinder pressures benefits the ring pack and pushes the rings further outwards towards the cylinder wall thereby improving the seal of the top ring and scraping of the second ring. A more plausible reason for the reduction in ring pack residence times when switching from motored to fired condition, is simply the increased cylinder pressure additionally increases the blow-by gas volume and rate through the ring pack which in turn is carrying lubricant downwards towards the crankcase. An increase in the engine speed also reduces the ring pack residence time. A greater lubricant throw rate from the crankshaft bearings and the connecting rod squirt onto the cylinder wall improves the oil availability at the higher speeds. This also improves the replenishment of the lubricant in the ring pack and reduces the residence time. Between the test lubricants, the XHVI 8.2 base lubricant constantly produces lower residence times than the fully formulated Shell Helix HX7 AG 5W30 lubricant. A difference on average of 3.60 seconds during motored conditions and 3.68 seconds during fired conditions across the engine speeds was measured. The greater viscosity of the fully formulated lubricant has an effect on the ring pack residence time as the flow of lubricant is reduced. This suggests that lower viscosity lubricants have greater lubricant flow and a reduced residence time. This was also suggested by Lee (Lee 2006).

When investigating the number of engine cycles required for lubricant to reach the ring pack, Figure 6-12, additional trends can be observed. In terms of lubricant viscosity, the same result is observed as the less viscous lubricant has greater flow through the ring pack. However, it appears as if the monograde lubricant, XHVI 8.2, is not as sensitive to engine speed as is the multigrade lubricant, HX7 5W30. At the higher speeds, the number of cycles to reach the ring pack is more for fully formulated lubricant possibly purely caused by the greater viscosity which is causing poorer oil flow through the ring pack.

Repeatability was also tested by repeating all test conditions at least once and the results fell within the repeatability of the first measurements taken for each test condition. The test condition at 1500 rpm and 50% engine load was repeated twice for determining the test error range. From the repeated measurements, the error was calculated to be a standard deviation of  $\pm 0.64$  seconds.



**Figure 6-12: The number of engine cycles required for the lubricant to reach the piston ring pack for both test lubricants when the supply is switched from Sump 1 to Sump 2**

The time taken for the lubricant to exit the ring pack was also measured when the lubricant supply was changed back from Sump 2 to Sump 1, Figure 6-13. The lubricant took longer to exit the ring pack, especially at the lower engine speeds (< 2000 rpm). A probable cause is when the supply was changed over to the lubricant without dye, it was possible that there was some residual dyed lubricant within the ring grooves and behind the piston rings. To remove this residual dye, a greater lubricant refreshment rate would be required to ensure that the all dyed lubricant had exited the ring pack. Hence the greater residence times when comparing the results in Figure 6-13 to the results in Figure 6-11.

In terms of the influence of lubricant viscosity, during fired engine operation, the same trend of the lower viscosity lubricant flowing through the ring pack at a greater rate is still valid. However, during motored conditions at engine speeds of 1500 and 2000 rpm, the opposite was observed, the lower viscosity lubricant having a greater residence time for the dyed lubricant to exit the ring pack. Without conducting further testing, it is difficult to say why this occurred other than this could be caused by sudden reduction in oil pressure which would reduce the oil flow. This is difficult to confirm since the oil pressure feed was not recorded. When comparing the number of cycles for the lubricant to exit the ring pack, Figure 6-14, the multigrade lubricant is now unaffected by the increase in engine speed as

was before whereas the monograde lubricant now is. Again, this could be caused by changes in oil pressure.

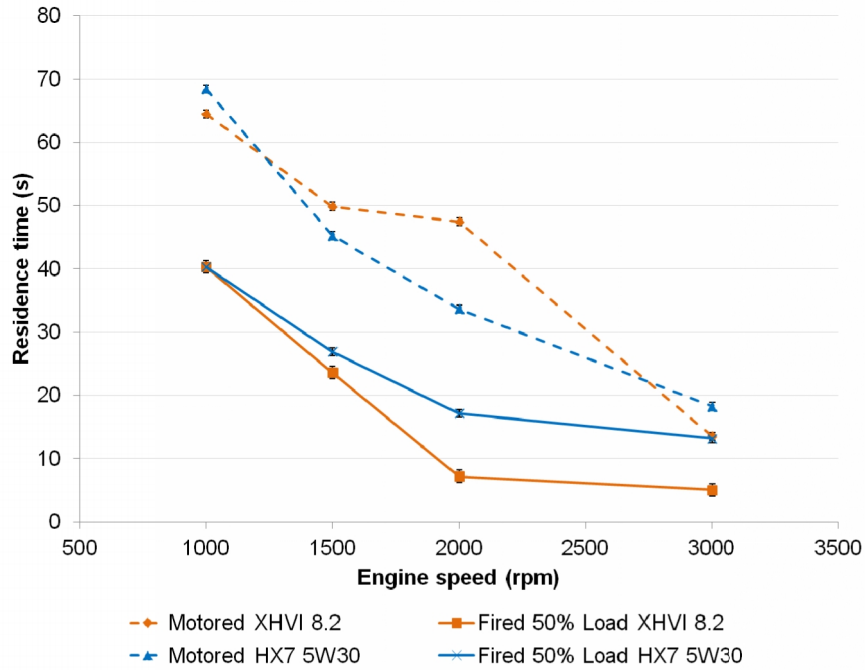


Figure 6-13: Piston ring pack residence time for lubricant switch from Sump 2 to Sump

1

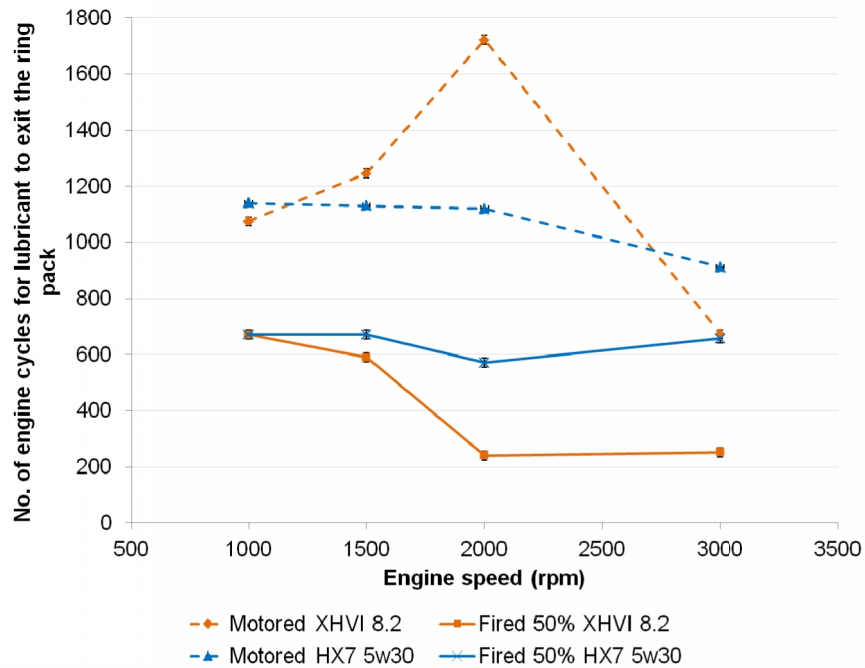
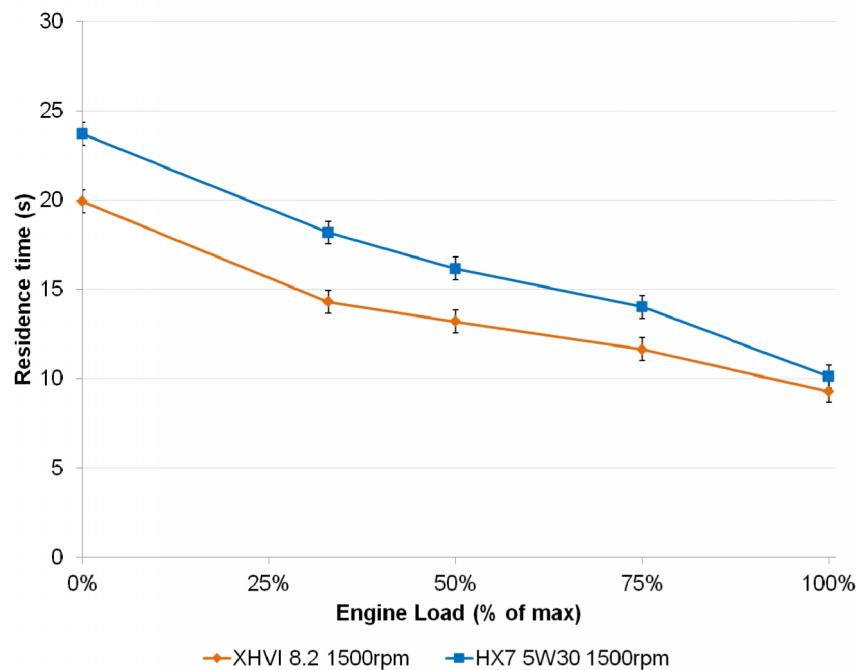


Figure 6-14: The number of engine cycles required for the lubricant to exit the piston ring pack for both test lubricants when the supply is switched from Sump 2 to Sump 1



**Figure 6-15: The influence of engine load on piston ring pack residence time**

The influence of engine load was also investigated, Figure 6-15. Test conditions were performed at 1500 rpm with increasing engine load; 0, 33, 50, 75 and 100% of maximum engine load. It was found that with increasing engine load the residence time of the test lubricants both decreased. Once again, the lower viscosity lubricant, XHVI 8.2, flows easier through the ring pack and produces lower residence times than the HX7 5W30 regardless of engine load. At 100% engine load the results for both appear to be similar, but fall just outside the error of repeatability of the tests. The increase in engine load pushes the rings out further towards the cylinder wall due to the increase in combustion pressure, and as assumed earlier, and increase in cylinder pressure may improve the sealing and scraping of the top two rings thereby displacing lubricant quicker and increasing the replenishment rate of the lubricant through the ring pack. An increase in engine load at the same engine speed also saw a decrease in the ring pack residence time as investigated by Lee (Lee 2006). However, his work was an indirect measurement and included the residence time of the lubricant in the TRZ sample pipe. Hence, his results were of the order of minutes as opposed to seconds as measured in this research.

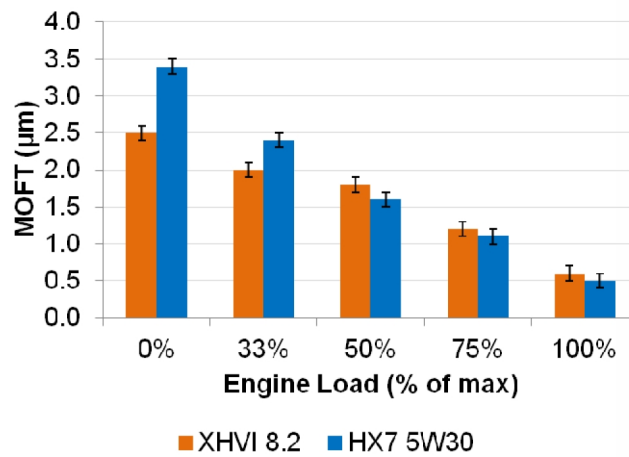


Figure 6-16: Compression ring MOFT of test lubricants at 1500 rpm with increasing load

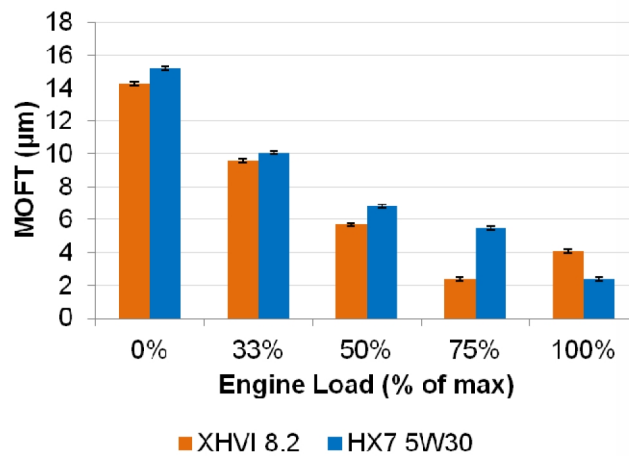


Figure 6-17: Scraper ring MOFT of test lubricants at 1500 rpm with increasing load

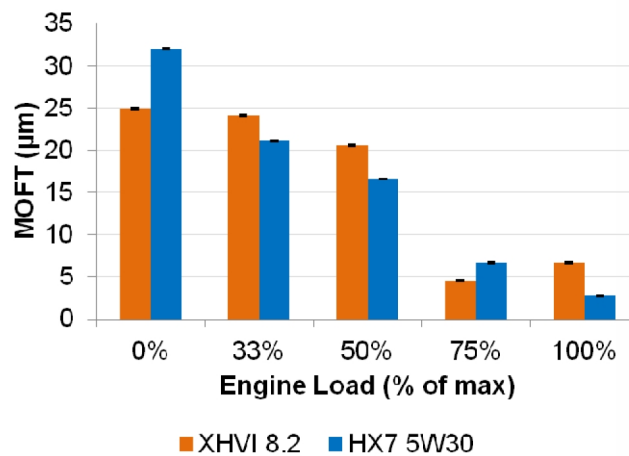


Figure 6-18: Oil control ring MOFT of test lubricants at 1500 rpm with increasing load

The piston ring pack MOFT at 1500 rpm with increasing engine load was also recorded; Figure 6-16, Figure 6-17 and Figure 6-18. The results of the compression stroke are only shown as similar results were observed over the complete engine cycle. As expected MOFT across the complete ring pack reduces with increasing load. However, the more viscous lubricant, HX7 5W30, begins to produce lower films under the compression ring as the load increases above 50 %. A possible cause for this is that this lubricant, containing polymer VI improvers, is suffering from shear thinning as the load increases whereas the monograde lubricant, XHVI 8.2, which does not contain VI improvers does not. Another possible reason for the modest differences in film thickness is that lubricant starvation is occurring, more so for the higher viscosity lubricant with poorer oil flow. This could be the reason why the difference between the measured residence times of the lubricants is much shorter at the higher loads (> 50 %) than the lower loads (< 50%), see Figure 6-15. The HTHS viscosity value for the HX7 5W30 lubricant from specification was found to be 3.5 mPa.s at 150 °C. Monograde XHVI 8.2 has no published HTHS viscosity data since it does not shear thin. However, using an ASTM chart (ASTM D341-03), and the available viscosity and density data from the XHVI 8.2 data sheet, it was possible to estimate the HTHS viscosity of this lubricant at 150 °C to be 2.7 mPa.s. This was an acceptable approach since the XHVI 8.2 lubricant does not contain any VI improvers and hence can be assumed not to shear thin. Knowing this data, it can be assumed that oil flow through the ring pack was the likely cause.

### 6.6.2 Top Ring Zone Sampling

Due to the scale of the following results, the standard error of 0.1  $\mu\text{m}$  is not displayed.

The results of the ring pack MOFT during the compression and the power strokes for the compression ring, scraper ring and the oil control ring against engine speed are presented as Figure 6-19, Figure 6-20 and Figure 6-21 respectively. The influence of the sampling technique can be clearly observed when the valve is open (sampling ON) or closed (sampling OFF). Generally, it was found that when the sampling valve was closed, thereby preventing sampling from the TRZ, the piston ring MOFT measured during this condition were either less or just fell outside the standard error (0.1  $\mu\text{m}$ ) than when sampling commenced. This was also regardless of engine speed or engine stroke.

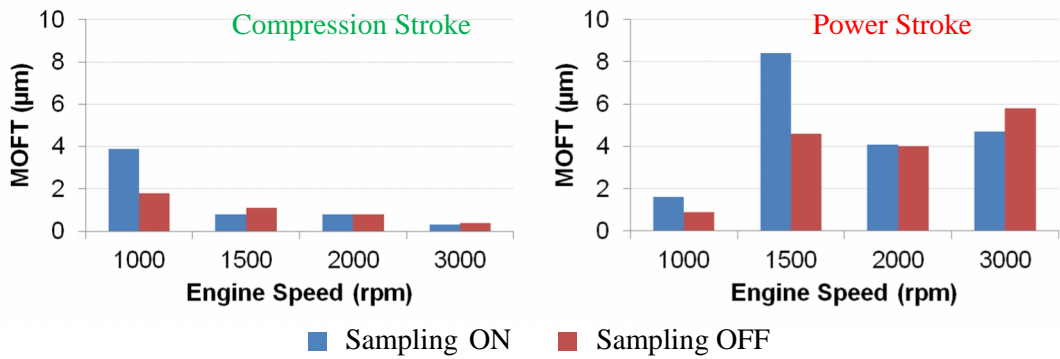


Figure 6-19: Effect of engine speed on TRZ sampling – compression ring, 50 % load

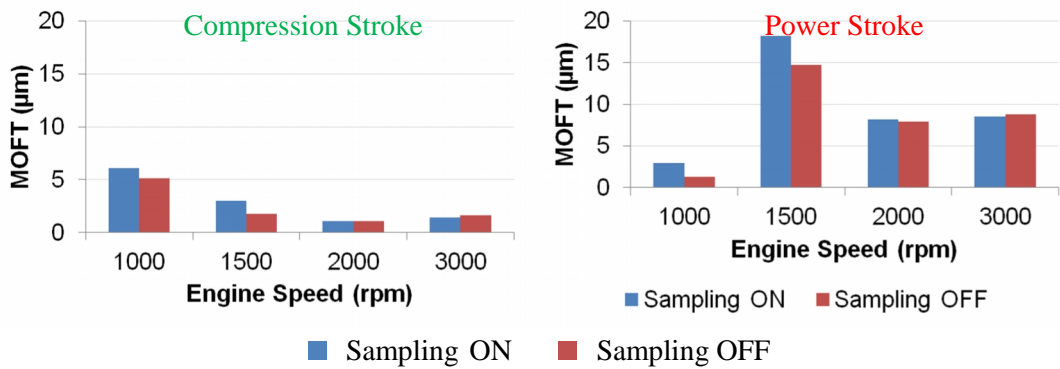


Figure 6-20: Effect of engine speed on TRZ sampling – scraper ring, 50 % load

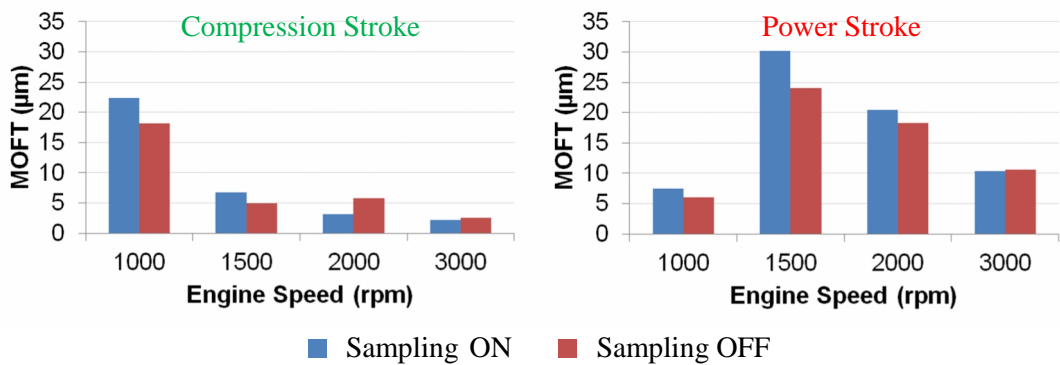


Figure 6-21: Effect of engine speed on TRZ sampling – oil control ring, 50 % load

		Engine Load (% of max)		
		0%	50%	100%
Engine speed (rpm)	1000		0.106	
	1500	0.072	0.113	n/a
	2000		0.123	
	3000		n/a	

**Table 6-5: TRZ sample pipe flow rate (l/min) as measured by Lee (Lee 2006)**

It was expected that sampling would reduce the amount of lubricant within the ring pack, especially at the compression ring since the sample hole was in the top ring groove, and as a result produce lower MOFT than without sampling. When sampling commenced a large volume of blow-by was present with the oil mist that collected in the vial outside the engine. Unfortunately, the sample volumetric flow rate was not measured on this occasion, but the results from Lee’s work are summarised as Table 6-5. From the his results, it can be concluded that as the engine speed increases the sample flow increases and also as the engine load increases for a given speed, the flow rate increases. The sample hole, which was 0.5 mm diameter, was at the top ring groove on the thrust side behind the top compression ring, but directly in line with the LIF probe position. A plausible reason why the film thickness was less when sampling was not occurring is possibly because the sampling system, when active, is reducing the maximum pressure in the ring pack and hence the loading on the rings. Priest measured the blow-by of the engine at 2500 rpm and 50 % load to be approximately 5 litres/min (Priest 1996) and using the data summarised in Table 6-5, it can be estimated that approximately 2 % of blow-by gas is diverted down the sample pipe. Since such a small variation, if any, in the load was not recorded, further testing would be required to confirm this. The MOFT trend results between the compression and power stroke are similar to those measured in the Chapter 5. However, the film thickness, regardless of TRZ sampling, was greatest on the power stroke at 1500 rpm than any other speed. It was not known why this occurred. Engines are very complex machines. It would be beneficial to repeat tests coupled with investigations into oil flow and ring dynamics to improve the understanding.

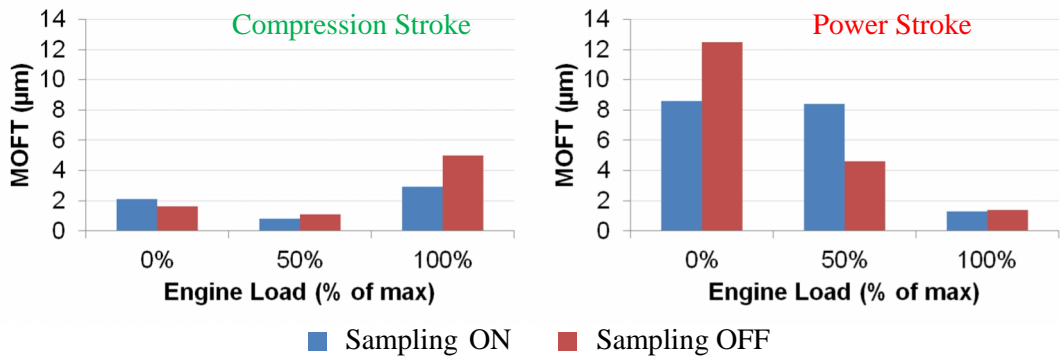


Figure 6-22: Effect of engine load on TRZ sampling – compression ring, 1500 rpm

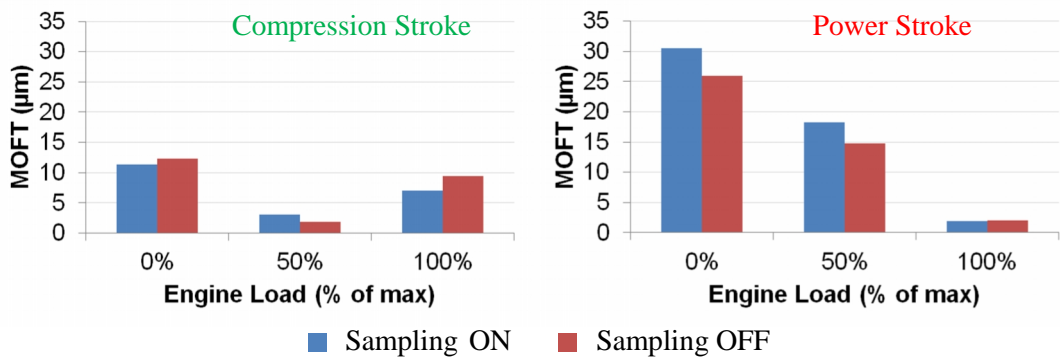


Figure 6-23: Effect of engine load on TRZ sampling – scraper ring, 1500 rpm

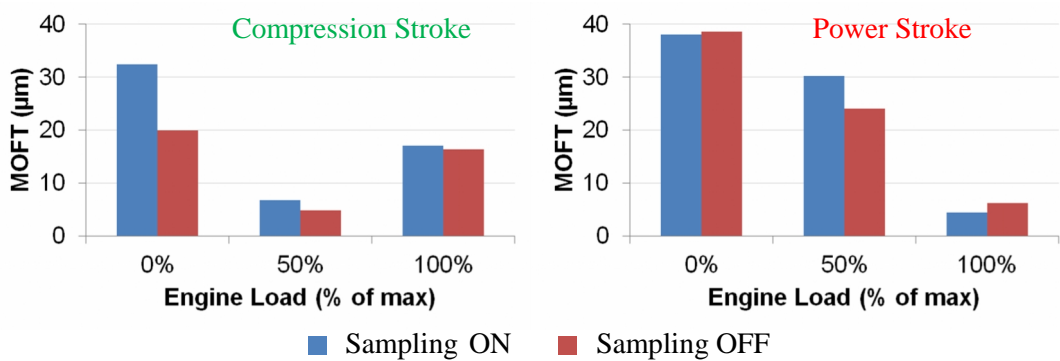


Figure 6-24: Effect of engine load on TRZ sampling – oil control ring, 1500 rpm

The results of the ring pack MOFT during the compression and the power strokes for the compression ring, scraper ring and the oil control ring against engine load are presented as Figure 6-22, Figure 6-23 and Figure 6-24 respectively. Similar to the results for the influence on TRZ sampling of engine speed, generally it was found that when no TRZ sampling was occurring, the ring pack MOFT measured during this condition were either less or just fell outside the standard error than when sampling commenced. Again, the influence of engine load on ring pack MOFT observed here shows that as the load increases the films reduce which is especially true of the results on the power stroke and similar to trends observed in previous chapters.

## 6.7 Conclusions

The LIF system was taken a step further and used to investigate the piston ring pack residence times and the influence of sampling lubricant from the TRZ on the MOFT. A wide range of engine operating conditions were tested with a selection of two fresh lubricants that had different viscosities. The results were obtained from the Ricardo Hydra engine and the following conclusions can be drawn:

- The use of a lubricant supply switching valve and twin system can be used to lubricate the bottom end of the engine successfully with repeatable results.
- It has been shown that increasing engine speed reduces the piston ring pack residence time of the lubricant thereby indicating an increasing in the oil flow through the ring pack.
- Piston ring pack residence times were measured directly and it was found that the times were of the order of seconds as opposed to minutes as previously indicated by indirect methods.
- The viscosity is proportional to the lubricant flow through the ring pack and hence the ring pack residence times. It was found that an increase in lubricant viscosity increased the residence time regardless of engine speed.
- Increasing engine load was found to reduce the piston ring pack residence times.

- It was generally found that the ring pack lubricant films reduced in thickness when no sampling was occurring. A possible reason was that the blow-by gas, which would escape down the sample pipe if sampling was on, was forced to flow past the rings thereby carrying the ring pack lubricant and reducing the film thickness here. This was regardless of engine speed, load and also engine stroke. Further investigations into piston ring pack oil flow rates would confirm this, but it can be concluded that TRZ sampling did not cause oil starvation issues in the piston ring pack.

## Chapter 7 Data Acquisition System

Measurement of the piston ring to cylinder wall oil film thickness in a high speed fired engine to such a high degree of refinement would not be possible without the use of an advanced data acquisition (DAQ) system. Data acquisition was at the heart of this research and was developed alongside the LIF system on the motored engine before a move to the Ricardo Hydra engine, where subtle changes to the DAQ software were made to accommodate the additional two engine strokes and the higher engine speeds.

Data was captured and recorded from various thermocouples, a single pressure transducer, spark plug ignition pulse and the crankshaft encoder simultaneously at high engine speeds. A description in detail of the various analogue and digital channels used to capture data from the multiple transducers and the crankshaft encoder is made in this chapter. The complete DAQ hardware, including the signal conditioning units, is explained along with the programming code used to communicate to hardware from the computer interface. Also, an account on averaging and standard error as employed for the LIF MOFT results is made.

### 7.1 LIF Data Acquisition System

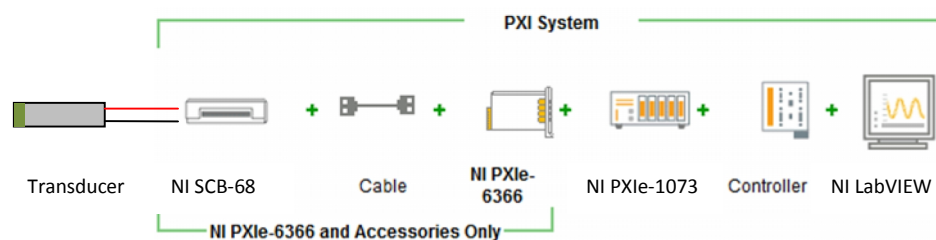


**Figure 7-1: Schematic diagram of transducer connection to NI hardware. Adapted from (NI 2013)**

When this project started, National Instruments (NI) data acquisition hardware for transducer instrumentation was available, but did not meet the requirements of this research. This system comprised of a NI PCI-6111 card having a maximum simultaneous sampling speed of 5 Mega-samples per second per channel with 2 analogue input channels, two digital TTL

(Transistor – Transistor logic) counter lines and 12-bit ADC (analogue to digital conversion). In this project, numerous thermocouples and transducers were used simultaneously and this meant that the lack of additional analogue and digital channels on the available hardware forced a new DAQ system purchase.

A high specification Dell computer with a high performance Xeon central processing unit with processing power of 2.40 GHz along with 3 GB of RAM (random access memory) was specifically used for this research to handle the mass of data captured from the engine instrumentation and process it. This computer was connected to a newly purchased NI PXIe-1073 chassis through a controller card added to the motherboard of the computer. This chassis had 5 slots to accept a different combination of card modules. One of the slots housed a NI PXIe-6366 multifunctional DAQ accessory card which had 8 analogue inputs at a sampling rate of 16 Mega-samples per second and 24 channel digital I/O (input and output) which were both 16-bit resolution, and four channel 32-bit resolution TTL counter lines. The system was well advanced at the time and even had the benefit of analogue and digital triggering. To allow physical wiring connections to plug into the DAQ hardware system, a shielded NI SCB-68 connector block was used which offered screw terminals for the wires. Some voltage signals can be affected with noise from surrounding electrical equipment and from the 50 Hz alternating current mains supply. Since this can cause poor signal to noise ratios in low voltage signals it is absolutely imperative that these signals are shielded. The SCB-68 block is a shielded box which is earthed to the mains powered chassis.

The NI hardware was controlled by an additional software programming language, NI LabVIEW (Laboratory Virtual Instrumentation Engineering Workbench). The schematic in Figure 7-1 summarises a typical connection of a transducer sensor signal to the hardware. An additional 24-bit USB (universal serial bus) device, NI USB-9211A, with four low voltage analogue input channels was used to connect thermocouples for temperature measurement.

## 7.2 DAQ Channels

As noted above, the data acquisition software was adapted slightly to accommodate the higher engine speeds and the addition of the power and exhaust strokes which the motored engine did not have.

The DAQ hardware has a large number of analogue and digital channels allowing various combinations of transducers to be used. The DAQ hardware system for the motored engine comprised the following data channels:

- a) Cylinder pressure transducer. This pressure transducer, a Kistler 601 sensor, was used to monitor the motored engine cylinder peak pressures. The sensor was wired directly to a Kistler 5011 charge amplifier whose voltage output was wired into one of the analogue inputs in the SCB-68 block for the PXIe-6366 card. The scale of the charge amplifier was set such that the maximum voltage at the maximum pressure tolerance of the transducer (25 bar) provided a maximum voltage output of 10 V. This was within the acceptable voltage range of the NI hardware.
- b) 3 liner temperature measurements. Three K-type thermocouples were mounted into the thrust side of the cylinder liner of the engine. These were used to monitor the temperature distribution. The three thermocouples were mounted at TDC, mid-stroke probe position and BDC of the piston stroke. These thermocouples were wired into analogue channels of the USB-9211A as voltage outputs. The USB-9211A has an internal cold-junction compensator to provide accuracy in the data acquisition of the thermocouple. K-type thermocouple wiring consists of two different wiring materials; Nickel-Chromium and Nickel-Aluminium. A thermocouple is produced once the two wires are fused together. Thermocouples produce very small voltage ranges and require no power source for operation since a current is produced based on the temperature difference between the cold (device) and hot junction (probe).
- c) Coolant temperature measurements. A single K-type thermocouple was positioned inside the engine barrel to monitor the coolant temperatures. This thermocouple was wired into the spare analogue channel of the USB-9211A device
- d) 2 photomultiplier (PMT) current output measurements. The PMTs were used to measure the laser excitation and the fluorescence emission intensities. These two outputs were wired into the SCB-68 connector block for the PXIe-6366 card. Hamamatsu Photonics H5783-20 PMT modules were selected since they worked well with the Hamamatsu Photonics C7169 power supply. They offered a high cathode radiant sensitivity (> 70%) from approximately 460 to 700 nm which covered the range of the LIF optical system. The specification sheet of the PMT module and the power supply is presented in Appendix A2 and A3.
- e) Crankshaft encoder to monitor crankshaft angle. The encoder produced 720 digital pulses per revolution along with a single TTL reference signal once every revolution. The single reference signal, Z line, was used to monitor the TDC position of the piston. This quadrature encoder had two output channels, A and B, which are 90° out of phase and are used to determine the direction of rotation. The direction of rotation is determined by the pulse channel that leads first. The additional benefit of this is that during data acquisition the rising and falling edges of both channels are

recorded allowing four times the resolution of the encoder therefore allowing a resolution of  $0.125^\circ$  of crank angle. This high resolution was used throughout this research. Each complete pulse, rise and fall, is  $0.50^\circ$  and is known as the pulse width. A schematic explaining this is presented in Figure 7-2. The shaft encoder had a separate 5 V power supply and the three outputs from the encoder; A, B and the reference line were wired into the SCB-68 as counter lines. The maximum pulse voltage is 5 V.

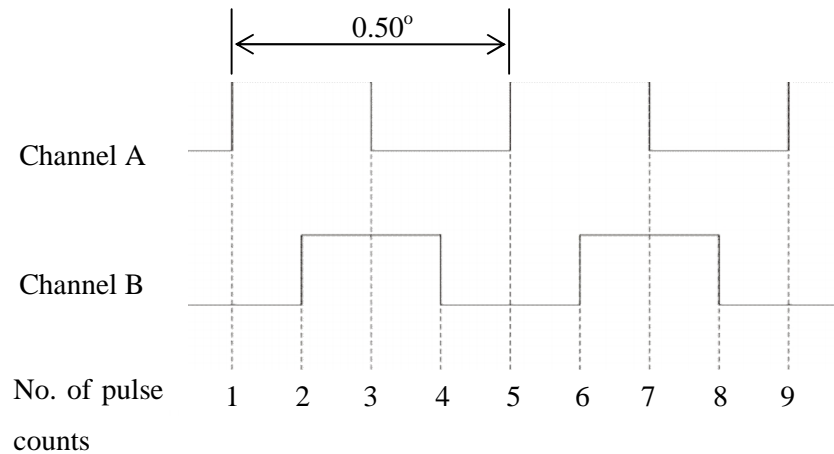


**Figure 7-2: Four times the resolution is possible with quadrature shaft encoders**

An additional thermocouple was placed in the motored engine crankcase to monitor the lubricant sump temperatures and was wired to a handheld display monitor and not into the DAQ hardware.

When the LIF was moved onto the Ricardo Hydra engine, the same DAQ system was used. The only difference in the hardware configuration was that cylinder pressure was not monitored and recorded since a cylinder pressure transducer was not installed. Instead the spark plug ignition pulse was wired in place of the channel used for the cylinder peak pressure of the motored engine. This was used to monitor the position of the engine strokes with respect to the crank angle. The encoder was different in form on the Hydra engine and the power supply for this was taken from the engine control unit. Both encoders were quadrature encoders with 720 pulses per revolution.

During LIF calibration, the voltage output from the LVDT was monitored and recorded for displacement measurements of the calibration stage. A summary of these output signals to the signal conditioning units and the computer is illustrated in flow chart in Figure 7-3.

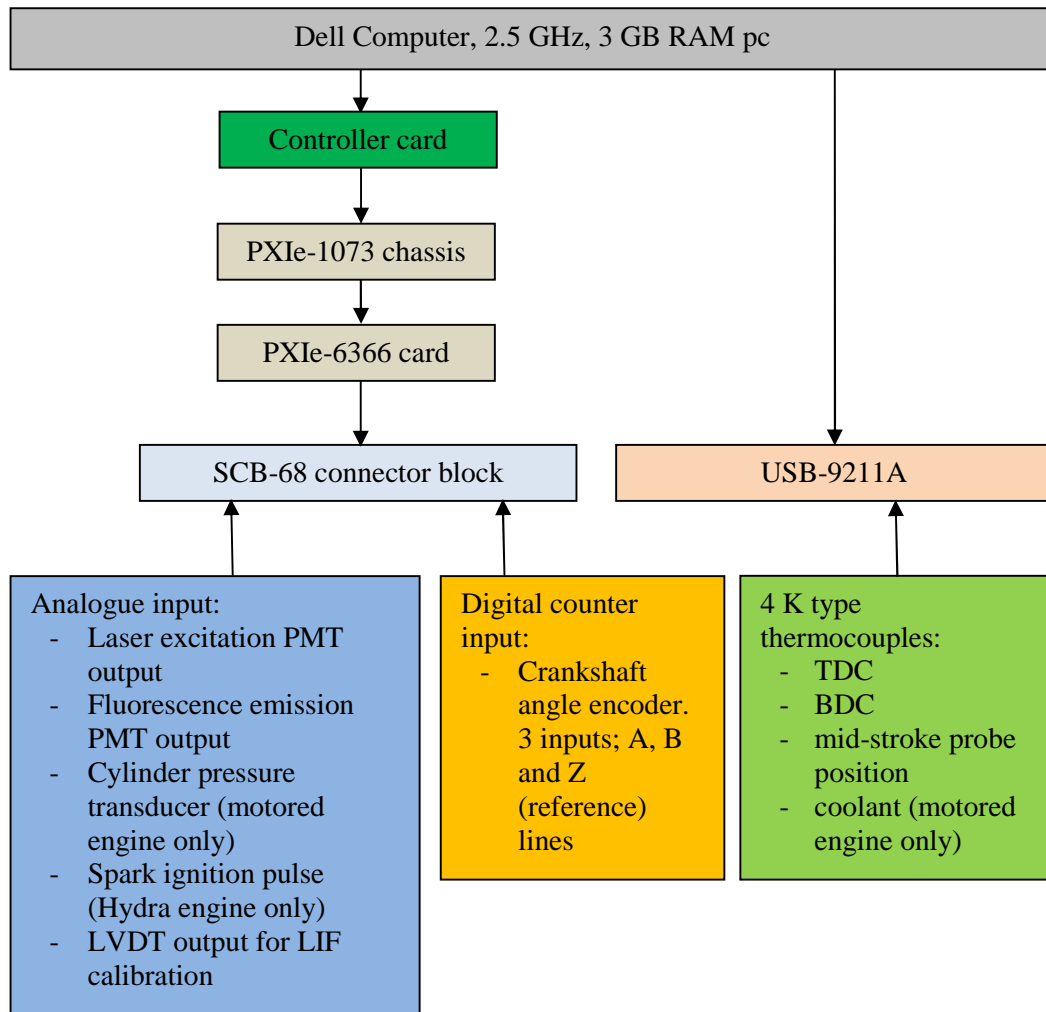


**Figure 7-3: Data flow chart of the DAQ system**

The analogue/digital inputs for the PXIe-6366 card and the analogue (thermocouple) inputs for the USB-9211A were wired into the devices via the screw terminals in the SCB-68 or the screw terminals on the device respectively. All analogue voltage inputs for the PXIe-6366 were wired as differential inputs whereby two wires are required, a positive and a negative, and the difference is measured between to give a readable signal. Connecting this way minimises the chance of signal noise (NI 2013). Just to note (NI 2010; NI 2011; NI 2013) are reference citations with the complete reference in the reference section. The PMT outputs are current signal outputs. For current measurements it is necessary to wire a resistor in parallel to prevent the chance of voltage overload and protect the DAQ device. The PMTs were wired into the SCB-68 block with a shunt resistor of 1 M $\Omega$  as the chassis could take up to a maximum signal of 10 V. As a result, the incoming PMT signals were very small in the

region of micro amperes, but the high resolution of the PXIe-6366 card meant that this was not a problem. Additionally, the PMT signal output is by default negative in value but this was corrected for in the software program.

### **7.3 Engine control unit**

The motored engine had a control box on the outside of the engine mounting frame, which was used to control the speed of the DC motor and thereby the crankshaft. There was an oil pressure switch on the panel to indicate low oil pressure and the motor would shut down if this was activated.

The fired engine was controlled by a CADET V14 Compact CP Engineering Systems chassis computer and software. This control unit was a purpose built system for the Hydra.

The CADET system was used to monitor:

- Thermocouple temperature measurements of the coolant in and out, crankcase oil, cylinder head and exhaust temperatures
- Oil pressure sensors for the lubricant supply at the crankshaft bearings and the valve train
- O<sub>2</sub> lambda sensor mounted on the exhaust manifold
- Air pressure at the inlet

The CADET system was used to monitor and control:

- Throttle position
- Ignition timing
- Injection timing
- Injection rate
- Operating load on the engine
- Dynamometer speed

### **7.4 Introduction to LabVIEW**

LabVIEW is system design programming software which is used to communicate with the DAQ hardware (Essick 2012). The manufacturer of both the DAQ hardware and the software are the same, allowing easy integration. The software is unique and different to other computer programming software, which are text based, and is purely graphical based.

A typical LabVIEW program is designed around two windows. One of the windows is known as the block diagram where the actual program is written and the other is known as the front panel and is the user interface (Essick 2012). LabVIEW consists of fundamental icons, wires, terminals, structures and nodes which are the building blocks of the program. Such include mathematical functions, DAQ hardware specific functions and also data storage functions.

The program executes in a data flow fashion, allowing certain functions to execute before others and allows multiple functions to execute at the same time (Essick 2012). This benefit allows simultaneous data acquisitions. Digital logic is the key to the programming and there is usually more than one method to perform the same task. However, if data performance and streaming is vital, it is important to remove or reduce the impact of bottlenecks, whereby the program hangs during execution, to reduce the load on the computers' resources and increase productivity. Further information on LabVIEW can be found in other sources such as (NI 2010; Essick 2012).

For this research, many different programs were developed and tested. When the move from the motored engine to the Hydra fired engine took place, the DAQ programs also needed to be altered to suit the changes in sampling rate to accommodate the higher engine speeds and the additional two engine strokes; the power stroke and the exhaust stroke.

## **7.5 LabVIEW DAQ Programs**

A LabVIEW software program was written for data acquisition from the engine and also for the LIF calibration procedure. The difference between the two programs for the DAQ was the sampling rate. The sample rate for the acquisition from the engine was much faster than that for the calibration procedure, rates above 200kHz as opposed to 1Hz. The data obtained from the engine was streamed to the disk at high speeds and as a result post processing of the data was required to make sense of the fluorescence PMT signal output in terms of film thickness measurements. If data was processed once acquired from the engine in the same program, the speed of the DAQ would be hindered and the recorded data would either be missing elements or a lag in the recording would cause not enough data points to be recorded. A description of the programs that were developed and used for this research is made in the next set of sections.

### 7.5.1 LIF Calibration Program

The purpose of this program was to facilitate the calibration of the LIF system. The static calibration rig as described in Chapter 3 was used to calibrate the PMT signal in terms of a measured film thickness. Data was acquired and recorded from both PMTs, for the laser signal strength check and the fluorescence signal, and the LVDT to measure the change in the movement of the height of the vertical stage, which in turn represented the film thickness between the probe window and the reflective calibration piece in the oil bath. The thermocouple that was placed in the oil bath, to measure the temperature of the test oil, was connected to a handheld monitor and the temperature was noted in the program and recorded to the data file as generated by the program. The PMT sensitivity was monitored from the display screen of the PMT power supply and also noted in the program to be recorded in the data file.

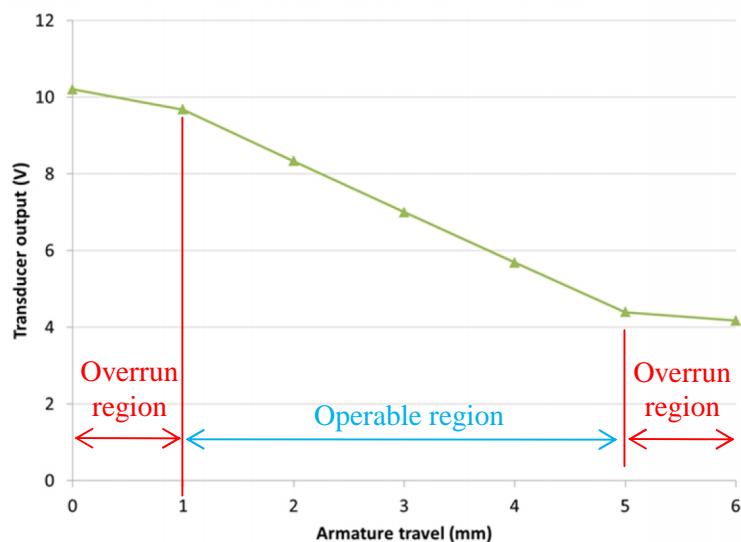


**Figure 7-4: LVDTs have a limited operable range**

The LVDT used for the calibration was an RDP Electronics GTX 2500 spring return displacement transducer connected to a RDPE 621 amplifier. This particular displacement transducer has an absolute resolution of  $0.25 \mu\text{m}$ . An LVDT consists of a moving armature in between two coils placed in parallel. As the armature moves past one coil and away from the other coil, the voltage through the coil nearest the armature increases positively and reduces in the coil it is moving away from. The combined potential difference of the two coils is used to monitor the displacement of the armature and hence measure the displacement of the LVDT plunger.

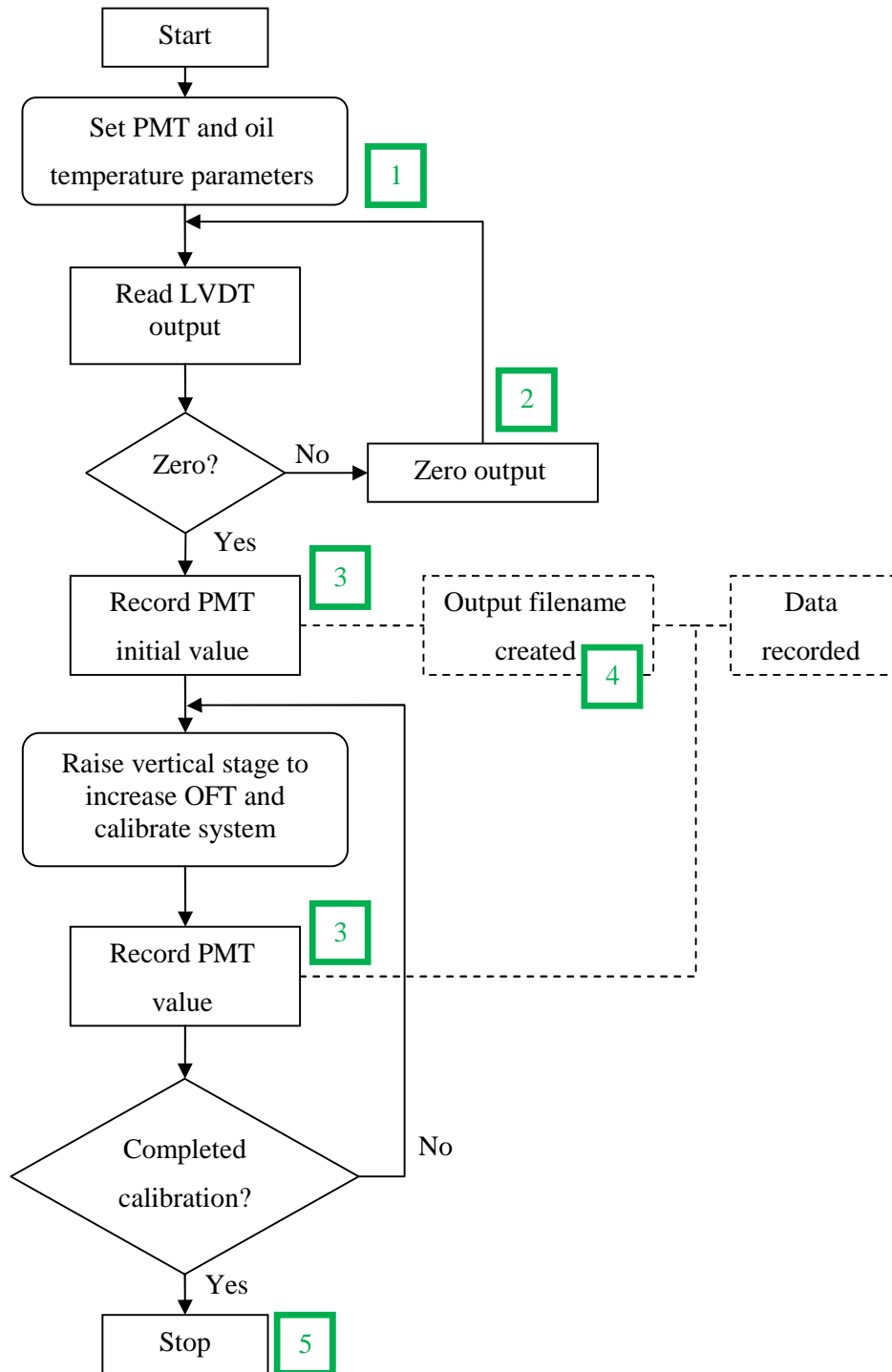


**Figure 7-5: Dataflow diagram of the LIF calibration program**

The amplifier can be set with a different level of gains depending on whether full stroke, 4.0 mm, or half stroke, 2.0 mm, operation is required. As a result, once the gain and range is set, it is necessary to calibrate the transducer. LVDT calibration was performed using slip gauges

of known thickness up to 5 mm and placing these in-between the plunger tip and a flat reference block. A total of five test runs were completed and an average of the linear relationship between the armature travel and the transducer output was taken. Calibration results were found to have a standard deviation of 24 mV and all test runs had a confidence level exactly equal to 1.0. LVDTs have an inherent ‘overrun’ position, which occurs at the inward and outward stroke ends, whereby the output deviates. This unusable overrun range was not used for calibration and can be clearly seen in the LVDT output trace in Figure 7-4.

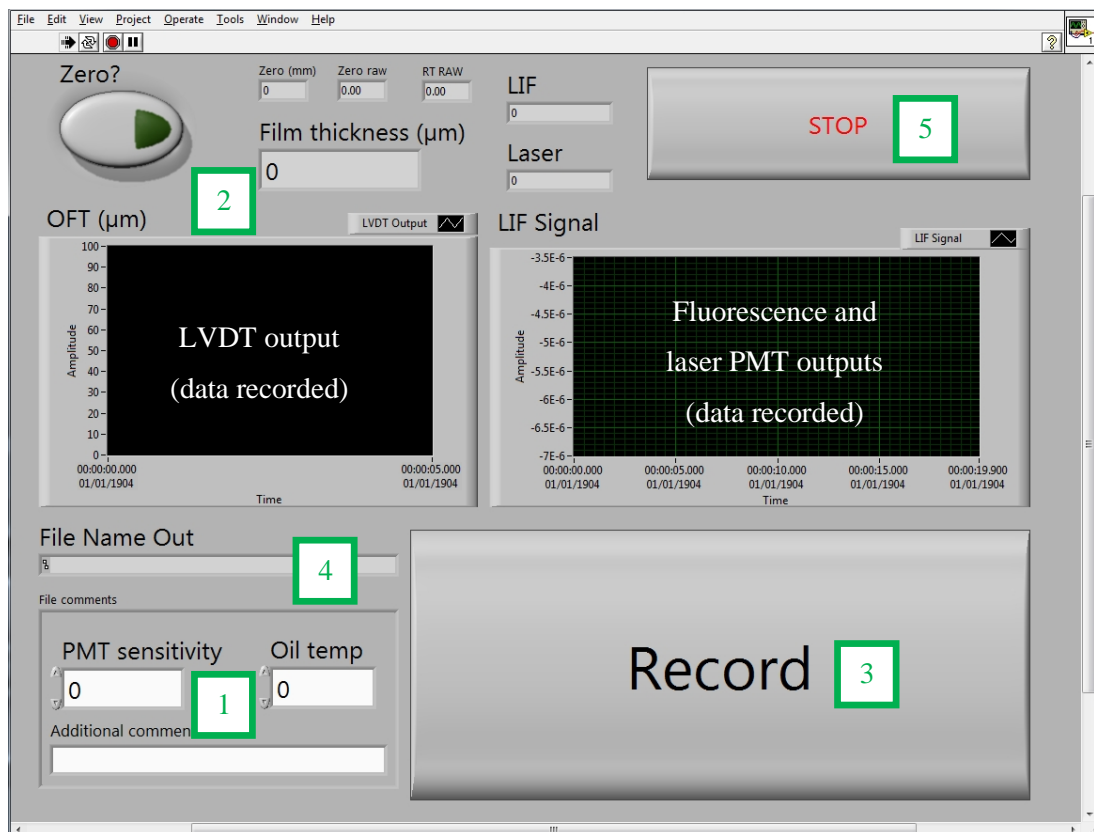


**Figure 7-6: Front panel of LIF calibration program**

During subsequent calibration tests of different lubricant test samples, the calibration setup needed to be disturbed to remove the oil bath and replace the sample. To allow this, the vertical stage needed to be raised to remove the bath and as a result the reference zero of the LVDT was lost. So during subsequent runs it was necessary to re-zero the LVDT. The zero reference was taken when the probe was at its lowest possible height when the oil bath plus sample was used. This was integrated into the software design, to first allow the software to zero the LVDT at its current position before actual calibration of the LIF system commenced.

The data flow chart in Figure 7-5 illustrates how the program works. Data is recorded from both PMTs and the LVDT. The relationship between the transducer output and the armature travel, the calibration equation, obtained from the LVDT calibration (see Figure 7-4) is used in the program to provide information of the oil film thickness as the armature moves. The front panel of the program is shown in Figure 7-6 and for clarity, data flow process numbers from Figure 7-5 are also shown on the illustration.

### 7.5.2 Piston Ring Pack Oil Film Thickness Measurement Program

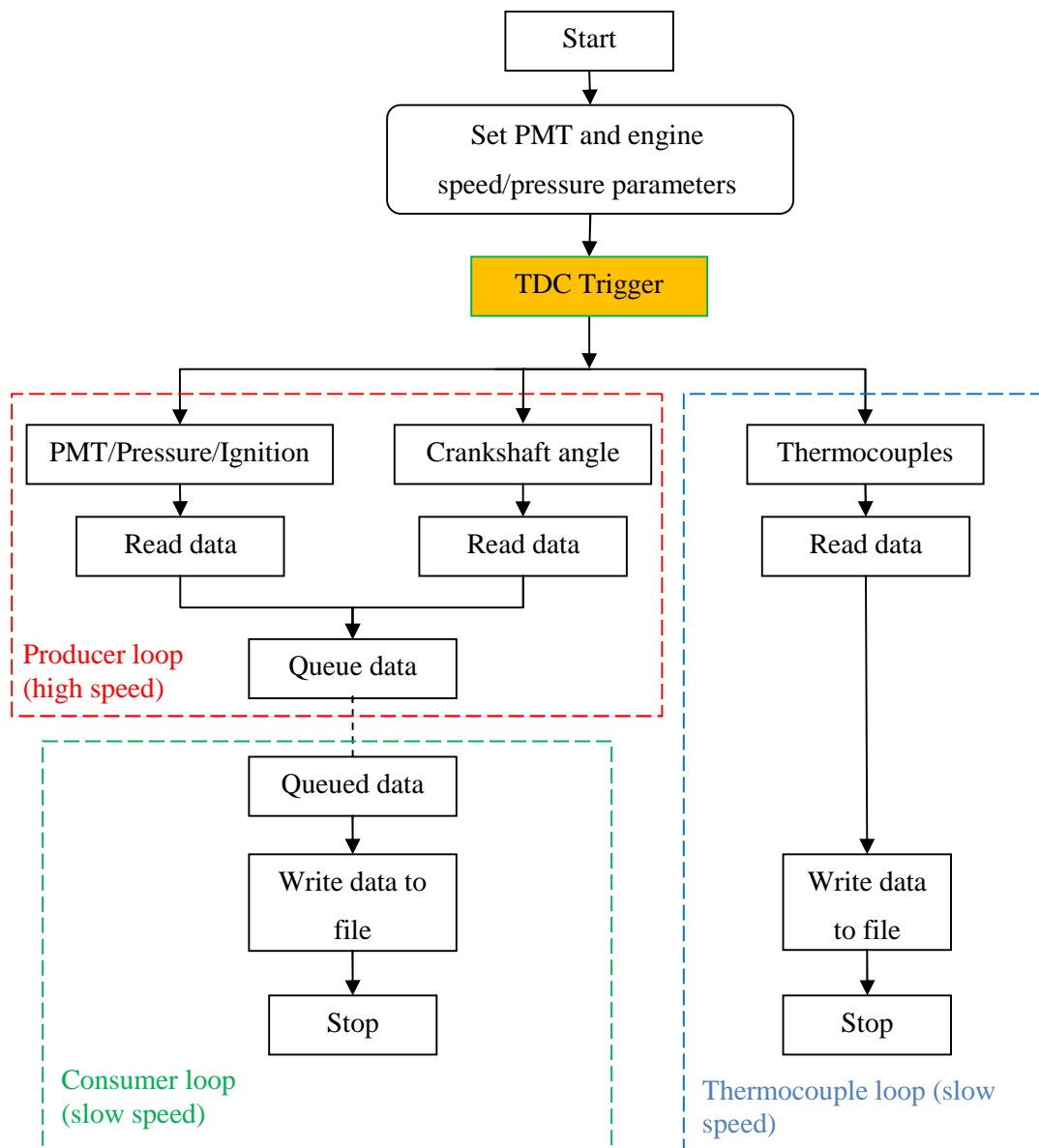


Figure 7-7: Dataflow diagram of the piston ring pack OFT measurement program

The program dedicated to the data acquisition of the fluorescence and laser intensity signals, along with data on the crankshaft angular position and the various transducers (pressure sensors and thermocouples), was developed with a view to performing the data acquisition at the fastest possible rate. This would allow high levels of refinement and minimal data loss at the higher engine speeds. The program was developed in conjunction with the hardware development of the LIF system on the motored engine with subtle changes made to the program when the fired Hydra engine was used. The data flow diagram in Figure 7-7 illustrates how the program works.

Simultaneous data capture between both PMTs, temperature/pressure sensors and the crankshaft encoder was the plan during program development. For simultaneous data acquisition, each acquisition channel needs to be referenced to the same time clock. The operating system used on the Dell computer was Windows XP 32-bit and the maximum internal clock speed capped by the operating system is at best 1ms (1 kHz). Since the Hydra engine can reach speeds up to 5000 rpm and the encoder pulses at 720 per revolution (see Section 7.2), the pulses occur at 60 kHz. For sampling this data and to prevent data loss, a sampling frequency of at least 10 times the rate of the data is necessary. So, that is a time clock of 600 kHz at an engine speed of 5000 rpm and this exceeds the time clock of the operating system. Fortunately, the 6366 card has its own 2 MHz clock and this was used as the external reference for simultaneous sampling.

For simultaneous sampling, apart from the clock source, a trigger event is required to allow data acquisitions from separate channels to occur at the same time. The Z line, the reference output, on the shaft encoder is used for TDC identification and was used to synchronise the crankshaft angular position (digital) to the PMT outputs (analogue). The pressure sensor output, used for the motored engine work, and the ignition pulse, used for the Hydra engine work, were also included in the simultaneous DAQ and recorded in the same data file. The thermocouples used for the liner temperature and the coolant pickup in the motored engine were not included in the simultaneous data capture since the speed of the temperature change is much slower than the speed of the acquisition and they were recorded in a separate data file. The DAQ for the thermocouples were, however, initialised on the same TDC triggering event.

Sampling speed performance and data integrity was the focus for the data capture. Reading data and writing the same data to a file causes sampling performance issues as the temporary memory (RAM) capacity of the computer is limited. It takes longer to write a data point than to read a data point. As a result, a queuing system of events was used whereby the data

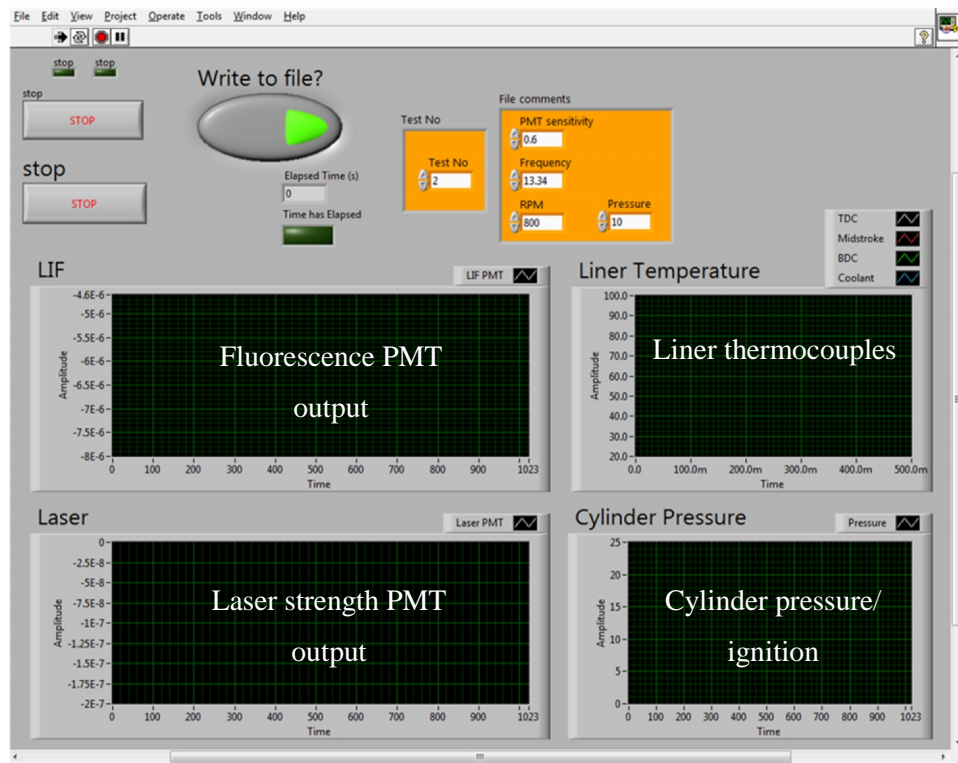


**Figure 7-8: Front panel of the piston ring pack OFT measurement program**

process follows a first in first out approach. Two data processing loops are used to allow this; a producer loop and a consumer loop. In the producer loop, the data is read at its required sampling rate and fed straight into a queue. The consumer loop runs at its own speed and handles the data queued up by processing it and recording the data to a file for output. The use of the two loops prevents data loss, provided the consumer loop is allowed to complete the queue before the loop is terminated and the program is stopped (NI 2010). The data capture and data recording for the thermocouples was performed in an additional separate loop since the sampling rate was set to less than 1 kHz. No processing of the data in terms of applying any calibration coefficients was performed during data acquisition as this was found to reduce the sampling performance of the program and instead a separate post processing program was used. Because the program was dedicated to just capture data, the front panel of the program was limited with only a few text inputs, for the input of the test number and engine speed and cylinder peak pressure (motored engine only). There were graphical displays, for the display of the PMTs and thermocouple outputs, and the ignition (Hydra engine only), but it was physically impossible to actually view the data as the

program ran rapidly due to the high speed of the data capture. The front panel of the program is shown as Figure 7-8.

### 7.5.3 Post Processing Program

As mentioned earlier, the program used to capture data whilst the engine was operating only performs acquisition to improve the performance of the program. The data captured is stored in a file format specific to LabVIEW known as technical data management streaming, more specifically a TDMS file output. As the name suggests the file format offers high speed data streaming and has been optimised for saving data to a recordable disk (NI 2011). Since the program is dedicated to high speed data acquisition, an additional program is used to process the data and make use of the calibration trends obtained from the calibration program. The data processed is outputted into a new file, thereby preserving the original, and provides information based on the oil film thickness, the laser strength and the cylinder pressure or ignition sequence against the crankshaft angle of the engine.

The data obtained from the engine can sometimes be sampled at too high a rate for the engine speed. It was found that there was more than one analogue data point per  $0.125^\circ$  crank angle since the speed of the analogue data capture is faster than the resolution of the crankshaft encoder. So for post processing it was decided to just take the first data point per  $0.125^\circ$  crankshaft resolution, thereby allowing a maximum of 2880 data points for a 2 stroke engine (motored engine) and 5760 data points for a 4 stroke engine (Hydra engine). This refinement was more than enough considering the size of the output data file, which could exceed 100 Mb of raw data when the engine was operating at high speeds in excess of 4000 rpm. The post processing data file was also averaged over 10 strokes for the motored engine and 50 strokes for the data collected from the Hydra engine. It was found that during motoring, the film thickness under the rings, the MOFT, did not vary engine cycle to cycle once the engine was stable at its test operating condition. The fired Hydra engine did produce slight variance in the piston ring MOFT across engine cycles which was found to be caused by the fluctuating nature of the combustion event per engine cycle and hence a greater level of averaging was required.

The post program also implemented the calibration trends from the calibration program for the test oil sample used in the engine (see Chapter 3) and the pressure calibration trend obtained earlier (see Chapter 4). The calibration trend for the fluorescence signal was in the form of:

$$\text{Fluorescence PMT output} = m(\text{oil film thickness}) + c_{bl} \quad \text{Equation 7-1}$$

Where  $m$  is the gradient obtained from the calibration trend and  $c_{bl}$  is the baseline of the laser; that being the signal output of the fluorescence PMT at zero fluorescence emission. The baseline of the laser was found to fluctuate slightly and believed to be caused by changes in room temperature on a day to day basis, which would affect the output of the PMT. This would cause the results of the fluorescence to fluctuate also for the same engine operating condition and same test lubricant. As a result it was decided to take the baseline based on the data obtained during engine operation where near zero fluorescence was most likely. This was the position in the engine cycle where the piston, on its downstroke, had passed the window completely with the laser emission diverging into the cylinder bore and illuminating it (i.e. no reflected laser light was returned to the detector). This occurred between 150 to 250° crank angle (when the piston was near or at 180° BDC) and the data obtained within this was averaged over the same number of strokes. It was found that this average was acceptable to be used as the baseline for the calibration. A lubricant sample was extracted from the sump during each test condition with the engine temperature noted for sample calibration purposes. This sample was then used to calibrate the fluorescence signal using the calibration program. Calibration included examination against both temperature and the opacity of the lubricant, since these factors were found earlier to influence the fluorescence signal. The influence of surface reflectivity was eliminated earlier in Chapter 3 as the PMT gain was set to the highest maximum sensitivity for fluorescence analysis, but such that it was not affected by surface reflectivity. Once calibration was completed, a calibration equation in a similar form to Equation 7.1 was obtained. This was then used in the post processing program to process the raw data obtained from the piston ring pack OFT measurement program.

Since the program is designed for data manipulation, it was decided not to include a data flow diagram in this chapter due to the size of the program, but the block diagram of the program itself does include information the data flow.

#### 7.5.4 Additional LabVIEW Programs

Since the data capture from the engine LIF program occurred at a rapid rate, it was virtually impossible to observe the data in the display charts, shown on Figure 7-8, and make sense of it. It was, however, necessary to monitor the engine operating conditions and parameters to make sure that the correct test condition was employed.

To monitor the engine operating condition 3 programs were developed. Two of these programs were used specifically for the motored engine, which did not have a separate engine control unit. They monitored the engine crankshaft speed in terms of rpm and the cylinder peak pressure. The third program was used to monitor the liner temperatures and the coolant temperature (motored engine only). Once the operating test condition was reached and the engine was under stable operation, all 3 of these additional programs were stopped to allow a greater computer resource to execute the high speed DAQ of the engine LIF program.

## 7.6 Data Averaging and Error Analysis

As mentioned earlier, data obtained from the engine was averaged over a number of engine cycles to improve the accuracy and reliability of the data. The LIF profile in Figure 7-9 shows data captured at 800 rpm, 120°C and 22 bar cylinder peak pressure from the motored engine during the compression stroke.

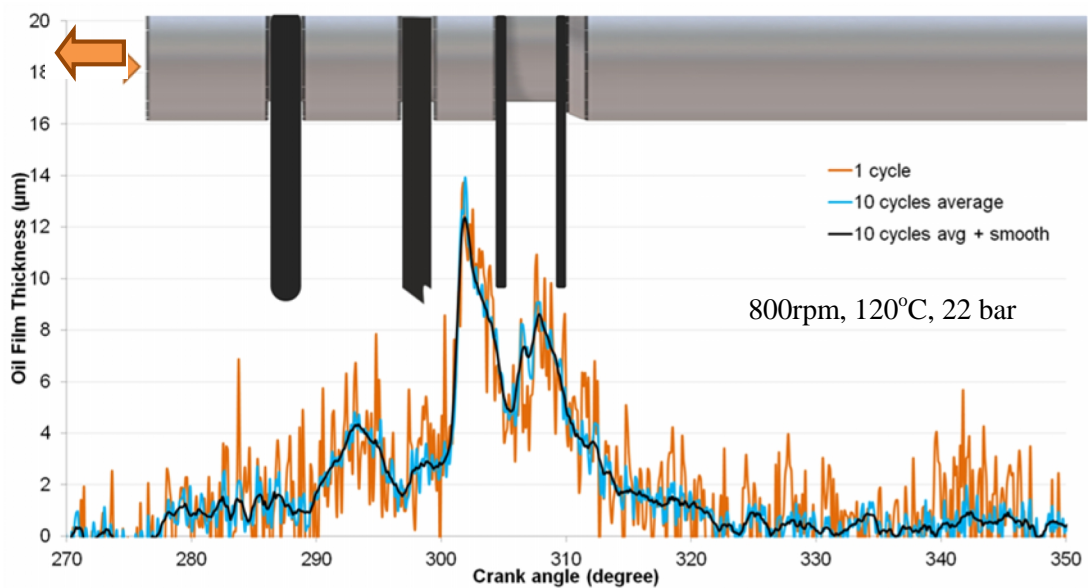


**Figure 7-9: Example of averaging process used for all LIF OFT profiles**

From Figure 7-9, it is apparent why it was necessary to average the data. A single engine cycle (orange trace in Figure 7-9) appears to be very noisy as there is a large fluctuation of data points. This 'noise' was actually found to be a characteristic of the PMT. The PMTs

have a rapid response time of less than 1 ns and fluorescence emission can be anything up to 10 ns (see Chapter 3). As a result, the 'noise' is the capture of photons from the individual fluorescent dye molecules, the fluorophores, fluorescing rapidly. An average of 10 engine cycles (blue trace in Figure 7-9) helps eliminate the majority of the PMT response issues but a further running average of 3 was applied for clarity (black trace in Figure 7-9). One point to note is that through this averaging process, no data is added or removed from the trace during the averaging process, thus showing that the technique is valid. The fluctuating combustion event of the fired Hydra engine meant that further analysis into the averaging technique was required to check the techniques validity for fired engine work. The Hydra engine was operated at 2000 rpm at both motored and fired conditions and data acquired from the engine under these conditions was averaged over 5, 50 and 100 cycles for the compression and power strokes. The LIF profiles during these conditions are shown as Figure 7-10, Figure 7-11, Figure 7-12 and Figure 7-13. This data underwent an extensive statistical analysis to investigate the standard deviation (SD) value of the mean.

From Figure 7-10, Figure 7-11, Figure 7-12 and Figure 7-13 it can be seen that regardless of engine operating condition, the films measured on the piston skirt have the largest variance when considering the standard deviation from the mean. Per engine cycle the skirt film thickness was observed to vary much more than the film thickness between the piston ring and the cylinder wall. This is quite evident when comparing the films around TDC as the piston slows down and prepares to change direction, and where piston secondary motion is one likely culprit for the large variation. This also confirms the fact that the film thickness measurements as such are not reliable to measure the films at the skirt since these are an ensemble of lubricant on the piston, lubricant on the cylinder wall and/or lubricant mist. As a result, it can never be known whether the film thickness between the piston skirt and the cylinder wall is correct in the film thickness profile. However, the film thickness under the rings, the MOFT, was the focus for this research.

A large fluctuation in the standard deviation is present when data is averaged over 5 engine cycles as opposed to either 50 or 100 cycles, deeming the technique unsuitable to average over a shorter number of cycles. There is very little difference between averaging over 50 and 100 engine cycles if any and as a result it was found that averaging over 50 engine cycles was more than enough and saved on post processing time.

As expected, the power stroke, during firing operation (see Figure 7-13), responds to the fluctuating nature of the combustion event and the standard deviation is quite large for the lower averaging range.

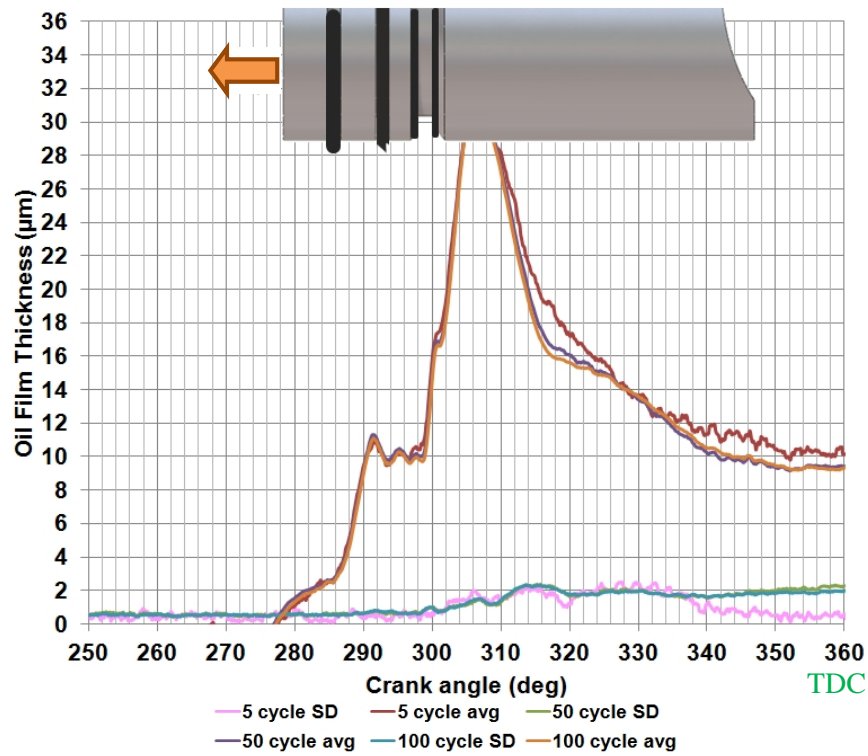


Figure 7-10: Standard deviation analysis for different averaging ranges during the compression stroke of the Hydra engine operating at a motoring speed of 2000 rpm

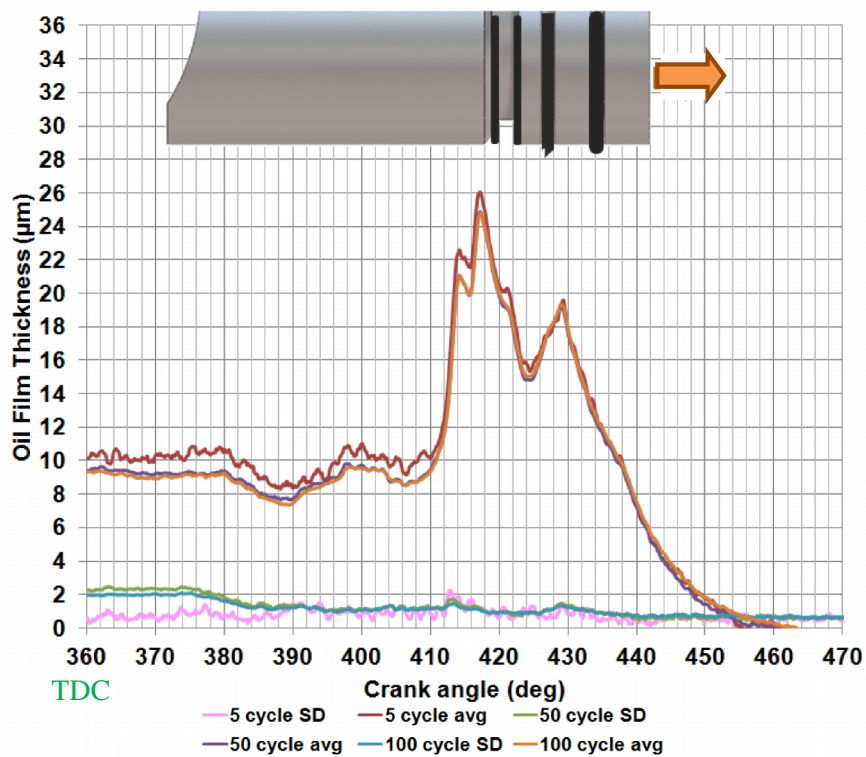


Figure 7-11: Standard deviation analysis for different averaging ranges during the power stroke of the Hydra engine operating at a motoring speed of 2000 rpm

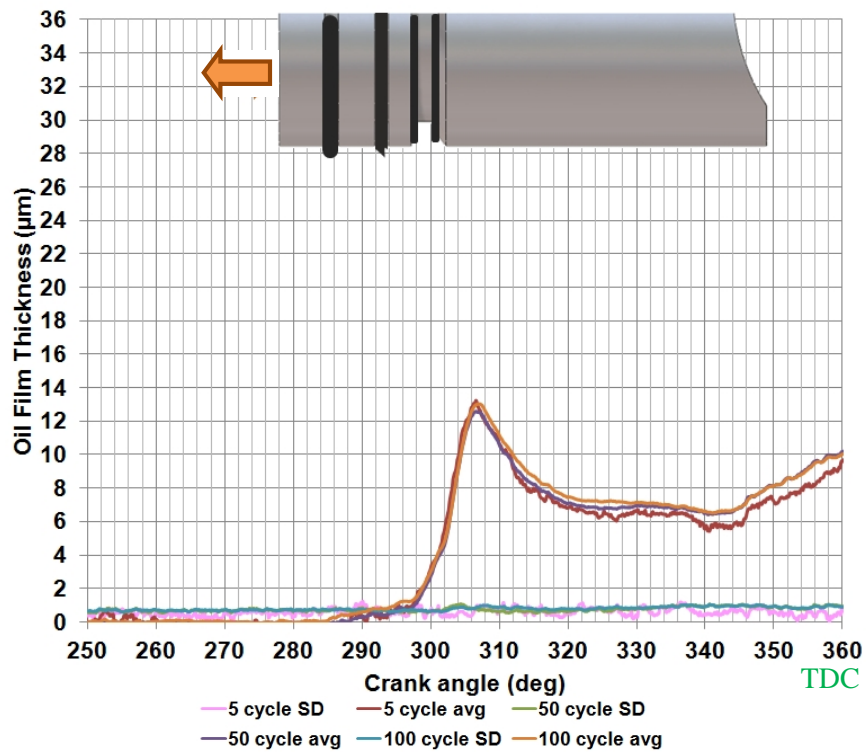


Figure 7-12: Standard deviation analysis for different averaging ranges during the compression stroke of the Hydra engine operating at a firing speed of 2000 rpm

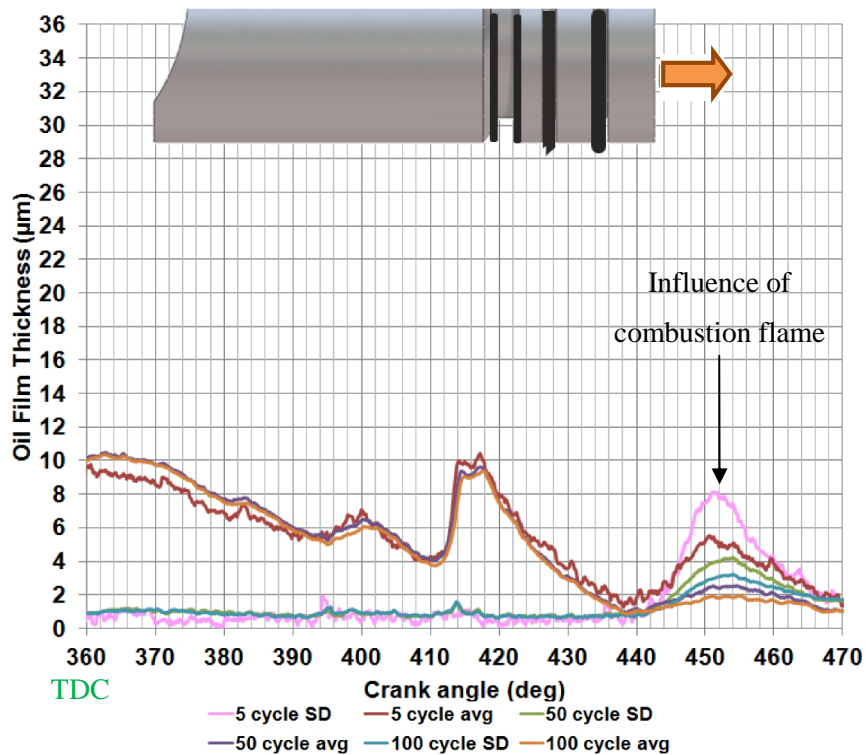


Figure 7-13: Standard deviation analysis for different averaging ranges during the power stroke of the Hydra engine operating at a firing speed of 2000 rpm

Since the films under the piston ring pack are most important for this research, the standard deviation around the ring pack was taken in the analysis of the standard error. The standard error is defined as:

$$\text{Standard error} = \frac{\text{Standard deviation}}{\sqrt{\text{number of observations}}} \quad \text{Equation 7-2}$$

Under the piston ring pack the standard deviation was found to remain a constant and approximately equal to 0.7  $\mu\text{m}$ . As a result the standard error was found to be 0.22  $\mu\text{m}$  for the motored engine with a cycle average of 10 and 0.10  $\mu\text{m}$  for the Hydra engine with a cycle average of 50. These values were taken forward in the results in Chapter 4 to 6.

## 7.7 Summary

To measure the lubricant film thickness profiles at a high degree of refinement at high engine speeds, a triggered simultaneous data acquisition sampling system was developed. Multiple programs were developed in the LabVIEW architecture to integrate with the National Instruments hardware. On both test engines, data was sampled from both PMTs for the laser strength and the fluorescence intensity, the liner thermocouples. The motored engine had an additional coolant thermocouple in the barrel and the cylinder pressure was also measured. The ignition sequence on both the motored and fired Hydra engines was recorded.

Standard deviation analysis was also performed and it was found that there was a variation in the films observed on the piston skirt, especially around top dead centre, possibly caused by an influence of the piston secondary motion and blow-by effects. It is however, difficult to confirm this since the film measured at the piston skirt and even between the rings is not certain to be exactly between the piston and the cylinder wall. This also varies whether the engine is operating motored or fired. Standard error results were also performed for the results obtained from both test engines. Based on the number of engine cycle averages, it was found that a 0.22  $\mu\text{m}$  and 0.1  $\mu\text{m}$  error for the motored and Hydra fired engine respectively was achieved.

# **Chapter 8 Conclusions and Recommendations for Future Research**

## **8.1 Introduction**

The purpose of this chapter is to bring together all the points from the discussions in previous chapters and to draw final conclusions. The main aim of this research was to investigate the influence of lubricant degradation on the oil film experienced by the piston ring pack of an engine and the effect on piston ring tribology. This was carried out through development of an in-situ piston ring to cylinder wall lubricant film thickness technique on a motored research engine which was furthered on to a fired research engine.

A laser induced fluorescence system including a bespoke optics setup was used to monitor the fluorescence intensity of engine lubricant doped with a special fluorescent dye. The intensity of the fluorescence was proportional to the film thickness and therefore, it was possible to investigate the oil behaviour around the piston ring pack during a wide range of engine operating conditions. This system was used to investigate a range of degraded gasoline lubricants supplied by Mercedes Benz Leasing in Leeds and a single diesel lubricant sample provided by Southwest Research Institute, Texas, USA. The lubricants were tested on a horizontally opposed motored engine and a progression to a Ricardo Hydra fired gasoline engine confirmed initial results.

The LIF system was taken a step further to investigate the oil flow through the piston ring pack by measuring the residence time of the lubricant. A twin switchable lubricant sump system was setup and allowed the crankshaft bearings and piston assembly to switch lubricant supply without any loss of lubricant or induced aeration. By using lubricant sumps with and without dye, it was possible to observe the fluorescence emission in the ring pack and hence the lubricant residence time when switching sump supply. Additionally, the influence of lubricant sampling from the top ring zone of a piston was also investigated with the laser induced fluorescence system.

## 8.2 Major Conclusions

The most important conclusions drawn from the research presented in the previous chapters can be summarised into the following points, ranked in order of most important first:

- A laser induced fluorescence system has been developed and implemented on a firing engine that can clearly distinguish between lubricants of different formulations (principally viscosity) and degradation state. A careful calibration of each lubricant sample is required to achieve this.
- The piston ring to cylinder wall minimum oil film thickness was found to be inversely proportional to lubricant viscosity. Degraded lubricants, typically having an increase in lubricant viscosity when compared to a fresh lubricant, were generally found to present the thickest films.
- Engine speed, load and lubricant viscosity were found to have a direct effect on the piston ring pack lubricant residence time and the replenishment of lubricant within the piston ring pack.
- Engine speed and load were also found to have a direct effect on the piston ring to cylinder wall minimum oil film thickness. Increasing engine speed was found to increase the oil availability in the ring pack and increase the piston ring to cylinder wall minimum oil film thickness. An increase in the engine load was found to decrease the piston ring to cylinder wall minimum oil film thickness.
- Sampling lubricant from the top ring zone of a piston of an operating engine for post chemical analysis was found not to be detrimental to the oil availability in the piston ring pack
- The piston ring to cylinder wall minimum oil film thickness was found to change per engine stroke. As a result of this, the lubricant shear rate was also found to be different per engine stroke; with differences across induction, compression, power and exhaust stroke.

### 8.3 Detailed Conclusions

For the ease of presentation and discussion, the conclusions have been divided into three main areas based on the original objectives of the thesis. These follow the progression of the research work and include the conclusions drawn from the:

- Motored engine experimental work
- Ricardo Hydra gasoline engine experimental work
- Piston ring pack lubricant residence time and top ring zone sampling investigation

The objectives from Section 1.5 are repeated below in italics.

#### 8.3.1 Motored Engine Experimental Work

*Develop a method of oil film thickness measurement for the piston ring – cylinder bore interface through the cylinder wall of a horizontally opposed motored engine.*

*Investigate the influence of lubricant degradation on lubricant film thickness within the piston ring – cylinder bore vicinity using lubricant samples of known degradation in the motored engine.*

An optical system was developed on the motored engine to measure the piston ring to cylinder wall lubricant film thickness using the laser induced fluorescence technique. The experiments were carried out using a range of degraded gasoline multigrade lubricants and a single monograde diesel lubricant over a wide range of engine temperature, cylinder peak pressures and engine speed conditions. Each test lubricant was analysed in terms of chemical degradation and lubricant viscosity. The outcomes of the research on this motored engine are as follows:

- The use of a both gasoline and diesel type lubricants showed that the laser induced fluorescence system is universally applicable to a wide range of lubricant viscosities and lubricant quality based on the lubricant degradation.
- A decrease in lubricant viscosity, due to an increase in cylinder temperatures, resulted in a reduction in piston ring to cylinder wall minimum oil film thickness, which was true regardless of lubricant type or quality.
- The high temperature high shear viscosity results measured for each lubricant tested correlated well with the piston ring to cylinder wall minimum oil film thickness.

- An increase in the cylinder pressure was found to reduce the overall piston ring to cylinder wall minimum oil film thickness.

### 8.3.2 Ricardo Hydra Gasoline Engine Experimental Work

*Adapt the same lubricant film thickness measurement system, as used on the horizontally opposed motored engine, to a Ricardo Hydra fired gasoline engine to investigate oil film profiles at higher engine speeds and loads.*

The laser induced fluorescence system developed and optimised on the motored engine, was moved and implemented on the Ricardo Hydra gasoline engine for fired engine investigation. The same gasoline lubricant samples as used on the motored engine were tested in this engine. A wider range of engine speeds and engine loads were now available and used to confirm the initial findings on the motored engine. The outcomes of the research on the Ricardo Hydra engine were as follows:

- The piston lubricant profiles and the piston ring to cylinder wall minimum oil film thickness were found to be engine stroke dependent. The piston motion direction and the piston ring profiles were found to be causing the difference in the laser induced fluorescence measurements per engine stroke.
- The introduction of combustion, and hence firing, increased the cylinder pressure and temperature which reduced the minimum oil film thickness of the piston ring to cylinder wall.
- A change in the film thickness per engine stroke; with differences across induction, compression, power and exhaust stroke, led to a cyclic variation in the lubricant shear rate.
- As the engine speed increased, the piston ring to cylinder wall minimum oil film thickness increased due to an increase in lubricant supply to the piston ring pack caused by an increase in ring pumping and lubricant availability on the cylinder wall. This was true regardless of the lubricant viscosity or quality.
- Degraded lubricants were generally found to present thicker lubricant films between the piston ring and cylinder wall. The high temperature high shear viscosity of the test lubricants correlated very well with the measured lubricant film thicknesses.

### **8.3.3 Piston Ring Pack Lubricant Residence Time and Top Ring Zone Sampling Investigation**

*Further this method to investigate residence time with the use of a switchable twin lubricant sump on the Ricardo Hydra engine.*

*Investigate the implications of sampling lubricant from the top ring groove of a piston, during engine operation, on the piston ring pack lubricant film thicknesses.*

The laser induced fluorescence system was adapted to investigate the flow of the lubricant through the piston ring pack. The lubricant residence time is important in determining the replenishment of the lubricant in the ring pack, since it is here where the lubricant degrades at a faster rate than in the sump (Lee 2006). A twin switchable sump was used with one of the test lubricants doped with fluorescent dye to examine the flow of the lubricant through the ring pack and provide quantitative information on the lubricant residence time. Engine tests were conducted over a wide range of operating speeds and loads, and with two test lubricants of different viscosities. A further investigation in this research also examined the influence of top ring zone lubricant sampling and the influence on oil availability, namely the minimum oil film thickness, within the piston ring pack. The outcomes of this part of the research are as follows:

- An increase in engine speed reduces the piston ring pack residence time. As mentioned earlier, there is an increase in the oil availability on the cylinder with increasing speed. Additionally, an increase in oil flow through the ring pack is possible at the higher speeds, but because this was not measured, this can only be hypothesised.
- Replenishment of the lubricant was observed to be inversely proportional to the lubricant viscosity. An increase in viscosity increased the piston ring pack residence time regardless of engine speed.
- Increasing the engine load was found to reduce the piston ring pack residence times.
- Top ring zone sampling was found not to cause oil starvation issues within the piston ring pack, confirming the technique is suitable for lubricant sampling from the top piston groove without causing a concern for oil availability.

## 8.4 Novel Aspects of the Research

For the very first time in engine tribology research:

- An experimental optical system to examine the piston ring to cylinder wall film thickness of degraded engine lubricants has been investigated with excellent spatial resolution in a real fired gasoline engine. The system was also found to be universally applicable to a wide range of engine lubricant types, quality and grades.
- Laser induced fluorescence examination of the piston ring to cylinder wall lubricant film thickness has been performed at high engine speeds, in excess of 4000 rpm in a gasoline engine.
- The piston ring pack lubricant residence time has been measured directly using laser induced fluorescence as a tracer technique. This allowed a detailed study of the effect of engine load, speed and lubricant viscosity on the ring pack residence times.
- The influence of lubricant sampling from the top piston ring groove has been examined in detail against engine speed and load. Before this study, it was not known what the consequence of sampling lubricant in this manner from an operating engine would do to the oil availability in the piston ring pack.

## 8.5 Recommendations for Further Work

The recommendations for further work are suggested for work to be completed should there be an additional sixth months to a year of time available. They are listed in order of highest priority.

- Investigate the influence of the lubricant degradation over a wider range of test lubricants. In this research, only a select few test lubricants were used and it would be beneficial to confirm the initial conclusions here over a greater range of test lubricants. A controlled set of engine tests to degrade lubricant from fresh over a specific period of service could be used to investigate the change in piston ring to cylinder wall minimum oil film thickness with time.
- The modern vehicle engine is now equipped with Stop-Start technology and cylinder deactivation technology as a means to improve the fuel economy and lower the

vehicle emissions. The difference between motoring engine operation and firing has been shown to influence the lubricant film thickness in this research. It would be beneficial to use the current system and investigate these current technology trends by examining the piston ring minimum oil film thickness and the exhaust unburnt hydrocarbon emissions at the same time. The CP CADET engine control system can be programmed to include the investigation of this technology.

- The current system is a single point laser induced fluorescence system. It would be beneficial to expand this to a twin point laser induced fluorescence system with an additional probe on the anti-thrust side. This would allow a greater detail of information of the oil availability around the piston. It could also be used to investigate the lubricant ring pack residence and determine if there is any difference in lubricant residence between the thrust and anti-thrust sides.
- Combine the laser induced fluorescence method for lubricant film thickness measurements with the indicated mean effective pressure piston assembly friction measurement as used by Mufti, see (Mufti 2004). This would indicate the influence of lubricant degradation on piston assembly friction and also provide greater insight into lubrication regimes as speed, load, etc. were varied.
- Combine the laser induced fluorescence method for lubricant film thickness measurements with investigation into the changes in lubricant film profiles during piston ring and cylinder liner running-in and wear studies.
- As vehicle engines are downsized, a need for a larger turbocharger unit is required to improve the power output and thermal efficiency of the unit. As a result, combustion temperatures are increasing which could have a direct effect on premature lubricant degradation, but this is yet unknown. As a result, piston under crown oil cooling jets are required and used in some modern engines. It is not known whether these would influence the oil availability in the piston ring pack. By using the laser induced fluorescence system and making an adaption to the Ricardo Hydra engine to allow for under crown oil cooling, it would be possible to investigate this over a wide range of engine operating conditions.

## 8.6 Recommendations for Future Research

The recommendations for future research are suggested for work to be completed if more than a year of time was available. They are listed in order of highest priority.

- It would be beneficial to investigate the lubricant film thickness nearer to the top ring reversal point. This would provide further information on the state of the lubricant film thickness as the piston experiences intermittent zero velocity on piston reversal. This would require a special Hydra barrel and possibly a new liner to be manufactured. Going further upwards towards top dead centre would possibly require additional neutral density filters to be put in place to avoid the possibility of damaging the sensitive photomultiplier tubes when combustion takes place.
- It would be interesting to examine the lubricant films towards the bottom dead centre to gain an overall understanding of changes of lubricant film thickness profiles during an engine cycle.
- As mentioned earlier about the use of downsized engines, by adapting the Ricardo Hydra engine for boosted application, it would be beneficial to examine the piston ring to cylinder wall lubricant film thickness at increased inlet air pressures thereby increasing cylinder pressures.

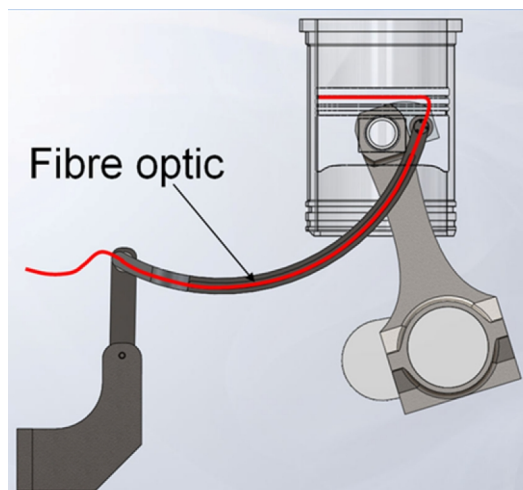


**Figure 8-1: Curved linkage design idea for in-situ LIF probe**

- Examining lubricant behaviour behind the piston ring in the ring groove would help provide additional information on the flow of the lubricant past the ring and the

direction of the lubricant flow. This requires a fibre optic to be positioned inside the engine behind the piston ring groove. This was investigated in this research to the point where a new curved linkage was designed and manufactured to retain a fibre optic cable, Figure 8-1. The linkage was designed so that no excessive bending of the fibre optic caused premature fatigue damage or cause issues with internal reflectance of the laser light in the fibre. This linkage was tested up to engine speeds of 1800 rpm for 10 hours in the Hydra engine. It failed due to a natural resonance occurring at high engine speeds, in excess of 2000 rpm.

- In-situ lubricant degradation infrared analysis as previously attempted in the past by only a few researchers (Natrass, Thompson et al. 1994; Thompson and Natrass 1996; Watson and Wong 2010). It would be beneficial to examine the chemical composition of the lubricant between the piston ring and cylinder wall during engine operation, without the need to extract lubricant samples. By examining just the oxidation region of a lubricant spectrum, it is possible to improve the spatial resolution and improve spectral analysis time. Coupling this with the laser induced fluorescence system would bring analysis of lubricant degradation and oil film thickness measurements together.

## References

ARAUJO, J. A. and BANFIELD, R. R. (2012). "Dlc as a Low Friction Coating for Engine Components." SAE Paper 2012-36-0255.

ARCOUMANIS, C., DUSZYNSKI, M., LINDENKAMP, H. and PRESTON, H. (1998). "Measurement of Lubricating Film Thickness in the Cylinder of a Firing Engine Using LIF." SAE Paper 982435.

ARCOUMANIS, C., DUSZYNSKI, M., PYKE, E. and PRESTON, H. (1998). "Cold-Start Measurement of the Lubricating Film Thickness in the Cylinder of a Firing Diesel Engine." SAE Paper 982436.

ASTM (D341-03). ASTM D341-03 - Standard Practice for Viscosity-Temperature Charts for Liquid Petroleum Products.

ASTM (D2896-07a). ASTM D2896 - 07a Standard Test Method for Base Number of Petroleum Products by Potentiometric Perchloric Acid Titration.

ASTM (D4485). ASTM D4485 - 11c Standard Specification for Performance of Active Api Service Category Engine Oils.

ASTM (D4683-10). ASTM D4683 - 10 Standard Test Method for Measuring Viscosity of New and Used Engine Oils at High Shear Rate and High Temperature by Tapered Bearing Simulator Viscometer at 150 °C.

ASTM (D-664-09). ASTM D664 - 09 Standard Test Method for Acid Number of Petroleum Products by Potentiometric Titration.

ASTM (E 2412-04). Practice E 2412-04 - Practice for Condition Monitoring of Used Lubricants by Trend Analysis Using Fourier Transform Infrared FT-IR Spectrometry, ASTM International.

AVAN, E. Y., MILLS, R. and DWYER-JOYCE, R. (2010). "Ultrasonic Imaging of the Piston Ring Oil Film During Operation in a Motored Engine - Towards Oil Film Thickness Measurement." SAE Paper 2010-01-2179.

AVAN, E. Y., MILLS, R. and DWYER-JOYCE, R. (2011). "Frictional Characteristics of Ultrasonically Measured Lubricant Films in a Simulated Piston Ring Liner Contact." SAE Paper 2011-01-1400.

AVAN, E. Y., SPENCER, A., DWYER-JOYCE, R. S., ALMQVIST, A. and LARSSON, R. (2013). "Experimental and Numerical Investigations of Oil Film Formation and Friction in a Piston Ring-Liner Contact." Proceedings of the Institution of Mechanical Engineers, Part J: Journal of Engineering Tribology 227(2): 126-140.

BABA, Y., SUZUKI, H., SAKAI, Y., WEI, D. L. T., ISHIMA, T. and OBOKATA, T. (2007). PIV/LIF Measurements of Oil Film Behavior on the Piston in I. C. Engine. 8th International Conference on Engines for Automobile, Capri, Naples, Italy, SAE Paper 2007-24-0001.

BAILEY, B. K. and ARIGA, S. (1990). "On-Line Diesel Engine Oil Consumption Measurement." SAE Paper 902113.

BASAKI, M., SAITO, K., NAKASHIMA, T. and SUZUKI, T. (2000). Analysis of Oil Consumption at High Engine Speed by Visualization of the Piston Ring Behaviors. SAE International Fall Fuels and Lubricants Meeting and Exhibition, Warrendale, Pennsylvania, USA, SAE Paper 2000-01-2877.

BELL, J. C. (1993). Engine Lubricants. Engine Tribology. C. M. Taylor, Elsevier Science Publishers B. V. ISBN 0444897550: 287-301.

BOONS, M., VAN DEN BULK, R. and KING, T. (2008). "The Impact of E85 Use on Lubricant Performance." SAE Paper 2008-01-1763.

BP (2012) "BP Statistical Review of World Energy." Available Online. Retrieved 20 October 2012. Available from <http://www.bp.com/sectionbodycopy.do?categoryId=7500&contentId=7068481>.

BROWN, S. R. and HAMILTON, G. M. (1977). "The Partially Lubricated Piston Ring." Journal Mechanical Engineering Science 19(2): 81-89.

BROWN, S. R. and HAMILTON, G. M. (1978). "Negative Pressures under a Lubricated Piston Ring." *Journal Mechanical Engineering Science* 20(1): 49-57.

BURNETT, P. J., BULL, B. and WETTON, R. J. (1995). "Characterisation of the Ring Pack Lubrication and Its Environment." *Proceedings of the Institution of Mechanical Engineers, Part J: Journal of Engineering Tribology* 209(2): 109-118.

CANTER, N. (2010). Special Report: Proper Additive Balance Needed to Meet GF-5. *Tribology & Lubrication Technology, STLE*. 66: 10-18.

CASEY, S. M. (1998). Analysis of Lubricant Film Thickness and Distribution Along the Piston/Ring/Liner Interface in a Reciprocating Engine. Master Degree. Department of Mechanical Engineering, Massachusetts Institute of Technology.

COATES, J. P. and SETTI, L. (1983). "Condition Monitoring of Crankcase Oils Using Computer Aided Infrared Spectroscopy." SAE Paper 831681.

COATES, J. P. and SETTI, L. C. (1986). Infrared Spectrometry as a Tool for Monitoring Oil Degradation. Aspects of Lubricant Oxidation, ASTM STP 916. W. H. Stadtmiller and A. N. Smith. Philadelphia, American Society for Testing and Materials: 57-78.

COURTNEY-PRATT, J. S. and TUDOR, G. K. (1946). "An Analysis of the Lubrication between the Piston Rings and Cylinder Wall of a Running Engine." *Proceedings of the Institution of Mechanical Engineers*, 155: 293.

DAHMANI, R. and GUPTA, N. (2002). Spectroscopic Analysis of Automotive Engine Oil. Instrumentation for Air Pollution and Global Atmospheric Monitoring. J. O. Jensen and R. L. Spellicy. Bellingham, Spie-Int Soc Optical Engineering. 4574: 179-183.

DEARLOVE, J. and CHENG, W. K. (1995). "Simultaneous Piston Ring Friction and Oil Film Thickness Measurements in a Reciprocating Test Rig." SAE Paper 952470.

DECC (2011) "UK Renewable Energy Roadmap." Department of Energy and Climate Change. , Page 97.

DEPARTMENT FOR ENVIRONMENT, F. R. A. (1999). Council Directive 1999/32/Ec - Relating to a Reduction in the Sulphur Content of Certain Liquid Fuels and Amending Directive 93/12/EEC. 1999/32/EC.

DFT (2011). ENV0101 Petroleum Consumption by Transport Mode and Fuel Type, Department for Transport. ENV0101.

DHAR, A., AGARWAL, A. K. and SAXENA, V. (2009). "Measurement of Dynamic Lubricating Oil Film Thickness between Piston Ring and Liner in a Motored Engine." *Sensors and Actuators A: Physical* 149(1): 7-15.

DONG, J., VAN DE VOORT, F. R., AKOCHI-KOBLE, E. and PINCHUK, D. (2000). "Rapid Determination of the Carboxylic Acid Contribution to the Total Acid Number of Lubricants by Fourier Transform Infrared Spectroscopy((C)) " *Lubrication Engineering* 56(6): 12-20.

DONG, J., VAN DE VOORT, F. R., YAYLAYAN, V., ISMAIL, A. A., PINCHUK, D. and TAGHIZADEH, A. (2001). "Determination of Total Base Number (TBN) in Lubricating Oils by Mid-FTIR Spectroscopy (C)." *Lubrication Engineering* 57(11): 24-30.

DOW, T. A., SCHIELE, C. A. and STOCKWELL, R. D. (1983). "Technique for Experimental Evaluation of Piston Ring—Cylinder Film Thickness." *Journal of Lubrication Technology* 105: 353.

DOWSON, D., ECONOMOU, P. N., RUDDY, B. L., STRACHAN, P. J. and BAKER, A. J. S. (1979). Piston Ring Lubrication. Part II. Theoretical Analysis of a Single Ring and a Complete Ring Pack. *Energy Conservation through Fluid Film Lubrication Technology: Frontiers in Research and Design*. S. M. Rohde, D. F. Wilcock and H. S. Cheng, The American Society of Mechanical Engineers: 23-52.

DOWSON, D., RUDDY, B. L. and ECONOMOU, P. N. (1983). "The Elastohydrodynamic Lubrication of Piston Rings." *Proceedings of Royal Society London. A* 386(1791): 409-430.

DWYER-JOYCE, R. S., GREEN, D. A., HARPER, P., LEWIS, R., BALAKRISHNAN, S., KING, P. D., RAHNEJAT, H. and HOWELL-SMITH, S. (2006). The Measurement of Liner-Piston Skirt Oil Film Thickness by an Ultrasonic Means. SAE 2006 World Congress, Warrendale, Pennsylvania, USA, SAE 2006-01-0648.

EILON, S. and SAUNDERS, O. A. (1957). "A Study of Piston Ring Lubrication." *Proceedings of the Institute of Mechanical Engineers*. 171(11): 427-443.

ENDO, M., WATANABE, T., TOCHIGI, H. and YAMAMOTO, K. (2009). A New Technique for Simple and Rapid Discrimination of the Stages of Used Oil degradation. SAE

International Powertrains, Fuels and Lubricants Meeting, Warrendale, Pennsylvania, USA, SAE International. SAE Paper 2009-01-1765.

ERIKSSON, L. (1998). "Requirements for and a Systematic Method for Identifying Heat-Release Model Parameters." SAE Paper 980626.

ESSICK, J. (2012). Hands-on Introduction to Labview for Scientists and Engineers, 2nd edition. OUP USA. ISBN 0199925151.

FEDERAL-MOGUL (2008). Goetze Piston Ring Handbook. Germany, Available Online. Retrieved 15 October 2012. Available from [<http://www.federalmogul.com/korihandbook/en/index.htm>].

FOX, M. (1997). Ring Zone Lubrication: Implications for Reduced Emissions and Enhanced Engine Life. The Tribology of Internal Combustion Engines, The University of Birmingham, UK, Mechanical Engineering Publications Limited. ISBN I860580718.

FUJIWARA, M., KUMAGAI, K., SEGAWA, M., SATO, R. and TAMURA, Y. (2008). "Development of a 6-Cylinder Gasoline Engine with New Variable Cylinder Management Technology."

FURUHAMA, S. (1959). "A Dynamic Theory of Piston-Ring Lubrication. (1st Report, Calculation)." Bulletin of JSME 2(7): 423-428.

FURUHAMA, S. (1961a). "On the Flow of Gas through the Piston-Rings (1st Report, the Discharge Coefficient and Temperature of Leakage Gas)." Bulletin of JSME 4(16): 684-690.

FURUHAMA, S. (1961b). "On the Flow of Gas through the Piston-Rings. (2nd Report, the Character of Gas Leakage)." Bulletin of JSME 4(16): 691-698.

FURUHAMA, S. and HIRUMA, M. (1972). "Axial Movement of Piston Rings in the Groove." ASLE Transactions 15(4): 278-287.

FURUHAMA, S. and SASAKI, S. (1983). "New Device for the Measurement of Piston Frictional Forces in Small Engines." SAE Paper 831284.

FURUHAMA, S. and SUMI, T. (1961). "A Dynamic Theory of Piston-Ring Lubrication (3rd Report, Measurement of Oil Film Thickness)." Bulletin of JSME 4(16): 744.

- GAMBLE, R. J., PRIEST, M., CHITTENDEN, R. J. and TAYLOR, C. M. (2000). Preliminary Study of the Influence of Piston Secondary Motion on Piston Ring Tribology. Thinning Films and Tribological Interfaces. D. Dowson, Elsevier Science: 679-693.
- GAMBLE, R. J., PRIEST, M. and TAYLOR, C. M. (2003). "Detailed Analysis of Oil Transport in the Piston Assembly of a Gasoline Engine." *Tribology Letters* 14(2): 147-156.
- GASNI, D., WAN IBRAHIM, M. K. and DWYER-JOYCE, R. S. (2011). "Measurements of Lubricant Film Thickness in the Iso-Viscous Elastohydrodynamic Regime." *Tribology International* 44(7-8): 933-944.
- HAMILTON, G. M. and MOORE, S. L. (1974a). "First Paper: Measurement of the Oil-Film Thickness between the Piston Rings and Liner of a Small Diesel Engine." *Proceedings of the Institution of Mechanical Engineers* 188(1): 253-261.
- HAMILTON, G. M. and MOORE, S. L. (1974b). "Second Paper: Comparison between Measured and Calculated Thicknesses of the Oil-Film Lubricating Piston Rings." *Proceedings of the Institution of Mechanical Engineers* 188(20).
- HAMMOND, C. (2003). A Mechanistic Study of the Autoxidation of Ketones in the Liquid Phase. PhD Thesis. Department Chemistry, University of York
- HANKE, W., FAHR, M., REHL, A., VOIGT, M. and ANDO, H. (2012). "Friction Reduction in Power Cylinder Systems for Downsize Gasoline Engines with Modern Surface Technologies of Aluminum Crankcases." SAE Paper 2012-01-1332.
- HARPER, P., DWYER-JOYCE, R. S., SJODIN, U. and OLOFSSON, U. (2005). "Evaluation of an Ultrasonic Method for Measurement of Oil Film Thickness in a Hydraulic Motor Piston Ring." *Tribology and Interface Engineering Series* 48: 305-312.
- HAUGLAN, R. P. (2005). Handbook of Fluorescent Probes and Research Chemicals, Molecular Probes. Invitrogen Corp, 10<sup>th</sup> Edition. ISBN 0971063648.
- HOLMBERG, K., ANDERSSON, P. and ERDEMIR, A. (2011). "Global Energy Consumption Due to Friction in Passenger Cars." *Tribology International* 47(0): 221-234.
- HOSHI, M. (1984). "Reducing Friction Losses in Automobile Engines." *Tribology International* 17(4): 185-189.

HOULT, D. P., LUX, J. P., WONG, V. W. and BILLIAN, S. A. (1988). "Calibration of Laser Fluorescence Measurements of Lubricant Film Thickness in Engines." SAE Paper 881587.

HSU, S. M., KU, C. S. and PEI, P. T. (1986). Oxidative Degradation Mechanisms of Lubricants. Aspects of Lubricant Oxidation. ASTM STP 916. W. H. Stadmler and A. N. Smith. Philadelphia, American Society for Testing and Materials: 27-48.

INAGAKI, H., SAITO, A., MURAKAMI, M. and KONOMI, T. (1997). "Measurement of Oil Film Thickness Distribution on Piston Surface Using the Fluorescence Method (Development of Measuring System)." JSME International Journal (Series B) 40(3): 487-493.

JUNG, S. and JIN, J. (1999). "Monitoring of Rotational Movements of Two Piston Rings in a Cylinder Using Radioisotopes." Journal of the Korean Nuclear Society 31(4): 423-431.

KATO, M., FUJITA, K., SUZUKI, H., BABA, Y., ISHIMA, T. and OBOKATA, T. (2009). "Analysis of Lubricant Oil Film Behavior on the Piston Surface According with Piston Shapes by Means of LIF and PIV." SAE Paper 2009-28-0003.

KORCEK, S. and JENSEN, R. K. (1976). "Relation between Base Oils Composition and Oxidation Stability at Increased Temperatures." ASLE Trans. 19(2): 83-94.

KORCEK, S. and JOHNSON, M. D. (1993). Effect of NO<sub>x</sub> on Liquid Phase Oxidation and Inhibition at Elevated Temperatures. Engine Oils and Automotive Lubrication. W. J. Bartz. New York, Marcel Dekker, Inc.: 177-199.

KOVACH, J. T., TSAKIRIS, E. A. and WONG, L. T. (1982). "Engine Friction Reduction for Improved Fuel Economy." SAE Paper 820085.

KUMAR, S., MISHRA, N. M. and MUKHERJEE, P. S. (2005). "Additives Depletion and Engine Oil Condition – a Case Study." Industrial Lubrication and Tribology 57(2): 69-72.

LAKOWICZ, J. R. (2006). Principles of Fluorescence Spectroscopy. New York, USA, Springer, ISBN 0-387-31278-1.

LEE, P. M. (2006). Lubricant Degradation, Transport and the Link to Piston Assembly Tribology. PhD Thesis. School of Mechanical Engineering. Leeds, University of Leeds.

LEE, P. M., PRIEST, M., STARK, M. S., WILKINSON, J. J., LINDSAY-SMITH, J. R., TAYLOR, R. I. and CHUNG, S. (2006). "Extraction and Tribological Investigation of Top Ring Zone Oil from a Gasoline Engine." *Proceedings of the Institution of Mechanical Engineers, Part J: Journal of Engineering Tribology*, 220(3): 171-180.

LEE, P. M., STARK, M. S., WILKINSON, J. J., PRIEST, M., SMITH, J. R. L., TAYLOR, R. I. and CHUNG, S. (2004). *The Degradation of Lubricants in Gasoline Engines: Development of a Test Procedure to Evaluate Engine Oil Degradation and Its Consequences for Rheology*. 31st Leeds-Lyon Symposium on Tribology. Life Cycle Tribology, Leeds, Elsevier.

LEONE, T. G. and POZAR, M. (2001). "Fuel Economy Benefit of Cylinder Deactivation - Sensitivity to Vehicle Application and Operating Constraints."

LLOYD, T. (1968). "The Hydrodynamic Lubrication of Piston Rings." *Proceedings of the Institution of Mechanical Engineers (Part 3P)*: 28-34.

LLOYD, T. (1969). *The Hydrodynamic Lubrication of Piston Rings*. Tribology Convention, I Mech E HQ.

LNG (2010). *Lubes 'N' Greases Europe, Middle East and Africa*. December 2010, LNG Publishing. 22: Page 32.

LUBRIZOL. (2010). "Global Implications of ILSAC GF-5. The Lubrizol Corporation." Available Online. Retrieved 3 March 2012. Available from [http://www.gf-5.com/the\\_story/globalimpact/](http://www.gf-5.com/the_story/globalimpact/).

MA, Z. (2010). "Oil Transport Analysis of a Cylinder Deactivation Engine." SAE Paper 2010-01-1098.

MCGEEHAN, J. A. (1983). "Effect of Piston Deposits, Fuel Sulfur, and Lubricant Viscosity on Diesel Engine Oil Consumption and Cylinder Bore Polishing." SAE Paper 831721.

MILLER, G. M. (1862). "On a Packing for Pistons of Steam Engines and Pumps." *Proceedings of the Institution of Mechanical Engineers* 13: 315-327.

MILLS, R., AVAN, E. and DWYER-JOYCE, R. (2013). "Piezoelectric Sensors to Monitor Lubricant Film Thickness at Piston-Cylinder Contacts in a Fired Engine." *Proceedings of the*

Institution of Mechanical Engineers, Part J: Journal of Engineering Tribology 227(2): 100-111.

MIN, B.-S., KIM, J.-S., OH, D.-Y., CHOI, J.-K. and JIN, J.-H. (1998). "Dynamic Characteristics of Oil Consumption - Relationship Between the Instantaneous Oil Consumption and the Location of the Piston Ring Gap."

MOORE, S. L. (1979). "Measurement of the Ring to Liner Oil Film Thickness in a Caterpillar 1-G Diesel Engine." SAE Paper 790730.

MOORE, S. L. (1981). "Piston Ring Lubrication in a Two-Stroke Diesel Engine." Wear 72(3): 353-369.

MOORE, S. L. (1985). Piston Ring Oil Film Thickness - The Effect of Viscosity, SAE Paper 850439.

MOORE, S. L. and HAMILTON, G. M. (1978). "The Starved Lubrication of Piston Rings in a Diesel Engine " Journal Mechanical Engineering Science 20: 345-352.

MORITANI, H. and NOZAWA, Y. (2003). "Oil Degradation in Second-Land Region of Gasoline Engine Pistons." R&D Review of Toyota CRDL 38(3): 36-43.

MORTIER, R. M., FOX, M. F. and ORSZULIK, S. T. (2009). Chemistry and Technology of Lubricants, Springer. ISBN 978-1-4020-8661-8.

MORTIER, R. M. and ORSZULIK, S. T. (1992). Chemistry and Technology of Lubricants. New York, USA, VCH Publishers, Inc. ISBN 0216929210.

MUFTI, R. A. (2004). Total and Component Friction in a Motored and Firing Engine. PhD Thesis. School of Mechanical Engineering. Leeds, University of Leeds.

MUFTI, R. A. and PRIEST, M. (2005). "Experimental Evaluation of Piston Assembly Friction under Motored and Fired Conditions in a Gasoline Engine." Journal of Tribology 127: 826-836.

MUFTI, R. A. and PRIEST, M. (2009). "Effect of Engine Operating Conditions and Lubricant Rheology on the Distribution of Losses in an Internal Combustion Engine." Journal of Tribology 131.

MUFTI, R. A., PRIEST, M. and CHITTENDEN, R. J. (2006). "Analysis of Piston Assembly Friction Using the Indicated Mean Effective Pressure Experimental Method to Validate Mathematical Models." Proceedings of the Institution of Mechanical Engineers, Part D: Journal of Automobile Engineering 222.

MUNRO, R. and PARKER, A. (1975). "Transverse Movement Analysis and Its Influence on Diesel Piston Design." SAE Paper 750800.

NAKASHIMA, K., ISHIHARA, S. and URANO, K. (1995). "Influence of Piston Ring Gaps on Lubricating Oil Flow into the Combustion Chamber." SAE Paper 952546.

NAKAYAMA, K., MORIO, I., KATAGIRI, T. and OKAMOTO, Y. (2003). A Study for Measurement of Oil Film Thickness on Engine Bearing by Using Laser Induced Fluorescence (Lif) Method. 2003 SAE World Congress, Detroit, Michigan, SAE 2003-01-0243.

NAKAYAMA, K., SEKI, T., TAKIGUCHI, M., SOMEYA, T. and FURUHAMA, S. (1998). "The Effect of Oil Ring Geometry on Oil Film Thickness in the Circumferential Direction of the Cylinder." SAE Paper 982578.

NATTRASS, S. R., THOMPSON, D. M. and MCCANN, H. (1994). "First In-Situ Measurement of Lubricant Degradation in the Ring Pack of a Running Engine." SAE Paper 942026.

NEALE, M. J. (1994). Drives and Seals: A Tribology Handbook, Butterworth-Heinemann Ltd. ISBN 0750609818.

NI (2010). Labview Core 1 Course Manual. National Instruments Corporation. Part Number 325290A-01

NI. (2011). "The NI TDMS File Format." Available Online. Retrieved 24 December 2011, from <http://www.ni.com/white-paper/3727/en>.

NI. (2013). "NI PXIE-6366." Available Online. Retrieved 30 January 2013, from <http://sine.ni.com/nips/cds/view/p/lang/en/nid/209217>.

NOTAY, R. S. (2008). Continuing Development of the Top Ring Zone Sampling System and Piston Linkage for the Hydra Engine. Masters Dissertation. Department of Mechanical Engineering, University of Leeds.

- OHSAWA, K., KIYAMA, S., NAKAMURA, Y., OCHIAI, Y., NAKAGAWA, S., ODA, T. and MIYAUCHI, Y. (2011). "Visualization Study on Lubricant Oil Film Behavior around Piston Skirt." SAE Paper 2011-01-2119.
- PARKER, C. A. (1968). *Photoluminescence of Solutions with Applications to Photochemistry and Analytical Chemistry*, Elsevier Publishing Co, Amsterdam.
- PARKER, D. A., ADAMS, D. R. and G, D. (1989). "The Measurement and Reduction of Piston Assembly Friction." *Proceedings of the Institution of Mechanical Engineers. Combustion Engines - Reduction of Friction and Wear*: 27-34.
- POWELL, J. R. and COMPTON, D. A. C. (1993). "Automated FTIR Spectrometry for Monitoring Hydrocarbon-Based Engine Oils." *Lubrication Engineering* 49(3): 233-239.
- PRIEST, M. (1996). *The Wear and Lubrication of Piston Rings*. PhD Thesis. Mechanical Engineering. Leeds, The University of Leeds.
- PRIEST, M., DOWSON, D. and TAYLOR, C. M. (2000). "Theoretical Modelling of Cavitation in Piston Ring Lubrication." *Proceedings of the Institution of Mechanical Engineers, Part C: Journal of Mechanical Engineering Science*. 214: 435-447.
- PRIEST, M. and TAYLOR, C. M. (2000). "Automobile Engine Tribology - Approaching the Surface." *Wear* 241(2): 193-203.
- RABUTE, R. and TIAN, T. (2001). "Challenges Involved in Piston Top Ring Designs for Modern Si Engines." *Transactions of the ASME* 123: 448-459.
- RADCLIFFE, C. D. (1993). *An Experimental and Analytical Study of a Piston Ring Pack*. PhD Thesis. Department of Mechanical Engineering. Leeds, University of Leeds.
- RAHIMIARDALI, B. (2008). *Oil-Film Thickness Measurement in Running Combustion Engine Using Laser Induced Fluorescence (LIF) Technique*. Bachelor Degree Dissertation. School of Mechanical Engineering. Leeds, University of Leeds.
- RAMSBOTTOM, J. (1854). "On an Improved Piston for Steam-Engines " *Proceedings of the Institution of Mechanical Engineers* 5: 70-74.
- RAMSBOTTOM, J. (1855). "On the Construction of Packing Rings for Pistons " *Proceedings of the Institution of Mechanical Engineers* 6: 206-208.

- READ, T., VAZQUEZ, C. and BLUHM, A. (2012). "Diamond Rings' Shine on Chevrolet Sonic, Cruze; Extra-Hard, Low-Friction Carbon Coating Prolongs Life of Piston Rings, Aids Fuel Efficiency." Available Online. Retrieved 19 August 2012. Available from [http://media.gm.com/media/us/en/gm/news.detail.html/content/Pages/news/us/en/2012/Jul/0710\\_sonic-cruze.html](http://media.gm.com/media/us/en/gm/news.detail.html/content/Pages/news/us/en/2012/Jul/0710_sonic-cruze.html).
- RICHARDSON, D. E. and BORMAN, G. L. (1992). "Theoretical and Experimental Investigations of Oil Films for Application to Piston Ring Lubrication." SAE Paper 922341.
- RUDDY, B. L., DOWSON, D. and ECONOMOU, P. N. (1981). "The Prediction of Gas Pressures within the Ring Packs of Large Bore Diesel Engines." *Journal Mechanical Engineering Science* 23(6): 295-304.
- RUOT, C. D., FAURE, D. and BLANC, G. (2000). "Adsorption of Engine Lubricant Dispersants and Polymers onto Carbon Black Particles." SAE Paper 2000-01-1991.
- SANDA, S., MURAKAMI, M., NODA, T. and KONOMI, T. (1997). "Analysis of Lubrication of a Piston Ring Package (Effect of Oil Starvation on Oil Film Thickness)." *JSME International Journal Series B* 40(3): 478-486.
- SAVILLE, S. B., GAINEY, F. D., CUPPLES, S. D., FOX, M. F. and PICKEN, D. J. (1988). "A Study of Lubricant Condition in the Piston Ring Zone of Single-Cylinder Diesel Engines under Typical Operating Conditions." SAE Paper 881586.
- SCHNEIDER, E. W., BLOSSFIELD, D. H., LECHMAN, D. C., HILL, R. F., REISING, R. F. and BREVICK, J. E. (1993). Effect of Cylinder Bore out-of-Roundness on Piston Ring Rotation and Engine Oil Consumption. International Congress and Exposition, Detroit, Michigan, SAE Paper 930796.
- SEKI, T., NAKAYAMA, K., YAMANDA, T., YOSHIDA, A. and TAKIGUCHI, M. (2000). "A Study on Variation in Oil Film Thickness of a Piston Ring Package: Variation of Oil Film Thickness in Piston Sliding Direction." *JSAE Review* 21(3): 315-320.
- SHERRINGTON, I. (2011). "Oil Film Thickness Measurement: A Contribution to the Understanding and Control of Lubrication in the Piston-Ring Packs of IC Engines." *Proceedings of the Institution of Mechanical Engineers, Part J: Journal of Engineering Tribology* 225(7): 595-601.

SHERRINGTON, I. and SMITH, E. H. (1985). "Experimental Methods for Measuring the Oil-Film Thickness between the Piston-Rings and Cylinder-Wall of Internal Combustion Engines." *Tribology International* 18(6): 315-320.

SHIN, K., TATEISHI, Y. and FURUHAMA, S. (1983). "Measurement of Oil-Film-Thickness Between Piston Ring and Cylinder." SAE Paper 830068.

SMITH, O., PRIEST, M., TAYLOR, R. I., PRICE, R., CANTLAY, A. and COY, R. C. (2006). "Simulated Fuel Dilution and Friction-Modifier Effects on Piston Ring Friction." *Proceedings of the Institution of Mechanical Engineer, Part J: Journal of Engineering Tribology* 220: 181-189.

SÖCHTING, S. J. and SHERRINGTON, I. (2009). "The Effect of Load and Viscosity on the Minimum Operating Oil Film Thickness of Piston-Rings in Internal Combustion Engines." *Proceedings of the Institution of Mechanical Engineers, Part J: Journal of Engineering Tribology* 223(3): 383-391.

SPEAROT, J. (1974). "Viscosity of Severely Oxidized Engine Oils." *Industrial & Engineering Chemistry Product Research and Development* 13(4): 259-266.

SREENATH, A. V. and RAMAN, N. (1976). "Mechanism of Smoothing of Cylinder Liner Surface During Running-In." *Tribology International* 9(2): 55-62.

SREENATH, A. V. and RAMAN, N. (1976). "Running-in Wear of a Compression Ignition Engine: Factors Influencing the Conformance between Cylinder Liner and Piston Rings." *Wear* 38(2): 271-289.

SREENATH, A. V. and VENKATESH, S. (1973). "Analysis and Computation of the Oil Film Thickness between the Piston Ring and Cylinder Liner of an Internal Combustion Engine." *International Journal of Mechanical Sciences* 15(8): 605-611.

STARK, M. S., GAMBLE, R. J., HAMMOND, C. J., GILLESPIE, H. M., LINDSAYSMITH, J. R., NAGATOMI, E., PRIEST, M., TAYLOR, C. M., TAYLOR, R. I. and WADDINGTON, D. J. (2005). "Measurement of Lubricant Flow in a Gasoline Engine." *Tribology Letters* 19(3): 163-168.

STARK, M. S., WILKINSON, J. J., LEE, P. M., LINDSAYSMITH, J. R., PRIEST, M., TAYLOR, R. I. and CHUNG, S. (2004). *The Degradation of Lubricants in Gasoline*

Engines: Lubricant Flow and Degradation in the Piston Assembly. 31st Leeds-Lyon. Life Cycle Tribology, Leeds, UK, Elsevier.

TAKIGUCHI, M., NAKAYAMA, K., FURUHAMA, S. and YOSHIDA, H. (1998). "Variation of Piston Ring Oil Film Thickness in an Internal Combustion Engine - Comparison between Thrust and Anti-Thrust Sides." SAE Paper 980563.

TAKIGUCHI, M., SASAKI, R., TAKAHASHI, I., ISHIBASHI, F., FURUHAMA, S., KAI, R. and SATO, M. (2000). "Oil Film Thickness Measurement and Analysis of a Three Ring Pack in an Operating Diesel Engine." SAE paper 2000-01-1787.

TAMMINEN, J., SANDSTRÖM, C.-E. and ANDERSSON, P. (2006). "Influence of Load on the Tribological Conditions in Piston Ring and Cylinder Liner Contacts in a Medium-Speed Diesel Engine." Tribology International 39(12): 1643-1652.

TAYLOR, H. R. (1997). Data Acquisition for Sensor Systems, Springer, ISBN 0412785609.

TAYLOR, R. I. (1997). "Engine Friction: The Influence of Lubricant Rheology." Proceedings of the Institution of Mechanical Engineers, Part J: Journal of Engineering Tribology 211(3): 235-246.

TAYLOR, R. I. (2002). Car Lubricants: Fact and Fiction. Physics World: 39-43.

TAYLOR, R. I. and EVANS, P. G. (2004). "In-Situ Piston Measurements." Proceedings of the Institution of Mechanical Engineers, Part J: Journal of Engineering Tribology 218(3): 185-200.

THIROUARD, B. and TIAN, T. (2003). Oil Transport in the Piston Ring Pack (Part 1): Identification and Characterization of the Main Oil Transport Routes and Mechanisms. 2003 JSAE/SAE International Spring Fuels and Lubricants Meeting, Yokohama, Japan, SAE International Paper 2003-01-1952.

THIROUARD, B., TIAN, T. and HART, D. P. (1998). "Investigation of Oil Transport Mechanisms in the Piston Ring Pack of a Single-Cylinder Diesel Engine, Using Two-Dimensional, Laser-Induced Fluorescence." SAE Paper 982658.

THOMPSON, D. M. and NATTRASS, S. R. (1996). "Full Mid-IR Spectral Characterization of Lubricant in the Ring Pack of a Running Diesel Engine by Time-Resolved FTIR Spectrometry." SAE Paper 962003.

- THOMPSON, M. (1990). "The Use of Top Ring Zone Sampling and Analysis to Investigate Oil Consumption Mechanisms." IMechE Conference on Automotive power systems—environment and conservation, Chester. Paper C394/041: 39-44.
- THOMSON, A. (1996). The Tribological Performance of Piston Ring Packs Designed for Low Emissions. PhD Thesis. Mechanical Engineering, University of Leeds.
- THOMSON, A., RADCLIFFE, C. D. and TAYLOR, C. M. (1997). "The Influence of Piston Ring Tribology on the Diffusion of Fuel through Oil Films." Proceedings of the Institution of Mechanical Engineers, Part J: Journal of Engineering Tribology 211: 223-233.
- TIAN, T. (2002). "Dynamic Behaviours of Piston Rings and Their Practical Impact. Part 1: Ring Flutter and Ring Collapse and Their Effects on Gas Flow and Oil Transport." Proceedings of the Institution of Mechanical Engineers, Part J: Journal of Engineering Tribology 216: 209-227.
- TING, L. L. (1980). "Development of a Laser Fluorescence Technique for Measuring Piston Ring Oil Film Thickness." Journal of Lubrication Technology 102(2): 165-170.
- TING, L. L. and MAYER, I. E. (1974a). "Piston Ring Lubrication and Cylinder Bore Wear Analysis, Part I - Theory." ASME Trans., Journal of Lubrication technology 96(3): 305-313.
- TING, L. L. and MAYER, I. E. (1974b). "Piston Ring Lubrication and Cylinder Bore Wear Analysis, Part II - Theory Verification." ASME Trans., Journal of Lubrication technology 96(2): 258-266.
- TOMS, L. (1998). Machinery Oil Analysis. Methods, Automation & Benefits. Virginia, USA, Coastal Skills Training.
- TUNG, S. C. and MCMILLAN, M. L. (2004). "Automotive Tribology Overview of Current Advances and Challenges for the Future." Tribology International 37(7): 517-536.
- WAKURI, Y., HAMATAKE, T., SOEJIMA, M. and KITAHARA, T. (1992). "Piston Ring Friction in Internal Combustion Engines." Tribology International 25(5): 299-308.
- WATSON, S. A. G. and WONG, V. W. (2010). In-Situ Measurements of Lubricant Composition at the Piston and Liner Interface. Presented at: STLE 65th Annual Meeting and Exhibition, Las Vegas, USA. 20th May 2010.

WENTWORTH, J. T. (1971). "The Piston Crevice Volume Effect on Exhaust Hydrocarbon Emission." *Combustion Science and Technology* 4(1): 97-100.

WILLIAMS, J. (2005). *Engineering Tribology*, Cambridge University Press, New York, USA. ISBN 0-521-60988-7.

WINBORN, L. D. and SHAYLER, P. J. (2001). "Fuel Losses to the Crankcase and Hydrocarbon Return with Recirculated Oil and Ventilation Flow " *Proceedings of the Institution of Mechanical Engineers, Part D: Journal of Automobile Engineering* 215(10): 1117-1130.

WING, R. D. and SAUNDERS, O. (1972). "Oil Film Temperature and Thickness Measurements on the Piston Rings of a Diesel Engine." *Proceedings of the Institution of Mechanical Engineers* 186(1).

YASUTOMI, S., MAEDA, Y. and MAEDA, T. (1981a). "Kinetic Approach to Engine Oil. 1. Analysis of Lubricant Transport and Degradation in Engine System." *Industrial & Engineering Chemistry Product Research and Development* 20(3): 530-536.

YASUTOMI, S., MAEDA, Y. and MAEDA, T. (1981b). "Kinetic Approach to Engine Oil .3. Increase in Viscosity of Diesel-Engine Oil Caused by Soot Contamination " *Industrial & Engineering Chemistry Product Research and Development* 20(3): 540-544.

YILMAZ, E., TIAN, T., WONG, V. W. and HEYWOOD, J. B. (2004). *The Contribution of Different Oil Consumption Sources to Total Oil Consumption in a Spark Ignition Engine. Powertrain and Fluid Systems Conference and Exhibition, Tampa, Florida, USA, SAE Paper* 2004-01-2909.

ZHANG, J., DRINKWATER, B. W. and DWYER-JOYCE, R. S. (2005). "Calibration of the Ultrasonic Lubricant-Film Thickness Measurement Technique." *Measurement and Science Technology* 16(9): 1784-1791.

# Appendix

## A. Optical Parts Inventory and Optical Specifications

### A.1 Optical Parts Inventory

Item No.	Description	Manufacturer	Part No.
1	Blue excitation filter	Thorlabs	MF475-35
2	25mm dia ND Filter, Optical density 2.0	Thorlabs	NE20A
3	Green emission filter	Thorlabs	MF535-22
4	105 $\mu$ m, SMA Fibre patch cable, 5m	Thorlabs	M15L05
5	Lens	Thorlabs	-
6	Dichroic mirror	Thorlabs	DMLP605
7	Optical cage system	Thorlabs	B3C, C4W, ER4,
8	H5873-20 Photosensor module	Hamamatsu	H5783-20
9	C7169 Photosensor module power supply	Hamamatsu	C7169
10	UV-silica lens, planoconvex	Comar Instruments	16PS10
11	16mm, TubeMount, lens size adapter	Comar Instruments	10MR16
12	16mm, TubeMount tube 40mm	Comar Instruments	40MU16
13	16mm, TubeMount SMA adapter	Comar Instruments	02FA32
14	16mm, TubeMount slotted retaining ring	Comar Instruments	01MW16

**Table A-1: Optical parts inventory**

## A.2 Photosensor Module Specification (H5783-20)

### Metal Package PMT

#### Photosensor Modules H5773/H5783/H6779/H6780 Series



The H5773/H5783/H6779/H6780 series are photosensor modules housing a metal package PMT and high-voltage power supply circuit. The metal package PMTs have a metallic package with the same diameter as a TO-8 package used for semiconductor photodetectors, and deliver high gain, wide dynamic range and high-speed response while maintaining small dimensions identical to those of photodiodes. The internal high-voltage power supply circuit is also compact, making the module easy to use.

Considering the mounting methods, a cable output type and a pin output type are provided, and a total of 7 types are available according to the wavelength range to be measured. A P-type is also available with selected gain and dark count ideal for photon counting under extremely low light conditions.

#### Product Variations

Type No.	Suffix	None	-01	-02	-03	-04	-06	-20	Output Type	Features
H5773		yes	yes	yes	yes	yes	yes	yes	On-board	Low power consumption
H5783		yes	yes	yes	yes	yes	yes	yes	Cable output	
H5773P		yes	no	no	no	no	no	no	On-board	For photon counting
H5783P		yes	no	no	no	no	no	no	Cable output	Low power consumption
H6779		yes	yes	yes	yes	yes	yes	yes	On-board	Low ripple noise
H6780		yes	yes	yes	yes	yes	yes	yes	Cable output	Fast settling time

Suffix	Spectral Response
None	300 nm to 650 nm
-01	300 nm to 850 nm
-02	300 nm to 880 nm
-03	185 nm to 650 nm
-04	185 nm to 850 nm
-06	185 nm to 650 nm
-20	300 nm to 900 nm

The suffix -06 type (synthetic silica window) has higher sensitivity than the -03 type below 300 nm in wavelength range.

#### Specifications

Parameter		H5773 / H5783 / H6779 / H6780 Series					Unit	
Suffix		None	-03, -06	-01, -04	-02	-20	—	
Input Voltage		+11.5 to +15.5					V	
Max. Input Voltage		+18					V	
Max. Input Current		H5773 / H5783 Series: 9 H6779 / H6780 Series: 30					mA	
Max. Output Signal Current		100					μA	
Max. Control Voltage		+1.0 (Input impedance 100 kΩ)					V	
Recommended Control Voltage Adjustment Range		+0.25 to +0.9					V	
Effective Area		φ8					mm	
Sensitivity Adjustment Range		1: 10 <sup>4</sup>					—	
Peak Sensitivity Wavelength		420	420	400	500	630	nm	
Cathode	Luminous Sensitivity	Min.	40	40	80	200	350	
		Typ.	70	70	150	250	500	
Blue Sensitivity Index (CS 5-58)		8					—	
Red/White Ratio		—					—	
Radiant Sensitivity *1		62	62	60	58	78	mA/W	
Anode	Standard Type	Luminous Sensitivity	Min.	10	10	15	25	35
		Typ.	50	50	75	125	250	
P Type	Radiant Sensitivity *1 *2	Typ.	4.3 × 10 <sup>4</sup>	4.3 × 10 <sup>4</sup>	3.0 × 10 <sup>4</sup>	2.9 × 10 <sup>4</sup>	3.9 × 10 <sup>4</sup>	
		Dark Current *2 *3	Typ.	0.2	0.2	0.4	2	2
		Max.	2	2	4	20	nA	
Gain *2		Min.	7.5 × 10 <sup>5</sup>	—			—	
		Typ.	1 × 10 <sup>6</sup>	—			—	
Radiant Sensitivity *1 *2		6.2 × 10 <sup>4</sup>					A/W	
Dark Count *2 *3		Typ. 80					s <sup>-1</sup>	
		Max. 400					—	
Rise Time *2		0.78					ns	
		H5773 Series	H5783 Series	H6779 Series	H6780 Series			
Ripple Noise *2 *4 (peak to peak) Max.		1.2		0.6		mV		
Settling Time *5		2		0.2		s		
Operating Ambient Temperature		+5 to +50		+5 to +45		°C		
Storage Temperature		-20 to +50					°C	
Weight		60	80	60	80		g	

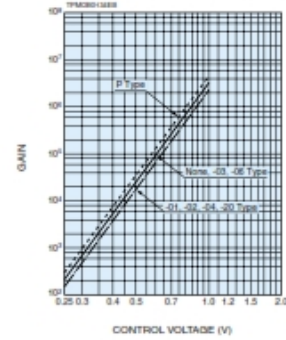
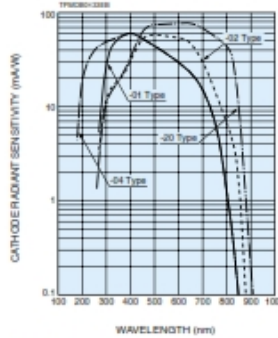
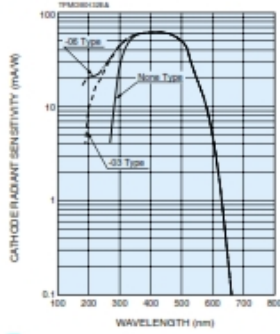
\*1: Measured at the peak sensitivity wavelength \*2: Control voltage = +0.8 V \*3: After 30 minute storage in darkness

\*4: Cable RG-174/U, Cable length 450 mm, Load resistance = 1 MΩ, Load capacitance = 22 pF

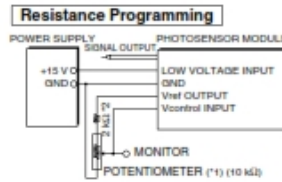
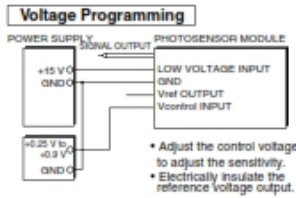
\*5: The time required for the output to reach a stable level following a change in the control voltage from +1.0 V to +0.5 V.

## Current Output Type Photosensor Modules

### Characteristics (Cathode radiant sensitivity, Gain)



### Sensitivity Adjustment Method

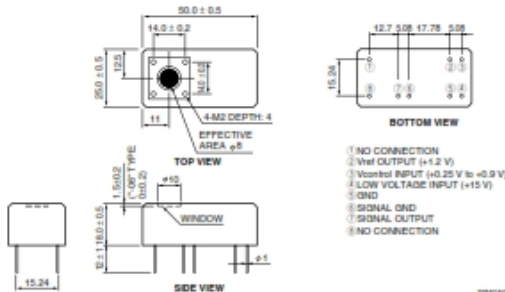


\*1: When using a potentiometer to adjust sensitivity, monitor the control voltage so it does not exceed +1.0 V.

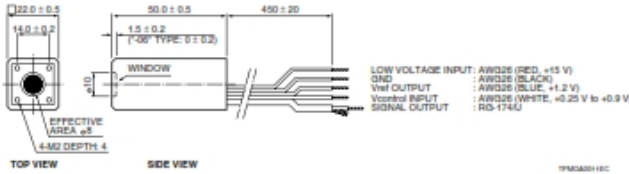
\*2: H6779/H6780 series has this 2 kΩ resistor. No external resistor is needed.

### Dimensional Outlines (Unit: mm)

#### H5773/H6779 Series

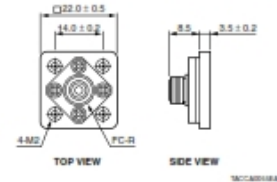


#### H5783/H6780 Series

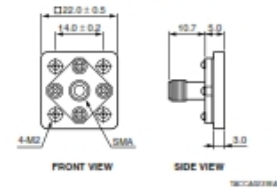


### Option (Optical Fiber Adapter) (Unit: mm)

#### E5776 (FC Type)



#### E5776-51 (SMA Type)



### A.3 Photosensor Module Power Supply (C7169)

**HAMAMATSU**  
PRELIMINARY DATA  
JUL. 2000

## POWER SUPPLY FOR PHOTOSENSOR MODULES C7169

C7169 is the power supply unit which can be used for various photosensor module produced by Hamamatsu commonly. The unit can provide both the driving voltage and the control voltage.



### APPLICABLE MODELS

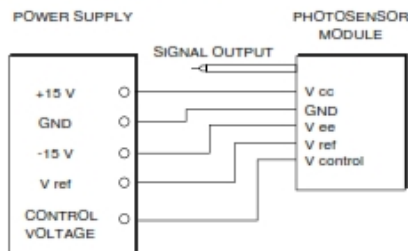
Type No.	Effective Area	Built-in Parts
H7710 SERIES	3.7 × 13 mm	Driving Circuit
H7711/H7712 SERIES		Driving Circuit + AMP
H6779 SERIES	8 mm Dia.	Driving Circuit
H6780 SERIES		
H5773 SERIES		
H5783 SERIES		
H5784 SERIES		
H7826 SERIES	15 mm Dia.	Driving Circuit
H7732 SERIES	4 × 20 mm	Driving Circuit

### SPECIFICATIONS

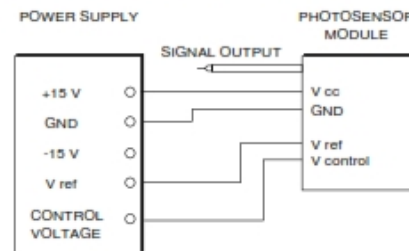
Type No.	Value	Unit
Output Voltage	±15	V
Output Current (MAX.)	0.3 (+15 V) 0.2 (-15 V)	A
Control Voltage	+0.25 to +1.2	V
Input Voltage	100 to 240	V ac
Input Line Voltage Frequency	50/60	Hz
Operating Temperature	+5 to +50	°C
Storage Temperature	+20 to +50	°C

### EXAMPLE OF CIRCUIT CONNECTION

WITH AMP (H5784/H7711/H7712)



WITHOUT AMP (H7710/H5773/H5783/H6779/H6780/H7826/H7732)



\* The connection of the unit and the photosensor module must be made while the unit power is "OFF".  
Please make proper wiring connection otherwise the photosensor module may be damaged.

Subject to local technical requirements and regulations, availability of products included in this promotional material may vary. Please consult with our sales office.  
Information furnished by HAMAMATSU is believed to be reliable. However, no responsibility is assumed for possible inaccuracies or omissions. Specifications are subject to change without notice. No patent rights are granted to any of the circuits described herein. ©2000 Hamamatsu Photonics K.K.

#### A.4 Thorlabs Excitation/ Emission Filters and Dichroic Mirror Specification

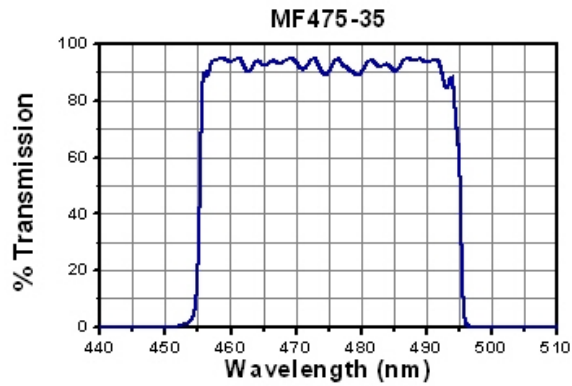


Figure A-1: MF475-35 – Blue Excitation Filter

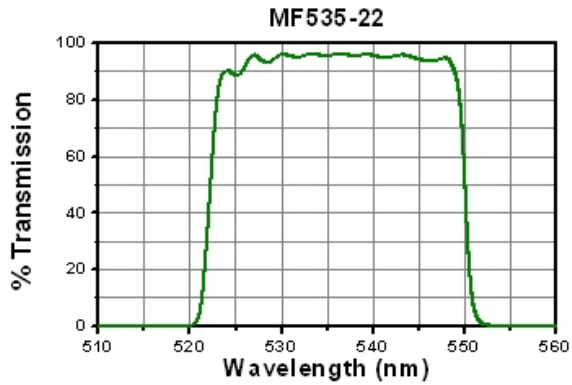


Figure A-2: MF535-22 - Green Emission Filter

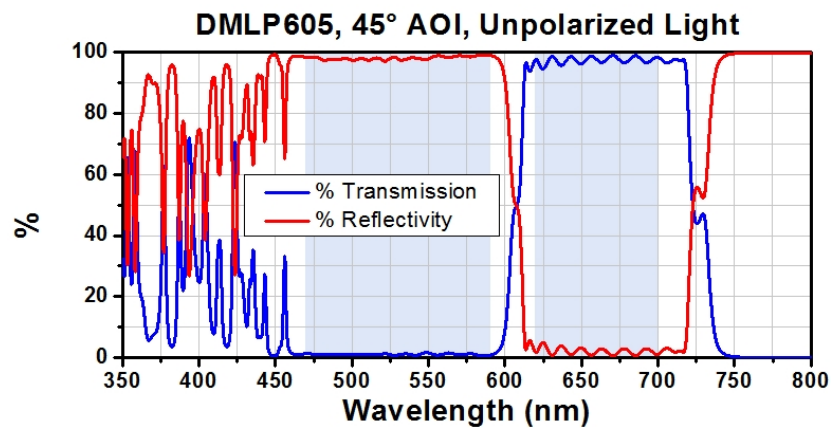
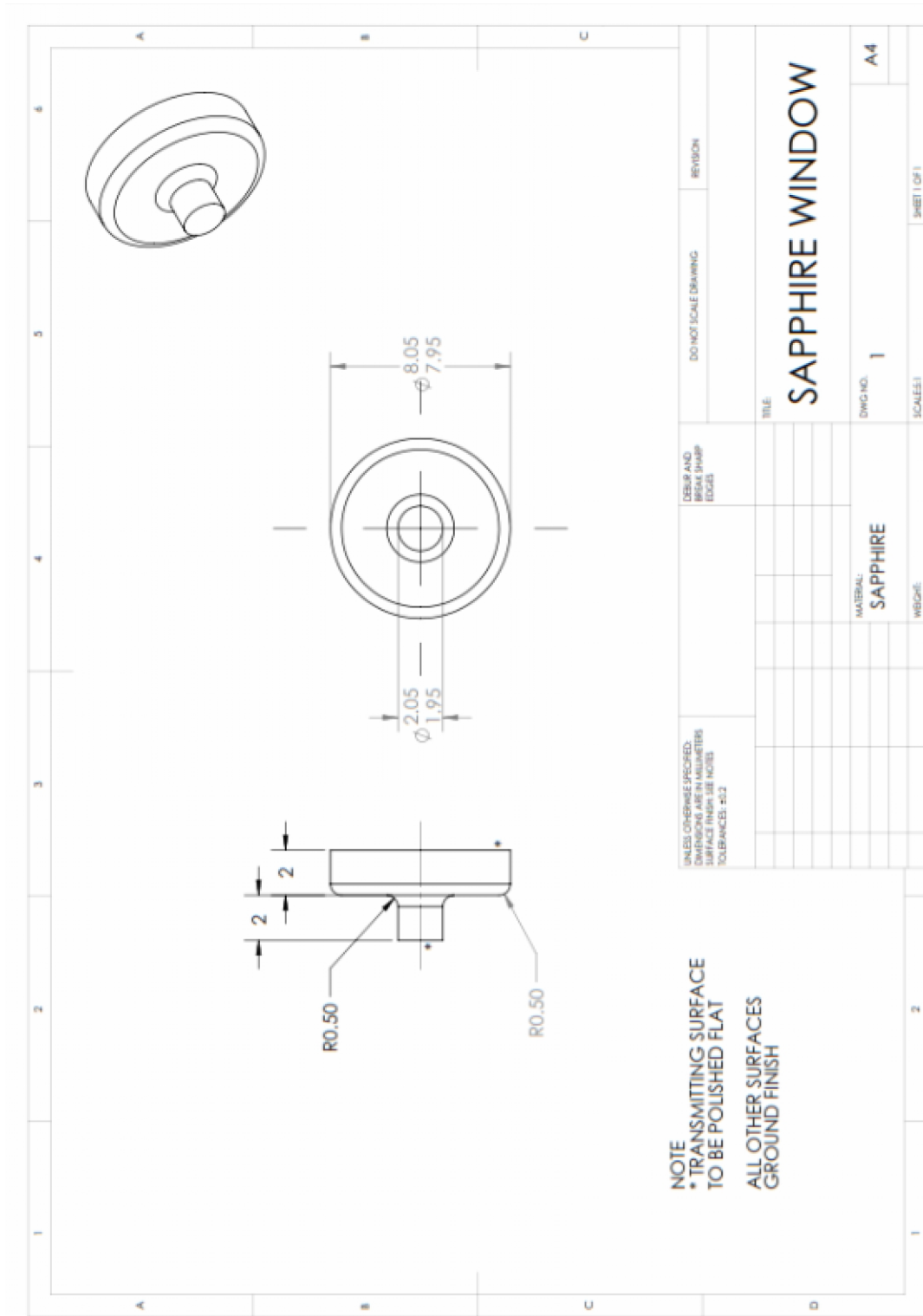


Figure A-3: DMLP605 – Dichroic Mirror

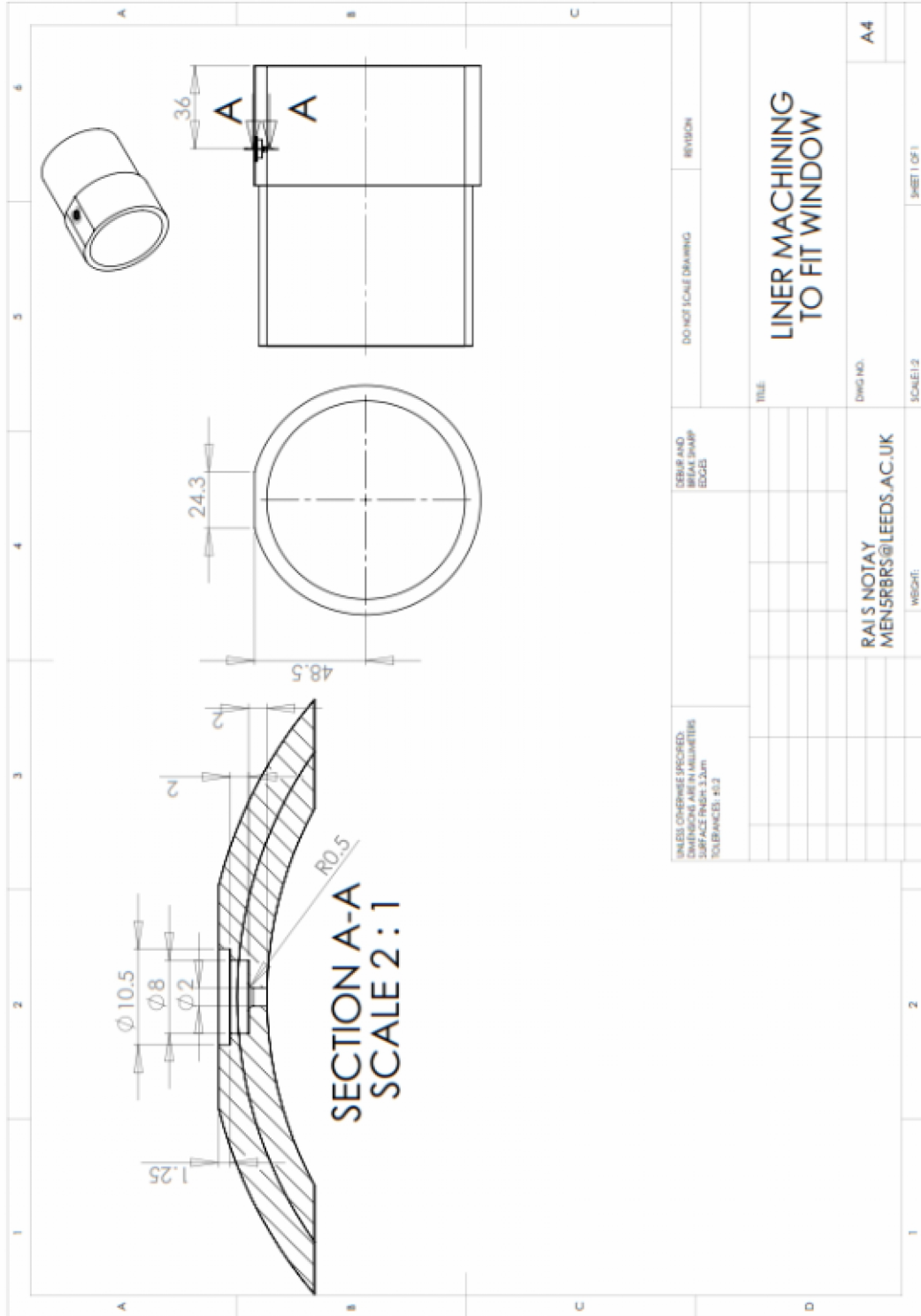
(Specification from Thorlabs Catalogue V20)

## B. Engineering Technical Drawings

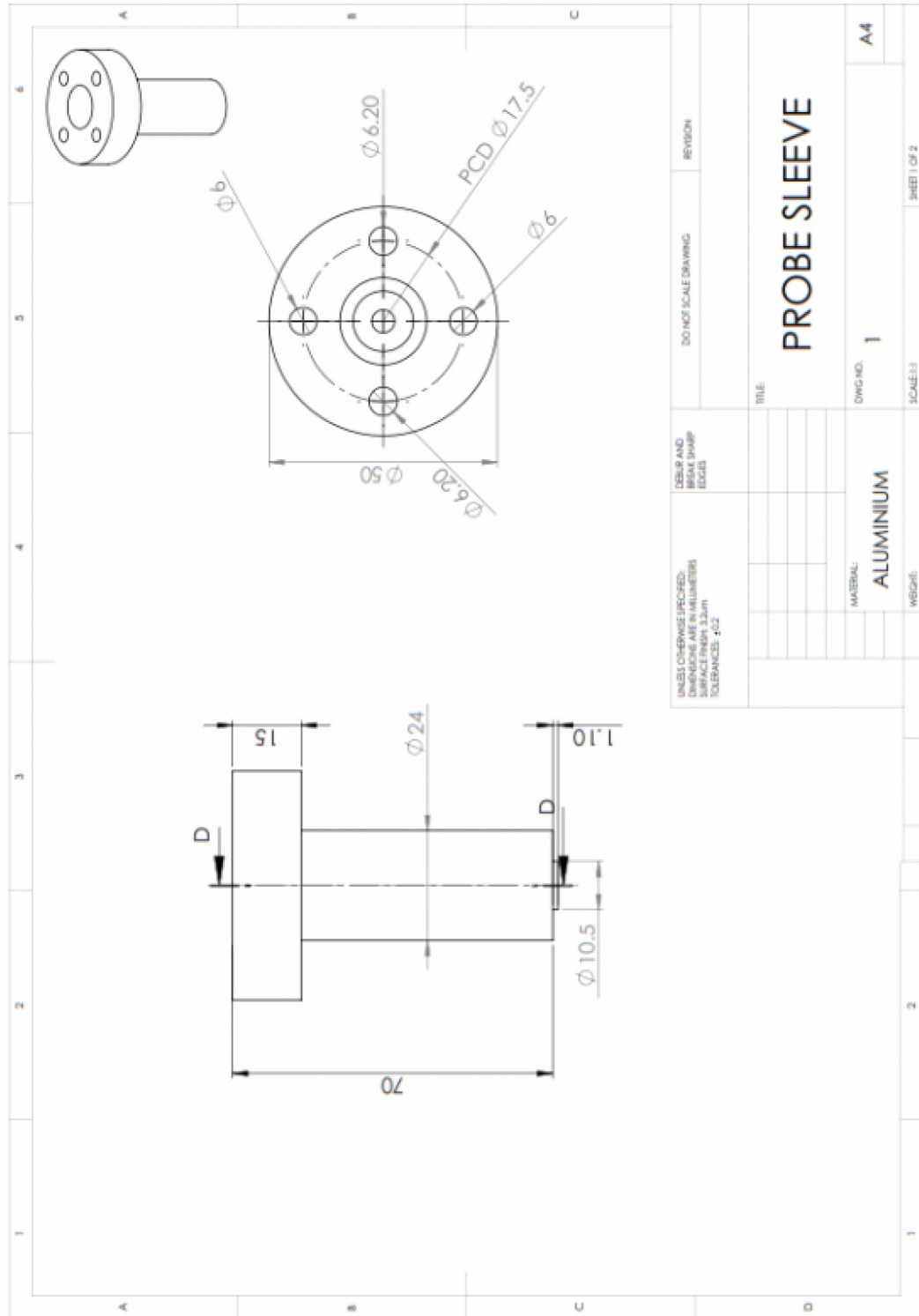
### B.1 Sapphire Window Technical Drawing



**B.2 Motored Engine Cylinder Liner Machining Guide to Fit Window**

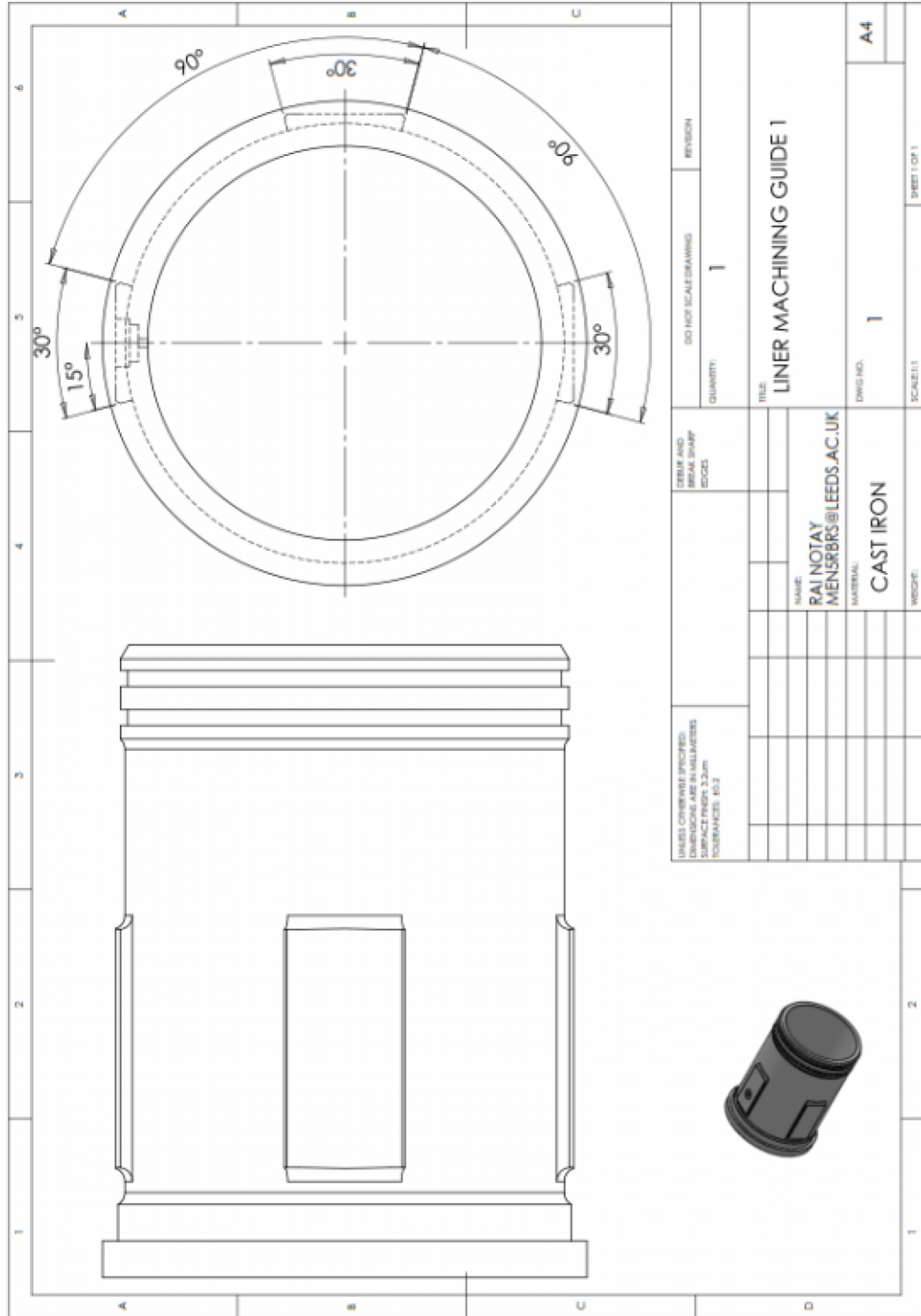


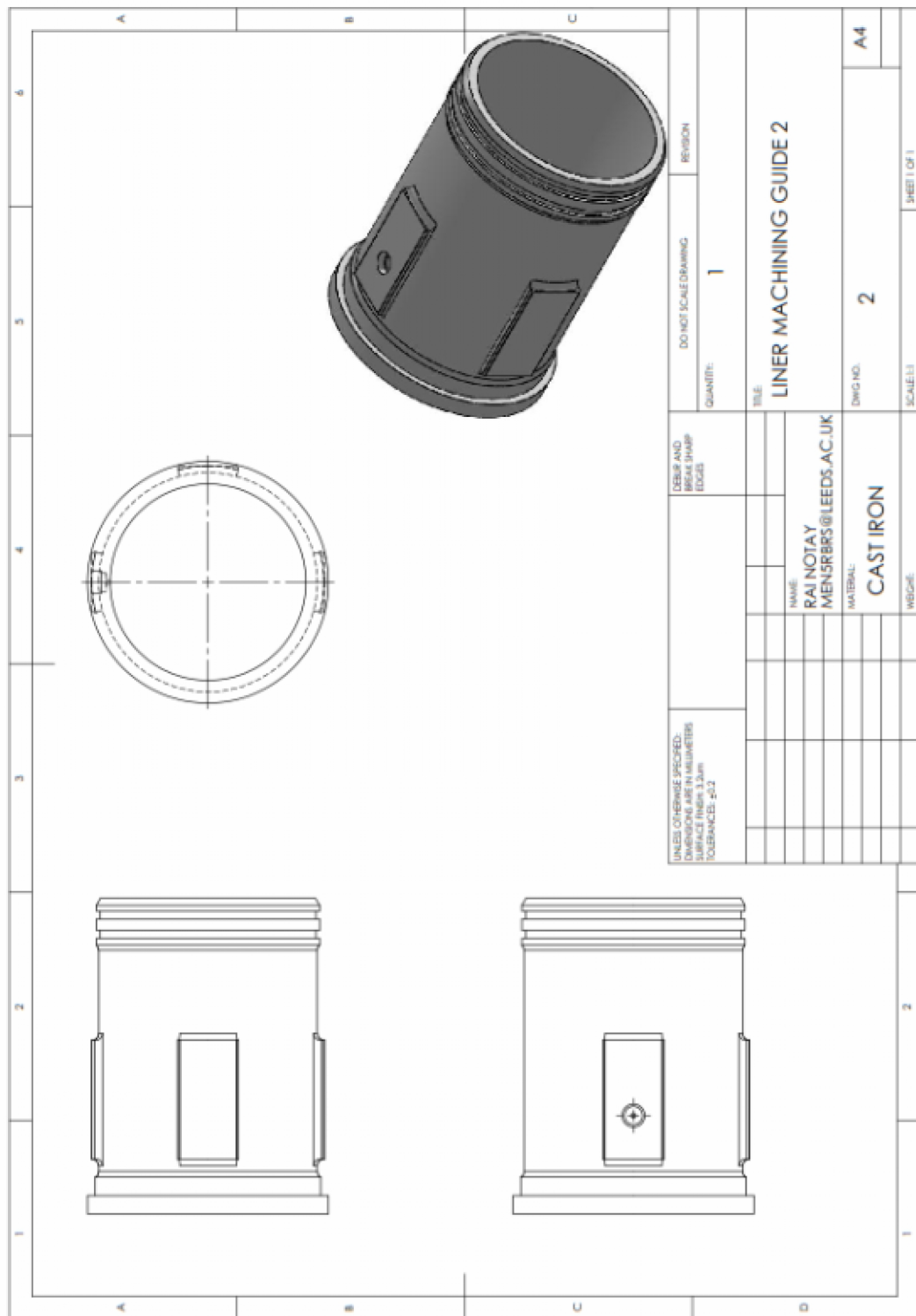
### B.3 Motored Engine LIF Collimator Probe Sleeve

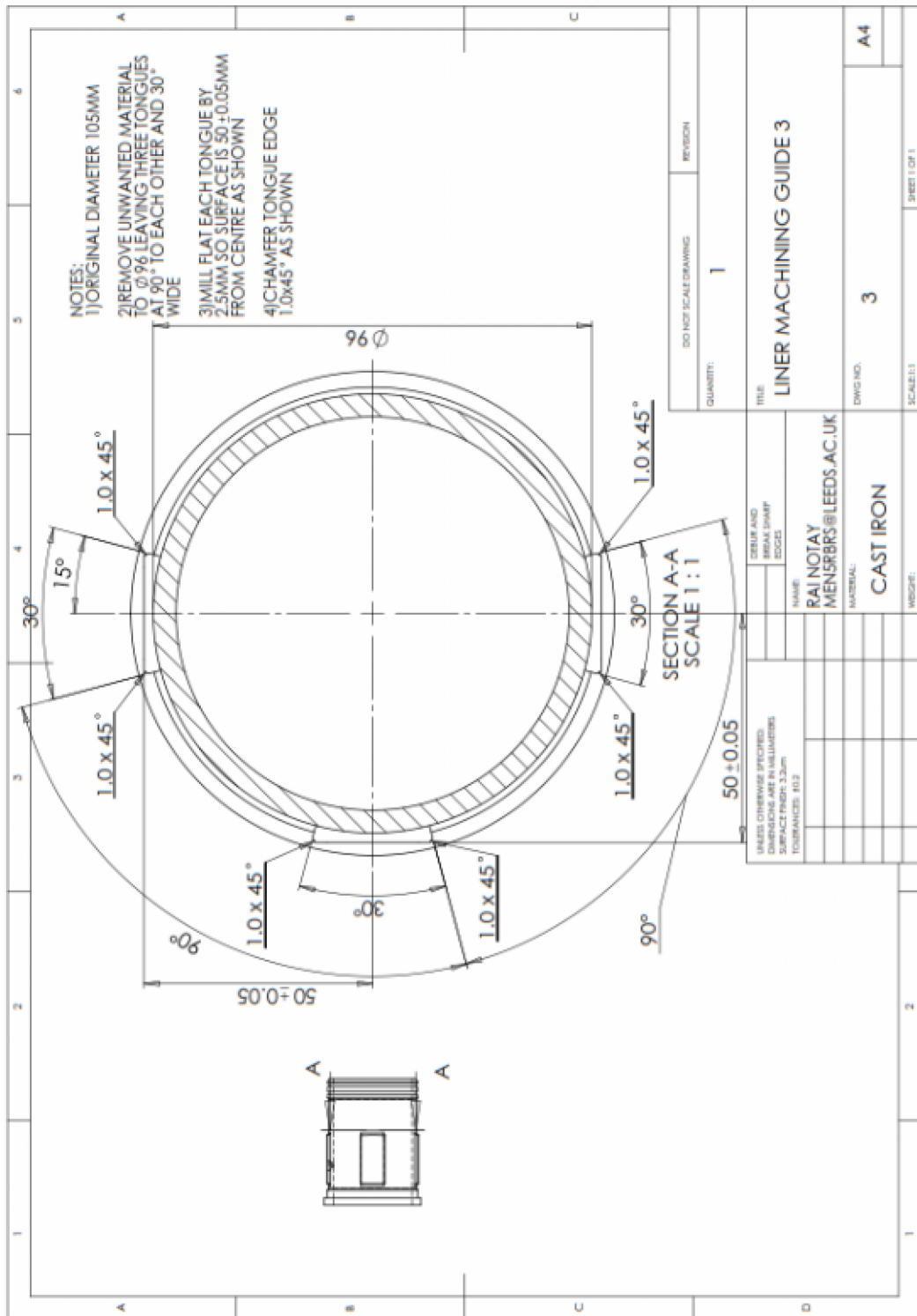


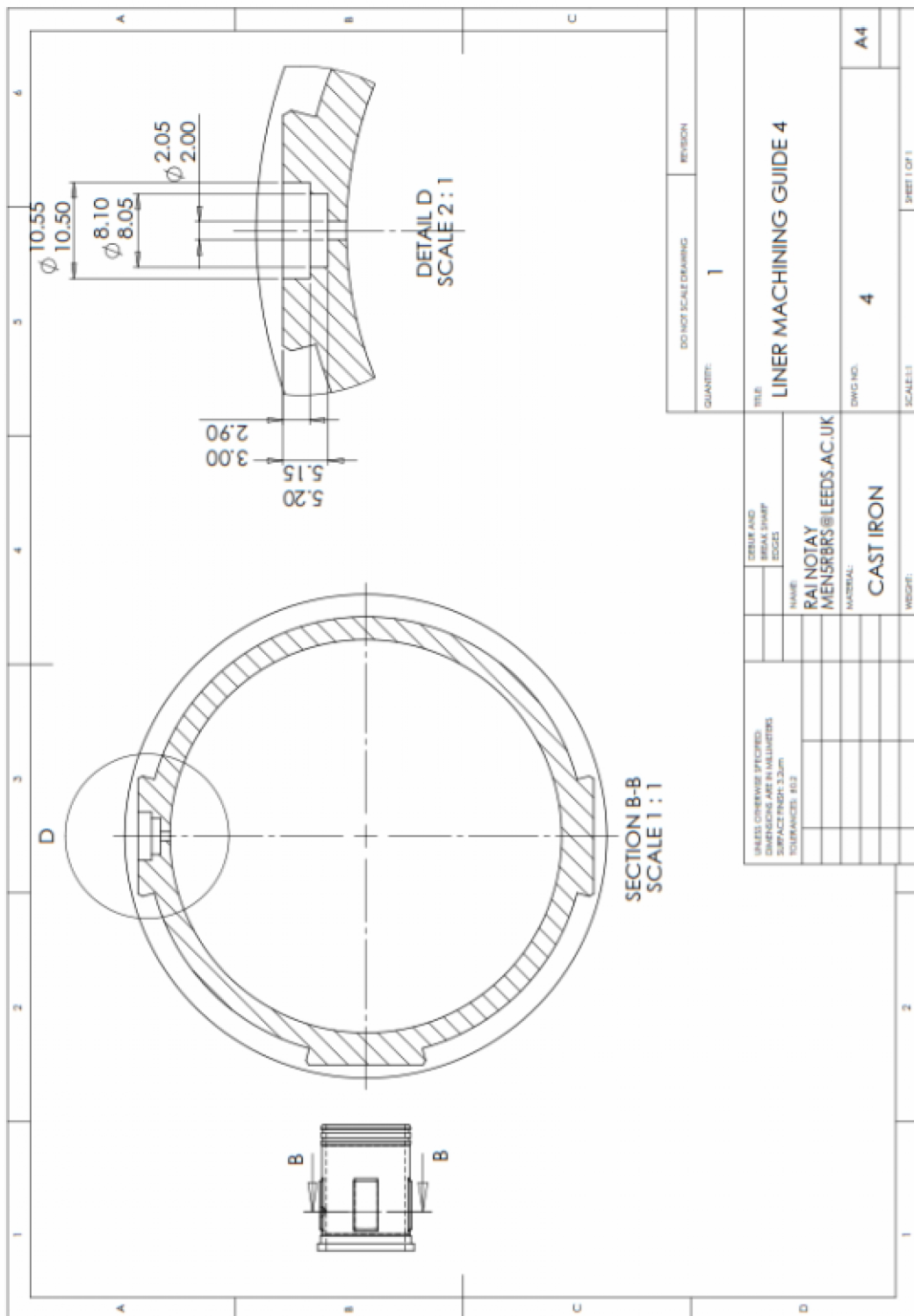


### B.4 Ricardo Hydra Cylinder Liner Machining Guide

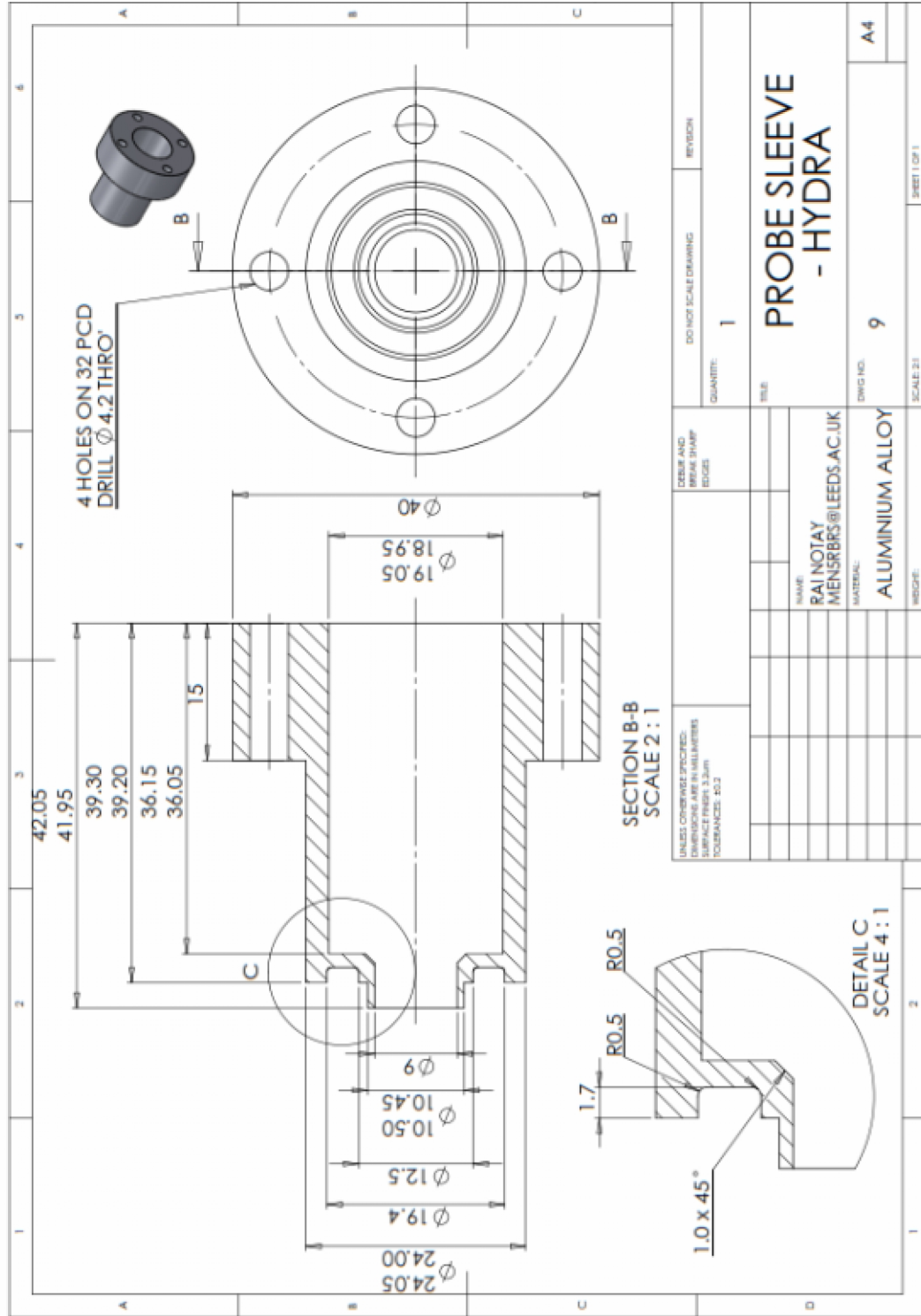






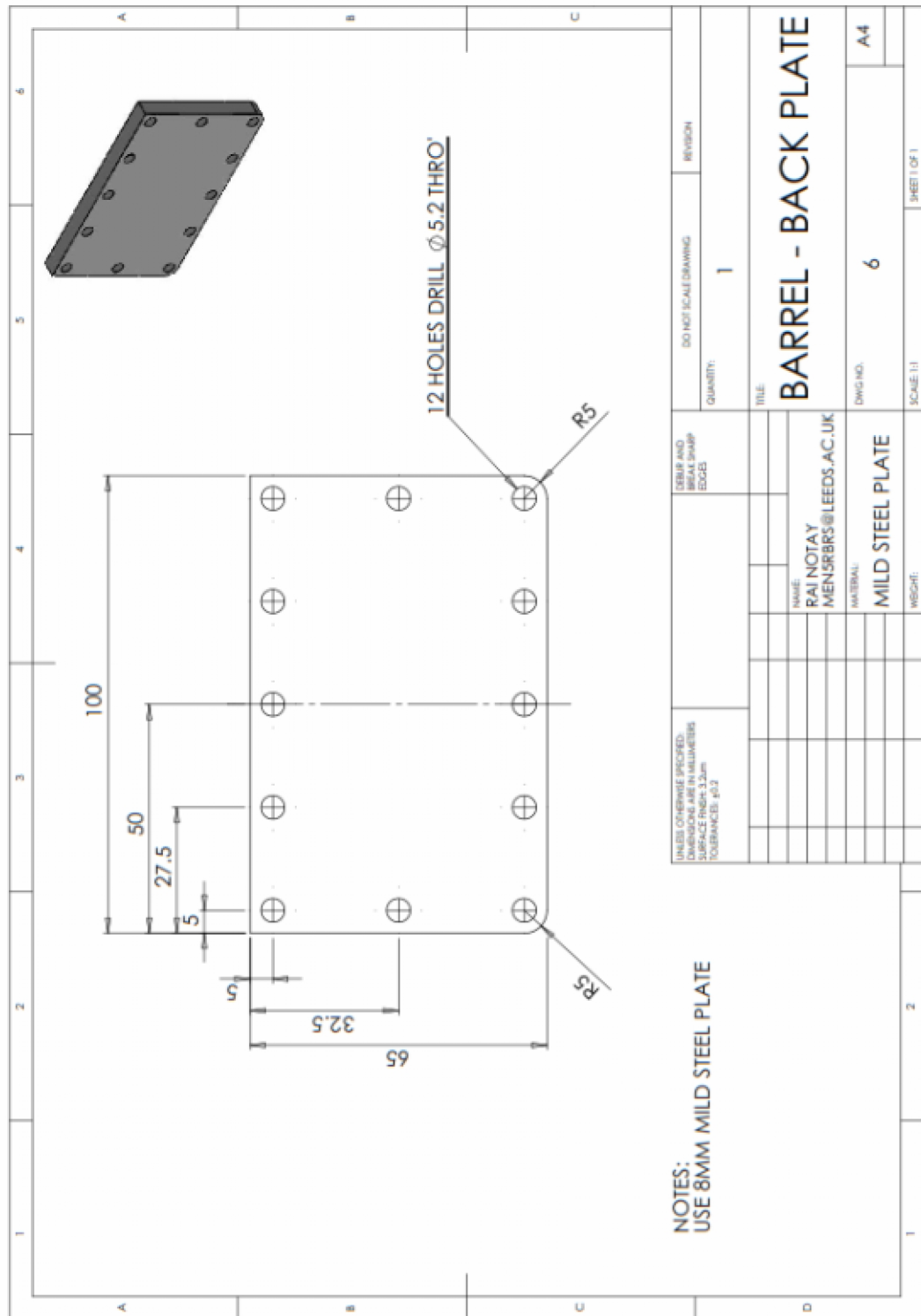


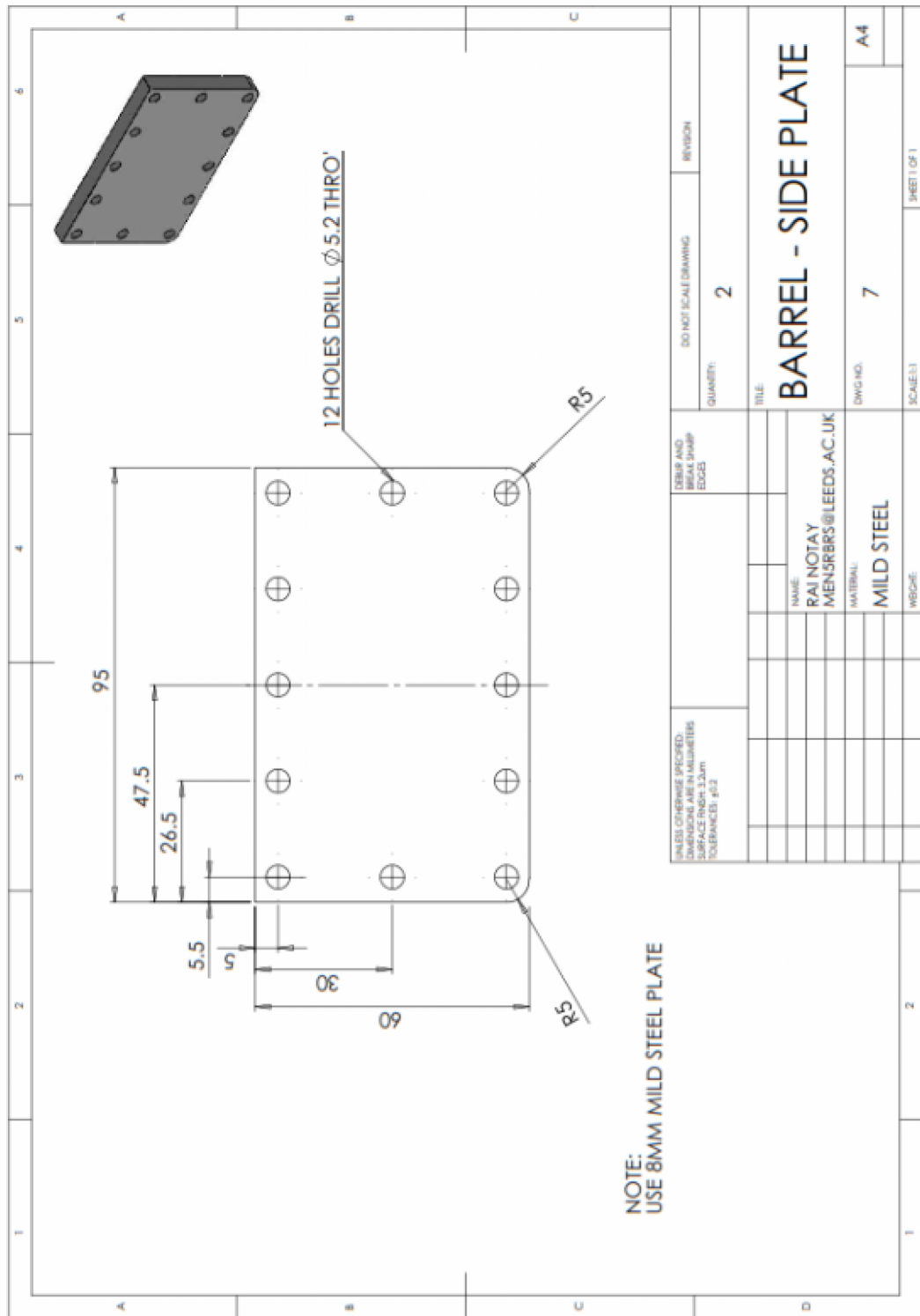
**B.5 Ricardo Hydra Engine LIF Collimator Probe Sleeve**

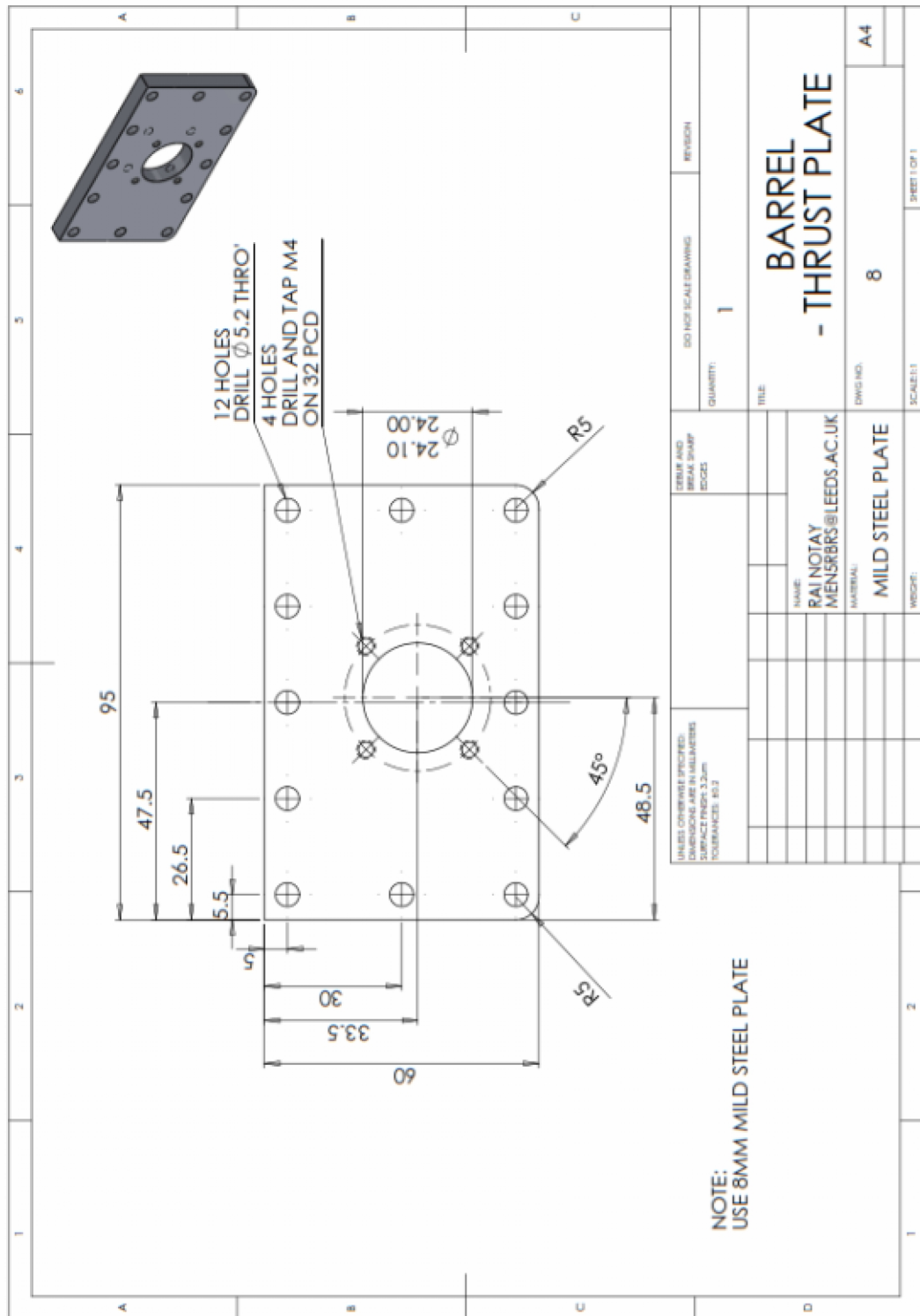






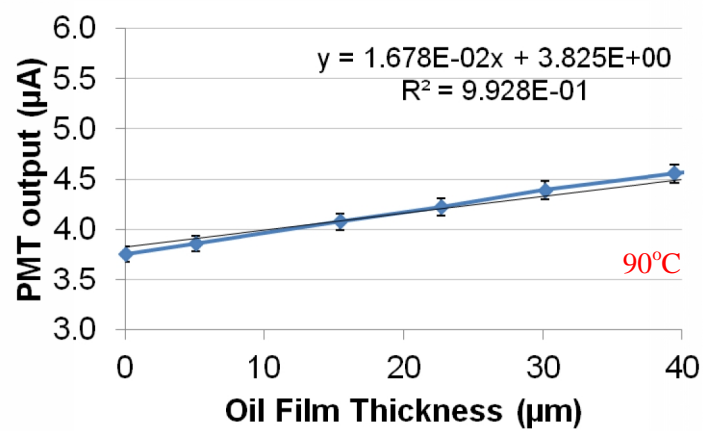
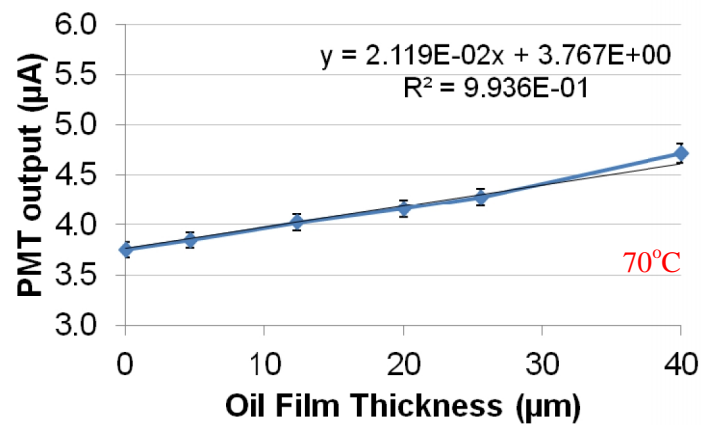
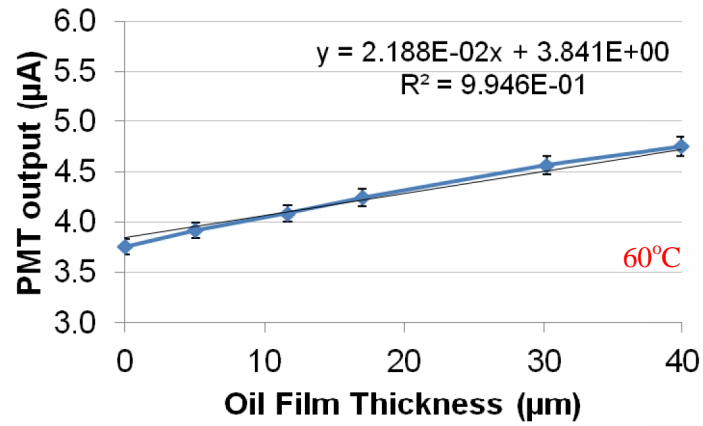






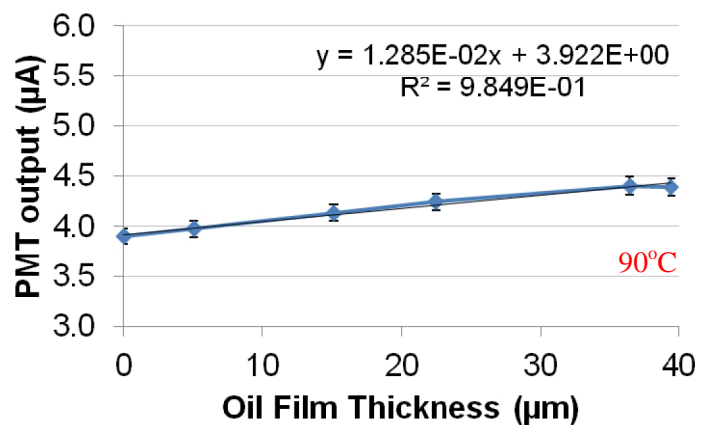
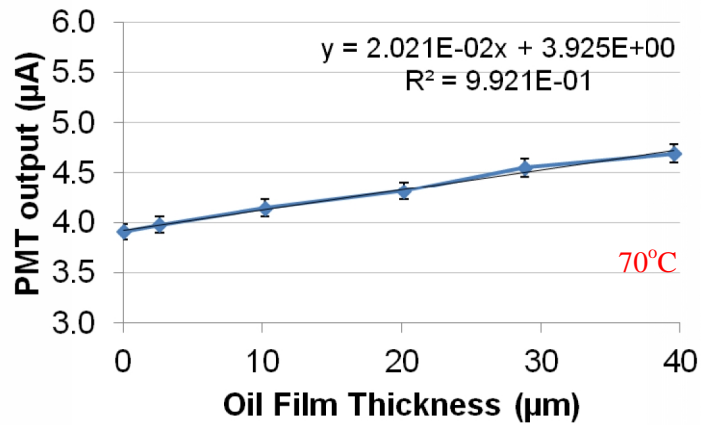
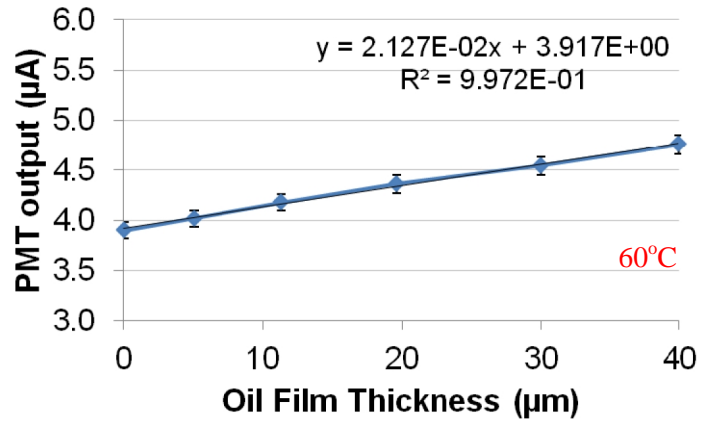
## C. Engine Lubricant LIF Calibration Tests

### C.1 Fresh Sample A – Castrol Edge SAE 0W30 plus 35mg/l dye



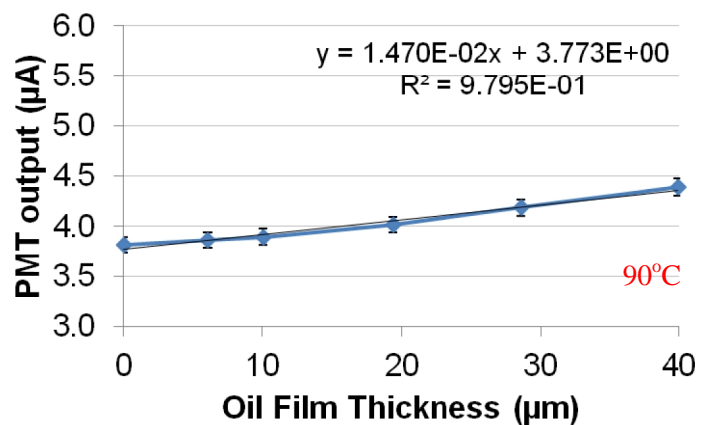
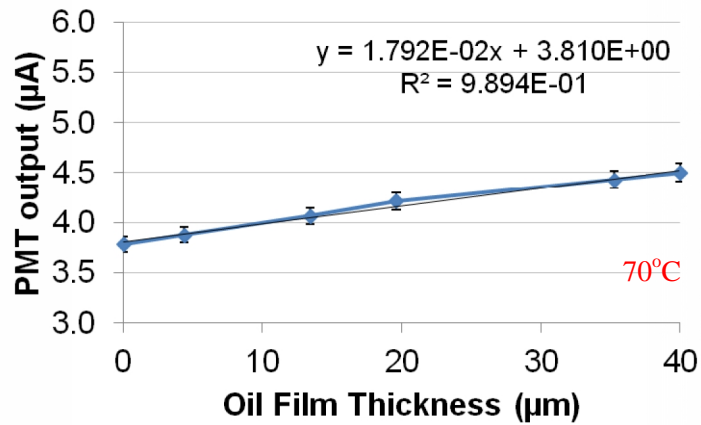
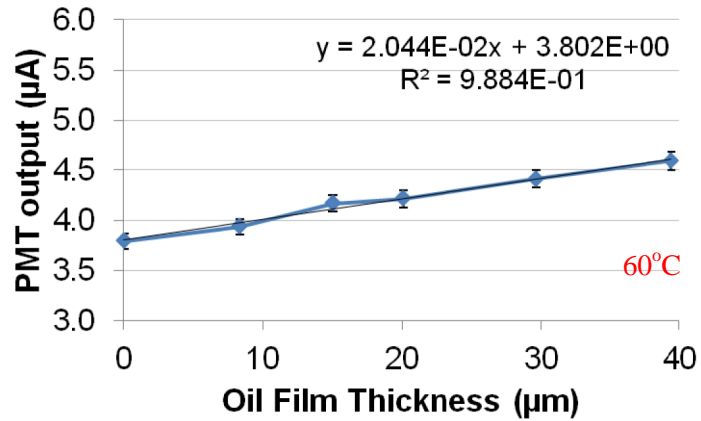
— Raw data    — Best fit

## C.2 Degraded Sample B – MB Medium Size Car, Castrol Edge SAE 0W30 plus 100mg/l dye



— Raw data      — Best fit

### C.3 Degraded Sample C – MB Sports Car, Castrol Edge SAE 0W30 plus 100mg/l dye



— Raw data      — Best fit

## D. Pyrromethene 567A Dye Specification



PO Box 31126  
Dayton, OH 45437  
Tel: 937.252.2989 Fax: 937.258.3937  
E-mail: [info@exciton.com](mailto:info@exciton.com)  
[www.exciton.com](http://www.exciton.com)

### PYRRROMETHENE 567A

**Synonyms:** 1,3,5,7-Tetramethyl-8-n-pentyl-2,6-diethylpyrromethene BF<sub>2</sub> complex

**Catalog No.:** 05678

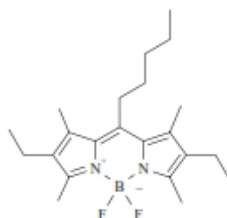
**CAS No:** N/A

**MW:** 374.32

**Chemical Formula:** C<sub>22</sub>H<sub>33</sub>N<sub>2</sub>BF<sub>2</sub>

**Appearance:** Bright orange crystalline solid

**Structure:**



#### Spectral Information:

$\lambda_{\text{max,abs}}$  519nm (ethanol), 522.5nm (gasoline), 521.64nm (Dow Corning 200 silicon oil), 520.5nm (PMMA), 518.85nm (ethyl acetate)

$\lambda_{\text{max,fl}}$  536nm (ethanol), 543nm (gasoline), 554nm (PMMA)

$\epsilon_{519}$  8.4x10<sup>4</sup> liter/mole cm

$\Phi_f$  not reported

#### Selected Solubility Limits (25°C):

Acetone	43 grams/liter	2-Ethoxyethyl Acetate	48 grams/liter
Acetonitrile	15 grams/liter	Ethyl Acetate	>133 grams/liter
p-Dioxane	>23 grams/liter	Gasoline	4.8 grams/liter
Dow Corning 200 Silicone Oil	0.85 grams/liter	Heptane	7.87 grams/liter
Ethanol	3.4 grams/liter	Methanol	3.7 grams/liter

Exciton, Inc.  
Pyrromethene 567A in Hydrocarbon Solvent  
Excitation Spectrum  
 $\lambda_{\text{max}} = 522.5\text{nm}$   
Concentration:  $\sim 9 \times 10^{-6}\text{M}$

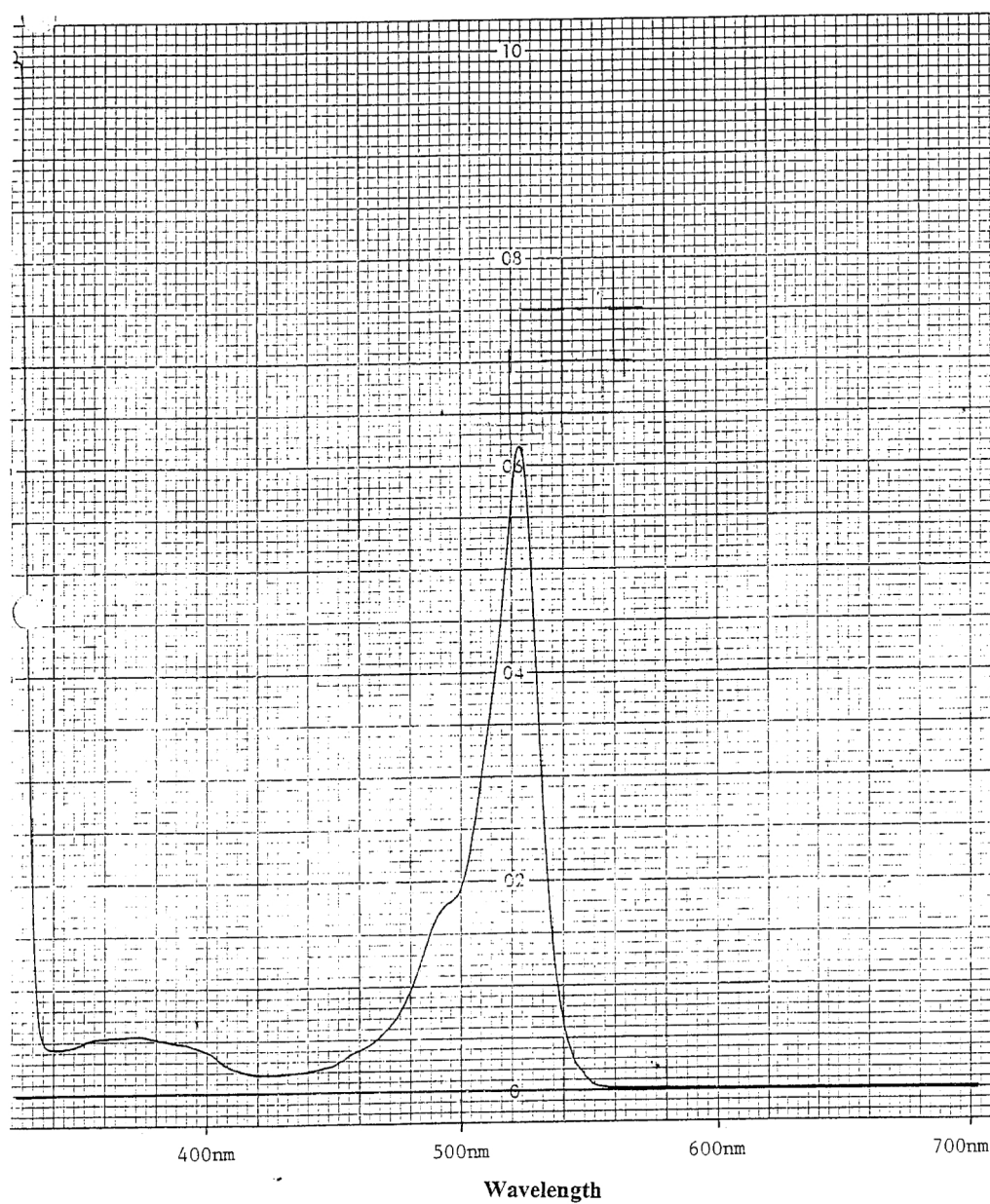


Figure D-1: Pyrromethene 567A dye absorption spectrum

## E. Monarch 280 Carbon Black Powder Specification

SPECIAL BLACK –  
UTILITY PIGMENT BLACK



### MONARCH® 280



MONARCH® 280 is a general purpose low color pigment black suitable for a variety of tinting applications. As a fluffy product, MONARCH 280 is a versatile and an easy to disperse carbon black that can be used to replace lamp blacks.

**Product Form:** Fluffy

#### Application Information

##### Printing Inks

MONARCH 280 is a high structure pigment black that is broadly applicable in a variety of inks. It is particularly suitable for web offset and gravure printing where matte finish is required. It also offers very blue undertone, excellent hold out or lay with excellent dispersibility.

##### Coatings

This pigment black can be used in a variety of coatings applications. It is recommended for underbody/underhood automotive, general industrial, or architectural trade sales applications where high jetness is not required. It is also recommended for use as a tinting black since the relatively large particle size allows for high loading while the high structure allows less mobility in the wet film of the applied coating. This reduces problems with floating and flooding in liquid tinting applications. It can be easily dispersed using a high speed disperser for liquid coatings or a single screw extruder for powder coatings.

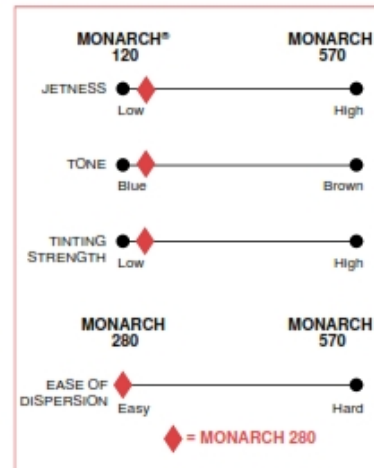
##### Other Applications

In addition to the applications listed above, this product is commonly used as a pigment in Concrete & Cement and Metallurgical Applications.

The dispersibility of MONARCH 280 pigment black depends on the equipment used and the formulation. Most low color pigment blacks exhibit the same ease of dispersion because of their relatively large particle size.

MONARCH 280 is a fluffy pigment black with a typical bulk density of 9 lbs/ft<sup>3</sup> (146 kg/m<sup>3</sup>).

#### Performance Comparison to Other Low Color Pigment Blacks



**Cabot Corporation**  
www.cabot-corp.com

## F. Test Oil Specifications

### F.1 Castrol Edge SAE 0W30

Typical Properties:\*

	Edge with SPT				
	Method	0W-20	0W-30	5W-20	5W-30
Viscosity @ 100C, cSt	ASTM D445	8.65	12.21	8.88	10.70
Viscosity @ 210F, SUS	ASTM D2161	54.59	67.22	55.37	61.72
Viscosity @ 40C, cSt	ASTM D445	45.08	72.0	49.35	62.64
Viscosity Index	ASTM 2270	174	167	161	159
Low Temperature ( C) Cranking Viscosity, cP max.	ASTM 5293	6,200 @ -35	6,200 @ -35	6,600 @ -30	6,600 @ -30
Low Temperature ( C) Pumping Viscosity, cP max.	ASTM 4684	60,000 @ -40	60,000 @ -40	40,000 @ -35	40,000 @ -35
HT /HS Viscosity, cP min	ASTM 4683	2.6	2.9	2.6	2.9
Pour Point, F (C) max	ASTM D97	-38 (-39)	-65 (-54)	-38 (-39)	-38 (-39)
Flash Point, PMCC, C min	ASTM D93	>200	>200	>200	>200
Density @ 15C, Relative	ASTM 4052	0.845	0.839	0.848	0.856
Pounds per Gallon		7.038	6.989	7.063	7.128

	Edge with SPT				
	Method	10W-30	10W-40	5W-40	5W-50
Viscosity @ 100C, cSt	ASTM D445	11.30	14.60	13.9	18.50
Viscosity @ 210F, SUS	ASTM 2161	63.88	76.36	73.6	92.18
Viscosity @ 40C, cSt	ASTM D445	75.10	91.89	82.6	114.36
Viscosity Index	ASTM 2270	151	162	174	170
Low Temperature ( C) Cranking Viscosity, cP max.	ASTM 5293	7,000 @ -25	7,000 @ -25	6,600 @ -30	6,600 @ -30
Low Temperature ( C) Pumping Viscosity, cP max.	ASTM 4684	50,000 @ -30	60,000 @ -30	60,000 @ -35	60,000 @ -35
HT /HS Viscosity, cP min	ASTM 4683	2.9	2.9	2.9	3.7
Pour Point, F (C) max	ASTM D97	-33 (-36)	-27 (-33)	-44 (142)	-22 (-30)
Flash Point, PMCC, C min	ASTM D93	>200	>200	>200	>200
Density @ 15C, Relative	ASTM 4052	0.858	0.859	0.850	0.854
Pounds per Gallon		7.145	7.202	7.076	7.111

\* Due to continual product research and development, the information contained herein is based on products purchased in the U.S. subject to change without notification. Typical properties may vary slightly.

## F.2 Shell Extra High Viscosity Index (XHVI) 8.2

### Shell XHVI 8.2

#### Extra high viscosity index base oil



Shell XHVI (Extra High Viscosity Index) base oils are special products from the Shell XHVI synthesis process. With the VI above 120 they are classified as API/ATIEL Group III type base oil. XHVI base oils are favourable blending components for high quality speciality lubricants in the automotive and industrial sector, where excellent viscosity-temperature behaviour and low volatility are required.

#### Typical Physical Characteristics

		XHVI 8.2	XHVI 8.2 Specification
Appearance		bright&clear	bright&clear
Colour (ASTM)	ASTM D 1500	L0.5	max 1.0
Density at 15 °C	kg/m <sup>3</sup> ASTM D 1298	834	
Flashpoint PMCC	°C ASTM D 93	240	min 210
Flashpoint COC	°C ASTM D 92	250	
Pour Point	°C ASTM D 97	-15	max -15
Kinematic Viscosity at 40 °C	mm <sup>2</sup> /s ASTM D 445	48	
Kinematic Viscosity at 100 °C	mm <sup>2</sup> /s ASTM D 445	8.3	7.8 - 8.5
Viscosity Index	ASTM D 2270	147	min 140
Acid Value	mgKOH/g ASTM D 974	<0.03	max 0.05
Ash	%m ASTM D 482	<0.01	
Sulphur Content	%m/m ASTM D 2622	<0.03	
Noack Volatility	%m ASTM D 5800	5	max 5

These characteristics are typical of current production. Whilst future production will conform to Shell's specification, variations in these characteristics may occur.

## F.3 Shell Helix HX7 AG SAE 5W30



Technical Data Sheet

# Shell Helix HX7 AG 5W-30

*For extra responsiveness right up to the next oil change*

Shell Helix HX7 AG is the latest generation synthetic technology engine oil designed specifically to meet the needs of almost all Opel and Vauxhall gasoline and diesel engines. Approved by these manufacturers for normal and extended service.

Specifically designed to provide exceptional engine responsiveness and protection for almost all Opel and Vauxhall gasoline and diesel engines.

Contains Shell's special active cleansing technology to continuously prevent dirt and sludge build-up, maintaining responsiveness right up to the next oil drain.

### DESIGNED TO MEET CHALLENGES

#### Performance, Features & Benefits

- **Specially selected synthetic base oils, lower evaporation loss**  
Reduces the oil volatility and therefore the oil consumption.  
The need for oil top-up is therefore reduced.
- **Special active cleansing technology**  
Twice as effective at removing sludge from dirty engines than mineral oil.
- **Enhanced oxidation stability**  
Up to 19% more protection than other synthetic technology leading brands tested.
- **Low viscosity, rapid oil flow and low friction**  
Greater fuel efficiency.
- **High shear stability**  
To maintain viscosity and stay in grade throughout the oil drain period.
- **Low Chlorine**  
For improved environmental disposal.

#### Special aeration control

Optimised hydraulic system control.

#### Lower Sulphur

For catalyst protection.

#### Minimise vibration and engine noise

Smoother, quieter drive.

#### Main Applications

- Meets the requirements of General Motors for their specification GM LL-A-025 and GM LL-B025.

#### Specifications, Approvals & Recommendations

- API: SL/CF
- ACEA: A3/B3, A3/B4
- GM-LL-A-025 equivalent to Opel B-040-2095
- GM-LL-B-025 equivalent to Opel B-040-2098

For a full listing of equipment approvals and recommendations, please consult your local Shell Technical Helpdesk, or the OEM Approvals website.

#### Typical Physical Characteristics

Properties		Method	Helix HX7 AG
Viscosity Grade			5W-30
Kinematic Viscosity	@40°C	mm <sup>2</sup> /s	EN ISO 3104 69.5
Kinematic Viscosity	@100°C	mm <sup>2</sup> /s	EN ISO 3104 11.7
Viscosity Index			ISO 2909 164
Density	@15°C	kg/m <sup>3</sup>	DIN 51757 854
Flash Point (COC)		°C	ISO 2592 230
Pour Point		°C	ISO 3016 -36

These characteristics are typical of current production. Whilst future production will conform to Shell's specification, variations in these characteristics may occur.

## G. Ricardo Hydra Engine Specifications

Number of cylinders	1
Bore	86mm
Stroke	86mm
Swept volume	0.4995 litres
Maximum speed	5000 rpm (CP software limited)
Maximum power (kW/ bhp)	15 kW/ 20 bhp
Maximum torque	36 Nm
Maximum cylinder pressure	120 bar
Compression Ratio	10.5:1
Valve per cylinder/ arrangement	4/ Overhead camshaft
Inlet opens	20° BTDC
Inlet closes	72° ABDC
Exhaust opens	60° BBDC
Exhaust closes	32° ATDC
Inlet clearance (cold)	0.3 – 0.4 mm
Exhaust clearance (cold)	0.3 – 0.4 mm
Induction system	Naturally aspirated
Injection	Gasoline Indirect
Timing range	70° BTDC - 20° ATDC (software set at 12° BTDC)
Spark plug	NGK BCPR 7ES
Spark plug gap	0.8 mm
Liner type	Removable sleeve
Liner material	Grade 14 Cast Iron

**Table G-1: Ricardo Hydra Engine specifications**

---

## H. List of Presentations

- [1] Notay, R. S., Priest, M., et al. (2013). *Influence of Lubricant Degradation on Measured Piston Ring Film Thickness in a Fired Gasoline Reciprocating Engine*. Abstract approved. To be presented at 5<sup>th</sup> World Tribology Congress. Torino, Italy. September 2013.
- [2] Notay, R. S. and Priest, M. (2012). *Influence of Lubricant Degradation on Measured Piston Ring Film Thickness in a Fired Reciprocating Engine*. Proceedings of 21<sup>st</sup> Mission of Tribology Research: Capturing the future of UK research. 5<sup>th</sup> December 2012
- [3] Notay, R. S., Priest, M., et al. (2012). *Influence of Lubricant Degradation on Measured Piston Ring Film Thickness in a Motored Reciprocating Engine*. Proceedings of 39<sup>th</sup> Leeds-Lyon Symposium on Tribology. Leeds, UK. September 2012.